MICROCOPY RESOLUTION TEST CHART

YALE UNIVERSITY

FINAL REPORT

To The Office of Naval Research
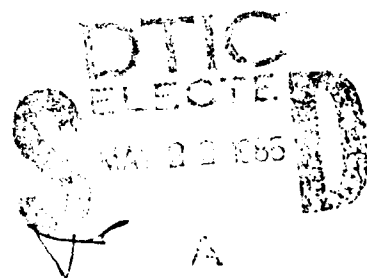
For Contract N00014-80-C-0075

by

Applied Physics Section

Yale University, New Haven, Connecticut 06520

RESEARCH ON GYROTRONS

Principal Investigator

J. L. Hirshfield

April 15, 1985

REPORT DOCUMENTATION PAGE		READ INSTRUCTIONS BEFORE COMPLETING FORM
1. REPORT NUMBER	2. GOVT ACCESSION NO. AD - A154032	3. RECIPIENT'S CATALOG NUMBER
4. TITLE *(and Subtitle)* Research on Gyrotrons		5. TYPE OF REPORT & PERIOD COVERED Final Technical Report
		6. PERFORMING ORG. REPORT NUMBER
7. AUTHOR*(s)* J. L. Hirshfield		8. CONTRACT OR GRANT NUMBER*(s)* N00014-80-C-0075
9. PERFORMING ORGANIZATION NAME AND ADDRESS Yale University, Physics Division Applied Physics Section New Haven, CT 06520		10. PROGRAM ELEMENT, PROJECT, TASK AREA & WORK UNIT NUMBERS 61153N RR011-07-0H0 NR 632-001
11. CONTROLLING OFFICE NAME AND ADDRESS Office of Naval Research 800 N. Quincy Street Arlington, VA 22217		12. REPORT DATE April 15, 1985
		13. NUMBER OF PAGES 263
14. MONITORING AGENCY NAME & ADDRESS*(if different from Controlling Office)*		15. SECURITY CLASS. *(of this report)* Unclassified
		15a. DECLASSIFICATION/DOWNGRADING SCHEDULE

16. DISTRIBUTION STATEMENT *(of this Report)*

Approved for public release; distribution unlimited.

17. DISTRIBUTION STATEMENT *(of the abstract entered in Block 20, if different from Report)*

18. SUPPLEMENTARY NOTES

19. KEY WORDS *(Continue on reverse side if necessary and identify by block number)*

Gyrotron
Cyclotron Resonance
Microwave Amplification
Millimeterwave Generation

20. ABSTRACT *(Continue on reverse side if necessary and identify by block number)*

    A summary is given of research on gyrotron-like mechanisms for anpli-
fying or generating electromagnetic radiation. These mechanisms include
slow-wave cyclotron-wave amplification in a dielectrically-loaded waveguide,
cyclotron harmonic oscillations in a quasi-optical millimeter-wave struc-
ture, a quasi-optical gyro-klystron, and cyclotron harmonic amplification
in irregular cross section waveguides. Both linearized theory and experi-
mental observations are described.

DD FORM 1473 EDITION OF 1 NOV 65 IS OBSOLETE
1 JAN 73
S N 0102-LF-014-6601

SUMMARY OF RESEARCH COMPLETED

Research on gyrotrons under this contract was carried out over a four-year period with support by the Office of Naval Research. The central emphasis of the research was to expand the theoretical base underlying gyrotron-type amplifying mechanisms and oscillators, and to test the theory and explore new mechanisms by direct experimentation.
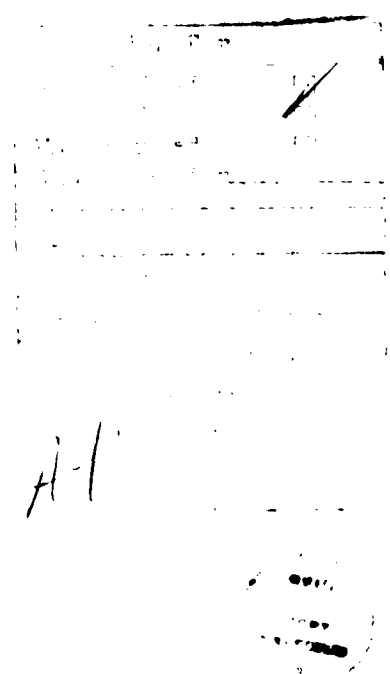
The most notable advances include the following:

1. Complete formulation of the linearized theory of gyrotron slow-wave amplification for TE_{on} and TM_{on}-modes including effects of finite beam geometry and finite thermal velocity spread.

2. Experimental demonstration of slow-amplification for TE_{01} modes, with observed gain of 53 db, power output of 20 kW, and electronic efficiency of 10% at 6 GHz.

3. Experimental operation of quasi-optical gyrotron oscillator, with power measurements on harmonics up to the ninth, giving sub-millimeter wave oscillations using magnetic fields below 15 kG and beam energies below 20 kV.

Copies of all major publications and reports which resulted from this research program are appended to this report. The list of these follows:

1. "Linear Theory of Gyro-Slow-Wave Amplifier for TE_{on}-Modes in a Dielectric-Loaded Cylindrical Waveguide," Soo Yong Park, J. Mark Baird, and J. L. Hirshfield, unpublished.

2. "Linear Theory of Gyro-Slow-Wave Amplifier for TM_{on}-Modes in a Dielectric-Loaded Cylindrical Waveguide," Soo Yong Park, J. Mark Baird, and J. L. Hirshfield, unpublished.

3. Invited paper. "Theory of a slow wave cyclotron amplifier," K. R. Chu, A. K. Ganguly, V. L. Granatstein, J. L. Hirshfield, S. Y. Park, and J. M. Baird, Int. J. Electronics, 51, 493 (1981).

4. "Measurements of Gain for Slow Cyclotron Waves on an Annular Electron Beam," H. Guo, L. Chen, H. Keren, and J.L. Hirshfield, Phys. Rev. Lett. <u>49</u>, 730 (1982).

5. "Cyclotron Harmonic Maser," J. L. Hirshfield, International Journal of Infrared and Millimeter Waves <u>2</u>, 695 (1981).

6. "Space Charge Effects in a Gyrotron Employing a Solid Electron Beam," H. Keren and J. L. Hirshfield, International Journal of Infrared and Millimeter Waves, <u>2</u>, 1097 (1981).

7. "Bernstein-Mode Quasioptical Maser Experiment," N. A. Ebrahim, Z. Liang, and J. L. Hirshfield, Phys. Rev. Lett. <u>49</u>, 1556 (1982).

8. "Bernstein Mode Quasi-Optical Gyroklystron," Z. Liang, N. A. Ebrahim, and J. L. Hirshfield, International Journal of Infrared and Milli-meter Waves <u>4</u>, 423 (1983).

9. "Electron Prebunching and High Harmonic Interaction in a Bernstein Mode Quasi-Optical Gyrotron," N. A. Ebrahim, Z. Liang, and J. L. Hirshfield, unpublished.

10. "Theory of Gyrotron Traveling Wave Amplifiers at Harmonics of the Gyration Frequency," Qiangfa Li, Ph.D. Thesis July 1984

Linear Theory of Gyro-Slow-Wave Amplifier

For TE_{on}-Modes in a

Dielectric-Loaded Cylindrical Waveguide

S. Y. Park[*] and J. M. Baird[+]

B-K Dynamics, Inc.
Rockville, Md 20852

and

J. L. Hirshfield

Yale University
New Haven, CT 06520

20 November 1981

[*]Present address: U.S. Naval Research Lab
[+]Present address: University of Utah

ACKNOWLEDGEMENTS

TABLE OF CONTENTS

LINEAR THEORY OF GYRO-SLOW-WAVE-AMPLIFIER FOR TE_{on}-MODES
IN A DIELECTRIC-LOADED CYLINDRICAL WAVEGUIDE

I. INTRODUCTION

Recently much interest has been shown in gyrotron-type microwave generating
(or amplifying) devices[1] utilizing transverse electron beam energy in a
strong guiding magnetic field. An electron gyrating in a magnetic field
shows negative mass response in its rotational motion when it interacts
with an electromagnetic wave. This negative mass behavior leads to an
azimuthal bunching and thus induces a negative mass instability.

There are two types of instability driving forces; a direct electric force
$\vec{E}$ and a magnetic pondromotive force $\vec{v} \times \vec{B}$; the former one leads to the
famous cyclotron maser instability (CMI)[2] and the latter one leads to
the Weibel instability[3]. Chu and Hirshfield[4] analyzed both mechanisms
in a unified treatment for a plane wave in a uniform (unbounded) plasma
and showed that they are competing with each other -- the cyclotron maser
instability dominating in a fast wave region and Weibel instability
dominating in a slow wave region. For a plane wave in an unbounded system,
the electrons in the plasma itself play the role of active medium to make the
phase velocity fast or slow. This requires a very dense electron beam.

In practice, it is desirable to provide this separation in a more efficient
way. A fast wave can be easily achieved by a waveguide with a bare conduc-
ting wall because the phase velocity in a waveguide is always greater than
the speed of light in a free space. Conventional gyrotrons operate near the
cutoff region where the cyclotron maser instability is dominating. In order
to provide a slow wave where Weibel instability is dominating, one must

introduce a slow wave structure inside the waveguide -- either a periodic
structure or dielectric layers.

A dispersion curve for a waveguide with slow wave structure shows a nearly-
straight section with a gentle slope within the range of moderate electron
beam energy over a wide range of frequencies. Then the electron beam line
can be chosen to be parallel and close to this section of the dispersion
curve inducing strong instability over a wide range of frequencies. This
broad band instability may provide us with a wide-band amplifier or slow-wave
gyrotron-type device.

The dispersion curve with dielectric layers shows an almost unlimited nearly
straight section, while the one with periodic structure bends over becoming
periodic which limits the intrinsic bandwidth. Of course, even with dielectric
layers the coupling between electron beam and electromagnetic wave is
substantially reduced at higher frequencies limiting its bandwidth. However,
this limitation seems to be less severe than that for waveguides with periodic
structure. Another advantage of dielectric layers over periodic structure
may be its simplicity in fabrication and theoretical analysis. In this
paper we restrict the analysis to an amplifier with dielectric layers.

We consider a hollow electron beam, initially with each electron gyrating in
an equilibrium orbit in a uniform guiding magnetic field, introduced into
an interaction region of a cylindrical waveguide loaded with an arbitrary
number of concentric dielectric layers. The electrons now interact with the
electromagnetic wave, get modulated and exchange energies. The development
of the electron state and the electromagnetic wave along the interaction tube
is completely determined by coupled Maxwell-Vlasov equations.

With our primary interest in the theory for an amplifier, we assume that the system is stationary in time (no absolute instability) and then one can reduce the problem into a one-dimensional boundary value problem which can be analyzed by Laplace transformation. The coupling between the input signal and the beam modes is completely determined by the boundary condition at the input end of the amplifier which means that one can calculate the insertion loss.

In this paper we wish to carefully develop a gain theory of an amplifier with dielectric slow wave structure for TE_{on}-modes. Whenever assumptions are made we point out their motivation and limitation. Throughout this paper we assume that electrons and electromagnetic waves are described by linearized Vlasov-Maxwell equations and that the space charge effect can be neglected. Furthermore, we make two more technical assumptions: the coupling through the electron beam between TE and TM modes, and between different radial modes, is negligible; otherwise the analysis is completely general.

In Section 2, an expression for the perturbed electron distribution function in terms of the integral over unperturbed characteristics is obtained for an arbitrary electromagnetic wave.

In Section 3, the linearized Maxwell equations with a source term from the perturbed electron beam are discussed. The TE_{on}-mode is separated out and the dispersion relation including the source term is derived. Here we extensively use the results of a general analysis[6] for an empty waveguide loaded with multilayers of dielectrics obtained previously.

In Section 4, the source term for a hollow electron beam is calculated. The calculation is straightforward but tedious, and two appendices at the end

are given for this section. Two major complexities are due to the finite geometry of the electron beam and the non-harmonicity of electromagnetic waves seen by electrons. The former one was often neglected in earlier work and the latter one requires a harmonic expansion using the Graf's Addition Theorem for Bessel functions.

In Section 5, the dispersion relation is solved to calculate gains. Some specific examples are calculated for various sets of parameters. In the last section, the physics learned from this work is discussed.

II. LINEARIZED VLASOV EQUATION

Consider that a hollow anular electron beam (such as from a magnetron injection gun) is introduced along a guiding magnetic field into one end of a cylindrical waveguide which is loaded with an arbitrary number of concentric dielectric layers. The electron beam is assumed to be sufficiently tenuous so that its space charge effect can be neglected initially in its equilibrium state in a uniform magnetic field, and thus each electron is gyrating about its guiding center at $r = R$ with its Larmor radius r_L. The electrons now interact with an electromagnetic wave and azimuthal bunching occurs, leading to a negative mass instability if the conditions are right.

Neglecting the collision effect between electrons, the dynamical development of the electron state in an electromagnetic field is governed by the Vlasov equation. With the electron distribution function $f(\vec{x}, \vec{u}; t)$ in the phase space, where

$$\vec{u} = \vec{p}/m = \gamma \vec{v} \text{ and thus } \gamma = (1 - v^2/c^2)^{-1/2} = (1 + u^2/c^2)^{1/2},$$

the relativistic Vlasov equation reads

$$\partial f / \partial t + \vec{u}/\gamma \cdot \nabla_x f - e/m \left(\vec{E} + \vec{u}/c\gamma \times \vec{H} \right) \cdot \nabla_u f = 0 \qquad (2.1)$$

which is coupled to the Maxwell equations through E and H.

Generally, it is not possible to solve such a problem analytically. However, in a strong magnetic field, one can linearize the equations by considering a

and

$$\tilde{J}_\theta(k) \equiv -Ne \int d^3u \, \frac{u_\perp}{\gamma} \cos\xi \, \tilde{f}_1(k) \qquad (4.6)$$

The source term $\tilde{P}_n(k)$ in (4.4) represents the amount of radiation in the n-th radial waveguide mode due to the induced current $\tilde{J}_\theta(k)$. The normalization factor C_N in (4.5) defined by (3.16) is related to the total power flow throughout the waveguide. The first step in solving (4.4) is to calculate the Laplace transformation of the perturbed electron distribution function $\tilde{f}_1(k)$.

$\tilde{f}_1(k)$: Perturbed Distribution Function

Let us first consider the perturbed electron distribution function (2.12) with the fields for TE_{on}-mode (3.10):

$$(4.7)$$

$$f_1(z) = \frac{e}{m} \int_{t-Z/v_\parallel}^{t} dt' e^{-i\omega t'} \left\{ \left[E_\theta(z') \frac{\partial f_0}{\partial u_\perp} + H_r(z') \left(\frac{u_\parallel}{c\gamma} \frac{\partial f_0}{\partial u_\perp} - \frac{u_\perp}{c\gamma} \frac{\partial f_0}{\partial u_\parallel} \right) \right] Z_1(|\alpha_n|r') \cos\xi' \right.$$

$$\left. - \left[\left(E_\theta(z') + H_r(z') \frac{u_\parallel}{c\gamma} \right) Z_1(|\alpha_n|r') \cos\chi' + H_z(z') \frac{u_\perp}{c\gamma} Z_0(|\alpha_n|r') i\sin\psi' \right] \frac{1}{\Omega_c} \frac{\partial f_0}{\partial R} \right\}$$

where the integration is to be carried out over the characteristic ("particle" trajectory) given by:

$$z' \equiv z + v \ (t'-t)$$

$$\psi' \equiv \psi + \omega_c (t'-t)$$

$$r' \equiv (R^2 + r_L^2 - 2Rr_L\cos\psi')^{1/2} \qquad (4.8)$$

$$v_\parallel \equiv \frac{u_\parallel}{\gamma}, \quad \omega_c \equiv \frac{\Omega_c}{\gamma}, \quad r_L \equiv \frac{u_\perp}{\Omega_c}$$

-19-

IV. LAPLACE TRANSFORMATION

An unstable system can be correctly analyzed by Laplace transformation (not Fourier analysis) defined by

$$\tilde{F}(k) \equiv \int_0^\infty dz e^{-ikz} F(z) \qquad (4.1)$$

where k is a complex variable with a sufficiently large negative imaginary part to guarantee that the integral (4.1) can be well defined. (Recall that in unstable system $F(z)$ can be an exponentially growing function of z.) The Laplace transformation of derivatives of function requires information on boundary values at the input end ($z = 0$) as

$$\frac{\widetilde{dF}}{dz}(k) \equiv ik\tilde{F}(k) - F(o)$$

$$(4.2)$$

$$\frac{\widetilde{d^2F}}{dz^2}(k) \equiv -k^2\tilde{F}(k) - ikF(o) - \frac{dF}{dz}(o)$$

Applying the Laplace transformation on the Maxwell equations (3.12) and (3.15) with the boundary condition (3.17), i.e., $E_\theta(o) = o$, one obtains

$$\frac{\omega}{c}\tilde{H}_r(k) = -k\tilde{E}_\theta(k)$$

$$(4.3)$$

$$\frac{\omega}{c}\tilde{H}_z(k) = |\alpha_n|\tilde{E}_\theta(k)$$

and

$$(k^2 - k_n^2)\tilde{E}_\theta(k) = \tilde{P}_n(k) - \frac{dE_\theta}{dz}(o)$$

$$(4.4)$$

where

$$\tilde{P}_n(k) \equiv i\frac{\omega}{c}e^{i\omega t}\frac{4\pi}{c}\frac{1}{C_N}\int 2\pi r dr\, Z_1(|\alpha_n|r)\tilde{J}_\theta(k)$$

$$(4.5)$$

-18-

Substituting (3.14) into (3.12) one obtains the equation for the n-th radial modes:

$$- d^2E(z)/dz^2 - k_n^2 E_\theta(z) = P_n(z) \tag{3.15}$$

where

$$P_n(z) \equiv 1/C_N \int 2\pi r dr \, Z_1(|\alpha_n|r) \, i \, \omega/c \, e^{i\omega t} \, 4\pi/c \, J_\theta$$

$$C_N \equiv \sum_{i=1}^{N} \int_{r_{i-1}}^{r_i} 2\pi r dr \, [A_i z_1(|\alpha_n^i|r) + \overline{A}_i \overline{Z}_1(|\alpha_n^i|r)]^2 \tag{3.16}$$

$(A_1 = 1, \overline{A}_1 = 0)$.

and

$$\sum_{n=1}^{\infty} [- d^2 E_\theta(z)/dz^2 - k_n^2 E_\theta(z)] Z_1 (|\alpha_n|r) = i \omega/c \ e^{i\omega t} \ 4\pi/c \ J_\theta$$

$$(\alpha_n^2 \equiv \omega^2/c^2 - k_n^2) \tag{3.12}$$

where

$$J_\theta = -e \int d^3u \ \hat{\theta} \cdot \vec{u}/\gamma \ f_1$$

$$J_r = J_z = 0. \tag{3.13}$$

The condition, $J_r = J_z = 0$, is an artifact of the assumption iv) which allowed us to concentrate on TE-mode field ($E_z = E_r = H_\theta = 0$). Actually, if one calculates J_z and J_r using the same f_1 in J_θ, they are not small, however, what is small is their coupling with fields. From (3.8), J_z and J_r are the sources of TM type fields (E_z, E_r, H_θ) and lead to a possible coupling to TM-mode. But, due to the assumption iv), the TM-modes are completely mistuned and their coupling to the TE-field is small. Therefore as far as one can neglect TE-TM coupling, one can neglect the condition $J_z = J_r = 0$.

Furthermore, with the assumption v), one can expand the source term in (3.12) in terms of radial modes as

$$i \omega/c \ e^{i\omega t} \ 4\pi/c \ J_\theta = P_n(z)Z_1 (|\alpha_n|r) + \sum_{n' \neq n} P_{n'}(z)Z_1 (|\alpha_{n'}|r) \tag{3.14}$$

and keep only the first term since that is the only term which couples to the n-th radial mode resonantly. The expansion of the source term in radial eigenmodes (3.14) can be easily done by applying the projection operator $1/C_N \int 2\pi r dr \ Z_1 (|\alpha_n|r)$ on the source term (C_N is a normalized constant).

and no assumption was made on the z and r dependency of the fields. However, for convenience, we have expanded the radial function in terms of a complete set of radial eigenmodes in empty waveguide. In practice radial eigenmodes with different n are well-separated and one can tune the electron beam so that it can interact resonantly with only one radial mode. Then one can neglect the coupling between different radial eigenmodes. So far, we have assumed:

     i)   linearity - small perturbation

    ii)   tenuous electron beam - neglect the space charge effect

   iii)   stationary in time - amplifier theory

    iv)   cylindrically symmetric TE-mode

     v)   only n-th radial mode is excited

The first two assumptions, i) and ii), are essential within the scope of the present work and the last two assumptions, iv) and v), are technical simplifying assumptions which could be easily removed as will be discussed in a separate work. The third assumption, iii), is for a true amplifier without absolute instability which will also be discussed in a separate paper. These are all the assumptions we make in this paper.

We emphasize that we have not made any assumption on the z-dependency of the fields. This will be completely determined by the dynamics and the boundary conditions at the input end.

Substituting (3.9) into (3.7), one obtains

$$i \, \omega/c \; H_r(z) = - \, dE_\theta(z)/dz$$

$$\omega/c \; H_z(z) = |\alpha n| \, E_\theta(z)$$

$$(3.11)$$

Since we are interested mainly in an amplifier theory, we assume that the system is stationary in time, and then one can write the most general fields for TE- mode $(E_z = E_r = H_\theta = 0)$ as

$$E_\theta = e^{-i\omega t} \sum_{n=1}^{\infty} E_\theta(z) Z_1 (|\alpha_n| r)$$

$$iH_z = e^{-i\omega t} \sum_{n=1}^{\infty} H_z(z) Z_0 (|\alpha_n| r)$$

$$H_r = e^{-i\omega t} \sum_{n=1}^{\infty} H_r(z) Z_1 (|\alpha_n| r)$$

$$(\alpha_n^2 \equiv \omega^2/c^2 - k_n^2)$$

(3.9)

in the innermost region, and

$$E_\theta^{(i)} = e^{-i\omega t} \sum_{n=1}^{\infty} [E_\theta^{(i)} (z) Z_1 (|\alpha_n^i| r) + \overline{E}_\theta^{(i)} (z) \overline{Z}_1 (|\alpha_n^i| r)]$$

$$iH_z^{(i)} = e^{-i\omega t} \sum_{n=1}^{\infty} [H_z^{(i)} (z) Z_0 (|\alpha_n^i| r) + \overline{H}_z^{(i)} (z) \overline{Z}_0 (|\alpha_n^i| r)]$$

$$H_r = e^{-i\omega t} \sum_{n=1}^{\infty} [H_r^{(i)} (z) Z_1 (|\alpha_n^i| r) + \overline{H}_r^{(i)} (z) \overline{Z}_1 (|\alpha_n^i| r)]$$

(3.10)

$$(\alpha_n^{i\,2} \equiv \epsilon_i \mu_i \omega^2/c^2 - k_n^2)$$

where k_n is a wave number determined by the boundary conditions of the empty waveguide and Z_ℓ, $\overline{Z}_\ell$ denote Bessel functions according to

$$Z_\ell(x) = \begin{cases} J_\ell(x) \\ I_\ell(x) \end{cases} \qquad \overline{Z}_\ell = \begin{cases} Y_\ell(x) & \text{if } \alpha_n^2 > 0 \\ K_\ell(x) & \text{if } \alpha_n^2 < 0 \ . \end{cases}$$

The fields in (3.10) are connected to those in (3.9) via a "transfer matrix" as shown in Paper I. Note that, in (3.9) and (3.10), the assumption of stationary in time allowed us to consider a single frequency $(\sim e^{-i\omega t})$ behavior

substantially alter the dynamic character (beside a possible small shift in the resonance frequency).

Now, let us study the perturbed part of electromagnetic field (RF part) given by (3.5) and (3.6). In the case of azimuthally symmetric states ($\partial/\partial\theta = 0$), the Maxwell equations (3.5) can be grouped into two parts: TE-mode part, which involves (E_θ, H_z, H_r; J_θ),

$$- \partial E_\theta/\partial z = - 1/c \; \partial H_r/\partial t$$
$$1/r \; \partial/\partial r \; (rE_\theta) = - 1/c \; \partial H_z/\partial t \qquad (3.7)$$
$$\partial H_r/\partial z - \partial H_z/\partial r = 1/c \; \partial E_\theta/\partial t + 4\pi/c \; J_\theta$$

and TM-mode part, which involves (H_θ, E_z, E_r; J_r, J_z),

$$\partial Er/\partial z - \partial E_z/\partial r = 1/c \; \partial H_\theta/\partial t$$
$$- \partial H_\theta/\partial z = 1/c \; \partial Er/\partial t + 4\pi/c J_r \qquad (3.8)$$
$$1/r \; \partial/\partial r \; (rH_\theta) = 1/c \; \partial E_z/\partial t + 4\pi/c \; J_z.$$

In general, these two sets of equations are coupled to each other through the source terms. In Paper I, we have shown that, for the azimuthal symmetric case, the boundary conditions between dielectric layers and on the conducting wall do not mix TE and TM modes. Therefore, in the azimuthally symmetric case the only place where TE and TM mode coupling can occur is through the source term. However, if the electron beam is sufficiently tenuous and the TE and TM modes are well-separated so that the electron beam can couple resonantly with only one of the modes, one may neglect the mixing. In this paper, we will concentrate on the TE-mode given by (3.7), neglecting the coupling to the TM mode.

First, by substituting the perturbation expansion (2.2) into (3.1) and (3.2) and separating the zeroth and the first order parts, one obtains, in the zeroth order,

$$\rho_0 \equiv -e\int d^3u f_0 = 0$$
$$\vec{J}_0 \equiv -e\int d^3u \ \vec{u}/\gamma \ f_0 = 0$$

(3.4)

and, in the first order.

$$\nabla \times \vec{E}_1 = -1/c \ \partial\vec{H}_1/\partial t \qquad \qquad \nabla \cdot \vec{E}_1 = 4\pi\rho_1$$
$$\nabla \times \vec{H}_1 = 1/c \ \partial\vec{E}_1/\partial t + 4\pi/c \ \vec{J}_1 \qquad \nabla \cdot \vec{H}_1 = 0$$

(3.5)

where

$$\rho_1 \equiv -e\int d^3u f_1$$
$$\vec{J}_1 \equiv -e\int d^3u \ \vec{u}/\gamma \ f_1.$$

(3.6)

Obviously, the condition (3.4) on the equilibrium part of electron distribution function cannot be fulfilled for a pure electron beam. This is because we have neglected the space charge effect which prohibits a simple perturbation expansion such as (2.2). With the space charge effect of the electron beam, the zeroth order fields in the perturbation expansion (2.2) should include the part of the static electric field and static diagmagnetic magnetic field in addition to the guiding magnetic field B_0. This again requires redefinition of the unperturbed beam function f_0 and leads to a whole new problem which is beyond the scope of this work. Therefore, throughout this paper, we assume that the electron beam is sufficiently tenuous so that one can neglect the space charge effect compared with the strong guiding magnetic field. Since we are mainly interested in instability properties which are due to a resonant interaction, one expects that such a static space charge effect may not
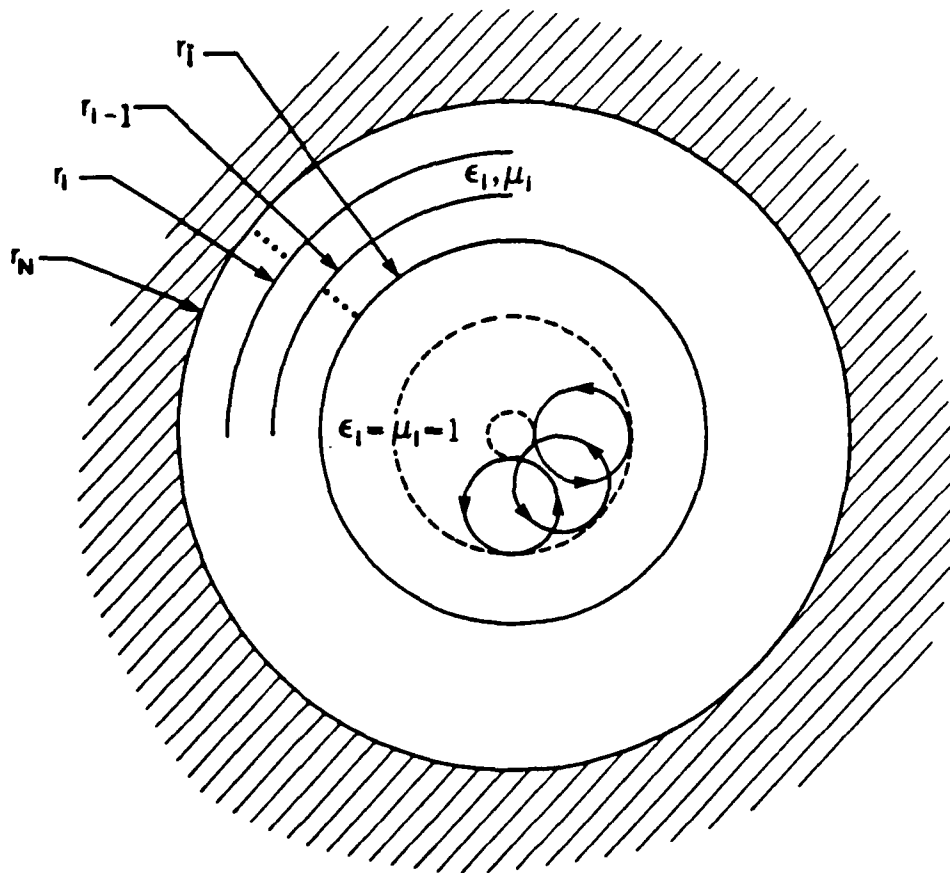
Figure 3.1 Cross-sectional view of the cylindrical waveguide loaded with an arbitrary number of dielectric layers. A hollow annular electron beam is confined only in the central vacuum region.

In case of no source term present (empty waveguide), the problem has been solved completely in the previous paper[6] which will be referenced to as Paper I from now on. Without source terms, the cylindrical symmetry allows us to use a Fourier transformation along z and the axial wave number k is an orthogonal eigenmode number. Furthermore, for azimuthally symmetric fields, TE and TM modes are decoupled. However, with the source terms which can in general couple all possible modes, one must be careful to make such a reduction. Since the source terms are present only in the innermost vacuum region, in this paper, we will concentrate on the Maxwell equations (3.1) with source (3.2) while referring to the Paper I for the part which can be handled in the same way as in the empty waveguide.

-11-

III. MAXWELL EQUATIONS

Consider a circular cylindrical waveguide loaded with an arbitrary number of
concentric dielectric layers which serve as a slow wave structure. We assume
that the innermost region is a vacuum ($\epsilon = \mu = 1$) where the hollow annular elec-
tron beam is present as shown in Figure 3.1.

Maxwell equations in the innermost region,

$$\nabla \times \vec{E} = -1/c \; \partial \vec{H}/\partial t \qquad\qquad \nabla \cdot \vec{E} = 4\pi\rho$$
$$\nabla \times \vec{H} = 1/c \; \partial \vec{E}/\partial t + 4\pi/c \; \vec{J} \qquad \nabla \cdot \vec{H} = 0$$

(3.1)

are coupled to the Vlasov equation through source terms,

$$\rho = -e \int d^3u \, f$$
$$\vec{J} = -e \int d^3u \; \vec{u}/\gamma \; f.$$

(3.2)

Electromagnetic fields in a dielectric layer satisfy sourceless Maxwell
equations,

$$\nabla \times \vec{E}^{(i)} = - \mu_i/c \; \partial \vec{H}^{(i)}/\partial t \qquad \epsilon_i \; \nabla \cdot \vec{E}^{(i)} = 0$$
$$\nabla \times \vec{H}^{(i)} = \epsilon_i/c \; \partial \vec{E}^{(i)}/\partial t \qquad \mu_i \; \nabla \cdot \vec{H}^{(i)} = 0 \qquad (3.3)$$
$$(i = 2, 3, \ldots, N).$$

These equations are supplemented by boundary conditions: The fields in one
region are connected to the fields in the adjacent region through the boundary
conditions that E_z, E_θ, H_z and H_θ be continuous (E_r and H_r are related to these
through Maxwell equations). Also fields in the innermost region must be
regular on the axis and the fields in the outermost region satisfy the boundary
condition that E_z and E_θ vanish on the conducting wall (again, the condition
on H_r is not independent).

notational convenience, we will suppress the subscript 1 in E and H):

$$f_1 = e/m \int_{t-z/v_\|}^{t} dt' \left\{ E_z' \, \partial f_0/\partial u_\| + \vec{E}_\perp \cdot \hat{e}_\perp' \, \partial f_0/\partial u_\perp + \right.$$

$$\vec{H}_\perp' \cdot \hat{e}_\phi' \, (u_\perp/c\gamma \, \partial f_0/\partial u_\| - u_\|/c\gamma \, \partial f_0/\partial u_\perp) + (-\vec{E}_\perp \cdot \hat{\Theta} \qquad (2.11)$$

$$\left. + \vec{H}_\perp \cdot \hat{R} \, u_\|/c\gamma + H_z' \, e_\perp' \cdot \hat{R} \, u_\perp/c\gamma) \, 1/\Omega_c \, \partial f_0/\partial R \right\}.$$

The first term in (2.11) is the driving term for a conventional TWTA insta-
bility, the second term is for the famous cyclotron maser instability and
the third term for the Weibel instability. Notice the characteristic
asymmetric derivative in the third term which picks out only the anisotropic
part of velocity distribution in f_0. Finally, the last term represents all
the effects of a bounded and spatially non-uniform plasma. In terms of
variables given in Figure 2.1, one can write (2.11) as

$$f_1 = e/m \int_{t-z/v_\|}^{t} dt' \left\{ E_z' \, \partial f_0/\partial u_\| + (E_r' \sin \xi' + E_\theta' \cos \xi') \, \partial f_0/\partial u_\perp \right.$$

$$+ (-H_r' \cos \xi' + H_\theta' \sin \xi') \, (u_\perp/c\gamma \, \partial f_0/\partial u_\| - u_\|/c\gamma \, \partial f_0/\partial u_\perp)$$

$$\qquad (2.12)$$

$$+ [(-E_r' \sin \chi' + E_\theta' \cos \chi') + (H_r' \cos \chi' + H_\theta' \sin \chi') \, u_\|/c\gamma$$

$$\left. - H_z' \sin \psi' \, u_\perp/c\gamma] \, 1/\Omega_c \, \partial f_0/\partial R \right\}.$$

In order to carry out the integral over the characteristics, one needs to
study the possible electromagnetic waves in the waveguide which are governed
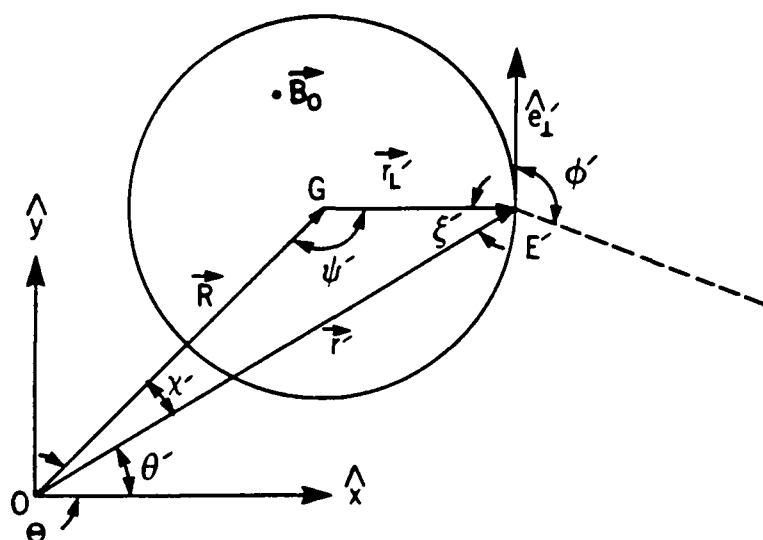by Maxwell equations and boundary conditions.

Figure 2.1. Cross-sectional view of the "unperturbed" characteristics (an electron "trajectory" in a uniform guiding magnetic field). O is the common center of the hollow annular electron beam and the waveguide, G is a guiding center of an electron and E' is the position of the electron at t'.

A set of the invariants of the unperturbed characteristics can be easily found: the longitudinal velocity component $v_{\parallel}$, the magnitude of transverse velocity $v_{\perp}$ (and thus γ) and the radius of guiding center R. These are three independent invariants convenient to use to represent a realistic equilibrium electron distribution function, $f_0 = f_0 (u_{\parallel}, u_{\perp}, R)$.

Noting the relation $R = (r'^2 + r_L^2 - 2r'r_L \cos\xi')^{1/2}$, the velocity gradient can be written as.

$$\nabla_u' f_0 = \hat{z} \, \partial f_0/\partial u_{\parallel} + \hat{e}_{\perp}' \, \partial f_0/\partial u_{\perp} + (\nabla_u \cdot R) \, \partial f_0/\partial R$$

$$\nabla_u' R = \hat{e}_{\perp}' \, \partial R/\partial u_{\perp} + \hat{e}_{\phi}' \, 1/u_{\perp} \, \partial R/\partial \phi' \qquad (2.10)$$

$$= 1/\Omega_c \, (\hat{e}_{\perp}' \cos\psi' - \hat{e}_{\phi}' \sin\psi') = - 1/\Omega_c \hat{\Theta}$$

where the capped quantities represent unit vectors for the corresponding variables. Substituting (2.10) into (2.8), one obtains (for the sake of

Equation (2.6) tells us that f_0 is an arbitrary function of invariants of the characteristics and equation (2.7) can be written as an integral form:

$$f_1 (\vec{x}, \vec{u}, t) = e/m \int_{t-z/v_{||}}^{t} dt' \ (\vec{E}_1' + \vec{u}'/c\gamma \times \vec{B}_1') \cdot \nabla_u' f_0' \qquad (2.8)$$

from which it is clear that the electron beam is introduced from one end of the guide in its equilibrium state and the perturbation grows in the direction of the velocity gradient of the equilibrium distribution function as the beam moves along the waveguide. The "unperturbed" characteristic, (2.5), which is nothing more than a "particle" trajectory in a uniform magnetic field, can be easily solved to be

$$\vec{u}' = \hat{z} \ u_{||} + \hat{e}_{\perp}' \ u_{\perp}$$
$$\vec{x}' = \vec{x}(t) + \hat{z} \ u_{||}/\gamma \ (t' - t) + (\hat{e}_{\phi} - \hat{e}_{\phi}')r_L \qquad (2.9)$$

where

$$\hat{e}_{\perp}' \equiv \hat{x} \ \cos\phi' + \hat{y} \ \sin\phi'$$
$$\hat{e}_{\phi}' \equiv -\hat{x} \ \sin\phi' + \hat{y} \ \cos\phi'$$
$$\phi' \equiv \phi(t) + \omega_c \ (t' - t), \quad \omega_c \equiv \Omega_c/\gamma$$

and $r_L \equiv u_{\perp}/\Omega_c = v_{\perp}/\omega_c \ (v_{\perp} \equiv u_{\perp}/\gamma)$ is the Larmor radius.

The geometrical representation of the characteristics is shown in Figure 2.1. The relation between angles is given by $\xi' \equiv \pi/2 - (\phi' - \theta'), \ \psi' \equiv \pi/2 + (\phi' - \Theta)$ and $\chi' \equiv \Theta - \theta'$.

small perturbation about an equilibrium state in a strong uniform magnetic field;

$$f = f_0 + f_1$$
$$\vec{H} = \vec{B}_0 + \vec{H}_1 \qquad\qquad (2.2)$$
$$\vec{E} = \vec{E}_1.$$

Substituting (2.2) into (2.1) and separating it into the equilibrium part (zeroth order) and the linear perturbed part (first order), one obtains

$$\partial f_0/\partial t + \vec{u}/\gamma \cdot \nabla_x f_0 + \Omega_c \,\hat{z} \times \vec{u}/\gamma \cdot \nabla_u f_0 = 0 \qquad\qquad (2.3)$$

and

$$\partial f_1/\partial t + \vec{u}/\gamma \cdot \nabla_x f_1 + \Omega_c \,\hat{z} \times \vec{u}/\gamma \cdot \nabla_u f_1 =$$
$$e/m \,(\vec{E}_1 + \vec{u}/c\gamma \times \vec{H}_1) \cdot \nabla_u f_0 \qquad\qquad (2.4)$$

where $\Omega_c \equiv eB_0/mc$ is the cyclotron frequency of an electron in its rest frame. Following a well-known technique[5], one can cast the left-hand side of both (2.3) and (2.4) into total derivatives along an "unperturbed" characteristic, $\vec{x}' \equiv \vec{x}'\,(\vec{x}(t), \vec{u}(t); t'-t)$ and $\vec{u}' \equiv \vec{u}'\,(\vec{x}(t), \vec{u}(t); t'-t)$ defined by

$$d\vec{x}'/dt' = \vec{u}'/\gamma' \qquad\qquad (2.5)$$
$$d\vec{u}'/dt' = \Omega_c \,\hat{z} \times \vec{u}'/\gamma'$$

such that $\vec{x}' = \vec{x}\,(t)$ and $\vec{u}' = \vec{u}\,(t)$ at $t' = t$.

Therefore one can write (2.3) and (2.4) as

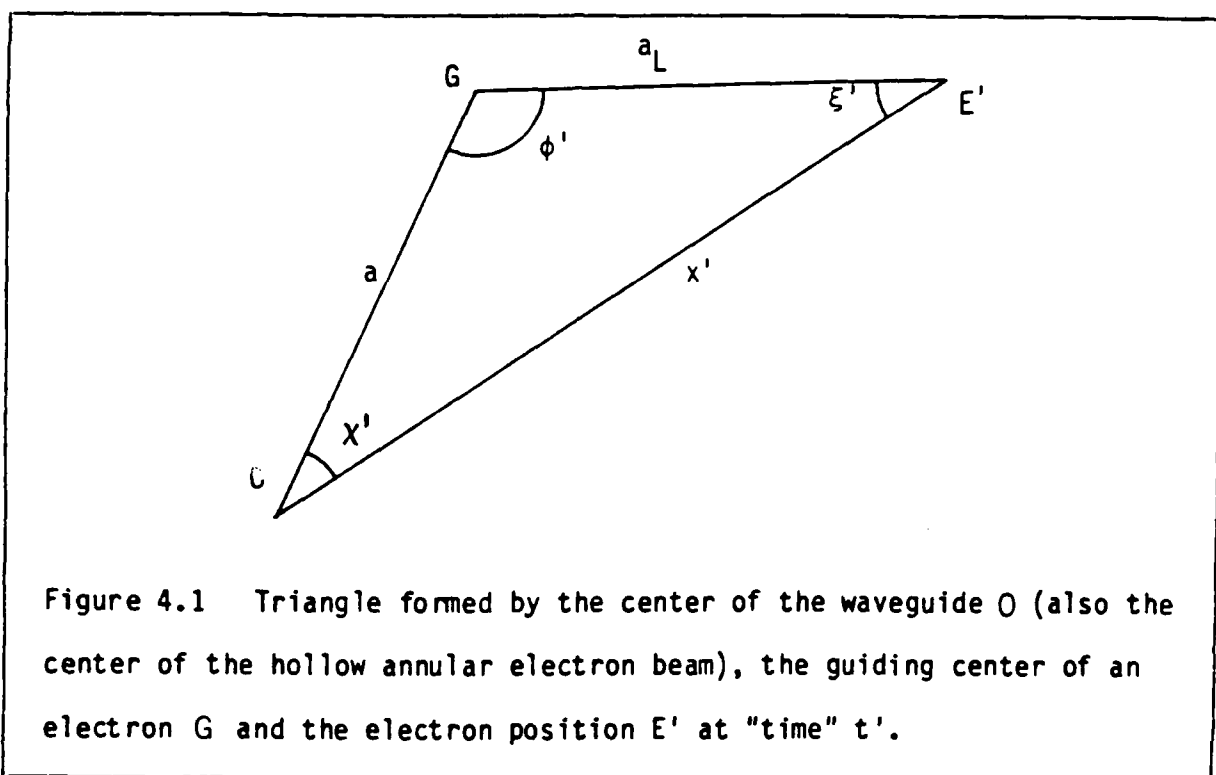$$df_0'/dt' = 0 \qquad\qquad (2.6)$$

and

$$df_1'/dt' = e/m \,(\vec{E}_1' + \vec{u}'/c\gamma' \times \vec{H}_1') \cdot \nabla_u' f_0 \qquad\qquad (2.7)$$

where the primed quantities are the values at a point on the characteristics defined by (2.5) and the total derivative is taken along them.

It will be convenient to introduce scale variables as

$$a \equiv |\alpha_n|R, \quad a_L \equiv |\alpha_n|r_L \equiv \frac{|\alpha_n|}{\Omega_c} u_\perp$$

$$x' \equiv |\alpha_n|r', \quad a_{||} \equiv \frac{|\alpha_n|}{\Omega_c} u_{||}$$

(4.9)

and then the geometric interpretation of the characteristics (4.8) in terms of these scale variables can be represented by a triangle as shown in Figure 4.1.

Figure 4.1   Triangle formed by the center of the waveguide O (also the center of the hollow annular electron beam), the guiding center of an electron G and the electron position E' at "time" t'.

It will also be convenient to introduce a sign factor $\hat{\alpha}$ as

$$\hat{\alpha} \equiv \alpha_n^2 / |\alpha_n|^2 = \begin{cases} 1 & \text{if } \alpha_n^2 > 0 \\ -1 & \text{if } \alpha_n^2 < 0 \end{cases}$$

(4.10)

$$(\alpha_n^2 \equiv \frac{\omega^2}{c^2} - k_n^2)$$

Recalling that the Bessel function $Z_\ell(|\alpha_n|r')$ represents either $J_\ell(|\alpha_n|r')$ or $I_\ell(|\alpha_n|r')$ depending on whether α_n^2 is positive (fast wave) or negative (slow wave), one can write Bessel function relations as

$$Z_\ell''(x) + \frac{1}{x} Z_\ell'(x) + (\hat{\alpha} - \frac{\ell^2}{x^2})Z_\ell(x) = 0$$

$$\frac{1}{2}(Z_{\ell-1}(x) - \hat{\alpha}E_{\ell+1}(x)) = Z_\ell'(x)$$

$$\frac{1}{2}(Z_{\ell-1}(x) + \hat{\alpha}Z_{\ell+1}(x)) = \frac{\ell}{x} Z_\ell(x)$$

$$Z_{-\ell}(x) = (-\hat{\alpha})^\ell Z_\ell(x).$$

(4.11)

One can write (4.7) in terms of the scale variables, (4.9), and convert the t'-integration into z'-integration using the characteristics, (4.8), as

$$f_1(z) = \frac{e}{mc} e^{-i\omega t} \int_0^z \frac{dz'}{v_\parallel} e^{i\omega \frac{z-z'}{v_\parallel}} \left\{ \left[E_\theta(z') \frac{c|\alpha_n|}{\Omega_c} \frac{\partial f_0}{\partial a} + H_r(z') \left(\frac{a_\parallel}{\gamma} \frac{\partial f_0}{\partial a_L} - \right. \right. \right.$$

$$\left. \frac{a_L}{\gamma} \frac{\partial f_0}{\partial a_\parallel} \right) \right] Z_1(x')\cos\xi' - \left[\left(E_\theta(z') \frac{c|\alpha_n|}{\Omega_c} + H_r(z') \frac{a_\parallel}{\gamma} \right) Z_1(x')\cos\chi' + \right.$$

$$\left. H_z(z') \frac{a_L}{\gamma} Z_1(x')i\sin\psi' \right] \frac{\partial f_0}{\partial a} \right\}.$$

(4.12)

Using the Graf's addition theorem of Bessel functions applied to the triangle shown in Figure 4.1 renders us

$$Z_1(x')\cos\xi' = \sum_{s=-\infty}^{\infty} \hat{\alpha}^s Z_{s+1}(a_L)Z_s(a)\cos s\psi'$$

$$= -\sum_{s=-\infty}^{\infty} \hat{\alpha}^{s+1} e^{is\psi'} Z_s'(a_L)Z_s(a)$$

(4.13)

-21-

$$Z_1(x')\cos x' = \sum_{s=-\infty}^{\infty} \hat{\alpha}^s \, Z_{s+1}(a) Z_s(a_L)\cos s\psi'$$

$$= -\sum_{s=-\infty}^{\infty} \hat{\alpha}^{s+1} e^{is\psi'} Z_s(a_L) Z_s'(a)$$

(4.13) (Cont'd)

$$Z_0(x')i\sin\psi' = \sum_{s=-\infty}^{\infty} \hat{\alpha}^s \, Z_s(a_i) Z_s(a)\cos s\psi' \, i\sin\psi'$$

$$= \sum_{s=-\infty}^{\infty} \hat{\alpha}^{s+1} e^{is\psi'} \left(Z_s'(a_L) \frac{s}{a} Z_s(a) + \frac{s}{a_L} Z_s(a_L) Z_s'(a) \right)$$

Substituting (4.13) into (4.12) and using (4.8) for ψ', one can cast (4.12) into the form

$$f_1(z) = -\frac{e}{mc} e^{-i\omega t} \sum_{s=-\infty}^{\infty} \hat{\alpha}^{s+1} e^{is\psi} \int_0^z dz' \, G(z-z') F(z')$$

(4.14)

$$G(z-z') \equiv \frac{1}{v_{\shortparallel}} e^{i(\omega - s\omega_c)\frac{z-z'}{v_{\shortparallel}}}$$

where

$$F(z') \equiv \left[E_\theta(z') \frac{c|\alpha_n|}{\Omega_c} \frac{\partial f_0}{\partial a} + H_r(z')\left(\frac{a_{\shortparallel}}{\gamma} - \frac{\partial f_0}{\partial a} - \frac{a_L}{\gamma} \frac{\partial f_0}{\partial a_{\shortparallel}} \right) \right] Z_s'(a_L) Z_s(a)$$

$$+ \left[\left(E_z(z') \frac{c|\alpha_n|}{\Omega_c} + H_r(z') \frac{a_{\shortparallel}}{\gamma} \right) Z_s(a_L) Z_s'(a) \right.$$

(4.15)

$$\left. - H_z(z') \frac{a_L}{\gamma} \left(Z_s'(a) \frac{s}{a} Z_s(a) + \frac{s}{a_L} Z_s(a_L) Z_s'(a) \right) \right] \frac{\partial f_0}{\partial a} \; .$$

The Laplace transformation of (4.15) can be readily obtained by the convolution theorem

$$\tilde{f}_1(k) = -\frac{e}{mc} e^{-i\omega t} \sum_{s=-\infty}^{\infty} \hat{\alpha}^{s+1} e^{is\psi} \tilde{G}(k)\tilde{F}(k)$$

(4.16)

-22-

where

$$\tilde{G}(k) = i \frac{\gamma}{\Omega_s(k)} \; ; \; \Omega_s(k) \equiv \omega\gamma - s\Omega_c - ku_{\parallel}$$

$$\tilde{F}(k) = \left[\tilde{E}_\theta(k) \frac{c|\alpha_n|}{\Omega_c} \frac{\partial f_0}{\partial a} + \tilde{H}_r(k) \left(\frac{a_{\parallel}}{\gamma} \frac{\partial f_0}{\partial a} - \frac{a_L}{\gamma} \frac{\partial f_0}{\partial a_{\parallel}} \right) \right] Z_s'(a_L) Z_s(a)$$

(4.17)

$$+ \left(\left[\tilde{E}_\theta(k) \frac{c|\alpha_n|}{\Omega_c} + \tilde{H}_r(k) \frac{a_{\parallel}}{\gamma} \right) Z_s(a_L) Z_s'(a) \right.$$

$$\left. - \tilde{H}_z(k) \frac{a_L}{\gamma} \left(Z_s'(a_L) \frac{s}{a} Z_s(a) + \frac{s}{a_L} Z_s(a_L) Z_s'(a) \right) \right] \frac{\partial f_0}{\partial a} \; .$$

Using the Maxwell equations (4.3) in (4.16) with (4.17), one obtains the final expression

$$\tilde{f}_1(k) = -i\tilde{E}_\theta(k) \frac{e}{mc} e^{-i\omega t} \frac{|\alpha_n|/\Omega_c}{\omega/c} \sum_{s=-\infty}^{\infty} \hat{\alpha}^{s+1} e^{is\psi}$$

$$\left\{ \frac{1}{\Omega_s(k)} \left[\omega\gamma \frac{\partial f_0}{\partial a_L} - k(u_{\parallel} \frac{\partial f_0}{\partial a_L} - u_{\perp} \frac{\partial f_0}{\partial a_{\parallel}}) \right] Z_s'(a_L) Z_s(a) \right.$$

(4.18)

$$\left. + \left[\frac{s\Omega_c}{\Omega_s(k)} \frac{a_{\parallel}}{a} Z_s'(a_L) Z_s(a) - Z_s(a_L) Z_s'(a) \right] \frac{\partial f_0}{\partial a} \right\}$$

The first term in the first bracket is from $\vec{E}_\perp$ (CMI), the second term is from $\vec{V}_\perp \times \vec{H}_\perp$ (Weibel), and the second bracket represents the effect of non-uniform plasma.

$\widetilde{J}_\theta(k)$: Induced Current

The integration in the induced current $\widetilde{J}_\theta(k)$ given by (4.5) and (4.18) requires a specific form of beam function f_0 ($u_\parallel$, $u_\perp$, R) while we still want to maintain its generality. One can do this by considering the following identity, for an arbitrary function $f_0(u_\parallel$, $u_\perp$, R);

$$f_0(u_\parallel,u_\perp,R) = du^o_\parallel \; 2\pi u^o_\perp du^o_\perp \; 2\pi R^o dR^o f_0(u^o_\parallel,u^o_\perp,R^o)\hat{f}(u_\parallel,u_\perp,R) \quad (4.19)$$

where

$$\hat{f}_0(u_\parallel,u_\perp,R) \equiv F_1(u_\parallel,u_\perp)F_2(R)$$

$$F_1(u_\parallel,u_\perp) \equiv \delta(u_\parallel-u^o_\parallel)\;\frac{1}{2\pi u_\perp}\;\delta(u_\perp-u^o_\perp) \quad (4.20)$$

$$F_2(R) \equiv \frac{1}{2\pi R^o}\;\delta(R-R^o).$$

Observe that the "δ-distribution" function $\hat{f}_0$ represents a "cold" beam with infinitely "thin" guiding center distribution and is normalized to be one electron per unit length. Equation (4.19) merely shows that an arbitrary beam function $f_0(u_\parallel$, $u_\perp$, R) can be constructed out of "δ-distribution" function $\hat{f}_0$ with the "weight" function $f_0(u^o_\parallel$, $u^o_\perp$, R^o) which contains all the information on the beam spread. The main advantage of using such a representation is that it allows us to carry out the required integration in (4.5) without introducing any specific assumption on the beam function f_0.

With (4.19), one can write (4.5) with (4.18) as

$$\widetilde{J}_\theta(R) = \int du^o_\parallel \; 2\pi u^o_\perp du^o_\perp \; 2\pi R^o dR^o \; f_0(u^o_\parallel,u^o_\perp,R^o)\;\hat{J}_\theta(k) \quad (4.21)$$

where

$$\hat{J}_\theta(k) \equiv i\tilde{E}_\theta(k) \frac{Ne^2}{mc} e^{-i\omega t} \frac{1}{\omega/c} \sum_{s=-\infty}^{\infty} \hat{\alpha}^{s+1} \int d^3 u \frac{a_L}{\gamma} \cos\xi e^{is\psi}$$

$$\left\{ \frac{1}{\Omega_s(k)} \left[\omega\gamma \frac{\partial F_1}{\partial a_L} - k\left(u_{\shortparallel} \frac{\partial F_1}{\partial a_L} - u_\perp \frac{\partial F_1}{\partial a_\shortparallel}\right)\right] F_2 Z_s'(a_L) Z_s(a) \right.$$

$$\left. + \left[\frac{s\Omega_c}{\Omega_s(k)} \frac{a_L}{a} Z_s'(a_L)Z_s(a) - Z_s(a_L)Z_s'(a)\right] F_1 \frac{\partial F_2}{\partial a} \right\}$$

(4.22)

represents the induced current for the "δ-distribution" function.
Recalling the relation, $R = (r^2 + r_L^2 - 2rr_L \cos\xi)^{1/2}$, and thus
$\partial R/\partial \xi = 1/R \ rr_L \sin\xi$, one can write

$$F_2(R) = \frac{1}{2\pi r} \frac{\delta(\xi-\xi_0) + \delta(\xi+\xi_0)}{r_L \sin\xi_0} \Delta(r;r_{\pm})$$

$$\left(\cos\xi_0 \equiv \frac{r^2+r_L^2-R_0^2}{2rr_L}; \quad o \le \xi_0 \le \pi\right)$$

(4.23)

where "step" function $\Delta(r; r_{\pm})$ is defined by

$$\Delta(r;r_{\pm}) \equiv \begin{cases} 1 & \text{if } r_- \le r \le r_+ \\ 0 & \text{otherwise} \end{cases}$$

(4.24)

$$(r_{\pm} \equiv R_0 \pm r_L)$$

In terms of the scale variables, (4.9), one can write (4.22) with (4.20) and
(4.23) as

$$\hat{J}_\theta(k) = i\tilde{E}_\theta(k) \; \frac{e^{-i\omega t}}{\omega/c} \; \frac{Ne^2}{mc} \; \frac{|\alpha_n|}{2\pi r} \; \frac{1}{2\pi r_L} \sum_{s=-\infty}^{\infty} \hat{\alpha}^{s+1} \int da_{\shortparallel} \; da_L \, d\xi \; \frac{a_L^2}{\gamma} \cos\xi e^{is\psi}$$

$$\left\{ \frac{1}{\Omega_s(k)} \left[\omega\gamma \frac{\partial\hat{F}_1}{\partial a_L} - k\left(u_{\shortparallel} \cdot \frac{\partial\hat{F}_1}{\partial a_L} - u_\perp \frac{\partial\hat{F}_1}{\partial a_{\shortparallel}} \right) \right] Z_s'(a_L) Z_s(a) \hat{F}_2 \right. \tag{4.25}$$

$$\left. + \left[\frac{s\Omega c}{\Omega_s(k)} \frac{a_L}{a} Z_s'(a_L) Z_s(a) - \;^\cdot Z_s(a_L) Z_s'(a) \right] \hat{F}_1 \; \frac{\partial\hat{F}_2}{\partial a} \right\}$$

where

$$\hat{F}_1 \equiv \delta(a_{\shortparallel} - a_{\shortparallel}^o) \delta(a_L - a_L^o)$$

$$\hat{F}_2 \equiv \frac{\delta(\xi-\xi_0) + \delta(\xi+\xi_0)}{a_L \sin\xi_0} \Delta(x; x_\pm) \tag{4.26}$$

$$(x_\pm \equiv a_0 \pm a_L)$$

Defining velocity angle integrals,

$$\Phi_s \equiv \int_{-\pi}^{\pi} d\xi \cos\xi \, e^{is\psi} Z_s(a)\hat{F}_2$$

$$\Psi_{s\pm 1} \equiv \int_{-\pi}^{\pi} d\xi \cos\xi \, e^{is\psi} Z_{s\pm 1}(a) \; \frac{\partial\hat{F}_2}{\partial a} \tag{4.27}$$

$$\Psi_s^{\pm} \equiv \tfrac{1}{2}(\Psi_{s-1} \pm \hat{\alpha}\Psi_{s+1})$$

One can write (4.25) as,

$$\hat{J}_\theta(k) = i\tilde{E}_\theta(k) \; \frac{e^{-i\omega t}}{\omega/c} \; \frac{Ne^2}{mc} \; \frac{|\alpha_n|}{2\pi r} \; \frac{1}{2\pi a} \sum_{s=-\infty}^{\infty} \hat{\alpha}^{s+1} \int da_{\shortparallel} \; da_L \; \frac{a_L^2}{\gamma}$$

$$\left\{ \frac{1}{\Omega_s(k)} \left[\omega\gamma \frac{\partial\hat{F}_1}{\partial a_L} - k(u_{\shortparallel} \frac{\partial\hat{F}_1}{\partial a_L} - u_\perp \frac{\partial\hat{F}_1}{\partial a_{\shortparallel}}) \right] Z_s'(a_L) \; \Phi_s \right. \tag{4.28}$$

$$+ \left[\frac{\Omega_c}{\Omega_s(k)} a_L Z_s'(a_L) \Psi_s^+ - Z_s(a_L) \Psi_s^- \right] \hat{F}_1 \Bigg\}$$

$$\Phi = Z_s(a_0) C_s^0$$

The integrals in (4.27) are calculated in Appendix to give,

$$\Psi_{s\pm 1} = \begin{Bmatrix} -1 \\ \hat{\alpha} \end{Bmatrix} Z_s(a_0) C_s^0 + Z_{s\pm 1}(a_0) \left[\frac{\partial}{\partial a_L} C_{s\pm 1}^0 \pm \frac{s+1}{a_L} C_{s\pm 1}^0 \pm \frac{1}{a_L} S_{s\pm 1}^0 \right]$$

$$(4.29)$$

where

$$C_s^0 = \frac{2\cos\xi_0}{a_L \sin\xi_0} \cos s\psi \; \Delta \; (x;x\underline{+})$$

$$(4.30)$$

$$S_s^0 = \frac{2}{a_L} \sin s\psi \; \Delta \; (x;x\underline{+})$$

The remaining integrations in (4.28) are trivial with $\hat{F}_1$ given by (4.26):

$$\hat{J}_\theta(k) = -i\tilde{E}_\theta(k) \frac{e^{-i\omega t}}{\omega/c} \frac{Ne^2}{mc} \frac{|\alpha_n|}{2\pi r} \frac{1}{2\pi a_L} \sum_{s=-\infty}^{\infty} \hat{\alpha}^{s+1}$$

$$\Bigg\{ \left[\omega \frac{\partial}{\partial a_L} - \frac{k}{\gamma_0} \left(u_\parallel^0 \frac{\partial}{\partial a_L^0} - u_\perp^0 \frac{\partial}{\partial a_\parallel^0} \right) \right] \left(\frac{a_L^{02}}{\Omega_s^0(k)} Z_s'(a_L) \Phi_s^0 \right)$$

$$(4.31)$$

$$- \frac{a_L^2}{\gamma_0} \left[\frac{\Omega_c}{\Omega_s^0(k)} a_L Z_s'(a_L) \Psi_s^{0+} - Z_s(a_i) \Psi_s^{0+} \right] \Bigg\}$$

where the superscript o ensures that the quantities are evaluated at $u_{\parallel} = u_{\parallel}^0$ and $u_{\perp} = u_{\perp}^0$. One can still trace back to the origins of the terms in (4.31); the first term is from $\vec{E}_{\perp}$-force (CMI). The second term is from $\vec{v}_{\perp} \times \vec{H}_{\perp}$ (Weibel), and the last term is due to the non-uniformity of (electron) plasma.

Lastly, one can observe that the induced current $\tilde{J}_{\theta}(k)$ can be put into the form

$$\tilde{J}_{\theta}(k) = \tilde{\sigma}(k)\tilde{E}_{\theta}(k) \tag{4.32}$$

where dynamical conductivity of the electron beam $\tilde{\sigma}(k)$ can be immediately read off from (4.21) and (4.31).

$\tilde{P}_n(k)$: Source Term

Substituting (4.21) into (4.4) one can write

$$\tilde{P}_n(k) = \int du_{\parallel}^0 \ 2\pi u_{\perp}^0 du_{\perp}^0 \ 2\pi R^0 \ dR^0 \ f_0(u_{\parallel}^0, u_{\perp}^0, R^0)\hat{P}_n(k) \tag{4.33}$$

where

$$\hat{P}_n(k) = i \ \frac{\omega}{c} \ e^{i\omega t} \ \frac{4\pi}{c} \ \frac{1}{C_N} \int 2\pi r \ dr \ Z_1(|\alpha_n|r)\hat{J}_{\theta}(k) \tag{4.34}$$

and $\tilde{J}_{\theta}(k)$ is given by (4.31) with (4.29) and (4.30).

Define $\langle A \rangle$ for an $A(x)$ as

$$\langle A \rangle \equiv \frac{\hat{\alpha}^{s+1}}{2\pi} \int dx Z_1(x)A(x) \tag{4.35}$$

and one can write (4.34) as

$$\hat{P}_n(k) = \hat{E}_{\theta}(k) \ \frac{4\pi\nu}{C_N} \ \frac{1}{a_L} \sum_{s=-\infty}^{\infty} \tag{4.36}$$

$$\left\{ \left[\omega\frac{\partial}{\partial a_L} - \frac{k}{\gamma_0}\left(u_{\parallel}^0 \ \frac{\partial}{\partial a_L} - u_{\perp}^0\frac{\partial}{\partial a_{\parallel}^0}\right)\right]\left(\frac{a_L^2}{\Omega_s(k)} Z_s'(a_L) \langle \Phi_s^0 \rangle\right)\right.$$

$$\left. - \frac{a_L^2}{\gamma_0}\left[\frac{\Omega_c}{\Omega_s(k)} \ a_L Z_s'(a_L) \langle \Psi_s^{0+} \rangle - Z_s(a_L) \langle \Psi_s^{0-} \rangle\right]\right\}$$

-28-

where

$$\nu \equiv \frac{Ne^2}{mc^2}$$ (4.37)

is the Budker parameter.

In the Appendix, we have calculated

$$<\Phi_s^0> = -Z_s'(a_L)Z_s^2(a_0)$$

$$<\Psi_s^{0+}> = Z_s'(a_L) \frac{s}{a_0} \left(Z_s^2(a_0)\right)'$$ (4.38)

$$<\Psi_s^{0-}> = Z_s'(a_L)[Z_s'^2(a_0) - (\hat{\alpha} - \frac{s^2}{a_0^2})Z_s^2(a_0)]$$

and therefore

$$\tilde{P}_n(k) = \tilde{E}_\theta(k) \frac{4\pi\nu}{C_N} \frac{1}{\gamma_0 a_L} \sum_{s=-\infty}^{\infty}$$

$$\left\{ \left[\omega \frac{\partial}{\partial a_L} - k\left(u_\parallel^0 \frac{\partial}{\partial a_L} - u_\perp^0 \frac{\partial}{\partial a_\parallel^0}\right)\right] \left(\frac{a_L^2}{\Omega_s(k)}Z_s'^2(a_L)\right)Z_s^2(a_0) \right.$$ (4.39)

$$- a_L^2 \left[\frac{s\Omega_c}{\Omega_s^0(k)} \frac{a_L}{a_0} Z_s'^2(a_L)\left(Z_s^2(a_0)\right)' - \frac{1}{2}\left(Z_s^2(a_L)\right)'\left(Z_s'^2(a_L)\right.\right.$$

$$\left.\left.- (\hat{\alpha} - \frac{s^2}{a_0^2})Z_s^2(a_0)\right)\right] \right\} .$$

-29-

It is now straightforward to carry out the differentiation recalling that $\Omega_s^0 = \omega\gamma_0 - ku_{\shortparallel}^0 - s\Omega_c$ and $Z_s''(x) + 1/x\, Z_s'(x) + (\hat\alpha - s^2/x^2)\, Z_s(x) = 0$ and one can finally obtain

$$\hat{P}_n(k) = \hat{E}_\theta(k)\, \frac{4\pi\nu}{C_N}\, \frac{a_L^0}{\gamma_0} \sum_{s=-\infty}^{\infty} \left\{ \frac{\Omega_c^2}{\Omega_s^{02}(k)} \frac{\frac{\omega^2}{c^2} - k^2}{|\alpha_n|^2}\, a_L^0 Z_s'^2(a_L^0) Z_s^2(a_0) \right.$$

$$+ \left(\frac{s\Omega_c}{\Omega_s^0(k)} + 1 \right) \left(\hat\alpha^0 - \frac{s^2}{a_L^{02}} \right) \left(Z_s^2(a_L^0) \right)' Z_s^2(a_0)$$

$$- \frac{s\Omega_c}{\Omega_s^0(k)} \frac{a_L^0}{a_0} \left(Z_s'^2(a_L^0)\, Z_s^2(a_0) \right)'$$

$$\left. + \tfrac{1}{2} \left(Z_s^2(a_L^0) \right)' \left(Z_s'^2(a_0) - (\hat\alpha - \frac{s^2}{a_0^2}) Z_s^2(a_0) \right) \right\}$$

(4.40)

With (4.33) and (4.40), one can now solve (4.3) as

$$\dot{E}_\theta(k) = \frac{-\frac{dE_\theta}{dz}(o)}{k^2 - k_n^2 - \tilde{S}_n(k)}$$

(4.41)

where

$$\tilde{S}_n(k) = \int du_{\shortparallel}^0\ 2\pi u_\perp^0 du_\perp^0\ 2\pi R^0 dR^0\ f_0(u_{\shortparallel}^0, u_\perp^0, R^0) \hat{S}_n(k)$$

(4.42)

and

$$\hat{S}_n(k) = \sum_{s=-\infty}^{\infty} \left\{ \frac{\Omega_c^2}{\Omega_s^{02}(k)} \frac{\frac{\omega^2}{c^2} - k^2}{|\alpha_n|^2}\, Q_2 + \frac{\Omega_c}{\Omega_s^0(k)}\, Q_1 + Q_0 \right\}$$

(4.43)

$$(\Omega_s^0(k) \equiv \omega\gamma_0 - s\Omega_c - ku_{\shortparallel}^0)$$

-30-

where

$$Q_2 \equiv \frac{4\pi\nu}{C_N} \frac{a_L}{\gamma_0} \cdot a_L Z_s'^2(a_L) Z_s^2(a_0)$$

$$Q_1 \equiv \frac{4\pi\nu}{C_N} \frac{a_L}{\gamma_0} \cdot S\left[(\hat{\alpha} - \frac{s^2}{a_L^2}) \left(Z_s^2(a_L)\right)' Z_s^2(a_0) - \frac{a_L}{a_0} Z_s'^2(a_L)\left(Z_s^2(a_0)\right)' \right]$$

$$Q_0 \equiv \frac{4\pi\nu}{C_N} \frac{a_L}{\gamma_0} \left(Z_s^2(a_L)\right)' \left[(\hat{\alpha} - \frac{s^2}{a_L^2}) Z_s^2(a_0) \right.$$

$$\left. + \tfrac{1}{2}\left(Z_s'^2(a_0) - (\hat{\alpha} - \frac{s^2}{a_0^2}) Z_s^2(a_0)\right) \right]$$

(4.44)

Lastly, the normalization constant C_N defined by (3.16) can be easily calculated to be

$$C_N \equiv \sum_{i=1}^{N} C_N^{(i)}$$

(4.45a)

where

$$C_N^{(i)} \equiv \int_{r_{i-1}}^{r_i} 2\pi r \, dr \left(A_i Z_1(|\alpha_n^i|r) + \overline{A}_i \overline{Z}_1(|\alpha_n^i|r) \right)^2$$

(4.45b)

$$= \begin{cases} \tfrac{1}{2}(|\alpha_n^i|r)^2 \left[\left(A_i Z_1(|\alpha_n^i|r) + \overline{A}_i \overline{Z}_1(|\alpha_n^i|r)\right)^2 \right. \\ \\ \left. - \left(A_i Z_0(|\alpha_n^i|r) + \overline{A}_i \overline{Z}_0(|\alpha_n^i|r)\right)\left(A_i Z_2(|\alpha_n^i|r) + \overline{A}_i \overline{Z}_2(|\alpha_n^i|r)\right) \right]_{r_{i-1}}^{r_i} \\ \\ \qquad\qquad\qquad\qquad\qquad : \text{ if } \alpha_n^{i^2} > 0 \\ \\ \tfrac{1}{2}(|\alpha_n^i|r)^2 \left[\left(A_i Z_1(|\alpha_n^i|r) + \overline{A}_i \overline{Z}_1(|\alpha_n^i|r)\right)^2 \right. \\ \\ \left. - \left(A_i Z_0(|\alpha_n^i|r) - \overline{A}_i \overline{Z}_0(|\alpha_n^i|r)\right)\left(A_i Z_2(|\alpha_n^i|r) - \overline{A}_i \overline{Z}_2(|\alpha_n^i|r)\right) \right]_{r_{i-1}}^{r_i} \\ \\ \qquad\qquad\qquad\qquad\qquad \text{ if } \alpha_n^{i^2} < 0 \end{cases}$$

Beam Spread Effect

Now let us consider the effect of beam spreads (velocity spread and guiding center spreads) in (4.42). In practice, the velocity spreads are non-thermal; mainly determined by the imperfact cathode surface, space charge effects, and electron optics from the acceleration stage to the beginning of the interaction region. The spreads in guiding centers are mainly determined by the finite size of electron emitting strips in addition to the same causes of velocity spread. The resulting distribution is close to the "water-bed" shape rather than Maxwellian. The water-bed shape distribution function may be best represented by a generalized Lorentzian distribution function:

$$F_p(x;\delta) \equiv \frac{C_p \, \delta^{2p}}{(x-\bar{x})^{2p} + \delta^{2p}} \tag{4.46}$$

where C_p is a normalization factor. When $p = 1$, (4.46) reduces to the standard Lorentzian distribution and the higher value of p gives the flatter shape. In the limit $p \to \infty$, (4.46) represents "box" distribution. Choosing x as $u_\parallel^0$, $u_\perp^0$ or R^0 with an appropriate p and δ, one can construct realistic distribution functions. The beam spread effect of the type (4.42) can be done analytically by contour integrals.

From the structure of (4.42) and (4.43), one can immediately see that the most sensitive one is the parallel velocity spread in $u_\parallel^0$ through the resonance denominator, $\Omega_s^0 = \omega \gamma_0 - k u_\parallel^0 - s\Omega c$. It is worth noting at this point that the Laplace transformation variable k which was introduced by (4.1) is a complex variable with sufficiently large negative in k to guarantee that the Laplace transformation (4.1) well-defined, and, therefore, the integral of (4.42) is well-defined.

In this paper, we will demonstrate the technique for the parallel velocity spread function,

$$f_0(u_{||}^0) = F_p(u_{||}^0 \; ; \; \Delta u_{||}) \equiv \frac{C_p \; \Delta u^{2p}}{(u_{||}^0 - \bar{u}_{||})^{2p} + \Delta u_{||}^{2p}}$$

$$1 = \int_{-\infty}^{\infty} du_{||}^0 \; F_2(u_{||}^0 \; ; \; \Delta u_{||})$$

(4.47)

where the normalization constant C_p is defined by

Then, the integral (4.42) can be written as

$$\tilde{S}_n(k) = \int_{-\infty}^{\infty} du_{||}^0 \; F_p(u_{||}^0 \; ; \; \Delta u_{||}) \hat{S}_n(k; u_{||}^0)$$

(4.48)

By writing (4.40) as

$$f_0 = \frac{C_p}{\zeta^{2p} + 1} \; ; \; \zeta \equiv \frac{u_{||}^0 - \bar{u}_{||}}{\Delta u_{||}}$$

(4.49)

One can identify that f_0 has poles at

$$\begin{cases} \zeta_k \equiv e^{i\pi \frac{2k+1}{p}} : & \text{in the upper-half } \zeta\text{-plane} \\ \\ \zeta_k^* \equiv e^{-i\pi \frac{2k+1}{p}} : & \text{in the lower-half } \zeta\text{-plane} \end{cases}$$

(4.50)

$$(k=0,1,\ldots, p-1)$$

Closing the contour in (4.47) by an upper-half circle or a lower-half circle, one can determine normalization constant C_p by

$$-C_p \frac{\Delta u_{||}}{2p} 2\pi i = \frac{1}{\sum\limits_{k=0}^{p-1} \zeta_k}$$

(4.51a)

or,

$$C_p \frac{\Delta u_{||}}{2p} 2\pi i = \frac{1}{\sum\limits_{k=0}^{p-1} \zeta_k^*}$$

(4.51b)

From (A.5), one can immediately obtain

$$<\Phi_s> = Z_s(a_0)<C_s^0> = -Z_s^2(a_0)Z_s'(a_L)$$

(A.15)

and from (A.9),

(A.16)

$$<\Psi_{s-1}> = \hat{\alpha}Z_s(a_0)<C_s^0> + Z_{s-1}(a_0)\,\frac{\partial}{\partial a_L}<C_{s-1}^0> - \frac{s-1}{a_L}<C_{s-1}^0> - \frac{1}{a_L}<S_{s-1}^0>$$

Using the Bessel equation, $Z_\ell''(x) + 1/x\,Z_\ell'(x) + (\hat{\alpha} - \ell^2/x^2)\,Z_\ell(x) = 0$, and the recursion formula, $Z_\ell'(x) - \ell/x\,Z_\ell(x) = -2\,Z_{\ell+1}(x)$, it is straightforward to simplify (A.16) as

$$<\Psi_{s-1}> = \left(-\hat{\alpha}Z_s^2(a_0) + Z_{s-1}^2(a_0)\right)Z_s'(a_L)$$

(A.17)

Similarily,

$$<\Psi_{s+1}> = \left(Z_s^2(a_0) - \hat{\alpha}Z_{s+1}^2(a_0)\right)Z_s'(a_L)$$

(A.18)

Then, from (A.17) and (A.18), one obtains

$$<\Psi_s^-> \equiv \tfrac{1}{2}\left(<\Psi_{s-1}> - \hat{\alpha}<\Psi_{s+1}>\right)$$

$$= \left[-\hat{\alpha}Z_s^2(a_0) + \tfrac{1}{2}\left(Z_{s-1}^2(a_0) + Z_{s+1}^2(a_0)\right)\right]Z_s'(a_L)$$

(A.19)

$$= \left[Z_s'^{\,2}(a_0) - (\hat{\alpha} - \frac{s^2}{a_0^2})Z_s^2(a_0)\right]Z_s'(a_L)$$

and

$$<\Psi_s^+> \equiv \tfrac{1}{2}\left(<\Psi_{s-1}> + \hat{\alpha}<\Psi_{s+1}>\right)$$

$$= \tfrac{1}{2}\left(Z_{s-1}^2(a_0) - Z_{s+1}^2(a_0)\right)Z_s'(a_L)$$

(A.20)

$$= \frac{s}{a_0}\left(Z_s^2(a_0)\right)'Z_s'(a_L)$$

A-4

Using the recursion formulas $Z_\ell(x) - \ell/x \, Z_\ell(x) = -\hat{\alpha} Z_{\ell+1}(x)$ and (A.7), it is straightforward to obtain from (A.8),

$$\Psi_{s-1} = \hat{\alpha} Z_s(a_0) C_s^0 + Z_{s-1}(a_0)\left(\frac{\partial}{\partial a_L} C_{s-1}^0 - \frac{s-1}{a_L} C_{s-1}^0 - \frac{1}{a_L} S_{s-1}^0\right) \qquad (A.9)$$

Similarly,

$$\Psi_{s+1} = -Z_s(a_0) C_s^0 + Z_{s+1}(a_0)\left(\frac{\partial}{\partial a_L} C_{s+1}^0 + \frac{s+1}{a_L} C_{s+1}^0 + \frac{1}{a_L} S_{s+1}^0\right) \qquad (A.10)$$

Radial Integration

Define a radial integration for a function $A(x)$, that

$$\langle A \rangle \equiv \frac{\hat{\alpha}^{s+1}}{2\pi} \int dx \, Z_1(x) A(x) \qquad (A.11)$$

Then, noting that from $x = (a_0^2 + a_L^2 - 2a_0 a_L \cos\psi_0)^{1/2}$, $dx = 1/x \, a_0 a_L \sin\psi_0 \, d\psi_0 = a_L \sin\xi_0 \, d\psi_0$, one can write the radial integration of C_s^0 given by (A.4)

$$\langle C_s^0 \rangle = \frac{\hat{\alpha}^{s+1}}{2\pi} \int_{x_-}^{x_+} d\psi_0 \, 2\cos\xi_0 Z_1(x)\cos s\psi_0 \qquad (A.12)$$

Applying Graf's addition theorem and (A.5), one obtains

$$\langle C_s^0 \rangle = \frac{\hat{\alpha}^{s+1}}{2\pi} \sum_{s'=-\infty}^{\infty} \hat{\alpha}^{s'} Z_{s'+1}(a_L) Z_{s'}(a_0) \int_0^\pi d\psi_0 \, 2\bar{\cos} s'\psi_0 \cos s\psi_0$$

$$= -Z_s(a_0) Z'_s(a_L) \qquad (A.13)$$

Similarly,

$$\langle S_s^0 \rangle = \frac{\hat{\alpha}^{s+1}}{2\pi} \int_{x_-}^{x_+} d\psi_0 \, 2\sin\xi_0 \, Z_1(x)\sin s\psi_0 \qquad (A.14)$$

$$= Z_s(a_0) \frac{s}{a_L} Z_s(a_L)$$

A-3

where

$$C_s^o \equiv \frac{2\cos\xi_0}{a_L \sin\xi_0} \cos s\psi_0 \cdot \Delta$$

(A.4)

$$S_s^o \equiv \frac{2}{a_L} \sin s\psi_0 \cdot \Delta$$

Using the above relations and Graf's addition theorem, one can easily show that

$$\Phi_s \equiv \int_{-\pi}^{\pi} d\xi \cos\xi \, e^{is\psi} Z_s(a)\overline{F}_2$$

$$= \sum_{s'=-\infty}^{\infty} \hat{\alpha}^{s'} Z_{s'+s}(a_L) Z_{s'}(x) C_{s'}$$

(A.5)

$$= Z_s(a_0) C_s^o$$

Consider

$$\Psi_{s-1} \equiv \int_{-\pi}^{\pi} d\xi \cos\xi \, e^{is\psi} Z_{s-1}(a) \frac{\partial \overline{F}_2}{\partial a}$$

(A.6)

$$= \int_{-\pi}^{\pi} d\xi \cos\xi \, e^{i(s-1)\psi} Z_{s-1}(a) \cdot e^{i\psi} \frac{\partial F_2}{\partial a}$$

From $a = (x^2 + a_L^2 - 2xa_L \text{ as } \xi)^{1/2}$, $\partial a/\partial a_L = \sin\psi$ and $1/a_L \, \partial a/\partial\xi = \sin\psi$, one obtains

$$e^{i\psi} \frac{\partial \overline{F}_2}{\partial a} = \frac{\partial \overline{F}_2}{\partial a_L} + \frac{i}{a_L} \frac{\partial \overline{F}_2}{\partial\xi}$$

(A.7)

Using (A.7) and the Graf's addition theorem, one can write (A.6) as

$$\Psi_{s-1} = \sum_{s'=-\infty}^{\infty} \hat{\alpha}^{s'} Z_{s'+s-1}(a_L) Z_{s'}(x) \left(\frac{\partial C_{s'}}{\partial a_L} + \frac{s'}{a_L} C_{s'} - \frac{1}{a_L} S_{s'} \right)$$

(A.8)

A-2

Velocity Angle Integrations

For the velocity-angle distribution function

$$\bar{F}_2 = \frac{\delta(\xi-\xi_0) + \delta(\xi+\xi_0)}{a_L \sin\xi_0} \Delta(x;x_{\underline{+}}) \tag{A.1}$$

where

$$\cos\xi_0 \equiv \frac{x^2+a_L^2-a_0^2}{2xa_L} \quad (0 \le \xi_0 \le \pi)$$

define

$$C_{s'} = \int_{-\pi}^{\pi} d\xi \, \cos\xi \, e^{is'\xi} \, \bar{F}_2$$

$$= \frac{2\cos\xi_0}{a_L \sin\xi_0} \cos s'\xi_0 \cdot \Delta$$

$$\tag{A.2}$$

$$S_{s'} \equiv \int_{-\pi}^{\pi} d\xi \, \frac{1}{i} \sin\xi \, e^{is'\xi} \bar{F}_2$$

$$= \frac{2}{a_L} \sin s'\xi_0 \cdot \Delta$$

Using Graf's addition theorem of Bessel function, one obtains the following identities:

$$\sum_{s'=-\infty}^{\infty} \hat{\alpha}^{s'} Z_{s'+s}(a_L) Z_{s'}(x) C_{s'} = Z_s(a_0) C_s^0$$

$$\tag{A.3}$$

$$\sum_{s'=-\infty}^{\infty} \hat{\alpha}^{s'} Z_{s'+s}(a_L) Z_{s'}(x) S_{s'} = Z_s(a_0) S_s^0$$

REFERENCES

1. J. L. Hirshfield and V. L. Granatstein, "The Electron Cyclotron
   Maser - A Historical Survey," IEEE, Trans. MTT-25, 522-527 (1977).

   V. A. Flyagin, A. V. Gaponov, M. I. Petelin, and V. K. Yulpatov,
   "The Gyrotron," IEEE Trans. MTT-25, 514-521 (1977).

   R. S. Symons and H. R. Jory, "Cyclotron Resonance Devices," Advances
   in Electronics and Electron Physics, Vol. 55, 1-75 (1981).

2. R. Q. Twiss, "Radiation Transfer and the Possibility of Negative
   Absorption in Radio Astronomy," Australian J. Phys. 11, 564-579 (1958).

   J. Schneider, "Stimulated Emission of Radiation by Relativistic Elec-
   trons in Magnetic Field," Phys. Rev. Lett. 2, 504-505 (1959).

   P. A. Sprangle and A. T. Drobot, "The Linear and Self Consistent Non-
   linear Theory of the Electron Cyclotron Maser Instability," IEEE Trans.
   MTT-25, 528-544 (1977).

   K. R. Chu, "Theory of Electron Cyclotron Maser Interaction in a Cavity
   at the Harmonic Frequencies," Phys. of Fluids 21, 2354-2364 (1978).

3. E. S. Weibel, "Spontaneously Growing Transverse Waves in a Plasma Due
   to an Anisotropic Velocity Distribution," Phys. Rev. Lett. 2, 83 (1959).

   K. R. Chu, P. A. Sprangle, and V. L. Granatstein, "Theory of a Dielectric
   Loaded Cyclotron Traveling Wave Amplifier," Bull. Am. Phys. Soc. 23,
   748 (1978).

   H. S. Uhn, J. Y. Choe, and S. Ahn, "Theory of Gyrotron in a Waveguide
   with Inner Dielectric Material," Int. J. Electronics, Special Issue on
   Gyrotrons (Oct 1981).

4. K. R. Chu and J. L. Hirshfield, "Comparative Study of Axial and Azimuthal
   Bunching Mechanism in Electromagnetic Cyclotron Instabilities," Phys.
   of Fluids 21, 461-466 (1978).

5. D. E. Baldwin, I. B. Bernstein, and M. P. H. Weenink, in Advances in
   Plasma Physics (Interscience, New York, 1969), Vol 3, p. 1.

6. S. Y. Park, J. M. Baird, and J. L. Hirshfield, "General Theory of
   Cylindrical Waveguide Loaded with Multilayer Dielectric," Bull. Am.
   Phys. Soc. 25, 910 (1980) and in B-K Dynamics Technical Report
   (N00173-79-C-0447) for NRL.

The effect of velocity spreads and the spreads in the guiding center of the beam are analyzed for generalized Lorentzian distribution which we believe represents more accurately the realistic situations. We have shown that the case of two waveguide modes and two beam modes applies to a "cold" beam or a standard Lorentzian distribution. A more realistic beam would require a generalized Lorentzian distribution which gives multiple beam modes and, in the limiting case of a box-shaped distribution, the number of beam modes will be infinitely many, all clustered on a branch cut.

The loss due to a dielectric layer and an imperfectly conducting wall is easy to take into account and is briefly mentioned in the text.

VI. DISCUSSION

In this paper, we have presented a careful analysis of the gyrotron-type
amplifier. The theory is based upon linearized Vlasov-Maxwell equations
in a strong guiding magnetic field. The space charge effect is neglected
and possible absolute instabilities are assumed to be absent. Then the
theory can be cast into a two-dimensional (axial and radial direction)
boundary value problem in the case of azimuthal symmetry. The dynamical
growth of the electron states and the electromagnetic fields along the
interaction tube is analyzed by Laplace transformation rather than Fourier
transformation as often found in earlier works. Fourier analysis, in the
case of instabilities such as the amplifiers (also oscillators), is not
only ill-defined, but also makes no connection to the boundary conditions.
In contrast, Laplace transformation is well-defined, even in the case of
strong instabilities, and also allows us to make a connection to the bound-
ary values. This way we can make definite determination of all the modes
(waveguide modes and beam modes) in terms of boundary values (input coupling
to the signal).

We have tried to carefully separate out TE_{on}-modes, noting exactly how TE
and TM modes could couple and how the different radial modes mix each
other. Analysis on the TM-modes will be presented elsewhere and the mixing
of the radial modes would be more interesting in the case of an azimuthally
non-symmetric situation such as the case of whistler modes. One important
technical feature of the analysis of a microwave device is that the electron
beam has a finite geometry which prevents the use of plasma theory for an
unbounded uniform plasma. The finite geometry of the electron beam introduces
an extra term which we have carefully identified. This term is important in
the determination of bandwidth, etc.

-41-

The loss due to the dielectrics and the finite conductivity of the wall can be easily taken into account by considering a complex dielectric constant $\epsilon = \epsilon' + i\epsilon''$. (Note that a conducting wall can also be considered as a dielectric layer with a large imaginary dielectic constant.)

can concentrate the z-dependency alone. With the radial function $A(r)$ which is a common factor, one obtains the power flow

$$S_z = - \frac{c}{8\pi} \, Re\left(\frac{i}{\omega/c} E_\theta^*(z) \, \frac{dE_\theta(z)}{dz}\right) A(r) \tag{5.10}$$

where $E_\theta(z)$ is given by (5.6). Separating the power flow inward (Re k<0) and outward (Re k>0), one obtains (5.11)

$$P_+(z) \equiv - \frac{c}{8\pi} \frac{A(r)}{\omega/c} \left|\frac{dE_\theta}{dz}(o)\right|^2 Re\left[\left(\sum_{Re k_i > 0} e^{-ik_i^* z} \frac{N^*(k_i)}{D'^*(k_i)}\right)\left(\sum_{Re k_i > 0} k_i \, e^{ik_i z} \frac{N(k_i)}{D'(k_i)}\right)\right]$$

$$P_-(k) \quad - \frac{c}{8\pi} \frac{A(r)}{\omega/c} \left|\frac{dE}{dz}(o)\right|^2 Re\left[\left(\sum_{Re k_i < 0} e^{-ik_i^* z} \frac{N^*(k_i)}{D'^*(k_i)}\right)\left(\sum_{Re k_i < 0} k_i e^{ik_i z} \frac{N(k_i)}{D'(k_i)}\right)\right]$$

In case 1) where the input signal is introduced at the gun end (z=0), the gain for the tube length L is given by

$$G(dB) = 10 \, \log_{10}\left(P_+(L)/P_+(o)\right) \tag{5.12}$$

and in case 2) where the input signal is introduced from the output pot, the gain is given by

$$G(dB) = 10 \, \log_{10}\left(P_+(L)/P_-(L)\right) \tag{5.13}$$

In general, these two methods of input signal coupling give nearly the same result when the loss is small, since the coupling of backward traveling waves to the electron beam is small in most amplifier applications. However, when a certain loss is introduced into the tube (either for stable operation or due to the dielectric and wall loss), method 2) suffers a substantial loss and method 1) would be preferred.

It is also interesting to notice that, since (5.6) with (5.4) must satisfy the boundary conditions at z=0, $E_\theta|_{z=0} = 0$ and $dE_\theta/dz|_{z=0} = dE_\theta/dz$ (0), one obtains sum rules.

$$\sum_{i=1}^{4} \frac{N(k_i)}{D'(k_i)} = 0$$

$$\sum_{i=1}^{4} k_i \frac{N(k_i)}{D'(k_i)} = 1$$

(5.8)

Power Flow and Gain

Having determined the fields as a function of z by (5.6) and (5.7), it is easy to calculate the gain of the amplifier. The gain is defined by the ratio of the output power to the input power and thus requires calculation of the power flow into the system (backward wave) and out of the system (forward wave).

Depending on the method of introduction of input signal, we consider two different cases: 1) the input signal is introduced at the gun end (z=0) and, 2) the signal is introduced from the output port (z=L) through a circulator.

The first step to calculate the gain is to calculate the power flow inward and the one outward. Consider the time averaged Poynting vector

$$\vec{S} = \frac{c}{8\pi} \text{Re}(\vec{E}^* \times \vec{H})$$

(5.9)

for the fields given by (5.6) and (5.7). For calculating the gain, we are interested in the ratio of power flows as a function of z and therefore one

and $\Omega_s^0 = \omega\gamma_0 - ku_{\parallel}^0 - s\Omega_c$ with $u_{\parallel}^0$ is replaced by $\bar{u}_{\parallel} \pm i\Delta u_{\parallel}$ according to (4.54). Then, $\widetilde{E}_\theta(k)$, given by (5.3), possesses poles given by roots of the dispersion relation

$$D(k_i) = 0 \qquad (5.5)$$

which is a quartic function giving four roots and $\widetilde{E}_\theta(k)$ is given by (5.2) as

$$E_\theta(z) = -\frac{dE_\theta}{dz}(o) \sum_{i=1}^{4} e^{ik_i z} \frac{iN(k_i)}{D'(k_i)} \qquad (5.6)$$

Clearly, $E_\theta(z)$ is a superposition of four modes: two empty waveguide modes moving to the forward and backward, and two beam modes. If there is no velocity spread ("cold" beam), $D(k)$ is a quartic function with real coefficients giving two complex conjugate roots, representing one growing mode (k_i with Im $k_i < 0$) and one decaying mode (k_i^*). With beam spread, the coefficients of $D(k)$ are no longer real and therefore the complex solutions need not be complex conjugates of each other. Physically one expects that the complexity of the coefficients of $D(k)$ through the shift in $u_{\parallel}^0 = \bar{u}_{\parallel} \pm i\Delta u_{\parallel}$ tends to reduce the growing part (Im $k_i < 0$) more. Once again, we emphasize that the two-foldness of beam modes (in addition to the two waveguide modes) in (5.6) is true only for the "cold" beam or standard Lorentzian distribution.

Having determined $E_\theta(z)$ as (5.6), the other non-vanishing fields are given by (3.12) as

$$i\frac{\omega}{c}H_r(z) = -\frac{dE_\theta(z)}{dz} \qquad (5.7)$$

$$\frac{\omega}{c}H_z(z) = |\alpha_n|E_\theta(z)$$

Fields

Applying the Bromwitz formula (5.1),

$$E_\theta(z) = \sum_i \text{Res}\left(e^{ikz}\, i\tilde{E}_\theta(k)\right)\Bigg|_{k=k_i:\text{poles}} \tag{5.2}$$

and therefore, the problem is essentially reduced to find poles of $\tilde{E}_\theta(k)$. From (4.41), (4.53) and (4.43), it is clear that there are, in general, an infinite number of poles in $\tilde{E}_\theta(k)$ when all the harmonics in (4.43) are included. In practice, however, for a reasonably strong magnetic field, different harmonics are fairly well-separated and the parameter can be chosen to tune to only one of the harmonic modes. For a given harmonic mode, there are $2 + 2p$ poles in $\tilde{E}_\theta(k)$ with generalized Lorentzian distribution of order p in $u_\parallel^0$. Two poles represent two empty waveguide modes while $2p$-poles represent beam modes. In the limit $p \to \infty$, that is for the "box" distribution, the infinite number of these poles is compactly distributed between $u_\parallel^0 \pm \Delta u_\parallel$ forming a branch cut. Only when $p=1$ (the standard Lorentzian distribution) are there four modes, as in the "cold" beam case.

For simplicity, from now on, we will consider the case $p=1$ for a specific harmonic mode s. In this case $\tilde{E}_\theta(k)$, given by (4.41), can be written as a quotient of two polynomial functions,

$$\tilde{E}_\theta(k) = -\frac{dE_\theta}{dz}(o)\,\frac{N(k)}{D(k)} \tag{5.3}$$

where

$$N(k) \equiv \Omega_s^{0^2}(k)\Big/\Omega_c^2$$

$$D(k) \equiv \Omega_s^{0^2}(k)\left(k^2 - k_n^2\right) - \left(Q_2 + Q_1\,\frac{\Omega_s^0(k)}{\Omega_c} + Q_0\,\frac{\Omega_s^{0^2}(k)}{\Omega_c^2}\right) \tag{5.4}$$

-36-

V. INVERSE LAPLACE TRANSFORMATION

Let us now consider the inversion of the Laplace transformation of $\widetilde{E}_\theta(k)$ given by (4.4) to obtain the field as a function of z, $E_\theta(z)$. The inverse Laplace transformation (4.1) is given by the Bromwitz inversion formula:

$$F(z) = \frac{1}{2\pi} \int_{-ic-\infty}^{-ic+\infty} dk \; e^{ikz} \; \widetilde{F}(k)$$

$$= \frac{1}{2\pi} \oint_C dk \; e^{ikz} \; i\widetilde{F}(k) \tag{5.1}$$

$$= \sum_i \text{Res}\left(e^{ikz} \; i\widetilde{F}(k)\right)\Bigg|_{k=k_i:\text{poles}}$$

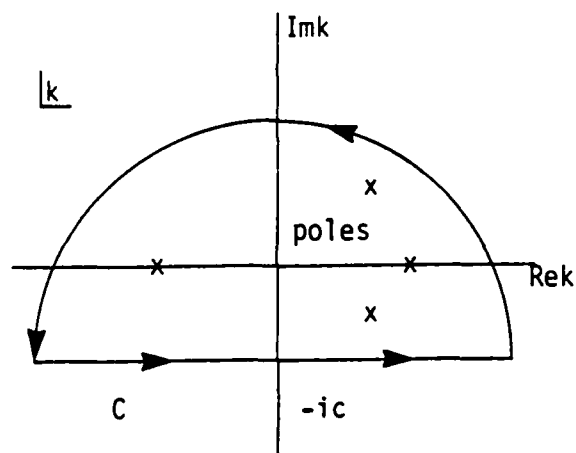Where the contour integral is done along C as shown in Figure 5.1.

Figure 5.1 The contour integral for the inverse Laplace transformation. c must be chosen to be large enough to include all the poles in $\widetilde{E}_\theta(k)$.

In terms of ζ-variable, (4.48) can be written as

$$\tilde{S}_n(k) = \Delta u_\parallel^0 \int_{-\infty}^{\infty} d\zeta \, \frac{C_p}{\zeta^{2p}+1} \, \hat{S}_n(k; \, \overline{u}_\parallel + \zeta \Delta u_\parallel)$$

(4.52)

Recalling that $\mathrm{Im} \, k < o$, one can show that the function S_n given by (4.43) has a pole in the upper ζ-plane if $\omega > s\omega_c$ and in the lower ζ-plane if $\omega < s\omega_c$. The contour in (4.52) can be closed to exclude this pole so that only the poles in the distribution function contribute to (4.52). Then, using the normalization constant C_p given by (4.51a) or (4.51b) accordingly, one obtains

$$\tilde{S}_n(k) = \sum_{k=0}^{p-1} \zeta_k^* \, \hat{S}_n(k; \, \overline{u}_\parallel + \zeta_k^* \, \Delta u_\parallel) \Bigg/ \sum_{k=0}^{p-1} \zeta_k^*$$

(4.53a)

if $\omega > s\omega_c$, and

$$\tilde{S}_n(k) = \sum_{k=0}^{p-1} \zeta_k \, \hat{S}_n(k; \, \overline{u}_\parallel + \zeta_k \Delta u_\parallel) \Bigg/ \sum_{k=0}^{p-1} \zeta_k$$

(4.53b)

if $\omega < s\omega_c$, where ζ_k and ζ_k^* are given by (4.50). In the case of the standard Lorentzian distribution for $p = 1$, $\zeta_0 = i$ and therefore, one obtains very simple results:

$$\tilde{S}_n(k) = \begin{cases} \hat{S}_n(k; \, \overline{u}_\parallel - i\Delta u_\parallel) & \text{if } \omega > s\omega_c \\ \hat{S}_n(k; \, \overline{u}_\parallel + i\Delta u_\parallel) & \text{if } \omega < s\omega_c \end{cases}$$

(4.54)

In other words, for standard Lorentzian distribution, the effect of spread in parallel velocity is merely shifting the center velocity to the complex one as (4.54). For generalized Lorentzian distribution $p > 1$, the effect is the average of the shifts by $\zeta_k \Delta u_\parallel$ or $\zeta_k^* \Delta u_\parallel$.

Linear Theory of Gyro-Slow-Wave Amplifier

For TM_{on}-Modes in a

Dielectric-Loaded Cylindrical Waveguide

S. Y. Park[*] and J. M. Baird[†]

B-K Dynamics, Inc.
Rockville, MD 20852

and

J. L. Hirshfield

Yale University
New Haven, CT 06520

20 November 1981

[*]Present address: U.S. Naval Research Lab
[†]Present address: University of Utah

ACKNOWLEDGEMENTS

TABLE OF CONTENTS

I. INTRODUCTION

A gyrotron is a microwave generating or amplifying device utilizing transverse energy of an electron beam gyrating in a strong dc-magnetic field. The basic mechanism responsible for this is the negative mass instability of rotating electrons resonantly interacting with the RF field. Due to the fact that the relativistic cyclotron frequency, $\omega_c = \Omega_c/\gamma$ $(\Omega_c \equiv eB_0/mc)$, is inversely proportional to the total energy of an electron, the rotational motion (angular velocity) decelerates when it gains energy and accelerates when it loses energy, resulting in azimuthal bunching in phase space. This azimuthal bunching induces a strongly enhanced coherent radiation (typically 10^{11-12} times over the incoherent radiation level).

A general analysis shows that there are three types of instability driving forces. The first one is a transverse electric force directly modulating the rotational motion of an electron and responsible for the familiar cyclotron maser instability (CMI). This is proportional to the transverse velocity gradient of the electron beam distribution function and is dominant in the fast wave region. The second force is a magnetic ponderomotive force due to a transverse magnetic field (linear combination of $\vec{v}_\perp \times \vec{H}_\perp$ and $\vec{v}_\shortparallel \times \vec{H}_\perp$) and is responsible for the Weibel instability. This force is effective only when the electron distribution function has an anisotropy in the velocity space. In a gyrotron, this effect usually competes with the CMI and becomes dominant in the slow wave region. The third kind is an axial electric force (therefore, not present for TE-modes) and is proportional to the axial velocity gradient of the electron distribution function. Unlike the CMI and Weibel which are proportional to $v_\perp^2$, this is the only instability driving force which survives in the limit $v_\perp \to 0$, leading to a type of conventional traveling wave tube with dielectric slow wave structure (or Cerenkov radiation device).

In addition to all these major instability driving forces, a careful analysis shows additional terms due to the inhomogeneity of the electron plasma for an electron beam with finite geometry. This geometric term gives a weak contribution to a case tuned to the top of resonance but it affects the detuning factor and bandwidth.

Previously, we have analyzed a gyrotron amplifier for the TE_{on}-mode. Here we report a similar analysis for the TM_{on}-mode. In many respects, the TM_{on}-mode analysis (with E_z, E_r, H_θ) is complementary to the one for the TE_{on}-mode (with H_z, H_r, E_θ). However, one major difference in the analysis for the TM_{on}-mode is that one must solve a coupled equation for E_z and E_r since there are two sources (J_z and J_r), both strongly coupled to E_z and E_r. This requires more care in projecting out the n-th radial mode radiation from a radially finite source which, in principle, could radiate in all radial modes. For this purpose we have derived an orthonormality relation in Appendix A which is used in projecting out the desired radial mode. The key factor which allows us to concentrate on a single radial mode at a time is that the radial mode dispersion relation is usually well-separated and only one of these modes is resonantly interacting with the electron beam in a controlled device. Bearing this difference in mind, we can proceed with the analysis much in parallel to the one for the TE_{on}-mode. In Section II, we have derived, from Maxwell equations, a coupled wave equation for E_z and E_r with source terms J_z and J_r. Using the properties of radial eigen-mode functions derived in Appendix A, we project out the n-th radial mode. As we have emphasized in the TE_{on}-mode analysis we use Laplace transformation which is suitable for an analysis dealing with instabilities. The Laplace transformation correctly accounts for the boundary values at the input end so that this analysis includes the insertion loss in a natural way.

In Section III, we calculate the source terms from a linearized Vlasov equation. The algebra is quite involved, mostly due to the cylindrical geometry we are interested in, but is rather straightforward, and freely uses Graf's addition theorem for Bessel functions. Appendix B is devoted to some of the integrals used in this section. Axial velocity spread is included in the source terms. A detailed discussion of this is included in the previous analysis for the TE_{on}-mode interaction.

In Section IV, we combine the results from Sections II and III to derive a complex dispersion relation and determine the fields as a function of z in terms of the input boundary values. This is done easily by an inverse Laplace transformation which, essentially, picks up pole contributions in the Laplace transformed fields. The complex dispersion relation leads to four poles (two beam and two waveguide modes), and the residue at each pole determines the relative strength of each mode. As a result, the present analysis allows us to determine completely the fields in terms of input boundary values. Thus, one can immediately calculate the gain vs. frequency for an amplifier application.

Some numerical examples are shown in Section V. These sample results (not yet optimized) show that the TM_{on}-mode interaction is comparable to the one for the TE_{on}-mode, at least in a slow wave region.

II. MAXWELL'S EQUATIONS

Consider an annular electron beam introduced along a strong uniform guiding magnetic field into the innermost (vacuum) region of a waveguide loaded with multilayer, concentric dielectric slow wave structure as shown in Fig. 1.
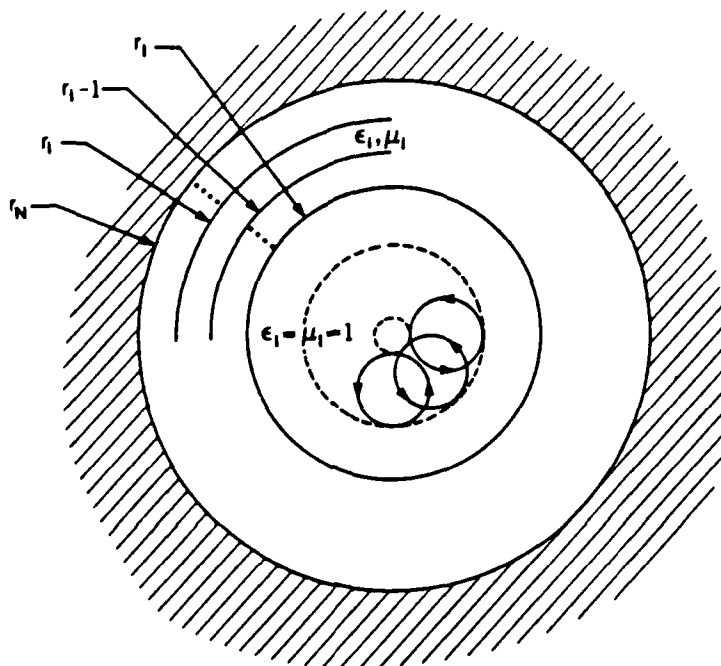
As we are interested in an amplifier theory for TM_{on} modes, we assume that the system is in a stationary state (with time dependence $\sim e^{-i\omega t}$) and is azimuthally symmetric ($\partial/\partial\theta = 0$). However, since the EM fields can grow or decay along the direction of propagation due to the interaction with the electron beam, one must leave the z-dependency to be determined consistently by the coupled Maxwell-Vlasov equations. Also, due to the presence of a radially localized source (the electron beam) which, in principle, can radiate into all radial modes, one cannot assume that the fields are given by a single radial eigenmode in the waveguide. Since the radial eigenmodes form a complete orthonormal set, one can certainly expand any radial function (satisfying the waveguide boundary conditions) in terms of these. Therefore

one can write a general ansatz as, in the i-th dielectric region,

$$E_z^{(i)}(r,z,t) = e^{-i\omega t} \sum_n \overline{E}_{z,n}(z) \, e_{z,n}^{(i)}(r)$$

$$E_r^{(i)}(r,z,t) = i \, e^{-i\omega t} \sum_n \overline{E}_{r,n}(z) \, e_{r,n}^{(i)}(r) \qquad (2.1)$$

$$H_\theta^{(i)}(r,z,t) = i \, e^{-i\omega t} \sum_n \overline{H}_{\theta,n}(z) \, h_{\theta,n}^{(i)}(r)$$

where the radial eigenmodes $e_{z,n}^{(i)}(r)$, $e_{r,n}^{(i)}(r)$, $h_{\theta,n}^{(i)}(r)$ and their properties
are given in Appendix A. Substituting this ansatz into Maxwell's equations,
$\nabla \times \vec{E} = i\mu \, \omega/c \, \vec{H}$ and $\nabla \times \vec{H} = -i\epsilon \, \omega/c \, \vec{E} + 4\pi/c \, \vec{J}$, one obtains

$$\sum_n (-i \, \dot{\overline{E}}_{r,n} \, e_{r,n}^{(i)} + \overline{E}_{z,n} \, e_{z,n}^{(i)\,'} - \mu_i \, \omega/c \, \overline{H}_{\theta,n} \, h_{\theta,n}^{(i)}) = 0 \qquad (2.2a)$$

$$\sum_n (-i\dot{\overline{H}}_{\theta,n} \, h_{\theta,n}^{(i)} - \epsilon_i \, \omega/c \, \overline{E}_{r,n} \, e_{r,n}^{(i)}) = 4\pi/c \, e^{i\omega t} J_r \qquad (2.2b)$$

$$\sum_n (\overline{H}_{\theta,n} \, 1/r \, (rh_{\theta,n}^{(i)})' + \epsilon_i \, \omega/c \, \overline{E}_{z,n} \, e_{z,n}^{(i)}) = -i \, 4\pi/c \, e^{i\omega t} J_z \qquad (2.2c)$$

where $\cdot \equiv d/dz$ and $' \equiv d/dr$. Note that the source terms J_r and J_z are localized
only in the innermost vacuum region ($i = 1$). This is why one needs all the
radial modes on the left-hand side of (2.2b) and (2.2c).

In practice the radial eigenmodes are fairly well separated, therefore,
one can tune the system so that the electron beam interacts resonantly with
only one specific radial eigenmode (n'). One would like to project out the
n'-th radial eigenmode from (2.2). This can be done easily by using the
orthogonality relation (A.19) derived in Appendix A. First, one writes the
radial fields in (2.2) in terms of $h_{\theta,n}$ using the relations given by (A.3);

- 5 -

$$\epsilon_i \, \omega/c \, e_{r,n}^{(i)} = k_{\shortparallel,n} \, h_{\theta,n}^{(i)}$$

$$\epsilon_i \, \omega/c \, e_{z,n}^{(i)\,\prime} = k_{\perp,n}^{(i)2} \, h_{\theta,n}^{(i)} \qquad\qquad (2.3)$$

$$(1/r \, (r \, h_{\theta,n}^{(i)})^{\prime})^{\prime} = - k_{\perp,n}^{(i)2} \, h_{\theta,n}^{(i)},$$

to cast (2.2) into

$$\sum_n (\overline{E}_{z,n} - \overline{H}_{r,n}) \, k_{\perp,n}^{(i)2} \, h_{\theta,n}^{(i)} = \sum_n (i \, \dot{\overline{E}}_{r,n} + \overline{H}_{\theta,n} k_{\shortparallel,n}) \, k_{\shortparallel,n} \, h_{\theta,n}^{(i)} \qquad (2.4a)$$

$$\sum_n (i \, \dot{\overline{H}}_{\theta,n} + \overline{E}_{r,n} \, k_{\shortparallel,n}) \, h_{\theta,n}^{(i)} = - \, 4\pi/c \, e^{i\omega t} J_r \qquad (2.4b)$$

$$\sum_n (-i \, \dot{\overline{E}}_{r,n} + \overline{H}_{\theta,n} \, k_{\shortparallel,n}) \, k_{\shortparallel,n} \, h_{\theta,n}^{(i)} = - \, i \, 4\pi/c \, e^{i\omega t} J_z^{\prime} \qquad (2.4c)$$

Now we multiply (2.4) by $h_{\theta,n^{\prime}}^{(i)}/\epsilon_i$, integrate $\int_{r_{i-1}}^{r_i} rdr$ and sum over all dielectric regions. Using the orthonormality (A.19) and (A.20), one obtains

$$k_{\perp,n^{\prime}}^2 \, \overline{E}_{z,n^{\prime}} = i \, \dot{\overline{E}}_{r,n^{\prime}} \, k_{\shortparallel,n^{\prime}} + \overline{H}_{\theta,n^{\prime}} \, \omega/c \qquad (2.5a)$$

$$i \, \dot{\overline{H}}_{\theta,n^{\prime}} + \overline{E}_{r,n^{\prime}} k_{\shortparallel,n^{\prime}} = - \, 4\pi/c \, e^{i\omega t} \, 1/C_{n^{\prime}} \int_o^{r_1} rdr \, h_{\theta,n^{\prime}}^{(i)} \, J_r \qquad (2.5b)$$

$$i \, \dot{\overline{E}}_{r,n^{\prime}} + \overline{H}_{\theta,n^{\prime}} k_{\shortparallel,n^{\prime}} = -i \, 4\pi/c \, e^{i\omega t} \, 1/C_n^{\prime} \int_o^{r_1} rdr \, h_{\theta,n^{\prime}}^{(i)} \, J_z^{\prime} / k_{\shortparallel,n^{\prime}} \qquad (2.5c)$$

$$(C_{n^{\prime}} \equiv \sum_{i=1}^{N} \int_{r_{i-1}}^{r_i} rdr \, h_{\theta,n^{\prime}}^{(i)2}/\epsilon_i),$$

where we have used the fact that the source terms J_r and J_z are nonvanishing only in the innermost region (vacuum, $\epsilon_1 = \mu_1 = 1$). By integration by parts on the right-hand side of (2.5c) and using (A.3b) and (A.3c), one can write (2.5) in a more transparent form as (dropping the subscript n' from now on),

$$k_{\perp}^2 \, \overline{E}_z = i \, \dot{\overline{E}}_r \, k_{\shortparallel} + \overline{H}_{\theta} \, \omega^2/c^2 \tag{2.6a}$$

$$i \, \dot{\overline{H}}_{\theta}(z) + k_{\shortparallel} \, \overline{E}_r(z) = - P_r(z) \tag{2.6b}$$

$$i \, \dot{\overline{E}}_r(z) + k_{\shortparallel} \, \overline{H}_{\theta}(z) = - P_z(z) \tag{2.6c}$$

where

$$P_r(z) \equiv 4\pi/c \; e^{i\omega t} \, \omega/c/k_{\shortparallel} \, \overline{J}_r(z)/C_n$$

$$P_z(z) \equiv i \; 4\pi/c \; e^{i\omega t} \, \omega/c/k_{\shortparallel} \, \overline{J}_z/C_n \tag{2.7}$$

and

$$\overline{J}_r(z) \equiv \int_0^{r_1} rdr \; e_r J_r$$

$$\overline{J}_z(z) \equiv \int_0^{r_1} rdr \; e_z J_z \tag{2.8}$$

$$\left(C_n \equiv \sum_{i=1}^{N} \int_{r_{i-1}}^{r_i} rdr \; e_{r,n}^{(i)} \, h_{\theta,n}^{(i)} \right).$$

The physical meaning of the source terms $P_r(z)$ and $P_z(z)$ is clearly that they are proportional to the work done by the induced current interacting with EM fields which are normalized to the total power flow through the waveguide.

The set of differential equations (2.6) can be converted into a set of algebraic equations by a Laplace transformation defined by

- 7 -

$$\widetilde{F}(k) \equiv \int_0^\infty dz \ e^{-ikz} \ F(z)$$

(2.9)

$$\overset{\sim}{\dot{F}}(k) = ik \ \widetilde{F}(k) - F(o)$$

with Im k sufficiently large and negative to make the transformation integral (2.9) well-defined even in the case of $F(z)$ exponentially increasing. Note that for a system involving an instability, the usual Fourier transformation is not well defined. A bonus of using the Laplace transformation rather than the Fourier transformation in the present case is that it completely determines the growth of the field from the boundary values at the input end.

Applying (2.9) to (2.6), one obtains

$$\hat{k} \ \widetilde{E}_{z,n} = - \widetilde{E}_{r,n} \ k \ k_{\shortparallel,n}/|k_{\perp,n}^{(i)}|^2 + \widetilde{H}_{\theta,n} \ \omega^2/c^2/|k_{\perp,n}^{(i)}|^2 - E_r(o) \ k_{\shortparallel,n}/|k_{\perp,n}^{(i)}|^2$$

$$-k \ \widetilde{E}_{r,n} + k_{\shortparallel,n} \ \widetilde{H}_{\theta,n} = 2/c/c_n \ \widetilde{W}_z + i \ \bar{E}_{r,n}(o)$$

(2.10)

$$k_{\shortparallel,n} \ \widetilde{E}_{r,n} - k \ \widetilde{H}_{\theta,n} = 2/c/c_n \ \widetilde{W}_r + i \ \bar{H}_{\theta,n}(o).$$

III. VLASOV EQUATION (LINEARIZED)

The perturbed electron distribution function f_1 (from its equilibrium state f_0) under the influence of EM fields is given by

$$f_1 (\vec{x},\vec{u},t) = e/m \int_{t-z/v_{\shortparallel}}^{t} dt' \; (\vec{E}' + \vec{u}'/c\gamma \times \vec{H}') \cdot \nabla_u \cdot f_0 \; , \quad (3.1)$$

The integration path is over the unperturbed characteristics -- a particle trajectory in a uniform magnetic field as shown in Fig. 3.1.
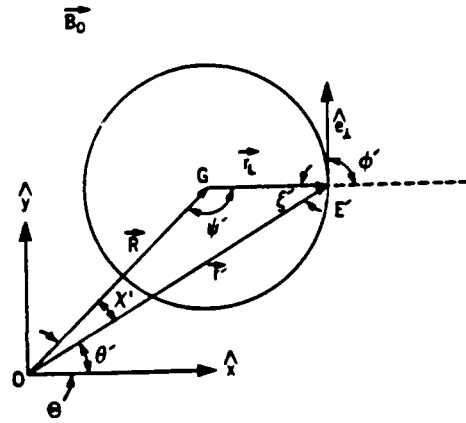

Figure 3.1. 0 is the center of waveguide; G is the guiding center of an electron; E' is the position of the electron at t'; $r_L \equiv u_\perp/\Omega_c$ is Larmor radius; and $\omega_c \equiv \Omega_c/\gamma$ ($\Omega_c \equiv eB_0/m_0$) is relativistic cyclotron frequency.

The primed quantities represent the values at t' and the position given by $z' = z + v_{\shortparallel} (t' - t)$ and $\varphi' = \varphi + \omega_c(t' - t)$. Note the relation between angles in Fig. 3.1: $\xi' = \pi/2 - (\varphi' - \theta')$, $\psi' = \pi/2 + (\varphi' - \Theta)$ and $\chi' = \Theta - \theta'$.

A realistic equilibrium beam function f_0 can be constructed from three invariants, $u_{\shortparallel}$, $u_\perp$ ($\vec{u} = \vec{p}/m = \vec{v}\gamma$ is a momentum variable) and the guiding center radius $R = (r'^2 + r_L^2 - 2r'r_L \cos\xi')^{1/2}$. In terms of the angles shown in Fig. 3.1, f_1 with TM - field components (E_z, E_r, H_θ) can be written as

$$f_1 = e/m \int_{t-z/v_{\shortparallel}}^{t} dt' \left\{ E_z' \, \partial f_0/\partial u_{\shortparallel} + [E_r' \, \partial f_0/\partial u_{\perp} + H_\theta' \, (u_{\perp}/c\gamma \, \partial f_0/\partial u_{\shortparallel} \right.$$

$$\left. - u_{\shortparallel}/c\gamma \, \partial f_0/\partial u_{\perp})] \sin \xi' + (E_r' - H_\theta' \, u_{\shortparallel}/c\gamma) \, 1/\Omega_c \, \partial f_0/\partial R \, \sin \chi' \right\}. \quad (3.2)$$

Note that the last term in (3.2) is essentially due to an inhomogeneous plasma such as annular electron beam. Substituting the ansatz (2.1) and noting that we have assumed that the electron beam is only in the innermost vacuum region of the waveguide, one obtains

$$f_1 = e^{-i\omega t} \, e/m \int_0^z dz'/v_{\shortparallel} \, e^{i\omega(z-z')/v_{\shortparallel}} \sum_n \left\{ \overline{E}_{z,n}(z') \, \partial f_0/\partial u_{\shortparallel} \, Z_0 \, (|k_{\perp,n}^{(i)}|r') \right.$$

$$- [\overline{E}_{r,n}(z') \, k_{\shortparallel,n}/|k_{\perp,n}^{(i)}| \, \partial f_0/\partial u_{\perp} + \overline{H}_{\theta,n}(z') \, \omega/c/|k_{\perp,n}^{(i)}| \, (u_{\perp}/c\gamma \, \partial f_0/\partial u_{\shortparallel}$$

$$- u_{\shortparallel}/c\gamma \partial f_0/\partial u_{\perp})] \, Z_1 |k_{\perp,n}^{(i)}|r') \, i \, \sin \xi'$$

$$- [\overline{E}_{r,n}(z') \, k_{\shortparallel,n}/|k_{\perp,n}^{(i)}| - \overline{H}_{\theta,n}(z') \, \omega/c/|k_{\perp,n}^{(i)}| \, u_{\shortparallel}/c\gamma] \, 1/\Omega_c \, \partial f_0/\partial R \, Z_1$$

$$(|k_{\perp,n}^{(i)}|r') \, i \, \sin \chi' \left. \right\}. \quad (3.3)$$

An immediate difficulty in carrying out the integral is due to the complexity of z'-dependency introduced by the arguments of the Bessel functions. This can be easily overcome by exploiting Graf's addition theorem for Bessel functions which allows us to expand in harmonic functions.

Consider a triangle shown in Fig. 3.2, with scale variables defined by

$$x' \equiv |k_{\perp,n}^{(i)}|r', \quad a_L \equiv |k_{\perp,n}^{(i)}|r_L, \quad a \equiv |k_{\perp,n}^{(i)}|R$$

and $\hat{k} \equiv k_{\perp,n}^{(i)2}/|k_{\perp,n}^{(i)}|^2$. Graf's addition theorem reads

$$Z_\ell(x') \, e^{i\ell\xi'} = \sum_{\ell'=-\infty}^{\infty} \hat{k}^{\ell'} \, e^{i\ell'\psi'} \, Z_{\ell'+\ell}(a_L) \quad Z_{\ell'}(a)$$

$$(3.4)$$

$$Z_\ell(x') \, e^{i\ell\chi'} = \sum_{\ell'='\infty}^{\infty} \hat{k}^{\ell'} \, e^{i\ell'\psi'} \, Z_{\ell'+\ell}(a) \quad Z_{\ell'}(a_L).$$
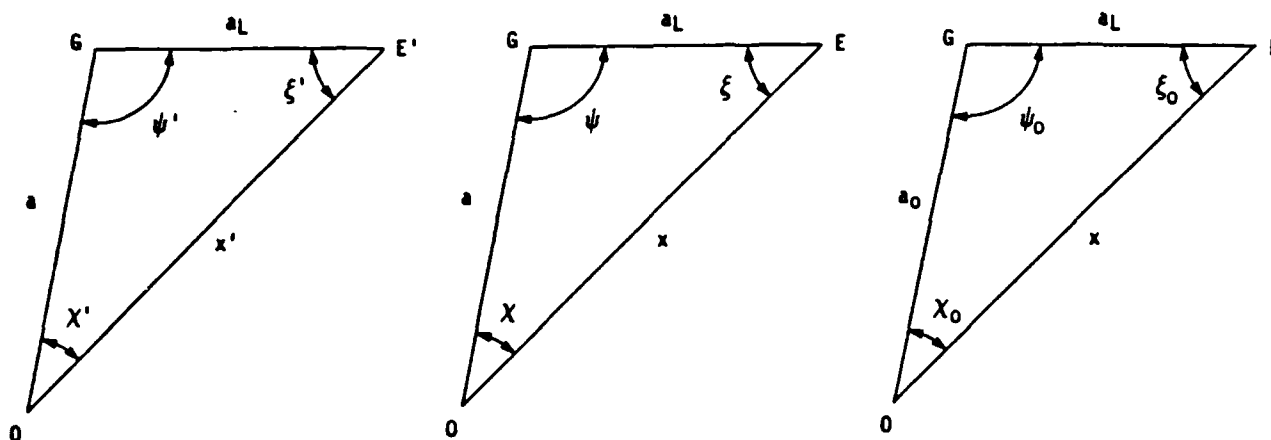

Figure 3.2. Triangles for Graf's addition theorem of Bessel function at various stages of integration.

Using (3.4) with $Z_{-\ell}(x) = (-\hat{k})^\ell Z_\ell(x)$, one obtains the desired harmonic expansion as

$$Z_0(x') = \sum_{S=-\infty}^{\infty} \hat{k}^S \, e^{iS\psi'} \, Z_S(a_L) \, Z_S(a)$$
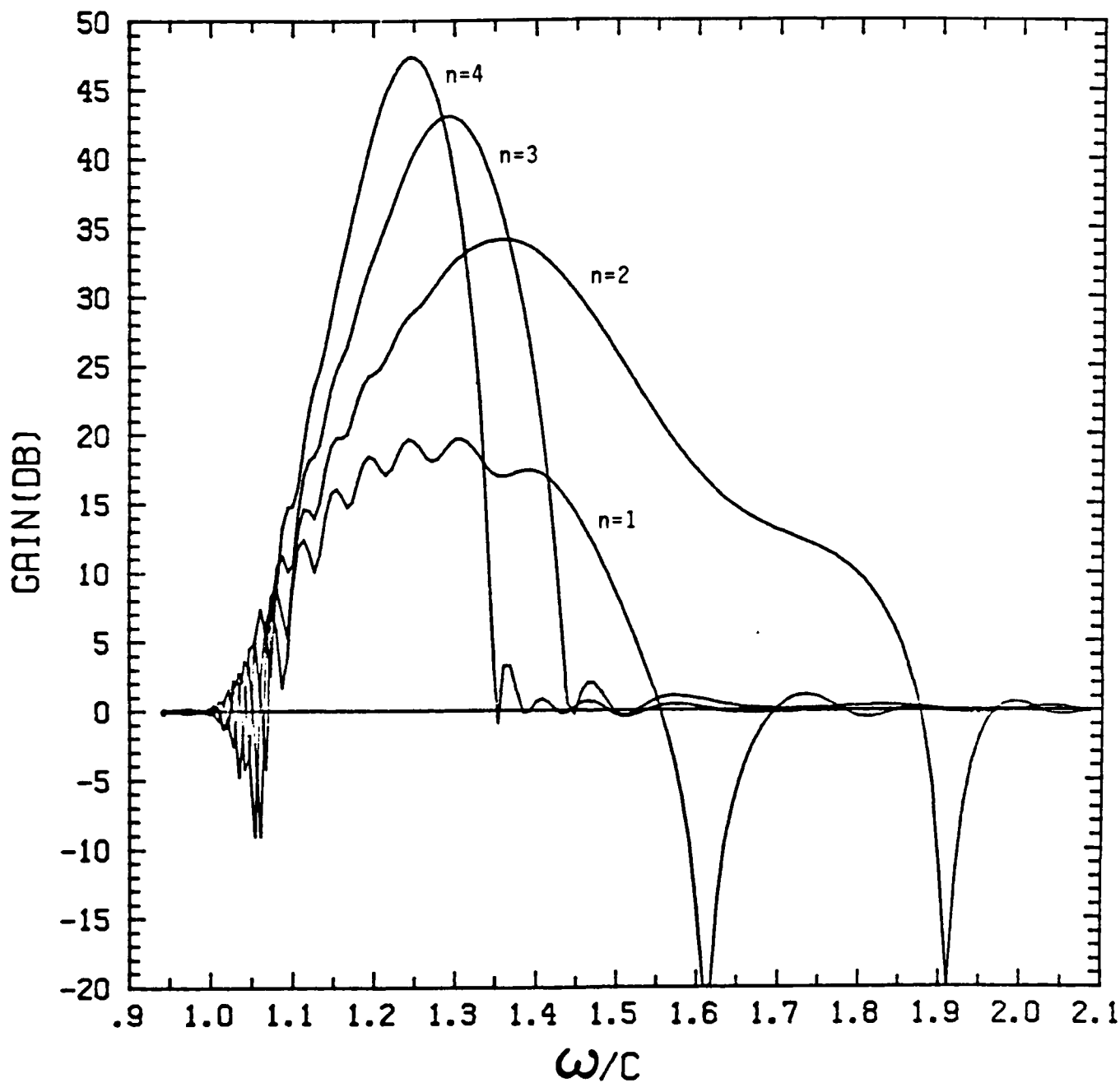
$$Z_1(x') \, i \, \sin\xi' = \sum_{S=-\infty}^{\infty} \hat{k}^{S+1} e^{iS\psi'} \, s/a_L \, Z_S(a_L) \, Z_S(a)$$

$$Z_1(x') \, i \, \sin\chi' = \sum_{S=-\infty}^{\infty} \hat{k}^{S+1} e^{iS\psi'} \, Z_S(a_L) \, s/a \, Z_S(a)$$

$$(\psi' = \psi + \omega_c \, (z'-z)/v_{\shortparallel})$$

and therefore, suppressing the obvious index n for notational simplicity,

GAIN VS. FREQUENCY

r_1 = 1.55 cm	ϵ_1 = 1	I = 5.2 Amp.	α = 2
r_2 = 1.75 cm	ϵ_2 = 4.6	R_G = 0.72 cm	ω_c/c = 0.75
r_3 = 2.033 cm	ϵ_3 = 19.	L = 100 cm	v_z/c = 0.17 + (n-1)x .005
		s = 1	Δv_z = 0

FIGURE 5.1

first harmonic (s=1). Instead, the zeroth harmonic s=0, which, of course, requires a steeper beam line to cross the dispersion line, gives a gain with narrow bandwidth. This is Cerenkov radiation from the axial energy of an electron beam rather than transverse energy as in the gyrotron. Certainly a more careful comparison study is necessary to compare the performance of a TM_{on}-mode amplifier to a TE_{on}-mode amplifier. However, the indication so far is that the TM_{on} mode amplifier seems to be at least comparable to the TE_{on}-mode amplifier.

V. RESULTS AND DISCUSSION

Based upon the analysis discussed so far, we have developed a computer code

to calculate and graph gain vs. frequency for a variety of parameters.

Some sample cases (not yet optimized) are shown in Figures 5.1 through 5.5.

For all these figures, we have considered a cylindrical waveguide with two

dielectric layers surrounding the central vacuum region with designated

parameters: r_1 = 1.55 cm, r_2 = 1.75 cm, r_3 = 2.033 cm and ϵ_1 = 1.0, ϵ_2

= 4.6, ϵ_3 = 19. (This particular choice of a waveguide is for comparison

to the Yale TE_{on} mode experiment.) The annular electron beam is assumed

to carry a current I = 5.2 Amp with a guiding center radius R = 0.72 cm in a

magnetic field corresponding to the cyclotron frequency ω_c/c = 0.75. All these

examples show the first harmonic interaction (s=1) with the TM_{on}-mode for

different velocities and the axial velocity spreads. For example, Figure 5.1

shows the gain vs. frequency for various axial velocities $v_{\shortparallel}/c$ = 0.17 +

(n-1) x 0.005 (n=1, ..., 4) with $\alpha \equiv v_\perp/v_{\shortparallel}$ = 2 and $v_{\shortparallel}$ = 0. Compared to

the similar results for the TE_{on}-mode, the gain is comparable. Figure 5.2 shows

the same case except the velocity spread ($\Delta v_{\shortparallel}$) is now 2%. It is obvious

that the slow wave amplifier is sensitive to the axial velocity spread,

particularly at higher frequencies (thus large $k_{\shortparallel}$). The next graph (Fig. 5.3)

shows the same case as Figure 5.2 except with slightly higher axial velocities

given by $v_{\shortparallel}$ = 0.185 + (n-1) x 0.005 (n=1, ..., 4). The gains are slightly

improved with smaller bandwidths. Apparently there seems to be a trade-off

between gain and bandwidth. Figure 5.4 shows the same case as Figure 5.3

except with a higher velocity spread $\Delta v_{\shortparallel}$ = 4%. The last figure (Figure 5.5)

is similar to Figure 5.1 except that α is 1 now. The gain is a very sensitive

function of the transverse velocity. This is a general characteristic of any

gyrotron device. In the limit $\alpha \to 0$, we do not get any positive gain for the

- 23 -

Applying (4.9) to (4.6) and noting that there are four poles corresponding to the four roots in the complex dispersion relation

$$d(k_i) = o,\qquad(4.10)$$

one obtains

$$\begin{pmatrix}\overline{E}_r(z)\\ \overline{H}_\theta(z)\end{pmatrix} = \sum_{i=1}^{4} e^{ik_iz}\begin{pmatrix}\widetilde{N}_r(k_i)\\ \widetilde{N}_\theta(k_i)\end{pmatrix}\Big/ d'(k_i)\qquad(4.11)$$

where

$$\begin{pmatrix}N_r(k)\\ N_\theta(k)\end{pmatrix} \equiv -\ \overline{\Omega}_s^2(k)\ \left\{\overline{H}_\theta(o)\begin{pmatrix}k_{,,} - S_{12}\\ k + S_{12}\end{pmatrix}+ \overline{E}_r(o)\begin{pmatrix}(1 + S_{10}) - S_{20}(k_{,,} - S_{12})\\ (1 + S_{10}) + S_{20}(k + S_{11})\end{pmatrix}\right\}.$$

$$(4.12)$$

Note that the relative field amplitude of each of the four possible modes is completely determined by the residues at the poles as a function of boundary values $(\overline{H}_\theta(o)$ and $\overline{E}_r(o))$.

Having determined the fields as functions of z, one can immediately calculate the gain as a function of interaction length r_L from the power flow compared to the input,

$$G(dB) = 10\ \log_{10}\ (S_z(L)/S_z(o))\qquad(4.13)$$

where

$$S_z(L)/S_z(o) = \text{Re}\ (\overline{E}_r(z)\overline{H}_\theta^*(z))/\text{R}_e\ (\overline{E}_r(o)\overline{H}_\theta^*(o))\Big|_{z=L}$$

$$= \text{Re}\ (\sum_i e^{ik_iL}\ H_r(k_i)/d'(k_i))\ (\sum_i e^{-ik_i^*L}\ N_\theta^*(k_i)/d'(k_i^*))/$$

$$\text{Re}\ (\sum_i N_r(k_i)/d'(k_i))\ (\sum_i N_\theta^*(k_i)/d'(k_i))^*$$

taking the summation over only Re $(k_i) > o$ for the forward gain, and Re $(k_i) < o$ for the backward gain.

and

$$S_{11}S_{22} - S_{12}S_{21} = (2/c_n)^2 \hat{k}\Omega_s \, ck_{\shortparallel}/|k_{\perp}|^2 \, [\zeta_1^2/\overline{\Omega}_s^2 \, \omega^2/c^2/|k_{\perp}|^2 \, s\Omega_c k_{\shortparallel}/|k_{\perp}|^2$$

$$- \zeta_1\zeta_2/\overline{\Omega}_s \, k_{\shortparallel} c\gamma_0/|k_{\perp}|^2 \, \omega/c/\Omega c] \; .$$

It is important to note that one can rationalize (4.6) by multiplying by $\overline{\Omega}_s^2(k)$ in the denominator and numerator. Then the denominator

$$d(k) \equiv \overline{\Omega}_s^2(k) \, \det(\widetilde{D}(k) \tag{4.8}$$

is a quartic polynomial in k.

The fields as functions of z can be immediately obtained from (4.6) by inverting the Laplace transformation. The Brownwitz inversion formula for the Laplace transformation (2.9) reads

$$F(z) = 1/2\pi \int_{-ic-\infty}^{-ic+\infty} dk \; e^{ikz} \; \widetilde{F}(k)$$

$$= 1/2\pi i \oint dk \; e^{ikz} \; i \; \widetilde{F}(k) \tag{4.9}$$

$$= \sum_i \text{Res} \left(e^{ikz} \; i \; \widetilde{F}(k) \right) \Big|_{k=k_i \, : \, \text{poles}}$$

where sufficiently large positive c guarantees that all the pole contributions in the contour integral shown in Fig. 4.1 are included.

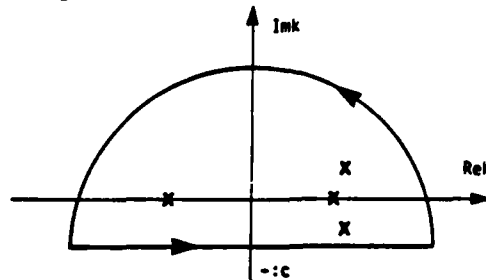Figure 4.1. Contour integral for (4.9).

$$A_2 \equiv \zeta_1 \bar{\Omega}_s^2 (\omega^2/c^2 - k^2) \, \omega/c\bar{u}_{\shortparallel}^{\circ}/|k_{\perp}|^2 - \zeta_1 \bar{\Omega}_s \, k \, \omega/c/|k_{\perp}|^2 - \zeta_2 \bar{\Omega}_s \, \omega/c\bar{u}_{\shortparallel}/\Omega c$$

$$A_0 \equiv - \zeta_1 \bar{\Omega}_s^2 \, k_{\shortparallel}/|k_{\perp}|^2 \, (\omega/c \, \bar{u}_{\shortparallel} - kc\gamma_0)$$

$$B_1 \equiv \zeta_1 \bar{\Omega}_s \, k_{\shortparallel} \, kc\gamma_0/|k_{\perp}|^2 , \qquad\qquad B_2 \equiv \zeta_1 \Omega_s^{\circ} \, \omega/c/|k_{\perp}|^2 \, (\omega\gamma_0 - s\Omega_c)$$

$$B_0 \equiv \zeta_1 \bar{\Omega}_s \, k_{\shortparallel} c\gamma_0/|k_{\perp}|^2 \tag{4.4}$$

$$(\bar{\Omega}s \equiv \omega\gamma_0 - s\Omega_c - k\bar{u}_{\shortparallel}) .$$

Substituting (4.2) into (4.1) one obtains

$$\begin{pmatrix} k + S_{11} & -k_{\shortparallel} + S_{12} \\ -k_{\shortparallel} + S_{21} & k + S_{22} \end{pmatrix} \begin{pmatrix} \tilde{E}_r \\ \tilde{H}_\theta \end{pmatrix} = i\bar{H}_\theta(o) \begin{pmatrix} 0 \\ 1 \end{pmatrix} + i\bar{E}_r(o) \begin{pmatrix} 1 + S_{10} \\ S_{20} \end{pmatrix} \tag{4.5}$$

which can be *immediately soluable by matrix inversion* as

$$\begin{pmatrix} \tilde{E}_r(k) \\ \tilde{H}_\theta(k) \end{pmatrix} = 1/\det(\tilde{D}(k)) \cdot \left\{ i\bar{H}_\theta(o) \begin{pmatrix} k_{\shortparallel} - S_{12} \\ k + S_{11} \end{pmatrix} \right.$$

$$+ i\bar{E}_r(o) \begin{pmatrix} (1 + S_{10}) + S_{20} \\ (1 + S_{10}) + S_{20} \end{pmatrix}$$

$$\left. \begin{pmatrix} (k_{\shortparallel} - S_{12}) \\ (k + S_{11}) \end{pmatrix} \right) \tag{4.6}$$

where

$$\det(\tilde{D}(k)) \equiv \begin{vmatrix} k + S_{11} & -k_{\shortparallel} + S_{12} \\ -k_{\shortparallel} + S_{21} & -k + S_{22} \end{vmatrix} \tag{4.7}$$

$$= (k^2 - k_{\shortparallel}^2) + k(S_{11} + S_{22}) + k_{\shortparallel}(S_{12} + S_{21}) + S_{11}S_{22} - S_{12}S_{21}$$

IV. DISPERSION RELATION AND GAIN

Let us go back to Maxwell equations (2.10) and write them in a matrix form as

$$\begin{pmatrix} k & -k_{\shortparallel} \\ -k_{\shortparallel} & k \end{pmatrix} \begin{pmatrix} \widetilde{E}_r \\ \widetilde{H}_\theta \end{pmatrix} = (2/c)/C_n \begin{pmatrix} \widetilde{W}_z \\ \widetilde{W}_r \end{pmatrix} + i\, \overline{H}_\theta(o) \begin{pmatrix} 0 \\ 1 \end{pmatrix} + i\, \overline{E}_r(o) \begin{pmatrix} 1 \\ 0 \end{pmatrix}, \quad (4.1)$$

with the source terms calculated in the previous section, (3.27) with (3.29). In the source terms, all the possible radial and temporal harmonics of TM_{on}-mode are included so far. However, each radial and temporal harmonic is weighted with resonance factor $1/\overline{\Omega}_s^2$ and $1/\overline{\Omega}_s$ with $\Omega_s \equiv \omega\gamma - k_{\shortparallel,n}\, \overline{u}_{\shortparallel} - s\Omega_c$ and, in practice, one can tune to only one of them since the radial modes and temporal harmonics are fairly well separated. Therefore, considering only this resonant mode term in the source term and using the relation (2.), one can write (3.27) as

$$- 2/c/C_n \begin{pmatrix} \widetilde{W}_z \\ \widetilde{W}_r \end{pmatrix} = \begin{pmatrix} S_{11} & S_{12} \\ S_{21} & S_{22} \end{pmatrix} \begin{pmatrix} \widetilde{E}_r \\ \widetilde{H} \end{pmatrix} + i\, \overline{E}_r(o) \begin{pmatrix} S_{10} \\ S_{20} \end{pmatrix} \quad (4.2)$$

where

$$S_{11} \equiv 2/C_n\, \hat{k}\, (u_{\shortparallel}^o\, A_1 + B_1) \qquad S_{12} \equiv -2/C_n\, \hat{k}\, (u_{\shortparallel}^o\, A_2 + B_2)$$

$$S_{21} \equiv 2/C_n\, s\Omega_c k_{\shortparallel}/|k_\perp|^2\, A_1 \qquad S_{22} \equiv -2/C_n\, s\Omega_c k_{\shortparallel}/|k_\perp|^2\, A_2 \qquad (4.3)$$

$$S_{10} \equiv 2/C_n\, \hat{k}\, (u_{\shortparallel}^o\, A_0 + B_0) \qquad S_{20} \equiv -2/C_n\, s\Omega_c k_{\shortparallel}/|k_\perp|^2\, A_0$$

and

$$A_1 \equiv \zeta_1/\overline{\Omega}_s^2\, (\omega^2/c^2 - k^2)\, k_{\shortparallel} c\gamma_0/|k_\perp|^2 - \zeta_1/\overline{\Omega}_s\, k_{\shortparallel}\, \omega/c/|k_\perp|^2$$

$$- \zeta_2/\overline{\Omega}_s^o\, k_{\shortparallel} c\gamma_0/\Omega c$$

which is the desired result for a "cold" beam with δ - function guiding center distribution. Beam spread effects should be included at this stage, according to (3.11). This has been discussed in detail in Ref. 1, and here we quote the result for the most important velocity spread effect in $u_{\shortparallel}$ for a Lorenzian distribution

$$f_0(u_{\shortparallel}^o) = 1/\pi \ \Delta u_{\shortparallel}^o/((u_{\shortparallel}^o - \overline{u}_{\shortparallel})^2 + (\Delta u_{\shortparallel}^o)^2) \quad . \tag{3.28}$$

We have shown in Ref. 1 that the result of this velocity spread effect is to merely replace $u_{\shortparallel}^o$ in (3.27) by

$$u_{\shortparallel}^o \ \rightarrow \ \overline{u}_{\shortparallel} - i \Delta u_{\shortparallel} \ \sin (\omega - \Omega_c/\gamma_0). \tag{3.29}$$

The remaining integration in (3.24) with $\hat{g}_1$ given by (3.17) can be done trivially by integration by parts,

$$
\begin{pmatrix} \widetilde{W}_z(k) \\ \widetilde{W}_r(k) \end{pmatrix} = - Ne^2/m \sum_{n,s} \Big\{ Z_s^2(a_o) \big[- \hat{k}\, \widetilde{E}_z\, \partial/\partial u_{\shortparallel}^o
$$

$$
+ s/a_L^o\, (\widetilde{E}_r\, k_{\shortparallel}/|k_{\perp}|\, \partial/\partial u_{\perp}^o + \widetilde{H}_\theta\, \omega/c\big/|k_{\perp}|\, (u_{\perp}^o/c\gamma_0\, \partial/\partial u_{\shortparallel}^o - u_{\shortparallel}^o/c\gamma_0\, \partial/\partial u_{\perp}^o))\big]
$$

$$
+ s/a_o\, (Z_s^2(a_o))'\, (\widetilde{E}_r\, k_{\shortparallel}/|k_{\perp}| - \widetilde{H}_\theta\, \omega/c\big/|k_{\perp}|\, (u_{\shortparallel}^o/c\gamma_0)\, |k_{\perp}|/\Omega c \Big\}
$$

$$
\begin{pmatrix} -k u_{\shortparallel}^o \\ s\Omega_c k_{\shortparallel}/|k_{\perp}|^2 \end{pmatrix} Z_s^2(a_L^o)/\Omega_s^o(k) \ . \tag{3.25}
$$

Defining

$$
\zeta_1 \equiv Ne^2/mc^2\gamma_0\, Z_s^2(a_L^o)\, Z_s^2(a_o) \tag{3.26}
$$

$$
\zeta_2 \equiv Ne^2/mc^2\gamma_0\, [Z_s^2(a_L^o)\, s/a_o\, (Z_s^2(a_o))' + s/a_L^o\, (Z_s^2(a_L^o))'\, Z_s^2(a_o)],
$$

one can further reduce (3.25) to

$$
1/c \begin{pmatrix} \widetilde{W}_z(k) \\ \widetilde{W}_r(k) \end{pmatrix} = \sum_{n,s} \Big\{ \begin{pmatrix} -\hat{k} u_{\shortparallel}^o \\ s\Omega_c k_{\shortparallel}/|k_{\perp}|^2 \end{pmatrix} \big[- \zeta_1/\Omega_s^{o2}\, (- k\, \widetilde{E}_z\, (\omega/c\, u_{\shortparallel}^o - kc\gamma_0)
$$

$$
+ (\widetilde{E}_r\, k_{\shortparallel} - \widetilde{H}_\theta\, k)\, s\Omega_c\, \omega/c\big/|k_{\perp}|^2
$$

$$
+ \zeta_2/\Omega_s^o\, 1/\Omega_c\, (\widetilde{E}_r\, k_{\shortparallel} c\gamma_0 - \widetilde{H}_\theta\, \omega/c\, u_{\shortparallel}^o)\big]
$$

$$
+ \begin{pmatrix} -\hat{k} \\ o \end{pmatrix} \zeta_1/\Omega_s^o(k)\, (-\hat{k}\, \widetilde{E}_z\, c\gamma_0 + \widetilde{H}_\theta\, s\Omega_c\, \omega/c\big/|k_{\perp}|^2) \ .
$$

$$
\tag{3.27}
$$

Defining the radial integrals as

$$\begin{pmatrix} \overline{I}_1 \\ \overline{I}_2 \end{pmatrix} \equiv \hat{k}^s/2\pi \int_0^{x_1} dx\ Z_0(x) \begin{pmatrix} I_1(x) \\ I_2(x) \end{pmatrix}$$

$$\begin{pmatrix} \overline{I}_3 \\ \overline{I}_4 \end{pmatrix} \equiv \hat{k}^s/2\pi \int_0^{x_1} dx\ Z_1(x) \begin{pmatrix} I_3(x) \\ I_4(x) \end{pmatrix} \tag{3.21}$$

one can write (3.20) with (3.19) as

$$\begin{pmatrix} \widetilde{W}_z(k) \\ \widetilde{W}_r(k) \end{pmatrix} = Ne^2/m \sum_{n,s} \int du_{\shortparallel}\ du_\perp\ u_\perp/u_\perp^o/\Omega_s(k)\ Z_s(a_L)$$

$$\bullet \begin{pmatrix} \hat{k} u_{\shortparallel}\ (\widetilde{F}_H\ \overline{I}_1 - \widetilde{F}_I\ \overline{I}_2) \\ (-\hat{k}\ k_{\shortparallel}/|k_\perp|u_\perp)\ (\widetilde{F}_H\ \overline{I}_3 + \widetilde{F}_I\ \overline{I}_4). \end{pmatrix} \tag{3.22}$$

The radial integrals (3.21) are carried out in Appendix C giving very simple results,

$$\overline{I}_1 = Z_s(a_L)Z_s^2(a_0), \qquad \overline{I}_3 = \hat{k}\ s/a_L\ \overline{I}_1$$

$$\overline{I}_2 = -Z_s(a_L)\ s/a_0\ (Z_s^2(a_0))', \quad \overline{I}_4 = \hat{k}\ s/a_L\ \overline{I}_2 \tag{3.23}$$

and one obtains

$$\begin{pmatrix} \widetilde{W}_z(k) \\ \widetilde{W}_r(k) \end{pmatrix} = -Ne^2/m \sum_{n,s} \int du_{\shortparallel} du_\perp\ u_\perp/u_\perp^o/\Omega_s(k) \begin{pmatrix} -\hat{k}u_{\shortparallel} \\ s\Omega_c\ k_{\shortparallel}/|k_\perp|^2 \end{pmatrix} Z_s^2(a_L)$$

$$(\widetilde{F}_H\ Z_s^2(a_0) + \widetilde{F}_I\ s/a_0\ (Z_s^2(a_0)')) \tag{3.24}$$

where F_H and F_I are given by (3.16).

- 16 -

$$g_1(u_{\shortparallel}, u_\perp) \equiv \delta(u_{\shortparallel} - u_{\shortparallel}^\circ) \ (u_\perp - u_\perp^\circ)$$

$$g_2(\xi) \equiv (\delta(\xi - \xi_0) + \delta(\xi + \xi_0))/a_L \sin\xi_0 \ \Delta(r) \ . \tag{3.17}$$

Defining the following phase angle integrals as

$$\begin{pmatrix} I_1(x) \\ I_2(x) \end{pmatrix} \equiv \int d\xi \ e^{is\psi} \begin{pmatrix} Z_s(a) \ \hat{g}_2 \\ s/a \ Z_s(a) \ \partial\hat{g}_2/\partial a \end{pmatrix} \tag{3.18}$$

$$\begin{pmatrix} I_3(x) \\ I_4(x) \end{pmatrix} \equiv \int d\xi \ 1/i \ \sin\xi \ e^{is\psi} \begin{pmatrix} Z_s(a) \ \hat{g}_2 \\ s/a \ Z_s(a) \ \partial\hat{g}_2/\partial a \end{pmatrix} \ ,$$

one can write (3.15) as

$$\begin{pmatrix} \tilde{J}_z(k) \\ \tilde{J}_r(k) \end{pmatrix} = e^{-i\omega t} \ Ne^2/m \sum_{n,s} |k_\perp|/(2\pi)^2 r \ \hat{k}^{s+1} \int du_{\shortparallel} du_\perp \ u_\perp/u_\perp^\circ/\Omega_s(k) \ Z_s(a_L)$$

$$\begin{pmatrix} -iu_{\shortparallel} \ (\tilde{F}_H \ I_1(x) - \tilde{F}_I \ I_2(x)) \\ u_\perp \ (\tilde{F}_H \ I_3(x) - \tilde{F}_I \ I_4(x)) \end{pmatrix} . \tag{3.19}$$

The integrals in (3.18) are calculated in Appendix B and the remaining integral in (3.19) is trivial, resulting in a rather complicated expression for the induced currents. However, what is interesting to us is the work done by fields on the induced current, given the source terms in the Maxwell equations (2.10).

$$\begin{pmatrix} \tilde{W}_z(k) \\ \tilde{W}_r(k) \end{pmatrix} = \int_0^{r_1} 2\pi r dr \begin{pmatrix} i \ e_z^{(1)}(r) \ e^{i\omega t} \ \tilde{J}_z(k) \\ e_r^{(1)}(r) \ e^{i\omega t} \ \tilde{J}_r(k) \end{pmatrix} \ . \tag{3.20}$$

- 15 -

With $R = (r^2 + r_L^2 - 2rr_L \cos \xi)^{1/2}$, one can consider $g_2(R)$ as a function determining the angle distribution and given by

$$g_2(R) = 1/2\pi r \ (\delta(\xi-\xi_0) + \delta(\xi+\xi_0))/r_L \sin \xi_0 \ \Delta(r) \qquad (3.13)$$

where $\cos \xi_0 \equiv (r^2 + r_L^2 - R_0^2)/2rr_L$ (see Fig. 3.2) and

$$\Delta(r) \equiv \begin{cases} 1 & \text{if } r_- \leq r \leq r_+ \\ 0 & \text{otherwise} \end{cases} \qquad (3.14)$$

$$(r_\pm \equiv R_0 \pm r_L) \ .$$

Putting all of this into (3.10) and understanding that the beam spread effects (both in velocities and guiding center) will be taken into account later (as dictated by (3.11)), one obtains

$$\begin{pmatrix} \tilde{J}_z(n) \\ \tilde{J}_r(k) \end{pmatrix} = -i \ e^{-i\omega t} \ Ne^2/m \sum_{n,s} |k_\perp|/(2\pi)^2 r \ \hat{k}^{s+1} \int du_{\shortparallel} \ du_\perp \ d\xi \ u_\perp/u_\perp^o \hat{/}\Omega_s(k)$$

$$e^{is\psi} \begin{pmatrix} u_{\shortparallel} \\ u_\perp \sin\xi \end{pmatrix} \cdot Z_s(a_L)$$

$$(\tilde{F}_H(k) \ Z_s(a) \ \hat{g}_2 - \tilde{F}_I(k) \ s/a \ Z_s(a) \ \partial\hat{g}_2/\partial a) \qquad (3.15)$$

where

$$\tilde{F}_H(k) \equiv \hat{k}\tilde{E}_z \ \partial g_1/\partial u_{\shortparallel} - s/a_L \ [\tilde{E}_r \ k_{\shortparallel}/|k_\perp| \ \partial\hat{g}_1/\partial u_\perp + \tilde{H}_\theta \ \omega/c/|k_\perp|$$

$$(u_\perp/c\gamma \ \hat{g}_1/\partial u_{\shortparallel} - u_{\shortparallel}/c\gamma \ \partial\hat{g}_1/\partial u_\perp)]$$

$$\tilde{F}_I(k) \equiv \hat{g}_1(\tilde{E}_r \ k_{\shortparallel}/|k_\perp| - \tilde{H}_\theta \ \omega/c/|k_\perp| \ u_{\shortparallel}/c\gamma) \ |k_\perp|/\Omega_c \qquad (3.16)$$

which represents the part for a homogeneous plasma and an inhomogeneity, respectively, and

- 14 -

The induced currents (Laplace transformed) are given by

$$\begin{pmatrix} \tilde{J}_z(k) \\ \tilde{J}_r(k) \end{pmatrix} \equiv - \, Ne \int d^3u \, \begin{pmatrix} u_{\shortparallel}/\gamma \\ u_{\perp}/\gamma \, \sin\xi \end{pmatrix} \tilde{f}_1(k) \qquad (3.10)$$

where N is number of electrons per unit length.

In order to carry out the integral over momentum space, we need to know a more specific form of the beam function f_0. This can be done without making any further assumption, other than f_0 being an arbitrary function of $u_{\shortparallel}$, $u_{\perp}$ and R, by invoking the following identity:

$$f_0(u_{\shortparallel}, u_{\perp}, R) \equiv \int du_{\shortparallel}^{\circ} \, 2\pi \, u_{\perp}^{\circ} \, du_{\perp}^{\circ} \, 2\pi \, R^{\circ} dR^{\circ} \, f_0 \, (u_{\shortparallel}^{\circ}, u_{\perp}^{\circ}, R^{\circ}) \, \hat{f} \, (u_{\shortparallel}, u_{\perp}, R)$$

$$(3.11)$$

with

$$\hat{f}_0 \, (u_{\shortparallel}, u_{\perp}, R) \equiv g_1 \, (u_{\shortparallel}, u_{\perp}) \, g_2(R)$$

$$g_1 \, (u_{\shortparallel}, u_{\perp}) \equiv \delta(u_{\shortparallel} - u_{\shortparallel}^{\circ}) \, 1/2\pi u_{\perp}^{\circ} \, \delta(u_{\perp} - u_{\perp}^{\circ}) \qquad (3.12)$$

$$g_2 \, (R) \equiv 1/2\pi R^{\circ} \, \delta(R - R^{\circ}).$$

Note that $\hat{f}_0$ represents a "cold" beam function with δ- function guiding center distribution and is normalized to be one electron per unit length. Equation (3.11) allows us to include the beam spread effects both in the velocity and the guiding center at the end of the calculation and to concentrate for the moment on the δ- function type of beam function $\hat{f}_0$ without losing any generality.

$$f_1 = e^{-i\omega t} \; e/m \sum_{n,s} \hat{k}^{s+1} \; e^{is\psi} \int_0^z dz'/v_\shortparallel \; e^{i(\omega - s\omega_c)(z'-z)/v_\shortparallel}$$

$$\left\{ \overline{E}_z(z') \partial f_0/\partial u_\shortparallel \; \hat{k} \; Z_s(a_L) \; Z_s(a) \right\}$$

$$- \left[\overline{E}_r(z') \; k_\shortparallel/|k_\perp| \; \partial f_0/\partial u_\perp + \overline{H}_\theta(z') \; \omega/c/|k_\perp| \; (u_\perp/c\gamma \; \partial f_0/\partial u_\shortparallel - u_\shortparallel/c\gamma \; \partial f_0/\partial u_\perp) \right]$$

$$s/a_L \; Z_s(a_L) \; Z_s(a)$$

$$- \left[\overline{E}_r(z') \; k_\shortparallel/|k_\perp| - \overline{H}_\theta(z') \; \omega/c/|k_\perp| \; u_\shortparallel/c\gamma \right] \; |k_\perp|/\Omega_c \; \partial f_0/\partial a \; Z_s(a_L) \; s/a \; Z_s(a) \Big\}$$

$$\equiv e^{-i\omega t} \; e/m \sum_{n,s} \hat{k}^{s+1} \; e^{is\psi} \int_0^z dz' \; G(z-z') \; F(z') \tag{3.5}$$

which shows characteristic hysteresis integral with Green's function

$$G\;(z-z') \equiv 1/v_\shortparallel \; e^{i(\omega - s\omega_c)\;(z-z')/v_\shortparallel} \; . \tag{3.6}$$

The Laplace transformation of (3.5) can be done immediately by invoking the convolution theorem,

$$\tilde{f}_1(k) = e^{-i\omega t} \; e/m \sum_{n,s} \hat{k}^{s+1} \; e^{is\psi} \; \tilde{G}(k) \; \tilde{F}(k) \tag{3.7}$$

with

$$\tilde{G}(k) \quad \int_0^\infty dz \; e^{-ikz} \; 1/v_\shortparallel \; e^{i(\omega - s\omega_c)\; z/v_\shortparallel}$$

$$= i\gamma/\Omega_s(k) \quad : \quad \Omega_s(k) \equiv \omega\gamma - ku_\shortparallel - s\Omega_c \tag{3.8}$$

and

$$\tilde{F}(k) = Z_s(a_L) \; \Big\{ \left[\hat{k} \; \tilde{E}_z(k) \; \partial f_0/\partial u_\shortparallel \right.$$

$$- s/a_L \; (\tilde{E}_r(k) \; k_\shortparallel/|k_\perp| \; \partial f_0/\partial u_\perp + \tilde{H}_\theta \; \omega/c/|k_\perp| \; (u_\perp/c\gamma \; \partial f_0/\partial u_\shortparallel$$

$$\left. - u_\shortparallel/c\gamma \; \partial f_0/\partial u_\perp)) \right] \; Z_s(a)$$

$$- (\tilde{E}_r(k) \; k_\shortparallel/|k_\perp| - \tilde{H}_\theta(k) \; \omega/c/|k_\perp| \; u_\shortparallel/c\gamma) \; |k_\perp|/\Omega_c \; \partial f_0/\partial a$$

$$s/a \; Z_s(a) \Big\} \; . \tag{3.9}$$

GAIN VS. FREQUENCY
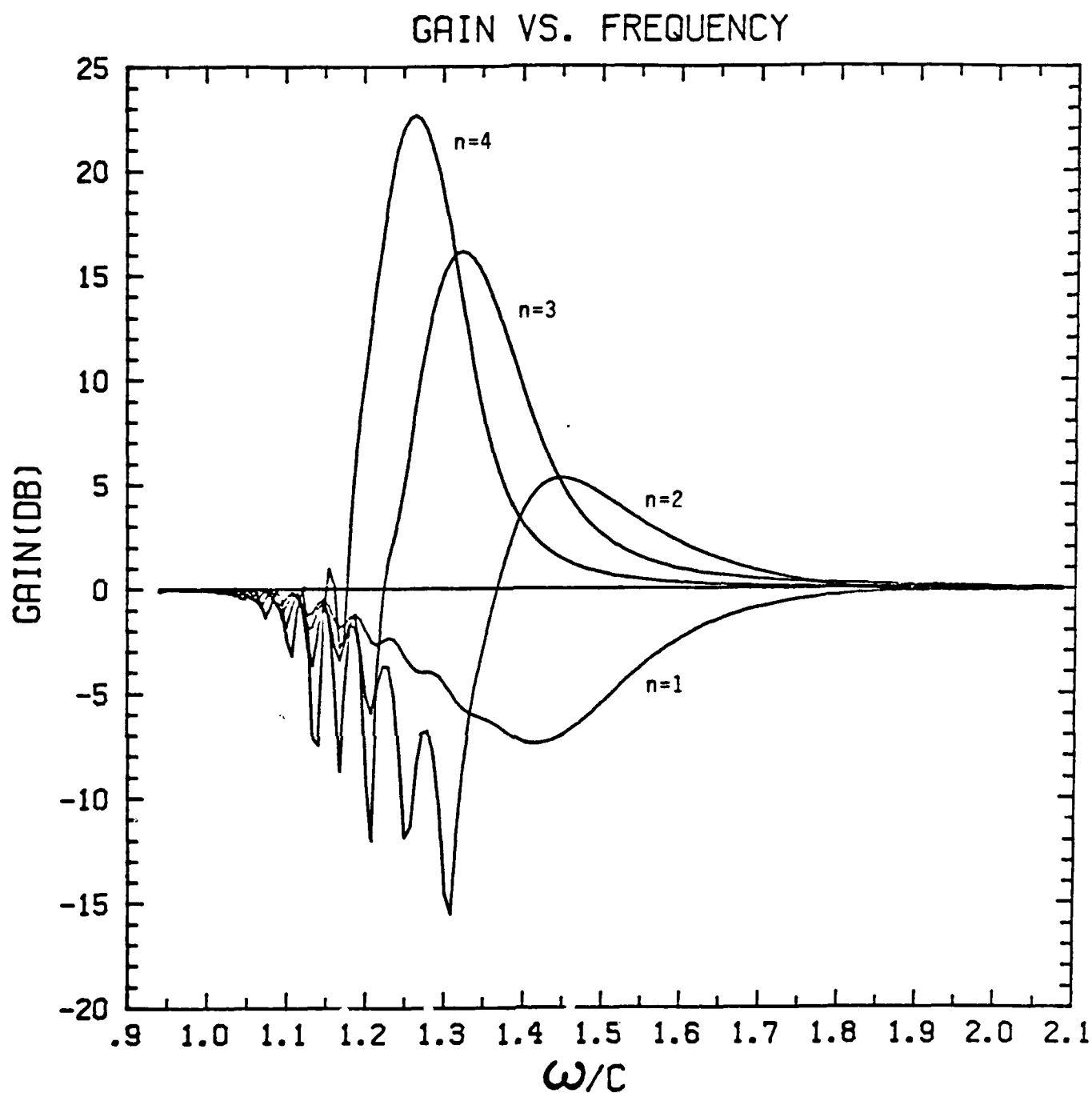
$r_1 = 1.55$ cm	$\epsilon_1 = 1$	$I = 5.2$ Amp.	$\alpha = 2$
$r_2 = 1.75$ cm	$\epsilon_2 = 4.6$	$R_G = 0.72$ cm	$\omega_c/c = 0.75$
$r_3 = 2.033$ cm	$\epsilon_3 = 19.$	$L = 100$ cm	$v_z = 0.17 + (n-1) \times 0.005$
		$s = 1$	$\Delta v_z = 2\%$

FIGURE 5.2

- 26 -
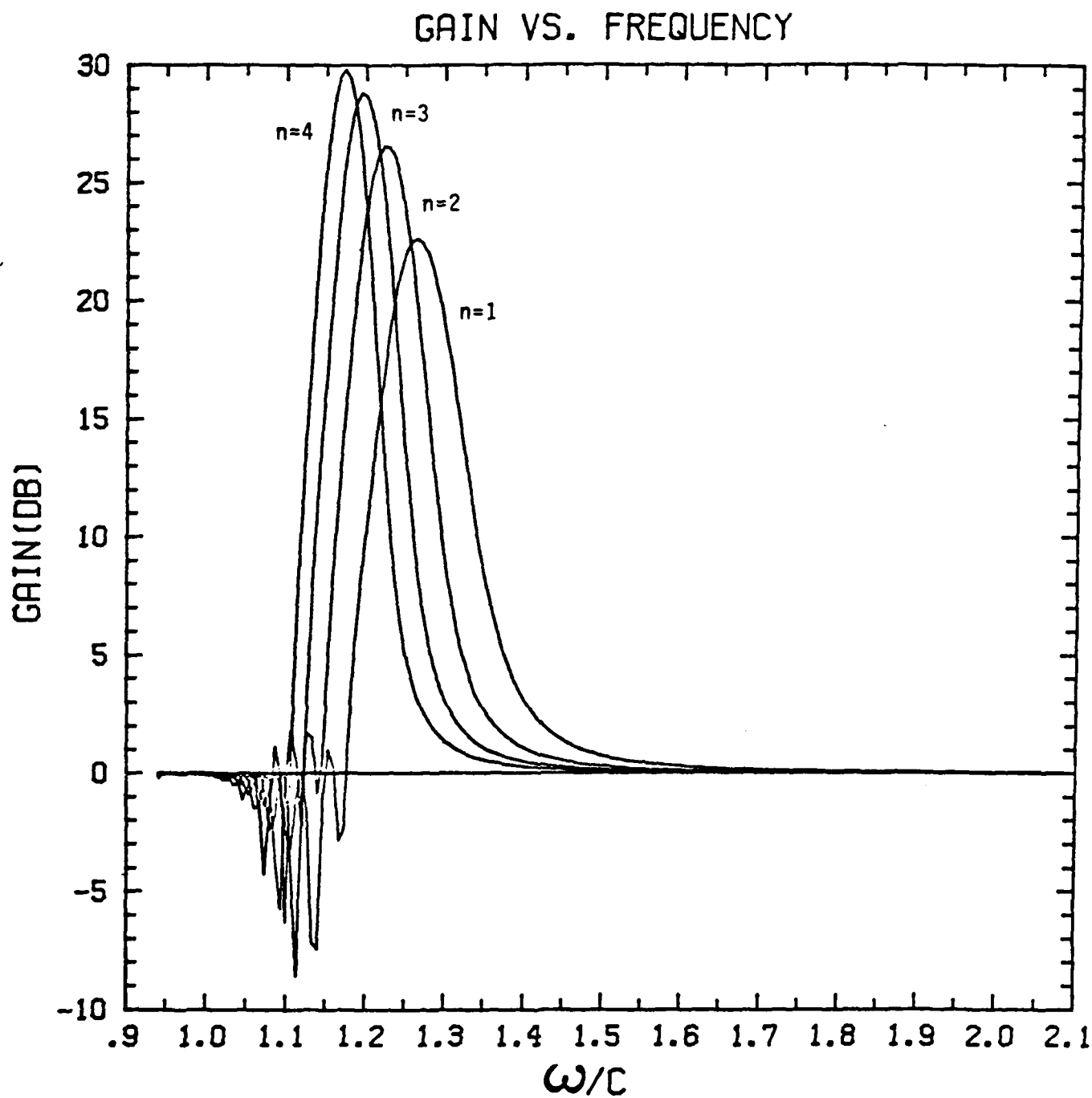
GAIN VS. FREQUENCY

$r_1 = 1.55$ cm $\epsilon_1 = 1$ $I = 5.2$ Amp. $\alpha = 2$

$r_2 = 1.75$ cm $\epsilon_2 = 4.6$ $R_G = 0.72$ cm $\omega_c/c = 0.75$

$r_3 = 2.033$ cm $\epsilon_3 = 19.$ $L = 100$ cm $v_z = 0.185 + (n-1) \times 0.005$

                                        $s = 1$ $\Delta v_z = 2\%$

FIGURE 5.3
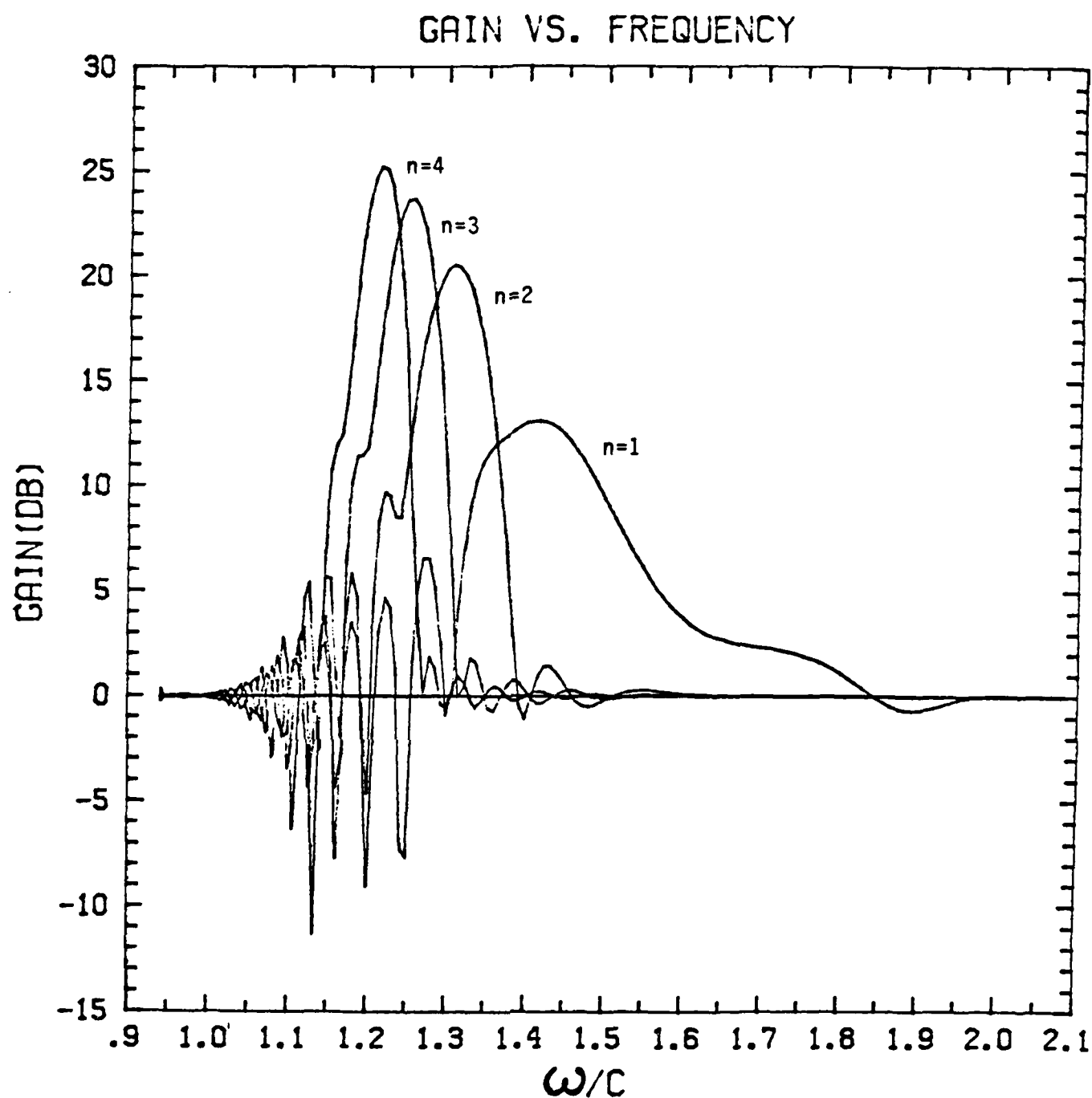
GAIN VS. FREQUENCY

$r_1 = 1.55$ cm	$\epsilon_1 = 1$	$I = 5.2$ Amp.	$\alpha = 2$
$r_2 = 1.75$ cm	$\epsilon_2 = 4.6$	$R_G = 0.72$ cm	$\omega_c/c = 0.75$
$r_3 = 2.033$ cm	$\epsilon_3 = 19.$	$L = 100$ cm	$v_z = 0.185 + (n-1) \times 0.005$
		$s = 1$	$\Delta v_z = 4\%$

FIGURE 5.4

GAIN VS. FREQUENCY
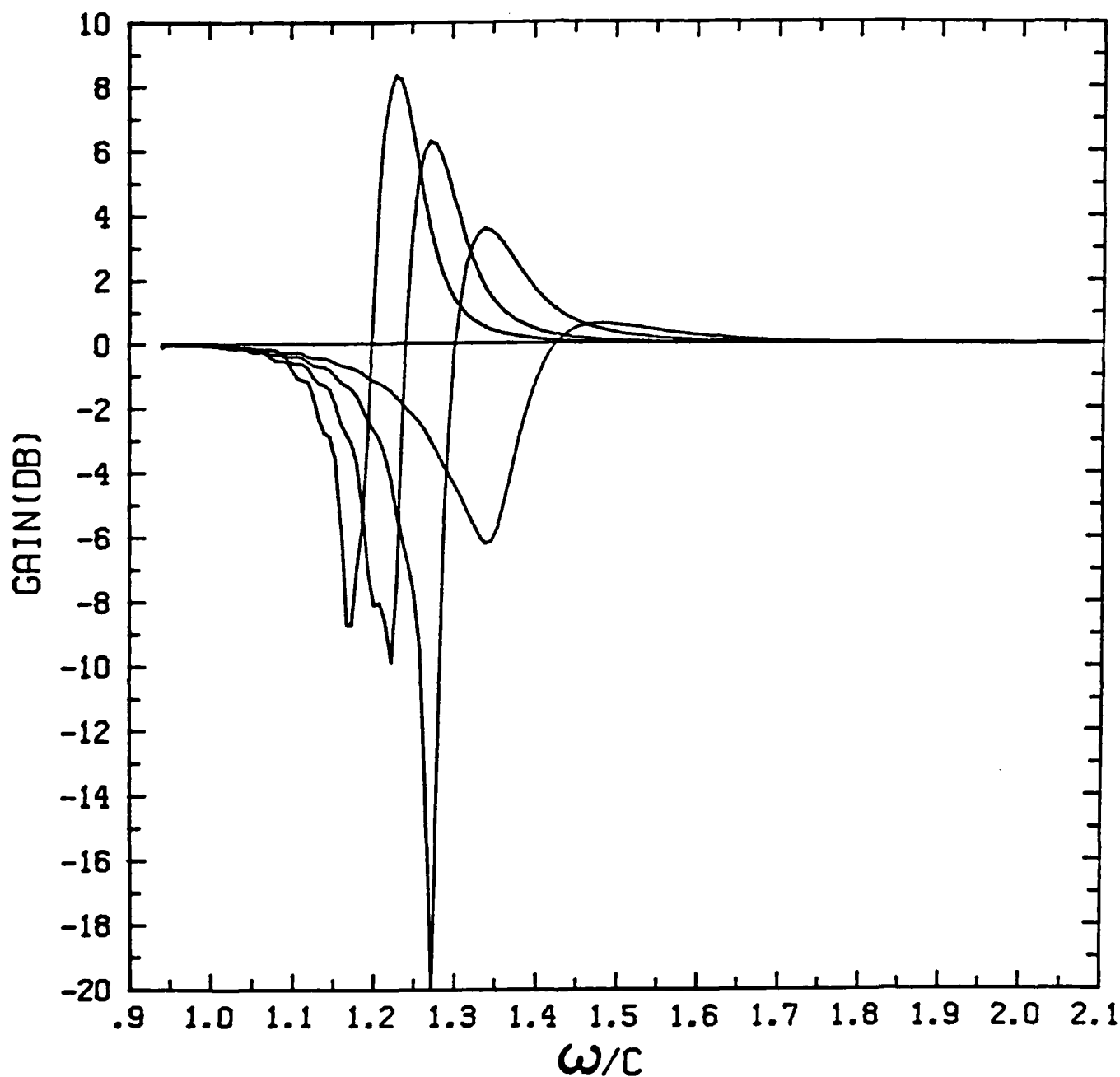
$r_1 = 1.55$ cm	$\epsilon_1 = 1$	$I = 5.2$ Amp.	$\alpha = 2$
$r_2 = 1.75$ cm	$\epsilon_2 = 4.6$	$R_G = 0.72$ cm	$\omega_c/c = 0.75$
$r_3 = 2.033$ cm	$\epsilon_3 = 19.$	$L = 100$ cm	$v_z/c = 0.170 + (n-1) \times .005$
		$s = 1$	$\Delta v_z = 0$

FIGURE 5.5

APPENDIX A

ORTHONORMAL TM$_{on}$ RADIAL EIGENMODES

We will derive here a complete set of orthonormal TM$_{on}$ radial eigenmodes in a waveguide loaded with an arbitrary number of concentric dielectric layers as in Fig. 1. (For more general and detailed treatment, see Ref. 1.)

For azimuthally symmetric modes ($\partial/\partial\theta = 0$), the sourceless Maxwell's equations in a linear dielectric medium ($\vec{D} = \epsilon\vec{E}$, $\vec{B} = \mu\vec{H}$, $\nabla \times \vec{E} = -\mu/c \, \partial H/\partial t$ and $\nabla \times \vec{H} = \epsilon/C \, \partial E/\partial t$), form a closed set of equations for E_z, E_r, H_θ;

$$\partial E_r/\partial z - \partial E_z/\partial r = -\mu/c \, \partial H_\theta/\partial t$$
$$-\partial H_\theta/\partial z = \epsilon/c \, \partial E_r/\partial t \tag{A.1}$$
$$1/r \, \partial/\partial r(rH_\theta) = \epsilon/c \, \partial E_z/\partial t \ .$$

Due to the cylindrical symmetry of the system, one can write the fields (stationary in time) as

$$E_z(r,z,t) = e^{-i\omega t} \, e^{ik_u z} \, e_z(r)$$

$$E_r(r,z,t) = i \, e^{-i\omega t} \, e^{ik_u z} \, e_r(r) \tag{A.2}$$

$$H_\theta(r,z,t) = i \, e^{-i\omega t} \, e^{ik_u z} \, h_\theta(r).$$

Substituting (A.2) into (A.1), one obtains a set of radial equations ($' \equiv d/dr$),

$$k_u e_r + e_z' = \mu \, \omega/c \, h_\theta \tag{A.3a}$$

$$k_u h_\theta = \epsilon \, \omega/c \, e_r \tag{A.3b}$$

$$1/r \, (rh_\theta)' + \epsilon \, \omega/c \, e_z = 0. \tag{A.3c}$$

Using (A.3b) one can eliminate e_r in (A.3a), to obtain

$$k_\perp^2 h_\theta = \epsilon \omega/c \; e_z'$$
$$(k_\perp^2 \equiv \epsilon \mu \, \omega^2/c^2 - k_{||}^2). \tag{A.4}$$

From (A.3c) and (A.4), one obtains, by eliminating h_θ,

$$1/r \; (r e_z')' + k_\perp^2 e_z = 0 \tag{A.5}$$

or, by eliminating e_z,

$$(1/r \; (r h_\theta)')' + k_\perp^2 h_\theta = 0. \tag{A.6}$$

Radial Eigenmodes

The solution of (A.5) is given in terms of the Bessel functions of order 0

$$e_z = A \, Z_0 \, (|k_\perp|r) + \overline{A} \, \overline{Z}_0 \, (|k_\perp|r) \tag{A.7}$$

and the solution of (A.6) is given in terms of the Bessel function of order 1,

$$h_\theta = B \, Z_1 \, (|k_\perp|r) + \overline{B} \, \overline{Z}_1 \, (|k_\perp|r) \tag{A.8}$$

where

$$Z_\ell(x) \equiv \begin{cases} J_\ell(x) \\ I_\ell(x) \end{cases}, \quad \overline{Z}_\ell(x) \equiv \begin{cases} Y_\ell(x) & \text{if } k_\perp^2 > 0 \\ K_\ell(x) & \text{if } k_\perp^2 < 0. \end{cases}$$

Of course, due to (A.4), the arbitrary constants (field coefficients) $(A, \overline{A})$ and $(B, \overline{B})$ are related to each other by

$$B = - \hat{k} \; \epsilon \omega/c \Big/ |k_\perp| \; A, \quad \overline{B} = - \epsilon \omega/c \Big/ |k_\perp| \; \overline{A} \tag{A.9}$$

since

$$Z_0'(x) = - \hat{k} \, Z_1(x)$$
$$\overline{Z}_0'(x) = - \overline{Z}_1(x)$$

$$(\hat{k} \equiv k_\perp^2/|k|_\perp^2).$$

Therefore, fields in a dielectric medfum are completely specified by two arbitrary constants $(A, \overline{A})$ - the field coefficients. The field coefficients in one dielectric layer and in another dielectric layer are related to each other by the boundary condition that e_z and h_θ be continuous. This can be shown as follows.

By defining

$$F(r) \equiv \begin{pmatrix} e_z(r) \\ h_\theta(r) \end{pmatrix} \qquad V \equiv \begin{pmatrix} A \\ \overline{A} \end{pmatrix}$$

$$M(r) \equiv \begin{pmatrix} Z_0(|k_\perp|r) & \overline{Z}_0(|k_\perp|r) \\ -\hat{k}\,\epsilon\,\omega/c/|k_\perp|\, Z_1(|k_\perp|r) & -\epsilon\,\omega/c/|k_\perp|\, \overline{Z}_1(|k_\perp|r) \end{pmatrix},$$

one can write (A.7) and (A.8) with (A.9) as in compact vector form as

$$F(r) = M(r)V. \tag{A.10}$$

Consider this relation in the i-th region and the i+1-st region,

$$F^{(i)}(r) = M^{(i)}(r)V^{(i)}$$

$$F^{(i+1)}(r) = M^{(i+1)}(r)\, V^{(i+1)}.$$

At the boundary $r = r_i$, $F^{(i)}(r_i) = F^{(i+1)}(r_i)$ and therefore one obtains the connection formula

$$V^{(i+1)} = S^{(i+1,i)}(r_i)\, V^{(i)} \tag{A.11}$$

with transfer matrix

$$S^{(i+1,i)}(r_i) \equiv (M^{(i+1)}(r_i))^{-1}\, M^{(i)}(r_i).$$

By applying (A.11) successively, one can express field coefficients in any dielectric layer in terms of the field coefficients in a particular dielectric region (for example, in the innermost region).

Actually, one can prove that the transfer matrices S form a transformation group in a discrete vector space V.

In the innermost region, fields must be finite at the origin (regularity condition) and therefore

$$v(1) = C\begin{pmatrix} 1 \\ 0 \end{pmatrix}. \qquad (A.12)$$

By applying (A.11) successively, one can find the field coefficients $v^{(N)}$ in the outermost region by

$$v(N) = S^{(N,1)}v(1) \qquad (A.13)$$

where

$$S^{(N,1)} \equiv S^{(N,N-1)}(r_{N-1})...S^{(2,1)}(r_1).$$

In the outermost region, the fields must satisfy the boundary condition that $e_z^{(N)}$ must vanish on the conducting wall at $r = r_N$;

$$e_z^{(N)}(r_N) \equiv A^{(N)}Z_0(|k_{\perp}^{(N)}|r_N) + \overline{A}^{(N)}\overline{Z}_0(|k_{\perp}^{(N)}|r_N) = 0$$

which can also be written in vector form as

$$P^{(N)\dagger} \cdot v(N) = 0 \qquad (A.14)$$

where

$$P^{(N)} = \begin{pmatrix} Z_0^{(N)}(|k_{\perp}^{(N)}|r) \\ \overline{Z}_0^{(N)}(|k_{\perp}^{(N)}|r) \end{pmatrix}.$$

Combining (A.12) - (A.14), one obtains a dispersion relation

$$P^{(N)\dagger} \cdot S^{(N,1)} \cdot v(1) = 0, \qquad (A.15)$$

which gives an eigenvalue condition on $k_{\shortparallel}$ for a given ω. The solutions of (A.15) for $k_{\shortparallel}$ form a discrete set of radial eigenmodes characterized by $k_{\shortparallel,n}$ or simply n. Having found the radial eigenvalue, the fields in all the dielectric layers are completely determined up to an overall normalization constant C.

Orthonormality

Let us now prove the orthogonality between two different radial eigenmodes and obtain the appropriate normalization constant for a given mode. This is an essential step in projecting out the correct TM_{on}-component field radiated from a radially localized source when we introduce an electron beam as in the text. Denoting the radial eigenmode by subscripts n and n', (A.6) reads, in the i-th dielectric region,

$$(1/r(rh_{\theta,n})')' + k_{\perp,n}^2 h_{\theta,n} = 0 \; ; \; k_{\perp,n}^2 \equiv \epsilon_i \mu_i \omega^2/C^2 - k_{\shortparallel,n}^2 \qquad (A.16)$$

$$(1/r(rh_{\theta,n'})')' + k_{\perp,n'}^2 h_{\theta,n'} = 0 \; ; \; k_{\perp,n'}^2 \equiv \epsilon_i \mu_i \omega^2/C^2 - k_{\shortparallel,n'}^2 .$$

(For notational simplicity, we have dropped the superscript i indicating the dielectric region on h_θ and $k_\perp$.) Multiplying (A.16) by $h_{\theta,n'}$ and $h_{\theta,n}$, respectively, subtracting one from the other and integrating over the dielectric region, $\int_{r_{i-1}}^{r_i} r dr$, one obtains

$$0 = \int_{r_{i-1}}^{r_i} dr \left\{ [rh_{\theta,n'}(1/r(rh_{\theta,n})')' - rh_{\theta,n}(1/r(rh_{\theta,n'}))'] \right.$$

$$\left. + (k_{\perp,n}^2 - k_{\perp,n'}^2)rh_{\theta,n'} h_{\theta,n} \right\}$$

$$= [h_{\theta,n'}(rh_{\theta,n})' - h_{\theta,n}(rh_{\theta,n'})']\Big|_{r_{i-1}}^{r_i} + (k_{\shortparallel,n'}^2 - k_{\shortparallel,n}^2) \times$$

$$\int_{r_{i-1}}^{r_i} r dr\, h_{\theta,n'} h_{\theta,n}$$

and, upon using (A.3c),

$$(k_{\shortparallel,n'}^2 - k_{\shortparallel,n}^2)\int_{r_{i-1}}^{r_i} r dr\, h_{\theta,n'} h_{\theta,n}/\epsilon_i = \omega/C\ [r(h_{\theta,n'}e_{z,n} -$$

$$h_{\theta,n}e_{z,n'})]\Big|_{r_{i-1}}^{r_i} . \qquad (A.17)$$

Now one can add expressions similar to (A.17) from all the dielectric regions. Note that the terms in the right-hand sides cancel out at the boundaries between dielectrics (because both h_θ and e_z are continuous) and vanish at the origin and on the conducting wall.

Thus one obtains

$$(k_{\shortmid\shortmid,n'}^2 - k_{\shortmid\shortmid,n}^2) \sum_{i=1}^{N} \int_{r_{i-1}}^{r_i} r dr \, h_{\theta,n'}^{(i)} \, h_{\theta,n}^{(i)}/\epsilon_i = 0 \qquad (A.18)$$

which is the desired relation.

If $k_{\shortmid\shortmid,n'}^2 \neq k_{\shortmid\shortmid,n}^2$, i.e., $n' \neq n$, (A.18) gives the orthogonality relation

$$\sum_{i=1}^{N} \int_{r_{i-1}}^{r_i} r dr \, h_{\theta,n'}^{(i)} \, h_{\theta,n}^{(i)}/\epsilon_i = 0 \qquad (A.19)$$

and, for $r' = n$, the field $h_{\theta,n}$ has a normalization factor

$$C_n \sum_{i=1}^{N} \int_{r_{i-1}}^{r_i} r dr \, h_{\theta,n}^{(i)2}/\epsilon_i. \qquad (A.20)$$

The physical meaning of this normalization constant C_n becomes more clear if one writes it as, using (A.3b),

$$C_n = \omega/c/k_{\shortmid\shortmid} \sum_{i=1}^{N} \int_{r_{i-1}}^{r_i} r dr \, h_{\theta,n}^{(i)} \, e_{r,n}^{(i)} \qquad (A.21)$$

which is nothing more than a quantity proportional to the total power flux of the entire waveguide, $S_z = \int 2\pi r dr \, R_e \, (c/8\pi E_r \, H_\theta^*) = c/4 \sum_{i=1}^{N} \int_{r_{i-1}}^{r_i} r dr \, e_{r,n}^{(i)} \, h_{\theta,n}^{(i)}$, that is,

$$C_n = 4/c \, \omega/c/k_{\shortmid\shortmid} S_{z,n}. \qquad (A.22)$$

APPENDIX B

ANGLE INTEGRALS

The angle integral defined by (3.12) can be calculated straightforwardly
by using Graf's addition theorem (3.4) for expanding and recombining
Bessel functions.

$$I_1(x) \equiv \int d\xi \; e^{is\psi} \, Z_s(a) \, \hat{g}_2(\xi) \quad [\hat{g}_2(\xi) \equiv (\delta(\xi-\xi_0) + \delta(\xi+\xi_0))/a_L \sin\xi_0 \, \Delta(x)]$$

$$= \sum_{s'} \hat{k}^{s'} \, Z_{s'+s}(a_L) \, Z_{s'}(x) \int d\xi e^{is'\xi} \, \hat{g}_2(\xi)$$

$$= 2\Delta/a_L \, \sin\xi_0 \sum_{s'} \hat{k}^{s'} \, Z_{s'+s}(a_L) \, Z_{s'}(x) \, \cos s'\xi_0$$

$$= Z_s(a_0) \, O_s(x) \quad [O_s(x) \equiv 2\Delta/a_L \sin\xi_0 \cos s\psi_0] \, . \tag{B.1}$$

Similarly,

$$I_3(x) \equiv \int d\xi \; 1/i \; \sin\xi \; e^{is\psi} \quad Z_s(a) \, \hat{g}_2(\xi)$$
$$= Z_s(a_0) \, S_s(x) \; ; \; S_s(x) \equiv 2_0/a_L \, \sin s\psi_0 \, . \tag{B.2}$$

For $I_2(x)$ and $I_4(x)$, note that

$$s/a \, Z_s(a) = 1/2 \, (Z_{s-1}(a) + \hat{k} \, Z_{s+1}(a))$$

and

$$a = (x^2 + a_L^2 - 2xa_L \cos\xi)^{1/2}$$

$$e^{\pm i\psi} \, \partial\hat{g}_2/\partial a = \partial\hat{g}_2/\partial a_L \pm i/a_L \, \partial\hat{g}_2/\partial\xi \, .$$

$$I_2(x) \equiv \int d\xi \, e^{is\psi} \, s/a \, Z_s(a) \, \partial\hat{g}_2/\partial a$$

$$= \int d\xi \, i/2 \, (e^{i(s-1)\psi} \, Z_{s-1}(a) e^{i\psi} \, \partial\hat{g}_2/\partial a + \hat{k} \, e^{i(s+1)\psi}$$

$$Z_{s+1}(a) \, e^{-i\psi} \, \partial\hat{g}_2/\partial a)$$

$$\equiv \quad 1/2 \, (I_2^-(x) + \hat{k} \, I_2^+(x)) \tag{B.3}$$

where

$$I_2^-(x) \quad \equiv \quad \int d\xi \, e^{i(s-1)\psi} \, Z_{s-1}(a) \, e^{i\psi} \, \partial\hat{g}_2/\partial a$$

$$= \sum_{s'} \hat{k}^{s'} \, Z_{s'+s-1}(a_L) \, Z_{s'}(x) \int d\xi \, e^{is'\xi} \, (\partial\hat{g}_2/\partial a_L + i/a_L \, \partial\hat{g}_2/\partial\xi)$$

$$= \sum_{s'} \hat{k}^{s'} \, Z_{s'+s+1}(a_L) \, Z_{s'}(x) \, (\partial/\partial a_L + s'/a_L) \, 2\Delta/(a_L \sin\xi_0) \cos s'\xi_0$$

$$= \hat{k} \, 2\Delta/(a_L \sin\xi_0) \, Z_s(a_0) \cos s\psi_0 + (\partial/\partial a_L - (s-1)/a_L) \, 2\Delta/(a_L \sin\xi_0)$$

$$Z_{s-1}(a_0) \, \cos(s-1)\psi_0$$

$$= \hat{k} \, Z_s(a_0) \, O_s(x) + Z_{s-1}(a_0) \, (\partial/\partial a_L - (s-1)/a_L) \, O_{s-1}(x)$$

$$\tag{B.4}$$

and similarly

$$I_2^+(x) \quad \equiv \int d\xi \, e^{i(s+1)\psi} \, Z_{s+1}(a) \, e^{-i\psi} \, \partial\hat{g}_2/\partial a \tag{B.5}$$

$$= - Z_s(a_0) \, O_s(x) + Z_{s+1}(a_0) \, (\partial/\partial a_L + (s+1)/a_L) \, O_{s+1}(x) .$$

Substituting (B.4) and (B.5) into (B.3), one obtains

$$I_2(x) = 1/2 \, [Z_{s-1}(a_0) \, (\partial/\partial a_L - (s-1)/a_L) \, O_{s-1}(x) + \hat{k} \, Z_{s+1}(a_0)$$

$$(\partial/\partial a_L + (s+1)/a_L) \, O_{s+1}(x)] . \tag{B.6}$$

Likewise,

$$I_4(x) \equiv \int d\xi \, 1/i \, \sin\xi \, e^{is\psi} \, s/a \, Z_s(a) \, \partial\hat{g}_2/\partial a$$

$$= 1/2 \, (I_4^-(x) + \hat{k} \, I_4^+(x)) \tag{B.7}$$

where

$$I_4^-(x) \equiv \int d\xi \; 1/i \; \sin\xi \; e^{i(s-1)\psi} \; Z_{s-1}(a) \; e^{i\psi}\partial\hat{g}_2/\partial a$$

$$= \sum_{s'} \hat{k}^{s'} \; Z_{s'+s-1}(a_L) \; Z_{s'}(x') \int d\xi \; 1/i \; \sin\xi \; e^{is\xi} \; (\partial\hat{g}_2/\partial a_L + i/a_L \; \partial\hat{g}_2/\partial \xi)$$

$$= \sum_{s'} \hat{k}^{s'} \; Z_{s'+s-1}(a_L) \; Z_{s'}(x') \; [(\partial/\partial a_L + s'/a_L) \; 2\Delta/a_L \; \sin s'\xi_0$$

$$- 1/a_L \; 2\Delta\cos\xi_0/(a_L \sin\xi_0) \; \cos s'\xi_0]$$

$$= \hat{k} \; 2\Delta/a_L \; Z_s(a_0) \; \sin s\psi_0 + (\partial/\partial a_L - (s-1)/a_L) \; 2\Delta/a_L \; Z_{s-1}(a_0) \; \sin (s-1)\psi_0$$

$$- 1/a_L \; 2\Delta\cos\xi_0/(a_L \sin\xi_0) \; Z_{s-1}(a_0) \; \cos (s-1)\psi_0$$

$$= \hat{k} \; Z_s(a_0) \; S_s(x) + Z_{s-1}(a_0) \; [(\partial/\partial a_L - (s-1)/a_L) \; S_{s-1}(x) - 1/a_L \; C_{s-1}(x)]$$

$$\text{(B.8)}$$

with $C_s(x) \equiv 2\Delta\cos\xi_0/(a_L \sin\xi_0) \; \cos s\psi_0$ and

$$I_4^+(x) \equiv \int d\xi \; 1/i \; \sin\xi \; e^{i(s+1)\psi} \; Z_{s+1}(a) \; e^{-i\psi}\partial\hat{g}_2/\partial a$$

$$= - Z_s(a_0) \; S_s(x) + Z_{s+1}(a_0) \; [(\partial/\partial a_L + (s+1)/a_L) \; S_{s+1}(x) + 1/a_L \; C_{s+1}(x)] \; .$$

$$\text{(B.9)}$$

With (B.8) and (B.9), (B.7) gives

$$I_4(x) = 1/2 \; [Z_{s+1}(a_0) \; ((\partial/\partial a_L - (s-1)/a_L) \; S_{s-1}(x) - 1/a_L \; C_{s-1}(x))$$

$$+ \hat{k} \; Z_{s+1}(a_0) \; ((\partial/\partial a_L + (s+1)/a_L) \; S_{s+1}(x) + 1/a_L \; C_{s+1}(x))] \; .$$

$$\text{(B.10)}$$

APPENDIX C

RADIAL INTEGRALS

For radial integration, note that

$$x = (a_0^2 + a_L^2 - 2a_0 a_L \cos\psi_0)^{1/2} \; ;$$

$$dx = 1/x \; a_0 a_L \sin\psi_0 \; d\psi_0 = a_L \sin\xi_0 \; d\psi_0 \; .$$

Define

$$\overline{O}_s \equiv 1/2\pi \int dx \; Z_0(x) \; O_s(x) \quad [O_s(x) \equiv 2\Delta(x)/(a_L \sin\xi_0)]$$

$$= 1/2\pi \int_{x-}^{x+} dx/(a_L \sin\xi_0) Z_0(x) \; 2 \cos s\psi_0$$

$$= \sum_{s'} \hat{k}^{s'} Z_{s'}(a_L) \; Z_{s'}(a_0) \; 1/2\pi \int_0^\pi d\psi_0 \; 2 \cos s'\psi_0 \cos s\psi_0$$

$$= \hat{k}^s \; Z_s(a_L) \; Z_s(a_0) \tag{C.1}$$

where the relation $Z_{-\ell}(x) = (-\hat{k})^\ell Z_\ell(x)$ was used.

Also,

$$\overline{S}_s \equiv 1/2\pi \int dx \; Z_1(x) S_s(x) \; [S_s(x) \equiv 2\Delta(x)/a_L \sin s\psi_0]$$

$$= 1/2\pi \int_{x-}^{x+} dx/(a_L \sin\xi_0) Z_1(x) \sin\xi_0 \; 2 \sin s\psi_0$$

$$= \sum_s \hat{k}^{s'} Z_{s'+1}(a_L) \; Z_{s'}(a_0) \; 1/2\pi \int_0^\pi d\psi_0 \; 2 \sin s'\psi_0 \sin s\psi_0$$

$$= \hat{k}^{s+1} \; s/a_L \; Z_s(a_L) \; Z_s(a_0) \tag{C.2}$$

and

$$\overline{C}_s \equiv 1/2\pi \int dx \; Z_1(x) C_s(x) \; [C_s(x) \equiv 2\Delta\cos\xi_0/(a_L \sin\xi_0) \cos s\psi_0]$$

$$= 1/2\pi \int_{x-}^{x+} dx/(a_L \sin\xi_0) Z_1(x) \cos\xi_0 \; 2 \cos s\psi_0$$
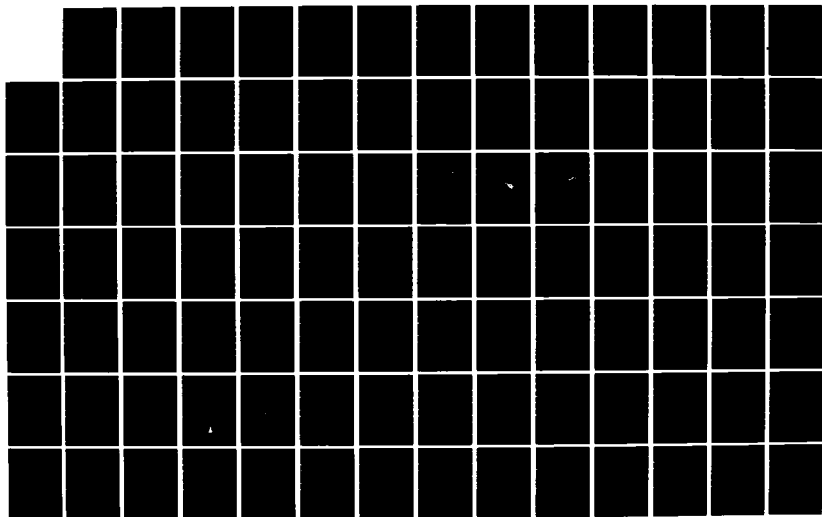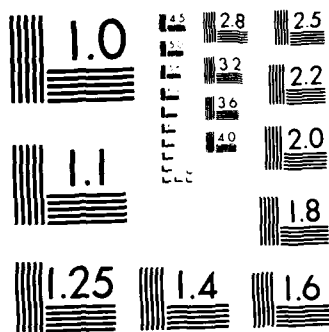
MICROCOPY RESOLUTION TEST CHART

NATIONAL BUREAU OF STANDARDS 1963-A

$$= \sum_{s'} \hat{k}^{s'} Z_{s'+1}(a_L) Z_{s'}(a_0) \, 1/2\pi \int_0^\pi d\psi_0 \, 2 \cos s'\psi_0 \cos s\psi_0$$

$$= -\hat{k}^{s+1} Z_{s'}(a_L) Z_s(a_0) \tag{C.3}$$

With these, one can easily carry out the radial integrals. From (B.1) and (B.2),

$$\overline{T}_1 \equiv \hat{k}^s/2\pi \int dx \, Z_0(x) \, I_1(x)$$

$$= \hat{k}^s Z_s(a_0) \, \overline{0}_s$$

$$= Z_s^2(a_0) Z_s(a_L) \tag{C.4}$$

and

$$T_3 \equiv \hat{k}^s/2\pi \int dx \, Z_1(x) I_3(x)$$

$$= \hat{k}^s Z_s(a) \, \overline{S}_s$$

$$= \hat{k} Z_s^2(a_0) \, s/a_L Z_s(a_L) \; = \; \hat{k} \, s/a_L \, \overline{T}_1. \tag{C.5}$$

For $\overline{T}_2$ and $\overline{T}_4$, using the recursion relations

$$(\partial/\partial a_L - (s-1)/a_L) \, Z_{s-1}(a_L) = -k \, Z_s(a_L)$$

$$(\partial/\partial a_L - (s+1)/a_L) \, Z_{s+1}(a_L) = Z_s(a_L) \; ,$$

one can easily show that

$$T_2 = k^s/2\pi \int dx \, Z_0(x) \, I_2(x)$$

$$= k^s/2 \left\{ Z_{s-1}(a_0) \, (\partial/\partial a_L - (s-1)/a_L) \, \overline{0}_{s-1} + \hat{k} \, Z_{s+1}(a_0) \right.$$

$$\left. (\partial/\partial a_L + (s+1)/a_L) \, \overline{0}_{s+1} \right\}$$

$$= - \, 1/2 \, (Z_{s-1}^2(a_0) - Z_{s+1}^2(a_0)) \, Z_s(a_L)$$

$$= - \, s/a_0 \, (Z_s^2(a_0))' \, Z_s(a_L) \tag{C.6}$$

and

$$\overline{T}_4 \equiv \hat{k}^s/2\pi \int dx \; Z_1(x) \; I_4(x)$$

$$= \hat{k}^s/2 \quad \left\{ Z_{s-1}(a_0) \; [(\partial/\partial a_L - (s-1)/a_L) \; \overline{S}_{s-1} - 1/a_L \; \overline{C}_{s-1}] \right.$$

$$\left. + \hat{k} \; Z_{s+1}(a_0) \; [(\partial/\partial a_L + (s+1)/a_L) \; \overline{S}_{s+1} + 1/a_L \; \overline{C}_{s+1}] \right\}$$

$$= - \hat{k}/2 \; (Z^2_{s-1}(a_0) - Z^2_{s+1}(a_0)) \; s/a_L \; Z_s(a_L)$$

$$= \hat{k} \; s/a_L \; \overline{T}_2 \; . \qquad\qquad\qquad (C.7)$$

Invited paper

Theory of a slow wave cyclotron amplifier

K. R. CHU†, A. K. GANGULY†, V. L. GRANATSTEIN†,
J. L. HIRSHFIELD‡, S. Y. PARK§ and J. M. BAIRD§

A new type of travelling wave amplifier is proposed which features a slow wave structure and wide bandwidth operation. It is based on the cyclotron interaction between a slow electromagnetic wave and helically moving electrons. Gain and bandwidths are calculated including the effect of beam velocity spread. It is shown that a bandwidth as high as 50% could be achieved with beam velocity spread $\leq 1\%$.

1. Introduction

We report the concept of a slow wave cyclotron amplifier (SWCA) based on the cyclotron interaction of a slow electromagnetic wave and a stream of helically moving electrons. The SWCA has the potential of wideband and high power operation at millimetre wavelength. As in typical microwave devices, the basic mechanism for radiation is electron bunching under the influence of the RF field. In the case of SWCA electron bunching is caused by the $\mathbf{v}_\perp \times \mathbf{B}_\perp$ Lorentz force, where $\mathbf{v}_\perp$ is the electron velocity and $\mathbf{B}_\perp$ is the magnetic component of the wave field, both transverse to the applied magnetic field. This mechanism is qualitatively different from the cyclotron maser mechanism involved in the gyrotron travelling wave amplifier (Gyro-TWA). A detailed comparison of the present mechanism and the cyclotron maser mechanism can be found in Chu and Hirshfield (1978). The potential use of the $\mathbf{v}_\perp \times \mathbf{B}_\perp$ bunching mechanism for high frequency wave radiation has been suggested and analysed by Hirshfield et al. (1978).

Before proceeding with the analysis, it is instructive to compare the SWCA with two other microwave devices—the Gyro-TWA and the travelling wave tube (TWT). The TWT (Pierce 1950) employs a longitudinal bunching mechanism driven by the axial electric field (E_z) of a slow wave structure such as the helix. The radiation energy in this device is derived from the electron streaming velocity v_z and no cyclotron resonance is involved. In contrast, both the Gyro-TWA (Granatstein et al. 1980, Barnett et al. 1980, Symons et al. 1981) and the SWCA depend on the free energy which resides in the transverse electron velocity, $\mathbf{v}_\perp$. These two devices are similar because they both extract energy from the beam through electron interactions with the transverse component of electric field, $E_\perp$: and they both radiate at the Doppler shifted electron cyclotron frequency or a harmonic. As described above (also in § 3) the difference between the two devices is in the mechanism

---

	SWCA	Gyro-TWA	TWT
Wave type	Slow wave	Fast wave	Slow wave
Condition of operation	$\omega - k_z v_z - s\Omega_c \lesssim 0$	$\omega - k_z v_z - s\Omega_c \gtrsim 0$	$\omega - k_z v_z \lesssim 0$
Cyclotron resonance	Present	Present	Absent
Field responsible for electron bunching	$B_\perp$	$E_\perp$	E_z
Field responsible for energy extraction	$E_\perp$	$E_\perp$	E_z
Nature of bunching mechanism	Non-relativistic	Relativistic	Non-relativistic
Free energy	$v_\perp$	$v_\perp$	v_z

Table 1.   Comparison of SWCA with Gyro-TWA and TWT.

which produces the phase bunching.   The principal advantage of the cyclotron resonance devices over the TWT is that the dimensions of the interaction structures permit much higher power outputs to be obtained at shorter wavelengths.   The above comparison is summarized in Table 1.

Preliminary results of our studies have been reported in several conference proceedings (Chu *et al.* 1978, Sprangle *et al.* 1979, Baird *et al.* 1980, Keren *et al.* 1980).   In this paper, we present a more complete theory of the SWCA. In § 2, a particular slow wave circuit—the dielectric loaded waveguide—is examined.   In §§ 3 and 4, the dispersion relation of the SWCA is derived and analysed.   On the basis of which a proof-of-principle experiment has been designed.   Finally, § 5 contains a summary of the present work and a brief review of related work.

2. Properties of the dielectric loaded waveguide

The beam-wave cyclotron resonance condition is given by

$$\omega - k_z v_z - s\Omega_c \simeq 0 \tag{1}$$

where ω is the wave frequency, k_z is the wave number, v_z is the beam axial velocity, s is the cyclotron harmonic number, and Ω_c is the electron cyclotron frequency.   Wide bandwidth operation requires that (1) holds over a broad range of frequencies.   Differentiating (1) with respect to k_z gives

$$\frac{d\omega}{dk_z} = v_z \tag{2}$$

Hence a wide band circuit is one whose group velocity $(d\omega/dk_z)$ coincides with the beam velocity over a wide frequency band.   One way to realize such a circuit is to load the waveguide with dielectric material.   In this section, we examine the properties of a dielectric loaded waveguide as shown in Fig. 1 (in the absence of electrons).   It is well known that TE and TM modes are separable only for modes without angular variation.   For simplicity, we shall restrict our consideration to the TE_{0n} modes, where the subscript n
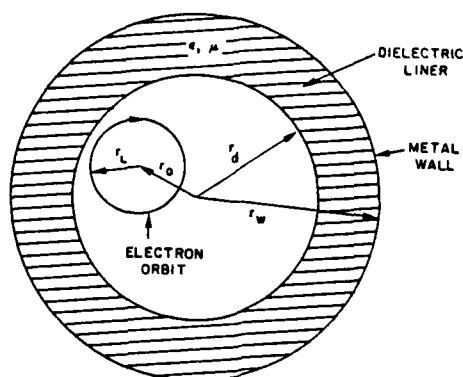
Figure 1. Cross-sectional view of a SWCA employing dielectric loaded waveguide. All the electrons have the same guiding centre position and are uniformly distributed on the circle of radius r_0. The applied magnetic field ($B_0 \mathbf{e}_z$) points toward the reader.

refers to the radial eigen-number. The TE_{0n} mode dispersion relation (in the absence of electrons) is given by

$$\frac{k_{n2}}{k_{n1}} J_1(k_{n1}r_d)[J_1(k_{n2}r_w)Y_0(k_{n2}r_d) - J_0(k_{n2}r_d)Y_1(k_{n2}r_w)]$$

$$+ \mu J_0(k_{n1}r_d)[J_1(k_{n2}r_d)Y_1(k_{n2}r_w) - J_1(k_{n2}r_w)Y_1(k_{n2}r_d)] = 0 \quad (3)$$

where

$$\left.\begin{aligned} k_{n1}^2 &= \frac{\omega^2}{c^2} - k_z^2 \\[2mm] k_{n2}^2 &= \mu\epsilon \frac{\omega^2}{c^2} - k_z^2 \end{aligned}\right\} \quad (4)$$

ϵ and μ are, respectively the dielectric constant and permeability of the dielectric liner, r_d is the inner radius of the dielectric liner, r_w is the wall radius (Fig. 1), J_n and Y_n are, respectively, Bessel functions of the first and second kind. For a given k_z, there are an infinite number of solutions for ω, which are denoted by the mode index n. The electromagnetic fields associated with the TE_{0n} mode are

$$B_z = \begin{cases} J_0(k_{n1}r), & r < r_d \\[2mm] aJ_0(k_{n2}r) + bY_0(k_{n2}r), & r > r_d \end{cases} \quad (5)$$

$$H_r = \begin{cases} \dfrac{-ik_z}{k_{n1}} J_1(k_{n1}r), & r < r_d \\[3mm] \dfrac{-ik_z}{\mu k_{n2}} [aJ_1(k_{n2}r) + bY_1(k_{n2}r)], & r > r_d \end{cases} \quad (6)$$

$$E_\theta = \begin{cases} \dfrac{i\omega}{k_{n1}c} \, J_1(k_{n1}r) & r < r_d \\[3mm] \dfrac{i\omega}{k_{n2}c} \, [aJ_1(k_{n2}r) + b Y_1(k_{n2}r)], & r > r_d \end{cases} \tag{7}$$

where

$$a = \frac{\pi}{2} k_{n2}r_d \left[\frac{k_{n2}}{k_{n1}} J_1(k_{n1}r_d) Y_0(k_{n2}r_d) - \mu J_0(k_{n1}r_d) Y_1(k_{n2}r_d) \right]$$

$$b = \frac{\pi}{2} k_{n2}r_d \left[\mu J_0(k_{n1}r_d) J_1(k_{n2}r_d) - \frac{k_{n2}}{k_{n1}} J_0(k_{n2}r_d) J_1(k_{n1}r_d) \right]$$

and all field components vary as $\exp(-i\omega t + ik_z z)$. A noticeable property of these electromagnetic fields is that (E_θ, H_r) forms an orthogonal pair, i.e.

$$\int_0^{r_w} rE_\theta H_r^* \, dr \begin{cases} =0 & \text{if } E_\theta \text{ and } H_r \text{ have the same mode number } n \\[2mm] \neq 0 & \text{if } E_\theta \text{ and } H_r \text{ have different mode numbers} \end{cases} \tag{8}$$

but (E_θ, E_θ), (H_r, H_r), (B_z, B_z) are not orthogonal pairs.
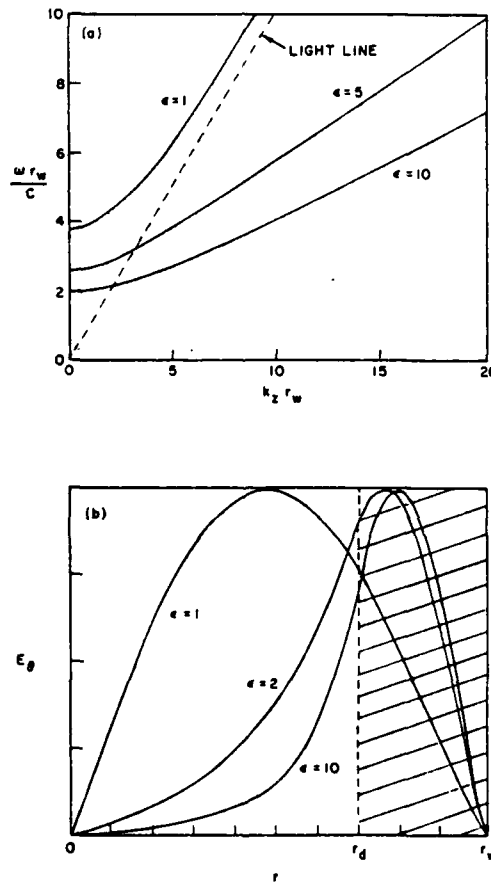
Figure 2. (a) ω versus k_z plots of the TE_{01} mode of the dielectric loaded waveguide. $r_d/r_w = 0.7$ and $\mu = 1$. Light line is defined by $\omega = k_z c$. (b) E_θ versus r of the same waveguide. Shaded area indicates dielectric region.

Figure 2 (a) plots the TE_{01} mode dispersion characteristics for $r_d/r_w = 0.7$, $\mu = 1$, and three values of the dielectric constant ϵ. The case $\epsilon = 1$ corresponds to an unloaded waveguide. In all three cases, the wave group velocity $(d\omega/dk_z)$ approaches a constant value (condition for wideband operation), while larger ϵ gives smaller group velocity. The unloaded waveguide $(\epsilon = 1)$ is impractical because its asymptotic group velocity approaches the speed of light. This is the reason that dielectric loading has been added to lower the asymptotic group velocity so that the wave could interact with a moderately energetic electron beam.

Figure 2 (b) shows typical E_θ profiles of the TE_{01} mode (eqn. (7)). As ϵ increases, E_θ tends to concentrate toward the dielectric region. When ϵ is so large that $\omega/k_z < c$ (i.e. k_{n1} becomes imaginary, see eqn. (4)), the electromagnetic wave can be regarded as a surface wave on the dielectric. A more sophisticated model of the dielectric loaded waveguide has been analysed by Park *et al.* (1980).

3. Dispersion relation of the SWCA

Figure 1 shows the present model of the SWCA. The electrons move along helical trajectories under the guidance of a uniform magnetic field $(B_0 \mathbf{e}_z)$. We assume that the beam is sufficiently tenuous that its space charge field can be neglected. Hence, the radial dependence of the RF field is that of an empty dielectric loaded waveguide (eqns. (5)–(7)). We let all quantities depend on t and z through $\exp(-\omega t + ik_z z)$. The presence of the electron beam, treated here as a perturbation, modifies slightly either ω or k_z such that ω or k_z has a small imaginary component to give rise to wave growth. The purpose of the following analysis is to derive a dispersion relation which determines k_z as a function of ω or vice versa. Using (5)–(7) and the Maxwell equations, we obtain

$$\left(\frac{\omega^2}{c^2} - k_z^2 - k_{n1}^2\right) E_\theta^{(1)} = \frac{-4\pi i \omega}{c^2} J_\theta^{(1)} \tag{9}$$

where the superscript (1) denotes first order quantities and $J_\theta^{(1)}$ is to be evaluated from the equation

$$J_\theta^{(1)} = -e \int f^{(1)}(\mathbf{x}, \mathbf{p}, t) v_\theta d^3 p \tag{10}$$

and the perturbed distribution function $f^{(1)}$ can be solved from the linearized relativistic Vlasov equation

$$\left(\frac{\partial}{\partial t} + \mathbf{v} \cdot \frac{\partial}{\partial \mathbf{x}} - e\mathbf{v} \times B_0 \mathbf{e}_z \cdot \frac{\partial}{\partial \mathbf{p}}\right) f^{(1)} = e(\mathbf{E}^{(1)} + \mathbf{v} \times \mathbf{B}^{(1)}) \cdot \frac{\partial}{\partial \mathbf{p}} f_0 \tag{11}$$

where f_0 is the equilibrium distribution function, $\mathbf{p}$ is the electron momentum, $\mathbf{E}^{(1)}$ and $\mathbf{B}^{(1)}$ are given by (5)–(7).

In the above, (9) is the field equation, (11) is the electron dynamics equation, and (10) serves to connect (9) and (11). To solve (9)–(11), one must first specify the form of the initial electron distribution function in terms of the constants of motion of the system, namely, the perpendicular and parallel momenta $p_\perp$ and p_z, and the canonical angular momentum P_θ. To be consistent with the usual experimental configuration that all the electron

guiding centres are approximately located on the same cylindrical surface defined by $r = r_0$, we choose f_0 to be of the form (Chu 1978)

$$f_0 = C\delta(r_L^2 - 2P_\theta/eB_0 - r_0^2)g(p_\perp, p_z) \qquad (12)$$

where $\delta(x)$ is the Dirac delta function, $r_L = p_\perp/eB_0$ is the electron Larmor radius, $g(p_\perp, p_z)$ is an arbitrary function of $p_\perp$ and p_z satisfying $\int g d^3 p = 1$, and C is a normalization constant chosen to satisfy $\int f_0 2\pi r dr d^3 p = N$, where N is the number of electrons per unit axial length. Methods for constructing f_0 as well as the steps leading to the dispersion relation are similar to those described elsewhere (Chu 1978, Chu *et al.* 1980). Here we present the result directly,

$$\frac{\omega^2}{c^2} - k_z^2 - k_{n1}^2 = \frac{-8\pi\nu}{r_w^2 K} \int_0^\infty p_\perp dp_\perp \int_{-\infty}^\infty dp_z g(p_\perp, p_z)$$

$$\times \left\{ \frac{(\omega^2 - k_z^2 c^2)p_\perp^2 H_s(k_{n1}r_0, k_{n1}r_L)}{\gamma^3 m^2 c^2 (\omega - k_z v_z - s\Omega_c)^2} - \frac{(\omega - k_z v_z)Q_s(k_{n1}r_0, k_{n1}r_L)}{\gamma(\omega - k_z v_z - s\Omega_c)} \right\} \qquad (13)$$

where $\nu = Nr_e$, $r_e = 2 \cdot 8 \times 10^{-12}$ cm is the classical electron radius

$$H_s(x, y) \equiv [J_s(x)J'_s(y)]^2$$

$$Q_s(x, y) \equiv 2H_s(x, y) + yJ'_s(y)J''_s(y)\{J_s^2(x)(1 + s^2/x^2) + [J'_s(x)]^2\}$$

$$+ 2s^2 J_s(x)J'_s(x)J'_s(y)[yJ'_s(y) - J_s(y)]/xy$$

and

$$K \equiv \frac{-2k_{n1}^2 c}{\omega k_z r_w^2} \int_0^{r_w} E_\theta H_r^* r \, dr$$

Note that K is a quantity proportional to the Poynting flux of the electromagnetic wave in the waveguide. Equation (13) has been written in a form to lend direct comparison with the dispersion relation of the Gyro-TWA (Chu *et al.* 1980). In the limit $\epsilon = 1$, eqn. (13) reduces to the dispersion relation of a TE_{0n} mode Gyro-TWA. This is expected because the SWCA differs in physical structure from the Gyro-TWA only in the addition of the dielectric liner.

Further comparison of the two devices is illustrated qualitatively in Fig. 3. Because of the presence of the dielectric liner, the phase velocity of the guide mode (eqn. (3)) falls below the speed of light at large k_z. This consequently renders the bunching process in SWCA qualitatively different from that in a Gyro-TWA. The bunching force is magnetic and the bunching mechanism is non-relativistic in the SWCA, while the bunching force is electric and the bunching mechanism is relativistic in a Gyro-TWA. The two mechanisms are in fact simultaneously present in either device and competing with one another. For fast waves $(\omega/k_z > c)$, the relativistic bunching mechanism dominates. For slow waves $(\omega/k_z < c)$, the non-relativistic bunching mechanism dominates (Chu and Hirshfield 1978). Thus, the fact that the SWCA operates in the slow wave regime and the Gyro-TWA operates in the fast wave regime (Fig. 3) represents a fundamental difference in the physical mechanism. As a consequence of this difference, the magnetic field is tuned such that the guide mode lies above the beam mode for the Gyro-TWA and below the beam mode for the SWCA (Fig. 3).
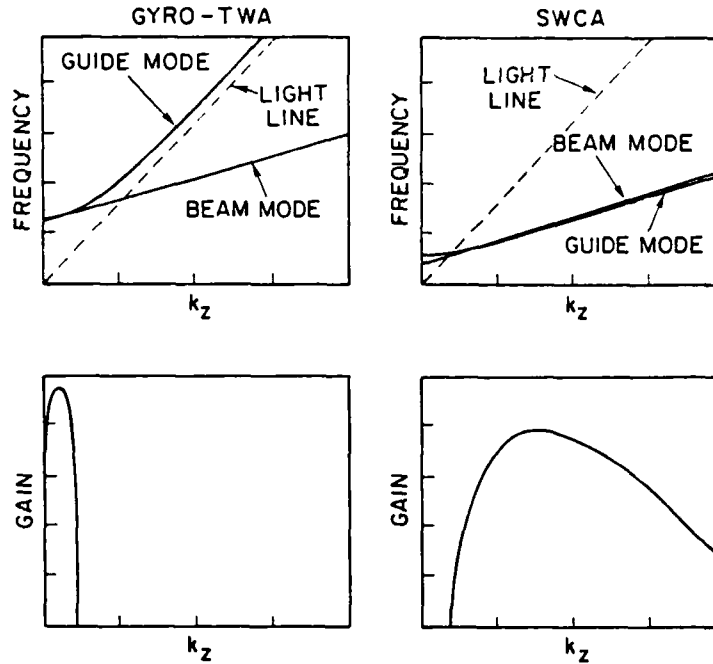
Figure 3. A qualitative comparison of dispersion curves between the Gyro-TWA
and the SWCA. The physical structures differ only in the absence (Gyro-
TWA) and presence (SWCA) of the dielectric liner. The guide mode is
plotted from eqn. (3). The beam mode is plotted from eqn. (1). The growth
rate is calculated from eqn. (13). The main feature is that the Gyro-TWA
operates in the fast wave regime with a smaller bandwidth, while the SWCA
operates in the slow wave regime with a wider bandwidth. Note that in the
region where there is gain, the guide mode line is above the beam mode line
for the Gyro-TWA and below the beam mode line for the SWCA.

4. Calculation of the small signal gain and design of a proof-of-principal experiment

The electromagnetic field in the waveguide varies as $\exp{(ik_z z)}$, hence in
the small signal regime the output power (P) depends on the input power
(P_0) through

$$P = P_0 \exp{(-2k_{zi}L)}$$

where k_{zi} is the imaginary part of k_z and L is the interaction length. The
total gain (G) is then

$$G \equiv 10 \log P/P_0 \simeq -8 \cdot 7 k_{zi}L \text{ dB} \tag{14}$$

Note that (14) gives the interaction gain of a single mode. The real gain
of an actual device is given by (14) minus the input coupling loss. The gain
per unit length (g) is given by

$$g = G/L = -8 \cdot 7 k_{zi} \text{ dB/unit length} \tag{15}$$

where k_{zi} is to be evaluated from (13).

2 c 2
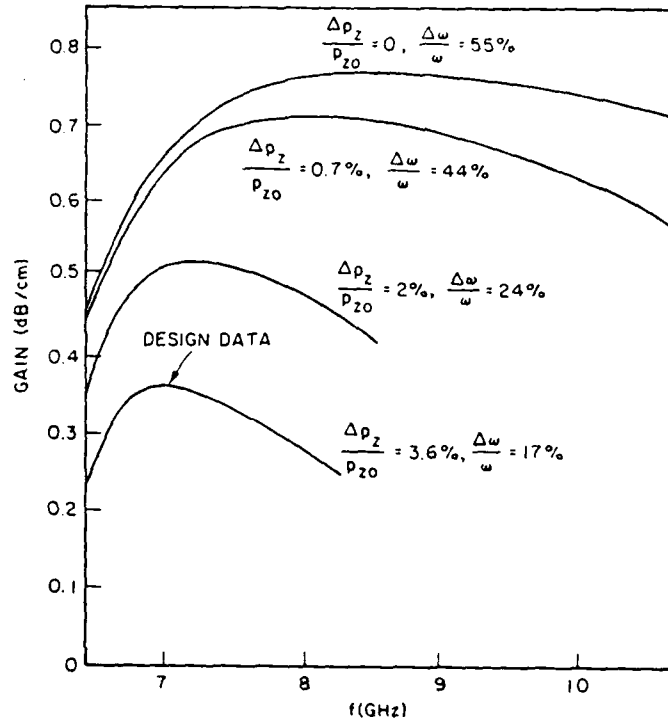
Figure 4. Gain/unit length versus frequency for different beam velocity spread. The point marked ' design data ' has been used in the design example (Table 2). Parameters used are $V_b = 60$ keV, $I_b = 5$ A, $r_d/r_w = 0.8$, $r_0/r_w = 0.51$, $\epsilon = 16$ and $\mu = 1$. The optimized magnetic fields for each curve (for top to bottom) are $B_0 = 1.89$ kG, 1.90 kG, 1.93 kG and 1.95 kG, respectively.

Figure 4 provides a specific example of the gain calculations for a mono-energetic electron beam with the following distribution in momentum space

$$g(p_\perp, p_z) = A\,\delta(\gamma - \gamma_0)\exp\left(\frac{-(p_z - p_{z0})^2}{2\Delta p_z^2}\right) \tag{15}$$

where $\delta(x)$ is the Dirac delta function, A is a normalization constant, $\gamma = [1 + (p_\perp^2 + p_z^2)/m^2c^2]^{1/2}$, γ_0 is the electron relativistic factor, p_{z0} is the mean axial momentum, and Δp_z is approximately the standard deviation of the electron axial momentum.

In Fig. 4, g is plotted as a function of the wave frequency for several values of momentum (or velocity) spread. The corresponding bandwidth ($\Delta\omega/\omega$) is also indicated, assuming a total small signal gain of 20 dB. Parameters used to generate Fig. 4 are indicated in the figure caption. For each velocity spread, there is a different optimal magnetic field, also indicated in the figure caption. One observes from eqn. (1) that a spread in v_z tends to spoil the resonance condition and thereby degrades the operation. Further, the sensitivity of the resonance condition is proportional to k_z as shown in (1). Since the SWCA operates at a relatively large wave number compared with the Gyro-TWA (Fig. 3), it is much more sensitive to electron velocity spread. The sensitivity is clearly exhibited in Fig. 4. For a perfectly cold beam, a

maximum bandwidth of $55\%_0$ is predicted but the bandwidth degrades rapidly to $17\%_0$ with a $3\cdot6\%_0$ velocity spread. In comparison, the Gyro-TWA can tolerate a much higher velocity spread (Lau *et al.* 1981). On the other hand, the Gyro-TWA, operating near the cut-off frequency of the waveguide, is known to be susceptible to band-edge oscillations caused by an absolute instability (Lau *et al.* 1981). The SWCA operates further away from the cut-off frequency and consequently is expected to be less susceptible to such oscillations.

The point in Fig. 4 marked 'design data' has been chosen for a proof-of-principle experiment design. Parameters of this design are shown in Table 2. Details of experimental considerations (Baird *et al.* 1978, Keren *et al.* 1980) have been described elsewhere.

Central frequency	6·9 GHz
Bandwidth	17%
Total gain	20 dB
Gain/unit length	0·36 dB/cm
Beam voltage	60 keV
Beam current	5 A
$v_\perp/v_z$	2
Applied magnetic field	1·95 kG
r_d	1·427 cm
r_w	1·784 cm
r_0	0·915 cm
r_L	0·405 cm
ϵ	16
μ	1

Table 2. Design parameters of a C-band SWCA.

5. Summary

We have presented the concept and small signal theory of the SWCA. It employs a physical mechanism not yet exploited for coherent microwave generation. The prospect of high-power, wideband operation at millimetre wavelength constititutes the main attraction of this device. However, the degrading effects of electron velocity spread may present a difficult problem in its implementation.

A dielectric loaded slow wave structure has been chosen to illustrate the principle of operation. Other slow wave structures, such as the periodically loaded waveguide and the helix, can also be employed and may even offer significant advantages over the dielectric structure in terms of high power and, most of all, the avoidance of loss and space charge build-up on the dielectric.

In this paper the basic principle is emphasized. Operation at a higher order (n) waveguide mode or at higher cyclotron harmonics (s) is included in the model but not analysed. Recently, Park *et al.* (1981) have developed a more refined theory of the SWCA and demonstrated some interesting features of harmonic operation. Ganguly and Chu (1980) have considered a SWCA model in slab geometry. Uhm *et al.* (1981) have studied a variation of SWCA

in which the dielectric material is inserted in the centre of the waveguide. A related device similar to the SWCA in structure and to the TWT in physical mechanism has been reported by Felch *et al.* (1981).

REFERENCES

BAIRD, J. M., PARK, S. Y., CHU, K. R., KEREN, H., and HIRSHFIELD, J. L., 1980, Design of a slow wave cyclotron amplifier. *Bull. Am. Phys. Soc.*, **25**, 911.

BARNETT, L. R., BAIRD, J. M., LAU, Y. Y., CHU, K. R., and GRANATSTEIN, V. L., 1980. A high gain single stage gyrotron traveling wave amplifier. *IEDM Technical Digest*, p. 314.

CHU, K. R., 1978, Theory of electron cyclotron maser interaction in a cavity at the harmonic frequencies. *Phys. Fluids*, **21**, 2354.

CHU, K. R., SPRANGLE, P. A., and GRANATSTEIN, V. L., 1978. Theory of a dielectric loaded cyclotron traveling wave amplifier. *Bull. Am. Phys. Soc.*, **23**, 748.

CHU, K. R., and HIRSHFIELD, J. L., 1978, Comparative study of the axial and azimuthal bunching mechanisms in electronmagnetic cyclotron instabilities. *Phys. Fluids*, **21**, 461.

CHU, K. R., DROBOT, A. T., SZU, H. H., and SPRANGLE, P., 1980, Theory and simulation of the gyrotron travelling wave amplifier operating at cyclotron harmonics. *I.E.E.E. Trans. microw Theory Tech.*, **28**, 313.

FELCH, K. L., BUSBY, K. O., LAYMAN, R. W., KAPILOW, D., and WALSH, J. E., 1981, Cerenkov radiation in dielectric lined waveguides. *Appl. Phys. Lett.*, **38**, 601.

FERGUSON, P. E., and SYMONS, R. S., 1981, A C-band gyro-TWT. *I.E.E.E. Int. Electron Dev. Meeting Tech. Digest*, p. 310.

GANGULY, A. K., and CHU, K. R., 1980, Slow wave cyclotron instability in dielectric loaded waveguide of rectangular cross section. *Naval Research Laboratory Memo Report No. 4215*.

GRANASTEIN, V. L., SPRANGLE, P., DROBOT, A. T., CHU, K.R., and SEFTOR, J. L., 1980, Gyrotron travelling wave amplifier. *U.S. Patent 4224576*.

HIRSHFIELD, J. L., CHU, K.R., and KAINER, S., 1978, Frequency up-shift for cyclotron wave instability on a relativistic electron beam. *Appl. Phys. Lett.*, **33**, 847.

KEREN, H., HIRSHFIELD, J. L., PARK, S. Y., CHU, K. R., and BAIRD, J. M., 1980, Design of a slow wave cyclotron wave amplifier. *Fifth Int. Conf. Infrared and mm Waves, Wurzburg*, p. 96.

LAU, Y. Y., CHU, K. R., BARNETT, L. R., and GRANATSTEIN, V. L., 1981, Gyrotron traveling wave amplifier. *Int. J. Infrared and mm Waves*, **2**, 395 and 373.

PARK, S. Y., BAIRD, J. M., and HIRSHFIELD, J. L., 1980, General theory of cylindrical waveguide loaded with multilayer dielectric. *Bull. Am. Phys. Soc.*, **25**, 910 ; 1981 (to be published).

PIERCE, J. R., 1950, *Travelling Wave Tubes* (Princeton : Van Nostrand).

SPRANGLE, P., CHU, K. R., SMITH, R. A., 1979. The theory of electron cyclotron maser devices. *Fourth Int. Conf. Infrared and mm Waves, Florida*. p. 93.

SYMONS, R. S., JORY, H. R., HEGJI, S. J., and FERGUSON, P. E., 1981. An experimental Gyro-TWT. *I.E.E.E. Trans. microw. Theory Tech.*, **29**, 181.

UHM, H. S., CHOE, J. Y., and AHN, S., 1981, Theory of gyrotron amplifier in a waveguide with inner dielectric material. *Int. J. Electron.* (this issue).

4. F. A. Korolev and A. F. Kurin, Radio Eng. Electron.
   Phys. 15, 1868 (1970).

5. L. C. Robinson, *Physical Principles of Far-Infrared
   Radiation*, Academic Press, New York (1973).

6. P. Sprangle, W. Manheimer, and J. Vomvoridis, NRL
   Memorandum Report 4366 (1980) (unpublished).

7. G. Landauer, J. Nucl. Energy C4, 395 (1962).

8. F. W. Crawford, G. S. Kino, and H. H. Weiss, Phys.
   Rev. Lett. 13, 229 (1964).

9. F. W. Crawford, J. Res. Natl. Bur. Stds./USNC-RUSI
   (Radio Science) 69D, 789 (1965).

10. D. E. Baldwin, I. B. Bernstein, and M.P. H. Weenink,
    Advances in Plasma Physics 3 (A. Simon and W. B.
    Thompson, eds.) Interscience (1969), pp. 87-95.

11. ibid, pp. 1-18.

$$J_s = 4.72 \times 10^8 \left(\frac{n}{Q}\right)^2 amp/cm^2 \quad .$$

If $Q = 10^4$, we find $J_s = 4.72 \, n^2 amp/cm^2$: a 10 ampere, 0.04 cm^2 area beam would, according to this criterion, support oscillations at harmonic value up to and including the seventh. According to Table II, this would correspond to frequencies as high as 1035 GHz.

This analysis, based upon an admittedly idealized model, suggests that the potent high cyclotron harmonic interactions, studied more than a decade ago in non-Maxwellian plasmas, may be exploited to generate coherent submillimeter wave power. The model presented here does not take into account the actual fields of a practical confocal Fabry-Perot resonator, the practical means of coupling power out, the actual spatial distribution of available electron beams, or the non-linear saturation levels for steady-state oscillations. All of these questions, and more, will have to be addressed before the cyclotron harmonic maser can be considered understood. Perhaps experimental demonstration can serve to stimulate interest in this promising mechanism.

Acknowledgment

References

* Research sponsored by the Office of Naval Research.

1. G. Bekefi, J. L. Hirshfield, and S. C. Brown, Phys. Fluids 4, 173 (1961); J. L. Hirshfield and G. Bekefi, Nature 198, 20 (1963).

2. G. N. Rapoport, A. K. Nemak, and V. A. Zhurakhovskiy, Radio Eng. Electron. Phys. 12, 587 (1967).

3. A. F. Kurin, G. A. Kurina, and V. V. Novikov, Radio Phys. Quantum Electron. 19, 742 (1976).

TABLE II

Solutions of the dispersion relation [Eq. (10)] giving the frequencies of oscillation for the first 10 harmonics (upper and lower ends of each harmonic band) for ℓ/r_g = 10 and $(L - \ell)/\ell$ = 20, and ℓ = 0.1 cm.

n	$k_n\ell$ (ℓ/r_g = 10)	$\dfrac{\cot(k_n\ell)}{k_n\ell}$	Lower end of band			Upper end of band		
			f_{nm} (GHz)	γB (kG)	mode no. m	f_{nm} (GHz)	γB (kG)	mode no. m
1	18.41	-0.1155	96.94	34.63	13	149.13	53.28	20
2	30.54	-0.02745	149.79	26.76	20	299.59	53.52	40
3	42.01	0.01003	300.15	35.74	40	442.72	52.72	59
4	53.18	-0.0835	448.12	40.03	60	590.03	52.70	79
5	64.16	0.00393	592.61	43.34	79	735.14	52.53	98
6	75.01	-0.0322	741.29	44.14	99	883.56	52.61	118
7	85.78	0.00825	835.35	42.64	118	1035.43	52.85	138
8	96.47	-0.00804	1042.06	46.54	139	1177.01	52.56	157
9	108.	0.00375	1177.71	46.75	157	1327.73	52.71	177
10	118.	-0.00163	1334.88	47.69	178	1477.3	52.78	197

For the anti-symmetric modes, it is a simple matter to show that the dispersion relation is given by a relation similar to Eq. (10), except that the left-hand side is replaced by $-\tan k_n \ell / k_n \ell$. Since for the parameter range of interest $[\ell/(L-\ell)]\cot k_n \ell / k_n \ell \ll 1$, Eq. (10) may be approximated as

$$\omega_{nm} = \frac{m \pi c}{L-\ell} \left[1 + \delta_n \left(\frac{\ell}{L-\ell} \right) \right] \qquad (11)$$

where $\delta_n = \cot k_n \ell / k_n \ell$ for symmetric modes, and $\delta_n = -\tan k_n \ell / k_n \ell$ for anti-symmetric modes. The discrete spectrum given by Eq. (11) contains two indices; n is the cyclotron harmonic number, and m is the resonator mode number.

We shall illustrate the nature of solutions to Eq. (10) by reference to a specific example. Suppose the electron beam thickness is such that $\ell \Omega / W = \ell / r_g = 10$, where r_g is the electron gyration radius. Then $k_n \ell = z_n \Omega \ell / W = 10 z_n$. Furthermore, we take $(L-\ell)/\ell = 20$ and $\ell = 0.1$ cm. Table II shows then, for each harmonic, the spectrum of frequencies predicted by Eq. (10), together with the associated magnetic field value. Only that portion of the spectrum available for magnetic field values below about 53 kG are given.

Of course, the existence of modes which satisfy the equation of real parts given by Eq. (10) does not insure that oscillations will in fact start. A rough criterion is that the rate of growth for the instability be balanced by the rate of energy dissipation into finite cavity losses. This is expressed as

$$\frac{Im\omega}{Re\omega} > \frac{1}{2Q} \qquad (12)$$

where Q is the resonator quality factor. If we take $Im\omega/Re\omega \simeq 0.3 W\omega_p/nc\Omega$, from Eq. (4), then Eq. (11) can be used to find a start-oscillation current density J_s. This can be expressed as

$$J_s = 1.65 \times 10^6 \left(\frac{nB}{Q} \right)^2 \frac{1}{V^{1/2}} \left(\frac{1 + \alpha^2}{\alpha^3} \right)$$

where J_s is in amperes/cm^2, B is in kG, V is the beam energy in kilovolts, and $\alpha = W/U$ is the momentum ratio. For B = 50 kG, V = 30 kV, and $\alpha = 2$, we have

$$\frac{E_x}{E_y} = \pm\, i\, \frac{c}{W}\, \gamma^{3/2} \frac{1}{\omega_p} \left[\frac{z_n}{nJ_n''(z_n)}\right] \quad . \tag{7}$$

This expression shows our approximation of nearly longitudinal polarization to remain valid throughout the range of parameters of interest.

We must now consider the matching of the fields within the electron beam $(0 < |x| < \ell)$

$$\underline{E}_i(x,t) = (\hat{e}_x E_L + \hat{e}_y E_T)\cos k_n x \cos\omega t \tag{8}$$

to the fields outside the beam $(\ell < |x| < L)$

$$\underline{E}_o(x,t) = \hat{e}_y E_o \sin[\tfrac{\omega}{c}(L - |x|)]\cos\omega t \quad . \tag{9}$$

Eq. (8) gives the symmetric modes $[\underline{E}_i(-x) = \underline{E}_i(x)]$; the anti-symmetric modes may be developed in parallel. Eq. (9) gives the vacuum field which matches the requirement of vanishing tangential electric field on the conducting boundary at $|x| = L$. At $|x| = \ell$, tangential electric field and its normal derivative must be continuous. Thus

$$E_T \cos k_n \ell = E_o \sin[\tfrac{\omega}{c}(L - \ell)]$$

and $$k_n E_T \sin k_n \ell = \tfrac{\omega}{c} E_o \cos[\tfrac{\omega}{c}(L - \ell)] \ ,$$

so that the dispersion relation which must be satisfied for the beam in the resonator is

$$\frac{\cot k_n \ell}{k_n \ell} = \left(\frac{L - \ell}{\ell}\right) \frac{\tan\left[\tfrac{\omega}{c}(L - \ell)\right]}{\left[\tfrac{\omega}{c}(L - \ell)\right]} \quad . \tag{10}$$

For the k_n which have already been specified as leading to the maximum growth rate for the instability, Eq. (10) gives the corresponding discrete values of ω. We shall find approximate roots of Eq. (10) by assuming $\mathrm{Im}\omega \ll \mathrm{Re}\omega$, and $\mathrm{Im}k_n \ll \mathrm{Re}k_n$. Then Eq. (10) holds for the real parts, to lowest order; $\mathrm{Im}k_n$ may then be found from $\mathrm{Im}\omega$ using a Taylor's expansion of Eq. (10) about its roots for real values. These complex corrections to the k_n are not of great consequence in what follows.

$$\frac{E_x}{E_y} = \frac{\epsilon P_{12}}{-y^2 + \epsilon P_{11}} \qquad (3)$$

and for $y^2 = \epsilon P_{11}$ is thus nearly longitudinal. Let us
first analyze the relation $y^2 = \epsilon P_{11}$, which is the disper-
sion relation for purely longitudinal waves propagating
across B ("Bernstein" modes). These modes are unstable
with approximate maximum growth rate for the lowest wave-
number such that $J_n'(z) = 0$. We designate this value as
z_n. In this case $y^2 = \epsilon P_{11}$ gives

$$\omega = \frac{n\Omega}{\gamma} \pm i \frac{\omega_p}{\gamma^{3/2}} \frac{W}{c} \left[\frac{n J_n(z_n)}{z_n} \right] . \qquad (4)$$

The value of $n J_n(z_n)/z_n$ is slowly varying with n; it has
the approximate value of 0.3 for n up to 20. The growth
rate given by Eq. (4) can thus be relatively large for par-
ameter values of practical interest, even for quite high
harmonic number n.

Anticipating instability for the wavenumber correspond-
ing to z_n at each harmonic, we can examine the full disper-
sion relation at this particular wavenumber. Here $X_{11} = X_{22} = Y_{12} = Y_{21} = Y_{22} \simeq 0$, and $X_{12} = -X_{21} \simeq i n J_n(z_n) J_n''(z_n)$.
Thus $P_{11} = -[y/(y - n/\gamma)]^2 Y_{11}$, $P_{22} = 0$, and $P_{12} = i[y/(y - n/\gamma)] X_{12}$. The full dispersion relation is then

$$\left[y^2 + \epsilon \left(\frac{y}{y - \frac{n}{\gamma}} \right)^2 Y_{11} \right] \left[\frac{c^2 z_n^2}{W^2} - y^2 \right] + \epsilon^2 \left(\frac{y}{y - \frac{n}{\gamma}} \right)^2 X_{12}^2 = 0 . \qquad (5)$$

For nearly longitudinal slow waves $c z_n/W \gg y$, and Eq. (5)
becomes

$$\omega = \frac{n\Omega}{\gamma} \pm i \frac{\omega_p}{\gamma^{3/2}} \frac{W}{c} \left[\frac{n J_n(z_n)}{z_n} \right] \left[1 - \epsilon n^2 J_n''^2(z_n) \right]^{1/2} . \qquad (6)$$

Clearly for $n^2 \epsilon \ll 1$, Eq. (4) is accurate. In this aprox-
imation Eq. (3) *becomes*

TABLE I

Elements of the dyadics $\underset{=}{X}_n$ and $\underset{=}{Y}_n$ for the distribution function $f_o(u,w) = (N/2\pi W)\delta(u-U)\delta(w-W)$. Here $J_n = J_n(z)$ and $J_n' = dJ_n(z)/dz$.

ij	X_{ij}	$\gamma^2 Y_{ij}$
11	$\dfrac{n^2}{z}(J_n^2)'$	$n^2 \dfrac{W^2}{c^2} \dfrac{1}{z^2} J_n^2$
12	$\dfrac{in}{z}(zJ_nJ_n')'$	$in \dfrac{W^2}{c^2} \dfrac{1}{z} J_nJ_n'$
13	$\dfrac{nU}{W}(J_n^2)'$	$n \dfrac{U}{c} \dfrac{W}{c} \dfrac{1}{z} J_n^2$
21	$-\dfrac{in}{z}(zJ_nJ_n')'$	$-in \dfrac{W^2}{c^2} \dfrac{1}{z} J_nJ_n'$
22	$\dfrac{1}{z}(z^2J_n'^2)'$	$\dfrac{W^2}{c^2} J_n'^2$
23	$-i\dfrac{U}{W}(zJ_nJ_n')'$	$-i \dfrac{W}{c} \dfrac{U}{c} J_nJ_n'$
31	$n \dfrac{U}{W}(J_n^2)'$	$n \dfrac{U}{c} \dfrac{W}{c} \dfrac{1}{z} J_n^2$
32	$i \dfrac{U}{W}(zJ_nJ_n')'$	$i \dfrac{U}{c} \dfrac{W}{c} J_nJ_n'$
33	$z \dfrac{U^2}{W^2}(J_n^2)'$	$\dfrac{U^2}{c^2} J_n^2$

momentum to be cold, i.e. $f_o(u,w) = (N/2\pi W)\delta(u-U)\delta(w-W)$; and we assume that linearized interaction of this beam with electromagnetic radiation is governed by the dispersion relation for plane waves in uniform hot plasma (11). The model should be viewed as an idealization, probably unachievable in the laboratory, since we assume the electron beam to be a uniform slab with sharp boundaries and we impose no boundaries along z. This model allows one to formulate a tractable theory which still retains the critical physics describing significant harmonic operation. For excitations which are independent of z, i.e. for $k_{\shortparallel} = 0$, the dispersion relation for these excitations (Eq. 1-99 of Ref. 11) reduces to det $\underline{\underline{R}} = 0$, where

$$
\frac{1}{\Omega^2} \underline{\underline{R}} = - y^2 \hat{e}_x \hat{e}_x + \left(\frac{c^2 z^2}{w^2} - y^2\right)\left(\hat{e}_y \hat{e}_y + \hat{e}_z \hat{e}_z\right)
$$
$$
+ \varepsilon \left\{ \hat{e}_z \hat{e}_z + \sum_{n=-\infty}^{\infty}\left[\left(\frac{y}{y - \frac{n}{\gamma}}\right)\underline{\underline{X}}_n - \left(\frac{y}{y - \frac{n}{\gamma}}\right)^2 \underline{\underline{Y}}_n\right]\right\} ,
\tag{1}
$$

with $\Omega = eB_o/m$, $y = \omega/\Omega$, $z = k_\perp W/\Omega$, and $\varepsilon = \omega_p^2/\gamma\Omega^2$. The elements of the dyadics $\underline{\underline{X}}_n$ and $\underline{\underline{Y}}_n$ are given in Table I. For electron beams of practical interest $\varepsilon \ll 1$, so that the solutions to Eq. (1) may be found harmonic-by-harmonic. That is, the summation may be suppressed and the harmonic number n considered as a parameter. We present a solution here in the beam frame, where $U = 0$. Then $X_{13} = X_{23} = X_{31} = X_{32} = X_{33} = Y_{13} = Y_{23} = Y_{31} = Y_{32} = Y_{33} = 0$. Eq. (1) then becomes

$$
\left[\frac{c^2 z^2}{w^2} - y^2 + \varepsilon\right]\left\{\left[- y^2 + \varepsilon P_{11}\right]\left[\frac{c^2 z^2}{w^2} - y^2 + \varepsilon P_{22}\right] + \varepsilon^2 P_{12}^2\right\} = 0
\tag{2}
$$

where $P_{ij} = [y/(y - n/\gamma)]X_{ij} - [y/(y - n/\gamma)]^2 Y_{ij}$.

The first square bracket in Eq. (2) set to zero gives $\omega^2 = k^2 c^2 + \omega_p^2$ for waves polarized along z (ordinary waves); since our interest is with waves polarized in the x-y plane we shall henceforth disregard this. The curley bracket in Eq. (2) set to zero gives the dispersion relation for waves of mixed x-y polarization (extraordinary waves). The polarization is

cyclotron maser at the fundamental and second-harmonic,
with a view towards high-power millimeter wave operation.

Operation of cyclotron masers at higher frequency
would seem to demand stronger wave-particle coupling at the
higher harmonics than has heretofore been demonstrated. In
other contexts, however, high harmonic cyclotron resonance
effects have been long observed in laboratory and ionospher-
ic plasmas with non-Maxwellian velocity distributions. Thus
Landauer (7) has reported observations of upwards of 40
harmonics in noise emission from low pressure discharges.
Crawford, et al. (8) have observed about 10 resonances in
transmission across a plasma column. These observations,
together with multiple harmonic observations in ionospheric
top-side soundings have been reviewed by Crawford (9).
These multiple harmonic interactions have been explained in
terms of coupling, at the plasma boundary, between long
wavelength electromagnetic modes, and short wavelength elec-
trostatic modes (10). The model presented in the present
paper is for a suggested means to exploit these multiple
harmonic couplings to produce useful cyclotron maser oscil-
lations at the higher harmonics. In this way it may be
possible to extend the useful frequency regime for cyclotron
masers to above 1000 GHz, using available laboratory mag-
netic fields.
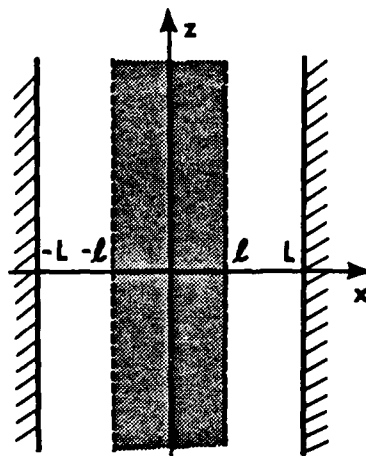
Fig. 1. Geometry for ideal-
ized cyclotron harmonic
maser. Plane mirrors are at
$x = \pm L$; the uniform slab
electron beam fills $-\ell < x < \ell$; the static magnetic field
is aligned along z; modes of
interest are polarized in
the x-y plane.

Our basic model is shown in Fig. 1. The electron beam
is guided by a uniform static magnetic field $\underline{B} = \hat{e}_z B_0$; we
take its distribution of parallel (u) and perpendicular (w)

CYCLOTRON HARMONIC MASER*

J. L. Hirshfield

Yale University
Department of Engineering and Applied Science
P.O. Box 2159, Yale Station, New Haven, CT 06520

A cyclotron resonance maser configuration is proposed which may allow operation at the higher cyclotron harmonics. Instability growth rates at the higher harmonics are shown to be significant when coupling between transversely- and longitudinally-polarized waves occurs at the electron beam boundary, for radiation propagating across the static magnetic field. With experimental parameters well within practical ranges, oscillation in a single device, tunable from about 100 to 1000 GHz, is shown to be possible.

Some of the earliest discussions of the cyclotron resonance maser gain mechanism stressed the existence of gain at the cyclotron harmonics, as well as at the fundamental (1). However, most device development in the past few years has been limited to fundamental or second-harmonic interactions. This, of course, would limit the applicability of cyclotron resonance masers to frequencies below about 300 GHz, corresponding to second-harmonic operation in a 53.6 kG magnetic field. At the shorter milli- meter- and sub-millimeter wavelengths, quasi-optical struc- tures must be employed to provide good mode selectivity without undue mode competition. Both theory (2,3) and de- vice development (4,5) have appeared in which quasi-opti- cal structures are employed. A recent work (6) reformu- lates linear and non-linear analysis for a quasi-optical

bandwidth values (~20%) were not observed in the slow-wave region. The conditions for wide bandwidth require grazing incidence between beam and guide lines (cf. Fig. 2). For this to be possible for the dispersion curve shown would have required a lower magnetic field (1.9 kG) and a higher slope, corresponding to $\alpha = 2$, $V = 60$ kV. But with $\alpha = 2$, our theoretical calculations indicate that beam velocity-spread values higher than 5% will severely degrade the gain; for the gun available the momentum spread, although not measured, was probably higher than 5%.[10] Thus to observe gain in the presence of large velocity spread evidently required higher α values, making the grazing condition inaccessible in these experiments. For intersecting conditions, such as those shown in Fig. 2(a), higher values of α result; gain can then occur even for large velocity spread. Beyond these qualitative points, a more detailed comparison between theory and experiment is probably not justified since the actual distribution function $f_0(\gamma, u)$ was not known.

In a subsequent experiment, the apparatus was arranged as a feedback amplifier, with a portion of the output signal returned to the input. With suitable phase adjustment, this arrangement allowed effective gain values as high as 53 dB to be observed at 6.2 GHz. Self-sustained oscillations did not occur since the gun voltage pulse did not remain at the gain condition for more than about 50 nsec. Under this high-gain condition, the amplifier power output was 20 kW, corresponding to an electronic efficiency of 10%.

Important discussions with B. Arfin, J. M. Baird, L. R. Barnett, P. Ferguson, A. Ginzburg, and V. L. Granatstein are gratefully acknowl-

---

[a]Present address: Weizmann Institute of Science, Rehovot 76100, Israel.

[b]Present address: Omega-P, Inc., 2008 Yale Station, New Haven, Conn. 06520.

[1]Y. Y. Lau, K. R. Chu, L. R. Barnett, and V. L. Granatstein, Int. J. infrared Millimeter Waves 2, 373 (1981).

[2]J. L. Seftor, V. L. Granatstein, K. R. Chu, and M. E. Read, IEEE J. Quantum Electron. 15, 848 (1979).

[3]J. L. Hirshfield, in Infrared and Millimeter Waves, edited by K. J. Button (Academic, New York, 1979), Vol. 1, pp. 1–54.

[4]K. R. Chu and J. L. Hirshfield, Phys. Fluids 21, 461 (1978).

[5]K. R. Chu, A. K. Ganguly, V. L. Granatstein, J. L. Hirshfield, S. Y. Park, and J. M. Baird, Int. J. Electron. 51, 493 (1981).

[6]L. R. Barnett, K. R. Chu, J. M. Baird, V. L. Granatstein, and A. T. Drobot, IEEE International Electron Devices Meeting Technical Digest (IEEE, New York, 1979), pp. 164–167.

[7]Type VUW-5080, Varian Assoc. Inc., Palo Alto, Cal. 94303.

[8]Pulse Generators, edited by G. N. Glasoe and J. V. Lebacqz (McGraw-Hill, New York, 1948), pp. 152–165.

[9]S. Y. Park, J. M. Baird, and J. L. Hirshfield, B-K Dynamics Technical Report No. TR-3-481, 1982 (to be published).

[10]An independent particle simulation to determine beam parameters for this gun was performed by N. Dionne (unpublished). He found a rms parallel momentum spread of 11% with $\alpha = 1.1$ at 42 kV.

st and then inserting whatever series attenuation was required to return the fast-rise-time output crystal-detector voltage to its value with the electron beam off. This method of measurement is independent of the detector linearity and is limited in accuracy only by the calibration accuracy of the attenuators used. Calibrated attenuators were placed in both the input and output guides to insure both linearity and absence of spurious oscillations.

A detailed small-signal theory has been developed for spatial amplification on axisymmetric wave guides penetrated by tenuous electron beams in a uniform magnetic field.[9] This theory applies to dielectric-loaded waveguides supporting TE_{0n}, TM_{0n}, and EH_{mn} modes and to empty waveguides with finite wall conductivity supporting TE_{mn} and TM_{mn} modes. The theory allows arbitrary input and output boundary conditions to be specified, so that the so-called input coupling loss arising from division of the input signal amongst several copropagating modes in an amplifier is automatically taken into account. Actual beam geometry (i.e., thick annulus, solid beam, radial density profile, etc.) may be included. Finite axial velocity spread is also included, modeled according to the equilibrium distribution function

$$f_0(\gamma, u) = A_s \delta(\gamma - \gamma_0)(\Delta u)^s [(u - u_0)^{2s} + (\Delta u)^{2s}]^{-1},$$

where γ is the total electron energy in units of mc^2, u is the axial velocity variable, $2\Delta u$ is the full width at half maximum for the distribution, γ_0 and u_0 are constants, A_s is a normalizing constant, and s is a parameter which governs the smear in f_0: For $s = 1$ the distribution is Lorentzian with its extended wings; as $s \to \infty$ the distribution approaches a box function, zero outside the interval $u_0 \pm \Delta u$. Examples of the predictions of this theory for the geometry of the apparatus described here are shown in Fig. 2(b), in which gain in decibels versus frequency is shown for two different sets of operating conditions (families of curves A and B) and for five values of parallel velocity spread $2\Delta u/u_0$. (The five cases meld together for family A.) The distribution with $s = 2$ was chosen for these examples as one which could reasonably approximate that produced by the electron gun used in the experiments. From the dispersion curve [Fig. 2(a)] one can determine that 5.80 GHz is the frequency at which $\omega k_z = c$; the gain curves of family A are thus for fast waves ($\omega/c < 1.215$ cm^{-1}) and those of family B for slow waves ($\omega/c > 1.215$ cm^{-1}). As remarked earlier, gain is not predicted at ω/c

= 1.215 cm^{-1}. Notable in Fig. 2(b) is the sensitivity of gain to velocity spread in the slow-wave region. The examples shown are for conditions of intersection between the dispersion curve and the beam line $\omega = \Omega/\gamma + k_z u$, where $\Omega = eB_z m$. Two such intersections are shown in Fig. 2(a) for fast- and slow-wave couplings. Examples are not shown here for cases of grazing incidence between dispersion and beam lines, a circumstance known to give rise to slow-wave gain characteristics with wide bandwidth, even for moderate parallel velocity spread.[5] This is because no substantial gain could in fact be observed for the grazing-incidence condition, a point we shall attempt to explain below.

The experimental results obtained are shown in Fig. 3. Six sets of data $(A-F)$ are given, corresponding to six combinations of gun voltage and magnetic field (values listed in the caption to Fig. 3). Both fast-wave ($f < 5.8$ GHz) and slow-wave ($f > 5.8$ GHz) interactions were observed, but gain at 5.8 GHz (where $\omega = k_z c$) was not observed, as predicted by theory. Experiments above ~6.6 GHz could not be performed, because of limits on the magnet power supplies; the tuning width in the slow-wave region is thus greater than the 700 MHz shown in Fig. 3, i.e., greater than 11%. The instantaneous −3 dB bandwidth for curve D is 220 MHz, or 3.7%, at a peak gain of 32 dB. In the fast-wave region (curve A) a bandwidth of 150 MHz, or 2.7%, was observed at a peak gain of about 30 dB. These values compare favorably with gain and bandwidth values reported[6] for fast-wave gyro traveling-wave amplifiers, i.e., 24 dB and 1.4%.
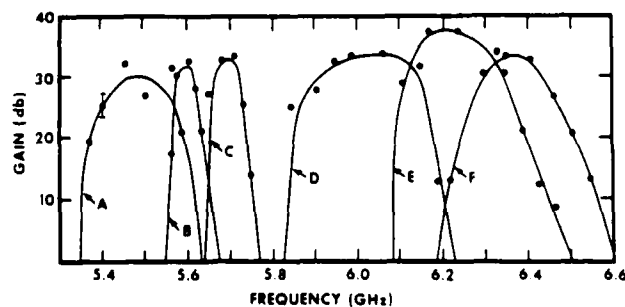
It remains to explain why the anticipated wide-

FIG. 3. Measured electronic gain vs frequency for six values of cathode voltage $(-V$ (kV)) and axial magnetic field $(B_z$ (kG)). A: $V = 34$, $B_z = 1.90$; B: $V = 39.7$, $B_z = 1.95$; C: $V = 39.7$, $B_z = 2.00$; D: $V = 42.0$, $B_z = 2.06$; E: $V = 42.0$, $B_z = 2.12$; F: $V = 45.4$, $B_z = 2.17$. For all cases $I = 5$ A. Solid curves connect measured points. Typical error bar is shown.

to a cylindrical copper waveguide of radius 3.7 cm. A mica vacuum window sealed with a old O ring provided reflection-free output coupling, and a Marié coupler provided output conversion from TE_{01} circular mode to TE_{10} rectangular mode. The Pyrex tube was coated on its interior with a thin carbon film (deposited from a dilute Alkadag solution) to drain off intercepted electron charge. The dc resistance of the film along the entire tube length was about 2 MΩ. The film was scraped off in thin axial stripes to minimize attenuation for the TE_{01} circular mode (TE_{mn} and TM modes were heavily attenuated). Microwave input signals (5–8 GHz) could be injected in the output guide or by means of a two-port coupler (shown in Fig. 1), with ports driven 180° out of phase to allow selective coupling to the TE_{01} mode. Dielectric pyramids were used to aid in coupling into the dielectric layer. Even so, the cold input coupling loss was about 10 dB, and the cold tube insertion loss was also about 10 dB.

The measured dispersion characteristic for this dielectric-loaded waveguide is shown by the heavy curve in Fig. 2(a); it is indistinguishable from the calculated curve. Mode filters were used to insure that TE_{01} was the only propagating mode, both in cold and hot operation. The dispersion curve was obtained by inserting a thin metal foil cylinder between the Pyrex and the dielectric annuli; this foil acted as a movable short circuit allowing measurement of the guide wavelength at each frequency.

The annular electron beam was injected along the dielectric-loaded waveguide from a magnetron injection gun. This gun, procured from an industrial manufacturer,[7] was built to operate at 60 kV, 5 A, 10^{-3} duty cycle under which conditions it was designed to produce a beam of mean radius 0.95 cm, annular thickness 0.75 cm, $\alpha = v_{\perp}/v_{\parallel} = 2.0$, and relative (rms) parallel velocity spread of 5%. As shall be seen, the gun operating conditions under which the data shown in this paper were obtained were different from the specified values. The gun was driven with ~5-μsec pulses at 100 sec^{-1} derived from a MIT model 9 modulator[8] feeding a 4:1 step-up pulse transformer. The gun's intermediate anode voltage was derived from the cathode voltage with a resistive voltage divider, and operated typically between 40% and 60% of cathode voltage. The beam collector was insulated, so that cathode current and transmitted current could be continuously monitored; for the data to be presented here the two were indistinguishable. Cathode cur-
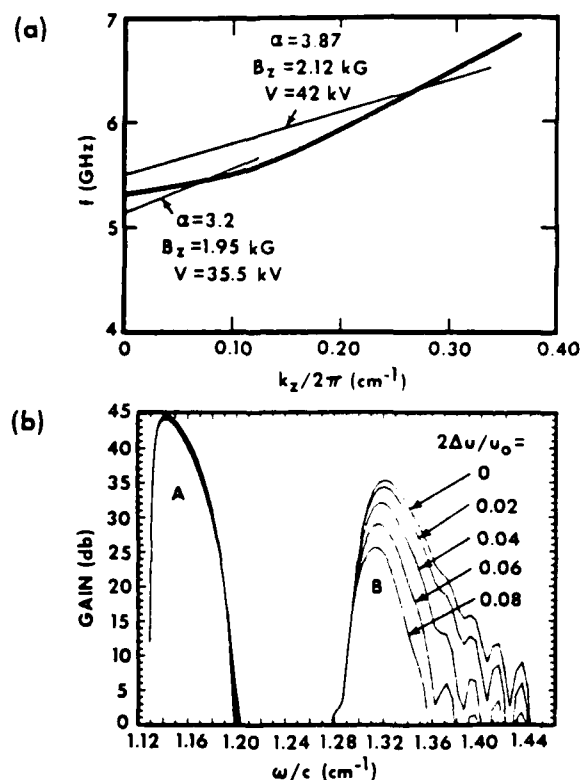
FIG. 2. (a) Measured dispersion curve (heavy line) and typical beam lines $\omega = \Omega/\gamma - k_z u$ for fast- and slow-wave couplings. (b) Calculated gain characteristics in the fast-wave (A) and slow-wave (B) regimes, for five values of parallel velocity spread $2\Delta u/u_0$, for the apparatus described. For curves A, $u = 0.0920c$, $\alpha = 4.2$, $I = 8.0$ A, $\Omega/\gamma c = 1.10$ cm^{-1} (i.e., $V = 45.8$ kV, $B = 2.043$ kG); for curves B, $u = 0.0920c$, $\alpha = 5.0$, $I = 8.0$ A, $\Omega/\gamma c = 1.17$ cm^{-1} (i.e., $V = 67.6$ kV, $B = 2.259$ kG). [Note: f (GHz) $= 4.775(\omega/c)$ (cm^{-1}).]

rent was measured with an integrating current transformer, and cathode voltage was measured with a compensated capacitive voltage divider.

Before and after cathode activation the entire apparatus was baked at 250 C for 48 h. System pressure, under continuous turbomolecular pumping, was ~10^{-9} Torr with the gun off, and < 5 ×10^{-7} Torr with the gun under full power. The electron beam was formed and guided along a magnetic field provided by five independently energized solenoid coil systems. Along the 60-cm interaction region a ~2-kG field was adjusted to ±2-G uniformity. Three coils around the gun provided the requisite broad field minimum of about 400 G at the cathode surface. Four-place digital measurement of all coil currents was essential for reproducibility.

Electronic gain was measured for this apparatus by injecting cw power at each frequency of inter-

Measurements of Gain for Slow Cyclotron Waves on an Annular Electron Beam

H. Guo, L. Chen, H. Keren,[a] and J. L. Hirshfield

Applied Physics Section, Yale University, New Haven, Connecticut 06520

and

S. Y. Park[b] and K. R. Chu

Naval Research Laboratory, Washington, D. C. 20375

(Received 1 June 1982)

Gain was measured for fast and slow waves propagating in a dielectric-loaded TE$_{01}$ axi-symmetric waveguide penetrated by an annular electron beam. This measurement is the first reported in the slow-wave regime, where axial velocity modulation dominates the azimuthal bunching. Small-signal gain at 6.0 GHz of over 30 dB, instantaneous bandwidth of 1.7%, and tuning bandwidth of over 11% are reported. In a feedback-amplifier configuration gain of 53 dB, power output of 20 kW, and 10% electronic efficiency are also reported.

PACS numbers: 41.70.+t, 52.35.Hr, 85.10.Hy

Considerable effort over the past decade has been directed towards understanding the convective instability for fast cyclotron waves interacting with electrons on orderly helical orbits in a uniform magnetic field.[1] This interaction is fundamental to the design of novel millimeter-wave gyrotron amplifiers.[2] The physical mechanism responsible for electromagnetic gain for this system originates with relativistic mass variations with energy which give rise to azimuthal phase bunching for orbiting electrons.[3] A competing physical mechanism, originating with axial velocity modulations, tends to oppose the azimuthal phase bunching, but the former mechanism dominates the latter so long as the wave's phase velocity exceeds the light velocity. These mechanisms have been carefully examined and contrasted by Chu and Hirshfield.[4]

For waves with phase velocity below the light velocity, the two mechanisms interchange their roles and the mechanism due to axial velocity modulation dominates the electromagnetic growth. This paper reports results of the first experiment deliberately designed to demonstrate this gain mechanism for slow electromagnetic waves. In fact, both slow and fast waves could be studied on the apparatus and their properties compared. The slow-wave mechanism has the potential for allowing wide-bandwidth operation,[5] a property not shared by the fast-wave interaction. However, a tapered-structure tapered-field variant based on the fast-wave mechanism has shown a bandwidth of 13% at 35 GHz[6]; gain is limited to about 20 dB for these fast-wave devices because of the need to use signal injection at the output in order to access the amplifying region in the device.

The apparatus built to study the slow-wave interaction is shown schematically in Fig. 1. The electromagnetic wave was guided by an axisymmetric structure consisting of a precision-bore Pyrex tube (interior diameter 3.10 cm; wall thickness, 0.20 cm), surrounded by a high-permittivity dielectric annulus (thickness, 0.29 cm), in turn surrounded by a helix waveguide formed by a closely spaced winding of No. 34 AWG copper wire. The helix waveguide was used to suppress lower modes, such as TE$_{11}$. At one end this composite waveguide tapered out gradually
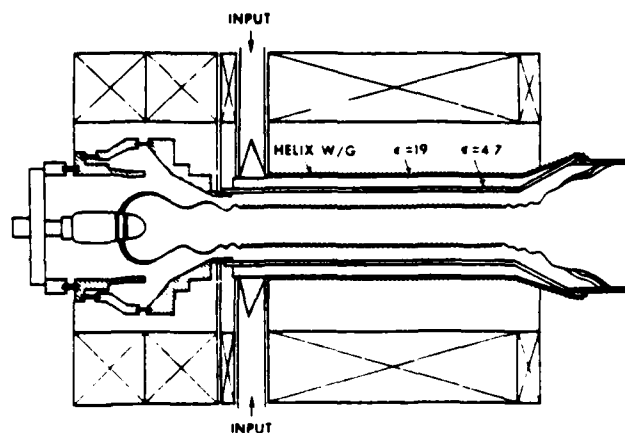
FIG. 1. Schematic outline of experimental configuration (not to scale). Magnetron injection gun at left generated annular electron beam (wiggly lines) which penetrated dielectric-loaded TE$_{01}$ circular waveguide with 60-cm uniform length. The Pyrex tube ($\epsilon = 4.7$) is surrounded by a dielectric layer ($\epsilon = 19$), which in turn is surrounded by a fine-pitch helical winding of No. 34 AWG copper wire.

SPACE CHARGE EFFECTS IN A GYROTRON EMPLOYING A SOLID ELECTRON BEAM*

H. Keren and J. L. Hirshfield

Section of Applied Physics, Yale University
P.O. Box 2159, Yale Station, New Haven, Connecticut 06520

The influence of space charge forces on the performance of
a single cavity gyrotron oscillator which uses a solid
electron beam was investigated. It was found that space
charge effects cause a large efficiency degradation as the
beam current is increased, if the other experimental para-
meters are unchanged. A small increase in the magnetic
field, however, can restore the efficiency to higher values.

Key words: microwave generators, space charge effects,
gyrotrons.

I. Introduction

The present work deals with the influence of space
charge forces on the operating characteristics of a single
cavity gyrotron oscillator. This problem was studied in
the linear regime by several authors (1-5). Here we pre-
sent results of simulations which cover both the linear and
the non-linear regimes. We calculate the response of a
solid electron beam with transverse gyrational motion, as
it passes through a cavity structure. Gyrotron experiments
along these lines are now under way (6,7). The parameters
used in our calculations are those of a 35 GHz gyrotron
oscillator which uses solid electron beams. The electron
beam enters the cavity with substantial transverse gyra-
tional motion for the beam electrons. The charge density

across the solid beam is approximately constant, and thus
gives a situation in which space charge effects can be
studied conveniently. Treating the space charge problem
for a gyrotron using an annular electron beam, which is
commonly used in experiments (8), is more complicated since
in that case the charge density across the beam is not
constant.

II. Model

Figure 1 shows the configuration of the system under
study. It consists of a solid electron beam propagating

(a)

(b)
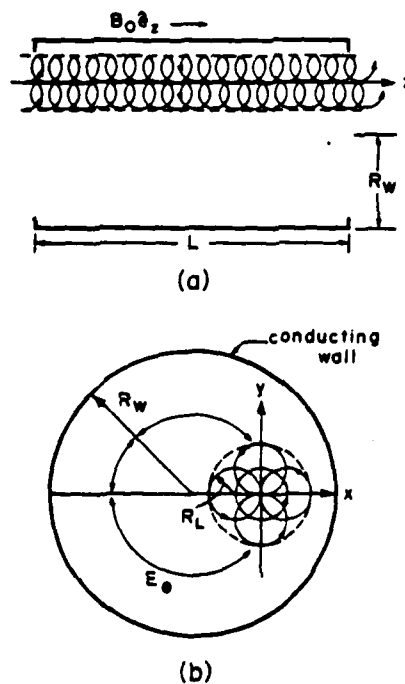
Figure 1. Side view (a) and end
view (b) of the 35 GHz gyrotron
oscillator cavity model. The solid
electron beam is axisymmetric about
the z-axis.

inside a circular cross section cavity (radius R_w and length L). The electrons, guided by an applied uniform magnetic field $B_o \hat{e}_z$, move along helical trajectories. The electrons have a substantial part of their kinetic energy in the form of transverse gyromotion and the balance in the form of axial motion. Inside the cavity, the electron beam gives up a portion of its energy through interaction with the electromagnetic fields. For fast wave cyclotron maser inter-actions it is well known (9) that the beam couples much more strongly with the TE mode than the TM mode. We thus restrict our consideration to the $TE_{on\ell}$ cavity mode, where n and ℓ are the radial and axial eigenmode numbers respectively. The field components of the $TE_{on\ell}$ cavity mode are:

$$E_\theta = E_o J_1(k_n r) \sin k_z z \cos \omega t \qquad (1)$$

$$B_r = (k_z/\omega) E_o J_1(k_n r) \cos k_z z \sin \omega t \qquad (2)$$

and
$$B_z = -(k_n/\omega) E_o J_0(k_n r) \sin k_z z \sin \omega t , \qquad (3)$$

where $k_z = \pi\ell/L$, $k_n = \chi_n/R_W$, χ_n is the nth nonvanishing root of $J_1(\chi) = 0$, and $\omega = (k_n^2 + k_z^2)^{1/2} c$ is the cavity resonant frequency.

The electron motion is governed by

$$d\underline{p}/dt = -e\underline{E} - (e/m\gamma)\underline{p} \times \underline{B} \qquad (4)$$

and
$$d\underline{r}/dt = \underline{p}/m\gamma , \qquad (5)$$

where $\underline{p} = \gamma m \underline{v}$ is the momentum, $\underline{v}$ is the velocity, $\gamma = (1 - v^2/c^2)^{-1/2}$, and $\underline{r} = \hat{e}_x x + \hat{e}_y y + \hat{e}_z z$. In case of an axisymmetric solid electron beam, with negligible longitudinal gradients in the beam radius and electron density, we can study fairly simply the influence of space charge forces on the electron orbits. We shall assume that the charge density across the beam is uniform and that the space charge forces are purely radial. Under this approxi-mation one obtains from Gauss's law, for the static elec-tric field of the beam:

$$\underline{E}_s = -\frac{N'er}{\epsilon_o R^2} \hat{e}_r \qquad (6)$$

where R is the radius of the beam envelope and N' is the
beam density per unit length which is I/ev$_z$, where I is
the beam current and v$_z$ is the axial velocity of the beam
electrons. Thus Eq. (6) becomes

$$\underline{E}_s = - \frac{Ir}{\epsilon_o R^2 v_z} \hat{e}_r \quad . \tag{7}$$

It should be pointed out that according to this model
the electrons move in an average space charge field and not
in the exact self-consistent field.

III. Particle Dynamics

The results presented in the present paper deal with
solid electron beams interacting with the fields of a TE$_{011}$
cylindrical cavity. The axis of symmetry for the solid
electron beam at the cavity entrance is the z-axis (see
Fig. 1). The cavity axis of symmetry, where the azimuthal
electric field is zero, is parallel to the z-axis but dis-
placed from it such that the azimuthal electric field has
its maximum values on the z-axis.

A three dimensional trajectory code, in cartesian co-
ordinates, was written to solve Eqs. (4) and (5). Explic-
itly, this code solves the following seven coupled equa-
tions as an initial value problem:

$$dp_x/dt = - eE_x - (e/\gamma m)(p_y B_z - p_z B_y) \tag{8}$$

$$dp_y/dt = - eE_y - (e/\gamma m)(p_z B_x - p_x B_z) \tag{9}$$

$$dp_z/dt = - (e/\gamma m)(p_x B_y - p_y B_x) \tag{10}$$

$$dx/dt = p_x/\gamma m \tag{11}$$

$$dy/dt = p_y/\gamma m \tag{12}$$

$$dz/dt = p_z/\gamma m \tag{13}$$

and $\qquad \gamma^2 = 1 + (p_x^2 + p_y^2 + p_z^2)/mc^2 \qquad .$ (14)

In these equations

$$B_x = (k_{\shortparallel}/\omega)E_o J_1(k_\perp r)\cos k_{\shortparallel} z \sin(\omega t + \phi)\cos\theta \qquad (15)$$

$$B_y = (k_{\shortparallel}/\omega)E_o J_1(k_\perp r)\cos k_{\shortparallel} z \sin(\omega t + \phi)\sin\theta \qquad (16)$$

$$B_z = B_o - (k_\perp/\omega)E_o J_o(k_\perp r)\sin k_{\shortparallel} z \sin(\omega t + \phi) \qquad (17)$$

$$E_x = - E_o J_1(k_\perp r)\sin k_{\shortparallel} z \cos(\omega t + \phi)\sin\theta - I\xi/\varepsilon_o R^2 v_z \quad (18)$$

$$E_y = E_o J_1(k_\perp r)\sin k_{\shortparallel} z \cos(\omega t + \phi)\cos\theta - I\zeta/\varepsilon_o R^2 v_z. \quad (19)$$

In Eqs. (15) – (19) ϕ is the temporal phase of the cavity fields at $t = 0$ when the electron enters the cavity structure at $z = 0$; $\theta = \tan^{-1}(\zeta/\xi)$ is the spatial angle at the instantaneous electron position $r = (x^2 + y^2)^{1/2}$; $x = x_o + \xi$, $y = y_o + \zeta$; $(x_o, y_o = 0)$ are the coordinates of the solid beam axis, and (ξ,ζ) are the coordinates relative to this axis; $k_\perp^2 = (\omega/c)^2 - k_{\shortparallel}^2$ and $k_{\shortparallel} = \pi/L$. We have _a priori_ chosen $x_o = 1.84/k_\perp$ so that the beam axis is located at the peak value of the cavity electric field.

The initial values are $p_{xo} = -\gamma_o m v_{\perp o}\sin\theta_o$, $p_{yo} = -\gamma_o m v_{\perp o}\cos\theta_o$, $p_{zo} = -\gamma_o m v_{\shortparallel o}$, $x_o = r_o\cos\theta_o$, $y_o = v_o\sin\theta_o$, and $z_o = 0$; here $v_{\shortparallel o} = v_o(1 + \alpha_o^2)^{-1/2}$ and $v_{\perp o} = \alpha_o v_o(1 + \alpha_o^2)^{-1/2}$, with $\alpha_o = v_{\perp o}/v_{\shortparallel o}$, $v_o = c(1 - \gamma_o^{-2})^{1/2}$, and $\gamma_o = 1 + eV/mc^2$ (V is the beam voltage). The axial velocity of the electron is but weakly influenced by the cavity fields. Moreover, the beam diameter remains approximately constant, since on the average we shall find that about 30% of the rotational energy is extracted from the beam. Therefore both v_z and R appearing in Eqs. (18) and (19) were assumed to be constants.

The amount by which an electron gains or loses energy to the field is determined by monitoring the relativistic energy factor γ. The efficiency η of the energy conversion for an electron with an initial value γ_o is given by $\eta = (\gamma_o - \gamma)/(\gamma_o - 1)$. In order to determine the oscilla-

tor efficiency, it is necessary to average the results over
the initial phases ϕ and θ_0. The effect of axial velocity
spread on the calculated efficiency can be studied by addi-
tional averaging over the initial velocity ratio α_0; in the
present work we have not done this.

IV. Electron Trajectories

We demonstrate our calculations for a set of experi-
mental parameters which characterize a 35 GHz gyrotron
oscillator. These parameters are summarized in Table I.

Table I. Design Parameters of the
35 GHz Gyromonotron

Cavity Mode	TE_{011}
Cavity Length	4 cm
Cavity radius	0.525 cm
Cavity Q	300
Beam voltage	10 kV
Beam current	1 Amp
Velocity ratio	2.0
Magnetic field	12.5 kG
Larmor radius	0.024 cm
Beam radius	0.048 cm
Efficiency	30%

(a) Small beam current. Fig. 2a shows the trajectory
of an electron which propagates from left to right along
the cavity, in the limit of zero current and for B_0 =
12.5 kG. Fig. 2b shows the projection of this trajectory
on the x-y plane in the cavity. It can be seen that this
electron continues to gyrate close to the beam axis of
symmetry. Initially this electron gains a small amount of
energy from the field; later on, when it becomes matched
in phase with the oscillating field, the electron loses
most of its rotational energy, mainly in the region where
E_θ is large. The orbit depicted in Fig. 2 is for a value

ELEC. TRAJEC. ØF SØLID ELECTRØN BEAM
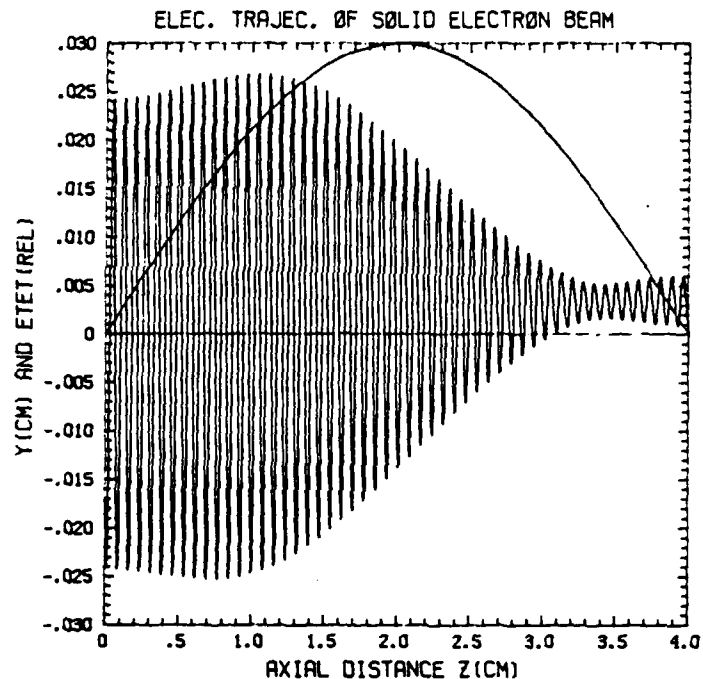
Figure 2a. The trajectory of an electron which
propagates from the left to the right along the
cavity, in case where $I = 0$ Amp and $B_0 = 12.5$
kG. Entrance phase was $\phi = 4\pi/3$. Also shown
is a normalized amplitude profile of the cavity
azimuthal electric field, proportional to
$\sin(\pi z/L)$.

of entrance phase $\phi = 4\pi/3$; for this phase the energy
given up is larger than for other phases.

(b) Space charge case. Fig. 3 shows the projected
trajectory of an electron which grazes the beam boundary
at the cavity entrance, and enters the cavity in the same
phase as the electron shown in Fig. 2, but now for a beam
current $I = 1.0$ Amp and $B_0 = 12.5$ kG. It can be seen that
in addition to the gyrational motion, this electron drifts
around the z-axis due to the $\underline{E} \times \underline{B}$ drift. Initially this
electron loses a significant part of its rotational energy

ELEC. TRAJEC. ØF SØLID ELECTRØN BEAM
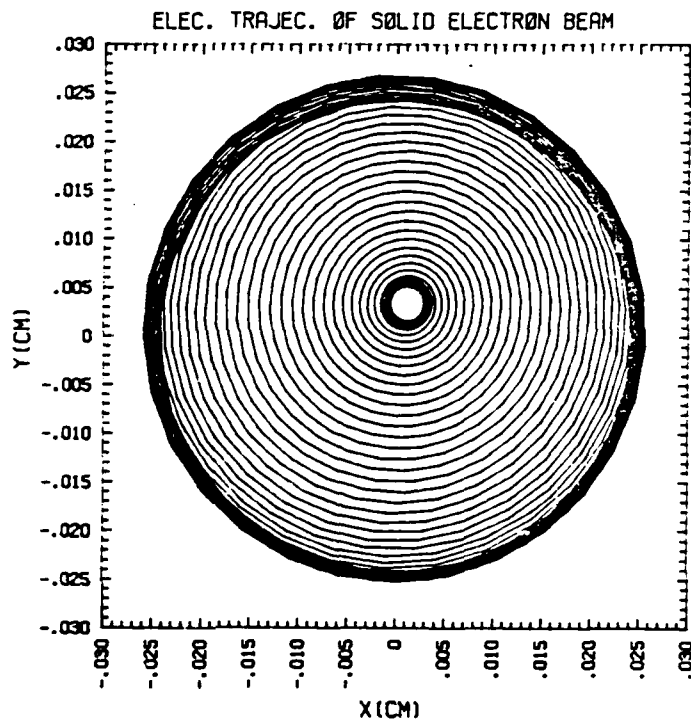
Figure 2b. The projection of the trajectory
of Fig. 2a on the x-y plane along the cavity.

as in the case of no space charge, but later on it regains
most of it due to mismatch in phase with the fields. A
small increase in the guide magnetic field, by only 1%,
changes the last situation dramatically (see Fig. 4); the
electron continuously transfers its energy to the cavity
field, similar to the case shown in Fig. 2. It should be
mentioned here that calculated trajectories of other elec-
trons, including the space charge forces, showed that the
axis of symmetry for the travelling solid electron beam
along the cavity remains the z-axis. Thus we can justify
the earlier assumption that inclusion of space charge
forces still leaves the beam axisymmetric with respect to
the z-axis.

ELEC. TRAJEC. ØF SØLID ELECTRØN BEAM
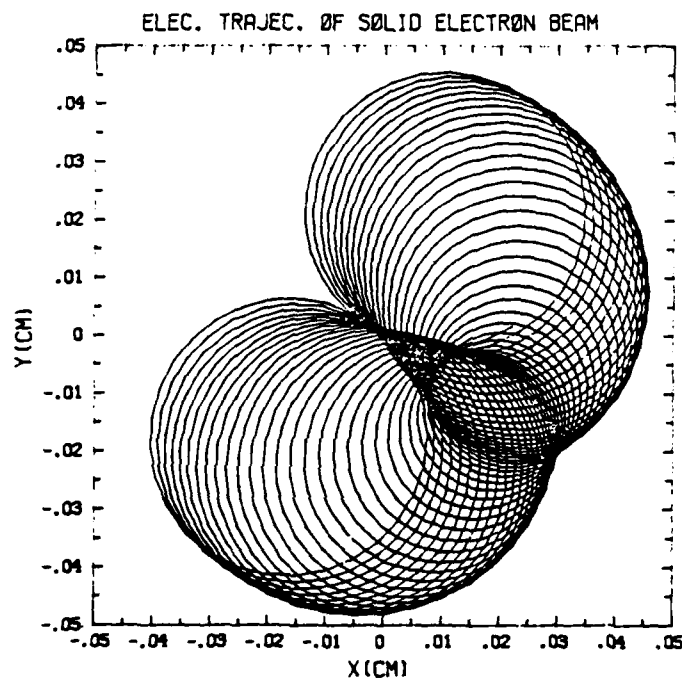
Figure 3. The projected trajectory of an elec-
tron which grazes the beam boundary at the
cavity entrance, and enters the cavity in the
same phase of the electron shown in Fig. 2,
in cases where I = 1 Amp and B_0 = 12.5 kG.

ELEC. TRAJEC. ØF SØLID ELECTRØN BEAM
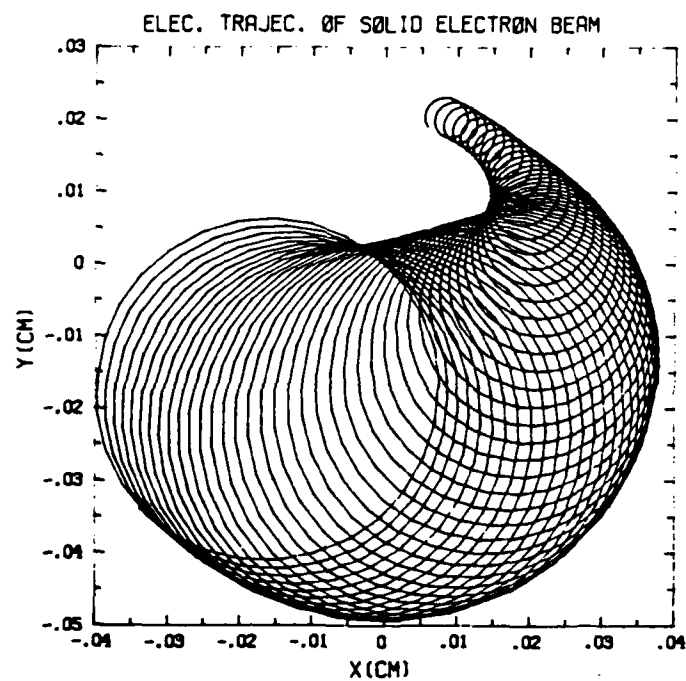
Figure 4. Same as Fig. 3 except an increase
of about 1% in the cavity static magnetic
field, i.e. B_0 = 12.65 kG.

V. Discussion

We recall that the kinetic energy of an electron is given by $(\gamma - 1)mc^2$, so the energy transfer rate from the electron to the cavity field is determined by monitoring γ. This transfer rate is twice the wave growth rate. Our calculations cover both the linear regime and the non-linear regime close to saturation. We shall define the energy growth rate as the time derivative of γ, where a negative sign for the derivative indicates transfer of energy from the electrons to the field, and vice versa.

Figure 5 shows γ as a function of time for the case

ELEC. TRAJEC. ØF SØLID ELECTRØN BEAM
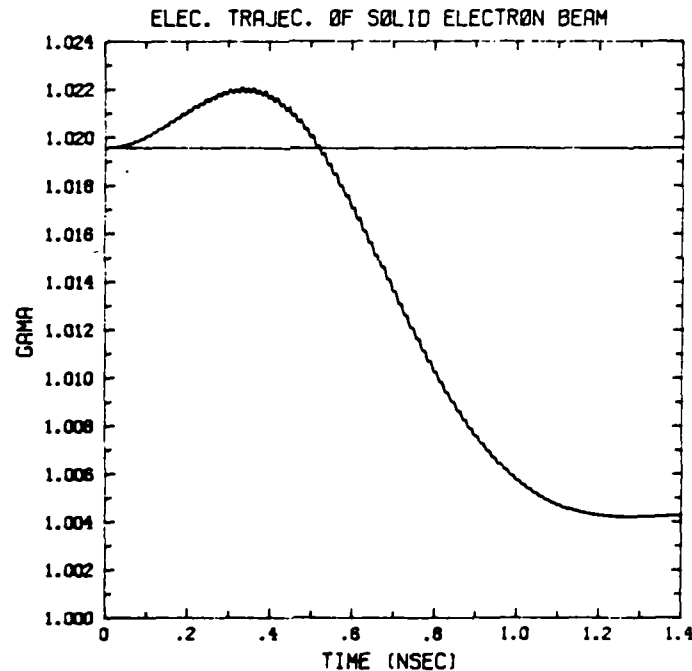
Figure 5. γ as a function of time for the case shown in Figs. 2a and 2b, i.e. I = 0 and B_0 = 12.5 kG. This electron enters the cavity at a time t = 0 and leaves the cavity at t = 1.4 nsec with 22% of its initial kinetic energy.

shown in Figs. 2a and 2b, i.e. I = 0 and B_O = 12.5 kG.
This electron enters the cavity at a time t = 0 and leaves
the cavity at t = 1.4 nsec with 22% of its initial
kinetic energy. Fig. 6 shows in curve (a) γ as a function
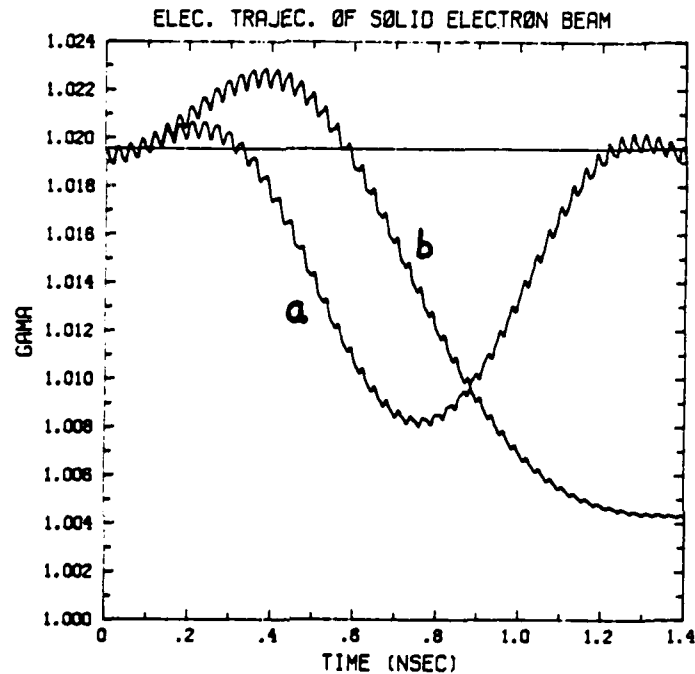
Figure 6. Trace (a) shows γ as a function of time
for the case shown in Fig. 3, i.e. I = 1 Amp and
B_O = 12.5 kG. Trace (b) is related to Fig. 4,
i.e. I = 1 Amp and B_O = 12.65 kG.

of time for the case shown in Fig. 3, i.e. I = 1 Amp and
B_O = 12.5 kG, and curve (b) γ versus time for the case
corresponding to Fig. 4, as in I = 1 Amp and B_O = 12.65 kG.
It can be seen that at a guide magnetic field of 12.5 kG,
the electron is trapped earlier by the cavity field and,
as a result, the electron leaves the cavity without losing
any of its kinetic energy. A small increase in the axial

field, by only 1%, restores the energy loss of the electron
to 76%.

Efficiency calculations for the above described gyro-
tron were done by averaging   η   over eight electrons
entering the cavity at eight different phases in space and
at three different phases with respect to the oscillating
field (see Fig. 7). These calculations predict 30%
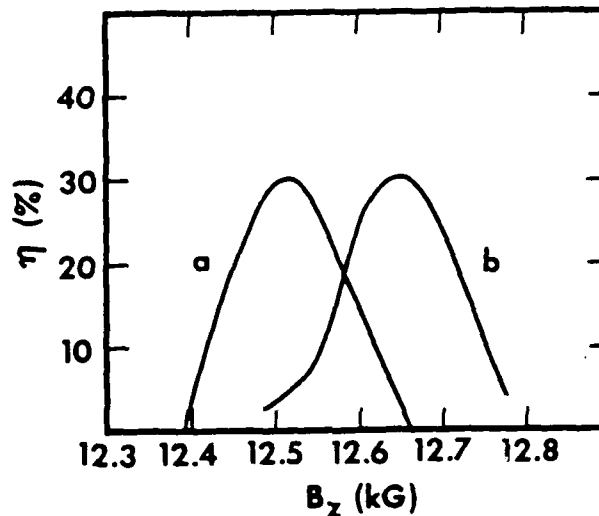
Figure 7. The gyromonotron efficiency as a
function of the cavity static magnetic field
without inclusion of space charge forces
(curve a) and with space charge forces due to
beam current of 1 Amp (curve b).

efficiency for the case of I = 0 and B_O = 12.5 kG, and
only 4% efficiency in the case of I = 1 Amp and B_O = 12.5 kG.
However, about 1% increase in the magnetic field, i.e.
B_O = 12.56 kG, predicts efficiency of 31% in the case of
I = 1 Amp. Fig. 8 correlates our calculations with the
prediction of th·. linear theory. This example shows γ in
in a short time interval (0.4 nsec) for an electron which
enters the cavity with phase corresponding to energy

ELEC. TRAJEC. ØF SØLID ELECTRØN BEAM
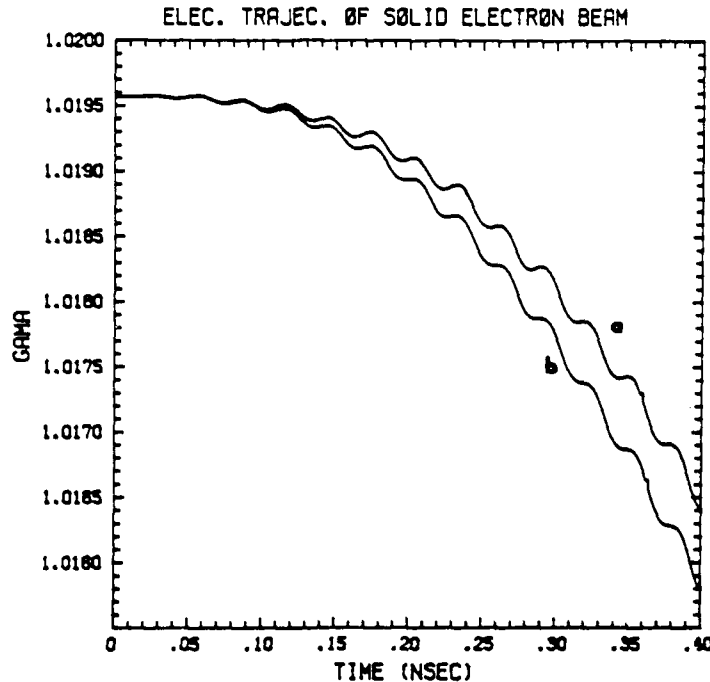
Figure 8. γ as a function of time in a short
time interval (0.4 nsec) for an electron which
enters the cavity with phase corresponding to
energy transfer to the oscillating wave. Curve
(a) corresponds to the case I = 0 and curve (b)
for I = 1 Amp, both for same B_0.

transfer to the oscillating wave. Curve (a) correspon;.
to the case of I = 0 and (b) for I = 1 Amp, both for same
B_0. The oscillatory behavior of these traces, clearly seen
on this time scale, shows that the gyrating electron is
strongly coupled to the azimuthal electric field only part
time in each period of oscillation. It can be seen that
the average growth rate in that short time interval, i.e.
the total decrease in γ, is higher for the space charge
case, as predicted also from the analytical expressions of
the linear theory (1-4). At a later time, in the case of

$$\overline{\Delta W} \simeq \sqrt{\pi} \, \frac{e p_{\perp 0} r_{02} E_{02}}{p_z} \, \frac{n J_n(\beta_0)}{\beta_0} \, \exp - \left[\frac{r_{02}^2 m^2 (n\Omega - \gamma_0 \omega)^2}{4 p_z^2} \right]$$

$$\times \, \sin[\phi_0 \, + \frac{m}{p_z} \, (n\Omega - \gamma_0 \omega) L] \int dy_g \, f(y_g) \tag{31}$$

$$\times \, \cos(k_\perp y_g - n\frac{\pi}{2}) J_1[q\cos(k_\perp y_g - n\frac{\pi}{2})] \qquad .$$

The power transfer from the electron beam to the wave is

$$\Delta P = \overline{\Delta W} I_b / e \qquad .$$

Finally, we have

$$\Delta P = \sqrt{\pi} \, \frac{I_b p_{\perp 0} r_{02} E_{02}}{p_z} \, \frac{n J_n(\beta_0)}{\beta_0} \, \sin[\phi_0 \, + \frac{m}{p_z} \, (n\Omega - \gamma_0 \omega) L]$$

$$\times \, \exp \left[- \frac{r_{02}^2 m^2 (n\Omega - \gamma_0 \omega)^2}{4 p_z^2} \right] \int dy_g \, f(y_g) \tag{32}$$

$$\times \, \cos(ky_g - n\frac{\pi}{2}) J_1[q\cos(ky_g - n\frac{\pi}{2})] \qquad .$$

III. Cyclotron Harmonic Gyroklystron Based On Electromagnetic Interactions

The physical configuration in this analysis is identical to that described at the beginning of Section II except that now we consider a TEM_{00} mode in a quasioptical Fabry-Perot cavity. We have for the electric and magnetic field components

$$E_x \simeq E_0 \exp(-z^2/r_0^2) \sin k_\perp y \cos \omega t \tag{33}$$

$$B_z \simeq E_0 \exp(-z^2/r_0^2) \cos k_\perp y \sin \omega t \quad , \tag{34}$$

where

$$\frac{k_\perp c}{\omega} = 1 \qquad . \tag{35}$$

Using the same procedure as we used in Section II, we obtain the following equations.

where

$$q \approx \frac{\sqrt{\pi} \; e\omega E_{01} \; \dfrac{nJ_n(\beta_0)}{\beta_0} \; P_{\perp 0} r_{01} L}{p_z^2 c^2} \; \exp\left[- \frac{(n\Omega - \gamma\omega)^2 \; m^2 r_{01}^2}{4p_z^2}\right] . \quad (25)$$

In Eq. (24) the variable z has been redefined so that z=0 is now at the center of the second cavity.

The energy that the electron transfers to the wave fields as it moves through the second cavity is

$$\Delta W = e \int v_y E_y dt = e \int \frac{p_y}{p_z} E_y dz \qquad (26)$$

where

$$E_y = E_{02} \exp(-z^2/r_{02}^2) \sin k_{\perp} y \cos(\omega t - \phi_0) \quad . \qquad (27)$$

E_{02} and r_{02} are the electric field amplitude and the minimum spot size in the second cavity, respectively. ϕ_0 is the temporal phase shift between the two cavities. Assuming $\omega \simeq n\Omega/\gamma$, we obtain

$$\Delta W \cong - e \; \frac{P_{\perp 0}}{p_z} \; E_{02} \; \frac{nJ_n(\beta_0)}{\beta_0} \; \cos(k_{\perp} y_g - n\frac{\pi}{2})$$

$$\times \int_{-\infty}^{\infty} dz \sin[n\theta_0 + \phi_0 + \Delta n\theta] \exp(-z^2/r_{02}^2) \quad . \qquad (28)$$

Substituting for $\Delta n\theta$, we obtain

$$\Delta W \simeq - \sqrt{\pi} \; \frac{ep_{\perp 0} r_{02} E_{02}}{p_z} \; \frac{nJ_n(\beta_0)}{\beta_0} \; \cos(k_{\perp} y_g - n\frac{\pi}{2})$$

$$\times \sin\left[n\theta_0 + \phi_0 + \frac{m}{p_z} (n\Omega - \gamma_0\omega) L + q\sin n\theta_0 \qquad (29)\right.$$

$$\times \left. \cos(k_{\perp} y_g - \frac{n\pi}{2})\right] \exp\left[-\left(\frac{r_{02}^2 m^2 (n\Omega - \gamma_0\omega)^2}{4p_z^2}\right)\right] \quad .$$

The average energy loss for a uniform distribution in θ_0 and arbitrary distribution $f(y_g)$ in y_g becomes

$$\overline{\Delta W} = \frac{1}{2\pi} \int dn\theta_0 \int \Delta W f(y_g) dy_g \quad . \qquad (30)$$

Substituting ΔW into Eq. (30) we obtain

If we assume $\omega \simeq n\Omega/\gamma$ and note that to lowest order $d\psi/dt \simeq \Omega/\gamma$, Eq. (18) can be reduced to

$$\frac{dp_\perp}{dz} = \frac{em\gamma}{p_z} E_0 \exp(-z^2/r_0^2) \; \frac{n J_n(\beta)}{\beta} \; \sin(\omega t - n\psi)\cos(k_\perp y_g - n \frac{\pi}{2}) \quad (19)$$

Introducing the slowly varying phase angle $n\theta = n\psi - \omega t$, Eq. (19) is reduced to

$$\frac{dp_\perp}{dz} = - \frac{em\gamma}{p_z} E_0 \exp(-z^2/r_0^2) \; \frac{n J_n(\beta)}{\beta} \; \sin n\theta \cos(k_\perp y_g - n \frac{\pi}{2}) \quad . \quad (20)$$

We can linearize Eq. (20) by setting $p_\perp = p_{\perp 0} + p_{\perp 1}$, and since $p_{\perp 0} \gg p_{\perp 1}$, we obtain

$$\frac{dp_{\perp 1}}{dz} \simeq - \frac{em\gamma}{p_z} E_{01} \exp(-z^2/r_{01}^2) \; \frac{n J_n(\beta_0)}{\beta_0} \; \sin n\theta \cos(k_\perp y_g - n \frac{\pi}{2}) \quad (21)$$

where $\beta_0 = k_\perp p_{\perp 0}/m\Omega$, E_{01} and r_{01} are the electric field amplitude and the minimum spot size in the first cavity respectively.

From Eq. (14) we obtain $n\theta \simeq n\theta_0 + m(n\Omega - \gamma\omega)z/p_{z0}$ where $n\theta_0$ is the slow phase angle at the center of the first cavity. Using $n\theta$ in Eq. (21) and assuming a weak electric field amplitude in the first cavity, we can calculate $p_{\perp 1}$, the change in the transverse momentum $p_\perp$ that a particle undergoes as it moves through the first cavity.

$$p_{\perp 1} \simeq - \sqrt{\pi} \; E_{01} \; \frac{n J_n(\beta_0)}{\beta_0} \; \frac{em\gamma_0 r_{01}}{p_z} \cos(k_\perp y_g - n \frac{\pi}{2})$$

$$\times \; \sin(n\theta_0) \exp\left[- \frac{(n\Omega - \gamma\omega)^2 r_{01}^2 m^2}{4 p_z^2} \right] \quad . \quad (22)$$

In the drift region we have

$$\frac{dn\theta}{dz} \simeq \left(n\Omega - \gamma_0 \omega - \frac{p_{\perp 0} p_{\perp 1} \omega}{m^2 c^2} \right) \frac{m}{p_z} \quad . \quad (23)$$

Substituting for $p_{\perp 1}$ in Eq. (23) and integrating this equation in a drift region of length L and a uniform magnetic field, we obtain the change in the slow phase angle $\Delta n\theta$ as

$$\Delta n\theta \simeq \frac{m}{p_z}(n\Omega - \gamma_0 \omega)(z + L) + q \sin n\theta_0 \cos(k_\perp y_g - n \frac{\pi}{2}) \quad (24)$$

where Ω is the electron cyclotron frequency.

Equations (9-11) then reduce to

$$\frac{dp_\perp}{dz} = -\frac{em\gamma}{p_z} E_x \cos\psi - \frac{em\gamma}{p_z} E_y \sin\psi \qquad (13)$$

$$\frac{d\psi}{dz} = \frac{em\gamma}{p_\perp p_z} (E_x \cos\psi - E_y \sin\psi) + \frac{e}{cp_z} (B_z + B_0) \qquad (14)$$

$$\frac{dy_g}{dz} = -\frac{\gamma e}{\Omega p_z} E_x - \frac{p_y B_z}{p_z B_0} \qquad . \qquad (15)$$

Since $E_y \gg E_x$, we have

$$\frac{dp_\perp}{dz} \simeq -\frac{em\gamma}{p_z} E_0 \exp(-z^2/r_0^2) \sin k_\perp y \sin\psi \cos\omega t \qquad . \qquad (16)$$

Substituting Eq. (11) into Eq. (16) we get

$$\frac{dp_\perp}{dz} \simeq -\frac{em\gamma}{p_z} E_0 \exp(-z^2/r_0^2) \cos\omega t \sin\psi \sin(k_\perp y_g - \beta\cos\psi) \qquad (17)$$

where $\beta = k_\perp p_\perp/m\Omega$.

In order to make simplifying approximations in Eq. (17), we note that the wave particle interaction is strong only for $\omega \simeq n\Omega/\gamma$ where n is an integer. The right hand side of Eq. (17) will then be the sum of rapidly and slowly oscillating terms in z (9). To first order in $E/(cB_0)$ we can neglect the rapidly oscillating terms and only retain the slowly oscillating terms in Eq. (17). Using the identity

$$\sin k_\perp(y_g - \frac{p_\perp}{m\Omega}\cos\psi) = \sin k_\perp y_g [J_0(\beta) + 2\sum_{\ell=1}^{\infty} (-1)^\ell J_{2\ell}(\beta)\cos 2\ell\psi]$$
$$- 2\cos k_\perp y_g \sum_{\ell=0}^{\infty} (-1)^\ell J_{2\ell+1}(\beta)\cos(2\ell+1)\psi \quad ,$$

we obtain

$$\frac{dp_\perp}{dz} = -\frac{em\gamma}{p_z} E_0 \exp(-z^2/r_0^2) \cos\omega t \sin\psi \{\sin k_\perp y_g$$
$$\times [J_0(\beta) + 2\sum_{\ell=1}^{\infty} (-1)^\ell J_{2\ell}(\beta)\cos 2\ell\psi] - 2\cos k_\perp y_g$$
$$\times [\sum_{\ell=0}^{\infty} (-1)^\ell J_{2\ell+1}(\beta)\cos(2\ell+1)\psi]\} \quad . \qquad (18)$$

are slow waves, the wavenumber $k_\perp$ and frequency ω must satisfy $k_\perp c/\omega > 1$. Also from Maxwell's equations, we can write

$$B_z = \frac{\epsilon k_\perp c}{\omega} E_0 \exp(-z^2/r_0^2) \cos k_\perp y \sin \omega t \quad . \tag{3}$$

The vector equation of motion for an electron is

$$\frac{d\vec{p}}{dt} = -e\left[\vec{E} + \frac{\vec{v}}{c} \times \vec{B}\right] \tag{4}$$

which in Cartesian coordinates reduces to the following set of equations

$$\frac{dp_x}{dt} = -eE_x - e\frac{v_y}{c}(B_0 + B_z) \tag{5}$$

$$\frac{dp_y}{dt} = -eE_y + e\frac{v_x}{c}(B_0 + B_z) \tag{6}$$

$$\frac{dp_z}{dt} = 0 \tag{7}$$

where E_x, E_y, and B_z are given by Eqs. (1-3). From Eq. (7) we can immediately write

$$p_z = p_{z0} = \text{const}$$

and

$$\frac{dz}{dt} = \frac{p_z}{m\gamma} = \frac{p_{z0}}{m\gamma_0} \tag{8}$$

where p_{z0} is the initial value of the parallel momentum upon entering the first cavity, $\gamma = (1 - v^2/c^2)^{-\frac{1}{2}}$ and γ_0 is the input γ.

Following the analysis of Ref. 9, we use $p_\perp$, ψ, x_g, and y_g as dependent variables in the equation of motion, where these variables are related to p_x, p_y, x and y respectively by

$$p_x = p_\perp \cos\psi \tag{9}$$

$$p_y = p_\perp \sin\psi \tag{10}$$

$$y_g = y + \frac{p_x}{m\Omega} \tag{11}$$

$$x_g = x - \frac{p_y}{m\Omega} \tag{12}$$

It has recently been suggested (6) that for high order
cyclotron harmonic operation, coupling to the Bernstein
modes on the electron beam should be possible, since these
modes exhibit strong wave-particle interaction even up to
the 20th cyclotron harmonic for device parameters easily
achievable in the laboratory. The first Bernstein mode
maser experiment (7), in which operation of a quasi-optical
gyromonotron was demonstrated up to the fourth cyclotron
harmonic, generally tends to support these theoretical
predictions. On the other hand, the operation of a gyro-
klystron with two open cavities has recently been analyzed
by Ganguly and Chu (8). Their analysis demonstrates that
the prebunching of the beam not only enhances the inter-
action efficiency but also improves mode stability. Thus
it is of some interest to investigate the performance of
a gyroklystron based on the Bernstein modes, particularly
for high order cyclotron harmonic operation. Such a
device is analyzed in this paper.

The paper is organized as follows. In Section II we
analyze the gyroklystron based on the Bernstein modes,
give the basic equations and derive the linear power out-
put. In Section III we analyze the quasi-optical gyro-
klystron based on electromagnetic interactions alone. In
Section IV comparisons on performance are made between the
two gyroklystrons, followed by a discussion.

II. Cyclotron Harmonic Gyroklystron Based On
Electron Bernstein Modes

The quasi-optical gyroklystron configuration is depic-
ted in Fig. 1. The gyrating beam electrons rotate in the
x-y plane and stream along the external magnetic field $\vec{B}_0$
which is directed along the z axis. In this analysis, we
assume that all electrons have the same transverse momen-
tum $p_{\perp}$ and parallel momentum p_z as they traverse the cavi-
ties from cavity 1 to cavity 2. For nearly longitudinal
standing waves across $\vec{B}_0$ (Bernstein modes) the electric
field components are (6)

$$E_y = E_0 \exp(-z^2/r_0^2)\sin k_{\perp}y\cos\omega t \qquad (1)$$

$$E_x = \varepsilon E_0 \exp(-z^2/r_0^2)\sin k_{\perp}y\cos\omega t \qquad (2)$$

where ω is the radiation frequency, E_0 is the field ampli-
tude at the origin, r_0 is the minimum spot size of the
radiation envelope and $|\varepsilon| \ll 1$. Since Bernstein modes

BERNSTEIN MODE QUASI-OPTICAL GYROKLYSTRON

Z. Liang, N. A. Ebrahim, and J. L. Hirshfield

Applied Physics Section, Yale University
P. O. Box 2159, Yale Station, New Haven, CT 06520

The performance of a quasi-optical cyclotron harmonic gyroklystron operating on electron Bernstein modes is investigated. An expression for the linear power output has been derived. It is found that, for high order cyclotron harmonic operation, a gyroklystron involving the Bernstein modes has higher linear efficiency than a corresponding gyroklystron based on electromagnetic interactions alone.

Key words: quasi-optical gyroklystron, electron Bernstein waves.

I. Introduction

In the past few years, there has been a great deal of interest in a high order cyclotron harmonic maser, because of potential applications in the millimeter and submillimeter regimes (1-4). However, most device development has been limited to fundamental or second harmonic interactions. Recently, McDermott, et al. (5) have demonstrated high harmonic gyrotron operation using a 200 kV rf-accelerated axis-encircling electron beam. However it would seem that operation of a high order cyclotron harmonic maser at lower voltages (< 50 kV) demands stronger wave-particle coupling than has hitherto been demonstrated.

Vol. 1, pp. 1–54.

[2]K. R. Chu and J. L. Hirshfield, Phys. Fluids 21, 461 (1978).

[3]F. A. Korolev and A. F. Kurin, Radio Eng. Electron. Phys. (Engl. Transl.) 15, 1868 (1970).

[4]D. E. Baldwin, I. B. Bernstein, and M. P. H. Ween-ink, in *Advances in Plasma Physics*, edited by A. Simon and W. B. Thompson (Interscience, New York, 1969), Vol. 3, pp. 87–95.

[5]F. W. Crawford, J. Res. Natl. Bur. Stand. 69D, 789 (1965).

[6]J. L. Hirshfield, Int. J. Infrared Millim. Waves 2, 695 (1981).

[7]Type MTF 1000 electron gun, Teledyne MEC, Palo Alto, CA 94304.

[8]P. Sprangle, W. Manheimer, and J. Vomvoridis, Naval Research Laboratories Memorandum Report No. 4366, 1980 (unpublished).

dius.

The start oscillation conditions for the two instabilities for the first four harmonics at 62.4 GHz are shown in Fig. 2, for several different values of the momentum ratio α. The operating values of the beam current observed experimentally when oscillations were sustained in the cavity are also shown for comparison. For reasonable experimentally achievable values of the momentum ratio the low values of starting current favor the Bernstein-mode instability as the gain mechanism in these experiments. The experimentally observed values of the beam current are larger than those predicted for the Bernstein-mode coupling because the experimental values are operating values rather than the minimum values required to start oscillations. In the present setup the beam current cannot be easily varied independently of other beam parameters. Although higher values of $\alpha(\sim 10)$ lower the starting conditions quite significantly, it is extremely unlikely that a momentum ratio of 10 was obtained in these experiments. Orbit calculations for the experimental conditions gave a value of α of 1.6. Furthermore, measurements of the collector current as a function of the kicker

magnetic field showed no abrupt cutoff in collector current, suggesting that these experiments were not conducted in a parameter regime close to the mirroring point of the beam electrons, where large values of α might be expected.

With use of the linear theory of the cyclotron maser instability, to calculate the small-signal efficiency, it can be shown that the output power at the nth harmonic normalized to the output power at the fundamental is given by

$$P_{0n}/P_{01} = 2(n/2)^{2n}(n!)^{-2}\beta_{\perp 0}^{2(n-1)}, \qquad (4)$$

where n is the harmonic number and $n \geq 2$. The normalized power according to Eq. (4) for the first four harmonics shows a very rapid decrease with harmonic number. For instance, for $\alpha = 2$, $(\beta_{\perp 0} = 0.243)$, the power output at the second harmonic is 2.8% of the fundamental power, at the third harmonic it is 0.2%, and at the fourth harmonic it is approximately 0.02% of the power at the fundamental. On the other hand, the experimentally observed detector output normalized to the fundamental showed a much slower decrease than that predicted by the cyclotron-maser instability theory. Experimentally observed signal at the second harmonic is 40% of the fundamental signal, at the third harmonic it is 6%, and at the fourth harmonic it is 1%. These comparisons are consistent with the observations that the present experiments have been in a regime where collective effects and mode conversion at the beam boundary determine the electromagnetic gain.

The results reported in this Letter confirm that strong interaction at the higher cyclotron harmonics is possible for very modest values of electron-beam currents. Our present interpretation is that this is due to the much larger instability growth rates at the higher harmonics for the electrostatic modes (Bernstein modes) compared to the case of electromagnetic interaction alone. This previously unexplored mechanism may have practical applications in the development of high-harmonic cyclotron masers operating at modest magnetic fields.
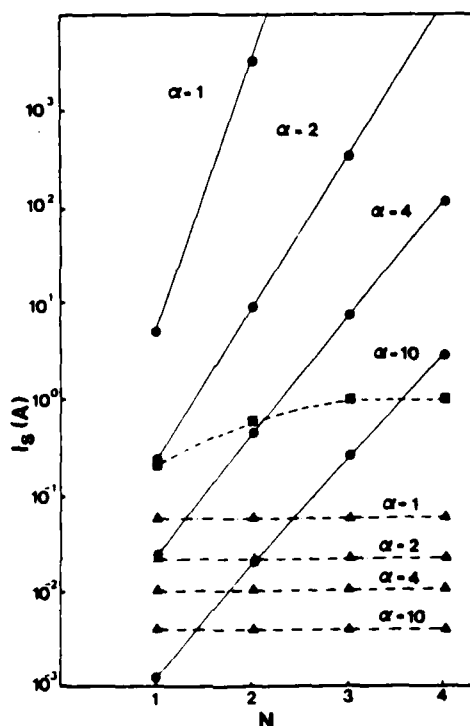
FIG. 2. Start oscillation current vs the harmonic number. Solid curves calculated from Eq. (1). Triangles, calculated from Eq. (3). Squares, experimental measurements of the operating current.

J. L. Hirshfield, in Infrared and Millimeter Waves, edited by K. R. Button (Academic, New York, 1979),

TABLE I. Conditions under which coherent output signals were observed and the frequency of the observed output. Intermirror spacing $L = 3.125$ cm, intermode frequency $\Delta f = 4.8$ GHz. $\gamma = 1.0371$, $f_0 = N\Omega_0/2\pi\gamma$, $\Omega_0 = |e|B_0/m_0$. f_{F-P} are the resonant modes of the Fabry-Perot. B_0 is in kilogauss and all frequencies are in gigahertz. N is the harmonic number.

HARMONIC NUMBER (N)	f_{F-P}	62.4	67.2	72.0	76.8	81.6	86.4	91.2	96.0	100.8	105.6
	Mode No. m	13	14	15	16	17	18	19	20	21	22
1	B_0	23.2	24.9	26.7	28.6	30.4	32.2	34.0	36.2	38.1	40.0
1	f_0	62.6	67.2	72.1	77.2	82.1	86.9	91.8	97.7	102.9	108.0
2	B_0	11.5	12.4	13.3	14.3	15.2	16.1	17.1	18.0	18.8	19.8
2	f_0	62.1	67.0	71.8	77.2	82.1	86.9	92.3	97.2	101.5	106.9
3	B_0	7.7	8.3	8.9	9.6	10.1	10.7				
3	f_0	62.4	67.2	72.1	77.8	81.8	86.7				
4	B_0	5.7									
4	f_0	61.6									

monic at 7.7 kG ($f_0 = 62.4$ GHz), and fourth harmonic at 5.7 kG ($f_0 = 61.6$ GHz). The small differences between the estimated cyclotron-harmonic frequencies and frequency of the resonant mode of the Fabry-Perot could be due to the accuracy of the axial magnetic field measurements (on the order of 2%) or to slight pulling of the resonator frequency by the electron beam. Between 67 and 86 GHz observations were made of up to the third cyclotron harmonic for every resonant mode of the Fabry-Perot cavity, and between 91 and 105 GHz we have observed up to the second harmonic. At the high values of the axial magnetic field, the lower electron-beam currents could only sustain up to the second harmonic. It should be noted that the estimated quality factor

Q of the empty Fabry-Perot is slightly greater than 10^4 over this frequency range but that Q drops at higher frequencies because of increased Ohmic and coupling losses. It is estimated that microwave output power levels of 1–2 W have been observed at the fundamental frequency at 86 GHz although the system was operated at conditions which were far from optimum.

The linear and nonlinear theory[8] for the cyclotron maser instability has recently been formulated for a quasioptical system of very similar geometry to that employed in the present experiment. With use of the linear small-signal efficiency at the nth harmonic it can be shown that the start oscillation conditions for the beam current are given by

$$I_s^{(n)} = (2^{n-1}n! \, r_0 B_0)^2 \omega L(1 - 1/\gamma_0)\exp[\xi_0^2(\Delta\omega/\omega)^2/2]\{\xi_0^2(kp_\perp/m_0\Omega_0)^{2(n-1)}[\xi_0^2\beta_\perp^2(\Delta\omega/\omega)/2 - n](2\pi QV)\}^{-1},$$

(1)

$$(\Delta\omega/\omega)_{min} = [n + (n^2 + \xi^2\beta_{\perp 0}^4)^{1/2}]/\xi^2\beta_{\perp 0}^2,$$

(2)

where $\xi_0 = (r_0\omega/c)/\beta_{\perp 0}$, $\Omega_0 = |e|B_0/m_0 c$, $\gamma = (1 + \vec{p} \cdot \vec{p}/m_0^2 c^2)^{1/2}$, $\vec{p}$ is the electron momentum vector, ω is the angular frequency, r_0 is the radiation spot size, B_0 is the axial magnetic field, $\beta_\perp$ is the normalized transverse component of the electron velocity, $\beta_{\perp 0}$ is the normalized parallel component of the electron velocity, V is the electron energy, Q is the Fabry-Perot quality factor $\sim 10^4$, and $\Delta\omega = \omega - n\Omega_0/\gamma_0$ is the frequency mismatch. We have assumed a value of $\Delta\omega/\omega$ which gives a minimum value for the starting current I_s.

By contrast, from the analysis of unstable Bern-

stein modes and their coupling to Fabry-Perot modes presented in Ref. 6, one can determine the starting current from the requirement for steady state, $Im\omega/Re\omega = 1/2fQ$, where f is a geometric filling factor. This reduces to

$$I_s^{(n)} = 6.6 \times 10^4 (nDB_0/Q)^2 V^{-1/2}(1 + \alpha^2)^{1/2}\alpha^{-2} \text{ A},$$

(3)

where D is the radiation waist radius in centimeters, B_0 is in kilogauss, V is in kilovolts, and f is taken as r_b/D with r_b the electron beam ra-

perimental observation of coherent higher-cyclo-
tron-harmonic oscillations for a system in which
the aforementioned mode conversion can occur.
The parameters of the experiment quantitatively
support the previously published simplified model
for the mode-coupling interaction.[5] The results
suggest that a previously unexplored mechanism
may now permit the development of higher-har-
monic cyclotron masers for submillimeter and
far-infrared application requiring modest mag-
netic fields.

The schematic of the experimental configuration
is shown in Fig. 1. The solid laminar-flow elec-
tron beam from a space-charge-limited Pierce
gun was injected along the axis of a cylindrical
stainless steel vacuum vessel located in the bore
of a superconducting solenoid. The gun,[7] designed
to operate at a maximum of 20 kV, 5.6 A, 10^{-3}
duty cycle, with a nominal beam radius of 0.3 cm,
was driven with 5-μsec, 10-sec^{-1} pulses from a
MIT model 9 modulator. The cathode and trans-
mitted currents were measured with Pearson inte-
grating transformers.

Immediately downstream of the gun exit, the
beam electrons underwent nonadiabatic passage
through a spatially localized transverse magnetic
field ("kicker") provided by a pair of tailored
Helmholtz coils which imparted controlled trans-
verse momentum to the beam electrons. The sub-
sequent passage of the beam through the increas-
ing axial magnetic field resulted in an increased
value of the transverse-to-axial momentum ratio
α, if one assumes the motion to be adiabatic.
Computer calculations of single-particle trajec-
tories in combined axial and kicker fields showed
that momentum ratios α of the order of 2 could
easily be achieved in this apparatus for kicker
fields of the order of 100 G in axial guide fields
of up to 10 kG.

The millimeter resonator was a confocal Fabry-
Perot resonator with a fixed intermirror spacing
$L = 3.125$ cm, mirror radii of curvature 11 cm,
and intermode frequency spacing $\Delta f = c/2L = 4.8$
GHz. The mirrors were made of polished oxygen-
free high-conductivity copper with a coupling hole
and WR-10 waveguide machined into the output
mirror to couple the millimeter-wave output from
the system. In cold tests of the Fabry-Perot
with a sweep oscillator, the complete longitudinal
mode spectrum between 62 and 105 GHz was
measured, with typical power coupling into the
resonator of approximately -3 dB at 91 GHz. The
resonator was designed for operation in the low-
est transverse mode with the polarization of the
electric field vector transverse to the axial guide
magnetic field.

Table I summarizes the conditions under which
coherent millimeter-wave output signals were
observed in the frequency range 62–105 GHz. The
low-frequency limit was determined by the low-
frequency cutoff of the WR-10 waveguide used in
these experiments which was about 59 GHz. The
upper frequency was limited by the maximum
value of the axial magnetic field used in these
experiments which was about 40 kG. Since co-
herent microwave output at several cyclotron
harmonics was expected for a given value of the
axial magnetic field at which the cyclotron fre-
quency coincided with a resonant mode of the
Fabry-Perot, the axial magnetic field was varied
slowly until oscillations were established in the
cavity. The output frequency was then estimated
by use of a series of waveguide cutoff filters.
Thus, for the Fabry-Perot mode at 62.4 GHz,
four cyclotron harmonics were observed corre-
sponding to the fundamental mode at an axial
magnetic field of 23.2 kG ($f_0 = 62.6$ GHz), second
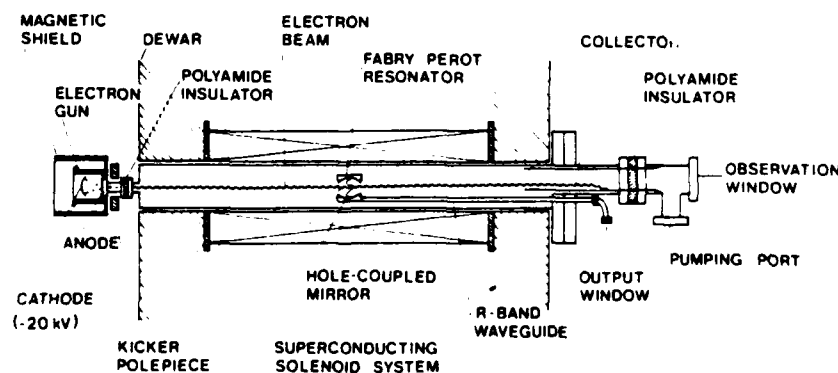harmonic at 11.5 kG ($f_0 = 62.1$ GHz), third har-

FIG. 1. Schematic diagram of the experimental arrangement.

Bernstein-Mode Quasioptical Maser Experiment

N. A. Ebrahim, Z. Liang, and J. L. Hirshfield

Applied Physics Section, Yale University, New Haven, Connecticut 06520

Experimental observations of coherent, millimeter-wavelength, higher-cyclotron-harmonic oscillations are reported for a system of an electron beam in a magnetic field traversing a Fabry-Perot resonator. The parameters of the experiment tend to support the interpretation that the strong multiple-harmonic interaction results from mode conversion of short-wavelength electrostatic waves (Bernstein modes) to long-wavelength electromagnetic resonator modes at the beam boundary.

Recently there has been a great deal of interest in electromagnetic gain mechanisms at millimeter wavelengths, because of potential applications to plasma heating in tokamaks, plasma diagnostics, radar, and far-infrared astronomy. One such mechanism is the electron cyclotron maser instability, in which the relativistic mass dependence of the electron cyclotron frequency results in azimuthal bunching of electrons gyrating in an external magnetic field.[1] A companion mechanism arises from the axial electron velocity modulation in the wave propagation direction.[2] Although electromagnetic gain has been predicted at the fundamental as well as the cyclotron harmonics, practical devices have been restricted to operations at the fundamental or second harmonic.[3]

On the other hand, it is well known that short-wavelength electrostatic waves (Bernstein modes) can propagate perpendicular to a magnetic field with loss in a collisionless plasma.[4] It is thought that the conversion of these modes to long-wavelength electromagnetic modes at a plasma boundary is responsible for multiple-harmonic interactions which have been observed in low-pressure discharges and ionospheric topside soundings.[5] A recent analysis of this problem suggests that when mode conversion occurs at an electron beam boundary, the instability growth rates at the higher harmonics can be much larger than for electromagnetic interactions alone.[6] This Letter reports the first ex-

4. L. Shengang and Yang Zhonghai, submitted for publication.

5. G. L. Chen, K. T. Chang, and T. C. Fan, International
   Journal of Infrared and Millimeter Waves $\underline{1}$, 247 (1980).

6. J. M. Wachtel, private communication.

7. P. Ferguson and R. Symons, private communication.

8. J. L. Seftor, A. T. Drobot, and K. R. Chu, IEEE
   Transactions on Electron Devices $\underline{26}$, 1609 (1979).

9. V. A. Flayagin, A. V. Gapanov, M. I. Petelin, and V. K.
   Yulpata, IEEE Trans. Microwave Theory Tech. $\underline{25}$, 514
   (1977).

I = 1 Amp, the electron is trapped earlier by the cavity field and the overall result is energy gain by the electron, while in the case of I = 0 the electron still loses some of its energy to the wave.

VI. Conclusions

We have studied the influence of space charge forces on the performance of a single cavity gyrotron oscillator which uses a solid electron beam. It was found that space charge effects cause a large efficiency degradation when the beam current is increased while holding other experimental parameters unchanged. A small increase in the magnetic field, however, causes the efficiency to be restored to its higher value. Our calculations for the linear regime are consistent with analytical results of others from linear theory which predict higher wave growth rate for the finite space charge case.

Although our results were derived for a gyrotron using solid electron beams, we believe that it is also applicable for the annular beam configuration which is widely used in gyrotrons. Our quantitative results were not derived from a self consistent treatment of the space charge problem. Rather, they serve as a useful guide for the experiment and also for full scale simulations.

The authors would like to acknowledge helpful discussions with Dr. K. R. Chu, who offered important inspiration and critical advice in the solutions presented here.

References

*   This research was supported by the U.S. Office of Naval Research.

1. G. Mourier, Internat. Symp. on Heating in Toroidal Plasmas, Grenoble, France, July 1978.

2. G. Mourier, Electronics and Communication $\underline{34}$, 473 (1980).

3. L. Shengang, 5th International Conference on Infrared and Millimeter Waves, Würzburg, Germany, Oct. 1980.

$$\frac{dp_\perp}{dz} = -\frac{em\gamma}{p_z} \cos\psi E_x \tag{36}$$

$$\frac{d\psi}{dz} = \frac{m\Omega}{p_z} + \frac{eB_z}{cp_z} + \frac{em\gamma\sin\psi E_x}{p_\perp p_z} \tag{37}$$

$$\frac{dy_g}{dz} = -\frac{e\gamma}{p_z\Omega} E_x - \frac{p_y}{p_z}\frac{B_z}{B_0} \qquad . \tag{38}$$

And as before Eq. (36) reduces to

$$\frac{dp_\perp}{dz} = -\frac{em\gamma}{p_z}E_0\exp(-z^2/r_0^2)J_n'(\beta)\cos(\omega t-n\psi)\cos(k_\perp y_g - n\frac{\pi}{2}), \tag{39}$$

where

$$\beta = \frac{k_\perp p_\perp}{m\Omega} \qquad . \tag{40}$$

Finally, the average energy loss from the electron to the wave fields for a uniform distribution in θ_0 and arbitrary distribution $f(y_g)$ in y_g, we obtain

$$\overline{\Delta W} \approx \sqrt{\pi}\,\frac{ep}{p_z}\frac{r_{02}E_{02}}{}\,J_n'(\beta_0)\exp\left[-\frac{r_{02}^2 m^2(n\Omega - \gamma_0\omega)^2}{4p_z^2}\right]$$

$$\times\,\sin[\phi_0 + \frac{m}{p_z}(n\Omega - \gamma_0\omega)L]\int dy_g f(y_g)\cos(k_\perp y_g - \frac{n\pi}{2}) \tag{41}$$

$$\times\,J_1[q\cos(k_\perp y_g - n\frac{\pi}{2})] \qquad ,$$

where

$$\beta_0 = \frac{k_\perp p_{\perp 0}}{m\Omega} \qquad , \tag{42}$$

$$q = \frac{\sqrt{\pi}\,e\omega E_{01}J_n'(\beta_0)p_{\perp 0}r_{01}L}{p_z^2 c^2}\exp\left[-\frac{(n\Omega - \gamma\omega)^2 m^2 r_{01}^2}{4p_z^2}\right], \tag{43}$$

and

$$J_n'(\beta_0) = dJ_n(\beta)/d\beta\big|_{\beta = \beta_0} \qquad .$$

Setting n=1 and noting that $J_1'(\beta_0) \simeq 1/2$, we find

$$\overline{\Delta W} \simeq \frac{\sqrt{\pi}}{2} \frac{e p_{\perp 0} r_{02} E_{02}}{p_z} \exp\left[- \frac{r_{01}^2 m^2 (\Omega - \gamma_0 \omega)^2}{4 p_z^2} \right]$$

$$\times \sin[\phi_0 + \frac{m}{p_z} (\Omega - \gamma_0 \omega)L] \int dy_g f(y_g) \qquad (44)$$

$$\times \sin k_\perp y_g J_1 (q \sin k_\perp y_g) \qquad .$$

Hence for n=1, Eq. (44) is identical to Eq. (III-7a) of Ref. 9, as expected. Finally, we can find the power transfer from the electron beam to the wave fields, as

$$\Delta P \simeq \sqrt{\pi} \frac{I_b p_{\perp 0} r_{02} E_{02}}{p_z} J_n'(\beta_0) \exp\left[- \frac{r_{02}^2 m^2 (n\Omega - \gamma_0 \omega)^2}{4 p_z^2} \right]$$

$$\times \sin[\phi_0 + \frac{m}{p_z} (n\Omega - \gamma_0 \omega)L] \int dy_g f(y_g) \qquad (45)$$

$$\times \cos(ky_g - n \frac{\pi}{2}) J_1 [q \cos(k_\perp y_g - n \frac{\pi}{2})] \qquad .$$

IV. Comparison Between Gyroklystrons With and Without Coupling to Bernstein Modes

To make the comparison easy, we assume that

$$f(y_g) = \delta(y_g - y_{g0}) \qquad ,$$

$$\cos(ky_{g0} - n \frac{\pi}{2}) = 1 \qquad ,$$

$$\sin[\phi_0 + \frac{m}{p_z} (n\Omega - \gamma_0 \omega)L] = 1 \qquad .$$

The first assumption corresponds to specification of a thin sheet beam of thickness one gyration diameter, the second places this beam at the standing wave maximum. The third corresponds to the best feedback phase between two cavities.

From Eqs. (32) and (45) we can write the expressions

for the power transfer from the electron beam to the wave
fields for the two types of interaction as follows:

$$\Delta P_B = AE_{02} \frac{nJ_n(\beta_0)}{\beta_0} J_1(q_B) \quad , \tag{46}$$

$$q_B = DE_{01}L \frac{nJ_n(\beta_0)}{\beta_0} \quad , \tag{47}$$

$$\Delta P_\perp = AE_{02}J_n'(\beta_0)J_1(q_T) \quad , \tag{48}$$

$$q_T = DE_{01}LJ_n'(\beta_0) \quad , \tag{49}$$

where

$$A = \frac{\sqrt{\pi} \ I_b p_{\perp 0} r_{02}}{p_z} \exp\left[- \frac{r_{02}^2 m^2 (n\Omega - \gamma_0 \omega)^2}{4p_z^2} \right]$$

$$D = \frac{\sqrt{\pi} \ e\omega p_{\perp 0} r_{01}}{p_z^2 c^2} \exp\left[- \frac{(n\Omega - \gamma\omega)^2 m^2 r_{01}^2}{4p_z^2} \right] \quad ,$$

and subscript B refers to Bernstein modes and T refers to
the TEM$_{00}$ electromagnetic mode.

   For small signal operation

$$J_1(q) \simeq \frac{1}{2} q \quad . \tag{50}$$

Substituting Eqs. (50) and (47) into Eq. (46), we obtain

$$\Delta P_B = \frac{1}{2} ADE_{01}E_{02}L \left[\frac{nJ_n(\beta_0)}{\beta_0} \right]^2 \quad . \tag{51}$$

Similarly for the electromagnetic interaction we obtain.

$$\Delta P_T = \frac{1}{2} ADE_{01}E_{02}L[J_n'(\beta_0)]^2 \quad . \tag{52}$$

We should point out that in Eq. (51) E_{01} and E_{02} are polar-
ized along the y-axis, which is also the direction of wave
propagation (longitudinal waves) whereas, in Eq. (52) E_{01}
and E_{02} are polarized along the x-axis with wave propaga-
tion along the y-axis (transverse waves). Thus Eq. (51)
and Eq. (52) can be rewritten as

$$\Delta P_B = \frac{1}{2} \ ADE_{01y}E_{02y}L \left[\frac{nJ_n(\beta_0)}{\beta_0} \right]^2 , \qquad (53)$$

$$\Delta P_T = \frac{1}{2} \ ADE_{01x}E_{02x}L \ [J_n'(\beta_0)]^2 \quad . \qquad (54)$$

For the Bernstein modes we find that (6)

$$\varepsilon = \frac{E_{01x}}{E_{01y}} = \frac{E_{02x}}{E_{02y}} = \frac{v_\perp}{C} \ \frac{\omega_p}{\Omega\gamma_0^{\frac{1}{2}}} \left[\frac{nJ_n''(\beta_0)}{\beta_0} \right] , \qquad (55)$$

where ω_p is the plasma frequency. Substituting Eq. (55)
into (53), we have

$$\Delta P_B = \frac{1}{2\varepsilon^2} \ ADE_{01x}E_{02x}L \left[\frac{nJ_n(\beta_0)}{\beta_0} \right]^2 \quad . \qquad (56)$$

$[nJ_n(\beta_0)/\beta_0]$ has the approximate value of 0.3 for n up to
20. For an electron beam of modest power $1/\varepsilon^2$ is of the
order of 10^6 for fundamental operation. As n increases up
to 10, $1/\varepsilon^2$ decreases gradually to about one tenth of the
fundamental value. On the other hand $[J'_n(\beta_0)]$ decreases
very rapidly as n increases.

Figure 2 shows the linear high harmonic power outputs
normalized to the output at the fundamental for several
cyclotron harmonics for gyroklystrons with $(\Delta P_{Bn}/\Delta P_{B1})$ and
without $(\Delta P_{Tn}/\Delta P_{T1})$ coupling to Bernstein modes. The calcu-
lations in Fig. 2 have been performed for radiation fre-
quency f = 65 GHz, beam voltage V_b = 19 kV, beam current
density J = 5A/cm^2 and a transverse to parallel momentum
ratio α = 2. These calculations show that for a gyrokly-
stron based on electromagnetic interaction only, the nor-
malized power output decreases very rapidly at the higher
harmonics. On the other hand, for a gyroklystron based
on the Bernstein modes, the normalized power output shows

a very weak dependence on the harmonic number up to very high harmonic numbers.

In Fig. 3 we show the linear power output for the Bernstein modes over the linear power output for electromagnetic interaction only $(\Delta P_{Bn}/\Delta P_{Tn})$, as a function of the harmonic number, for the same parameter regime as in Fig. 2. We observe a significant increase in linear power output at the higher harmonics for a gyroklystron based on the Bernstein modes compared to one based on electromagnetic interaction alone.

From our analysis, we can draw three major conclusions. Firstly, since $1/\epsilon^2$ is of the order of $10^5 \sim 10^6$, a gyroklystron based on the electron Bernstein modes has a higher linear efficiency than a corresponding gyroklystron involving only the electromagnetic interactions. Secondly, since both $[nJ_n(\beta_0)/\beta_0]$ and $1/\epsilon^2$ decrease slowly as the harmonic number n increases, the linear efficiency of the gyroklystron involving the Bernstein modes will decrease slowly for high order harmonic operations. Finally, since $[J_n'(\beta_0)]$ decreases very rapidly as the harmonic number n increases, the linear efficiency of a gyroklystron based only on electromagnetic interactions will decrease very rapidly for high order harmonic operations.

In the present analysis we have developed a simple theoretical model which takes into account the basic physics of a quasi-optical gyro-klystron based on the electron Bernstein modes. The model is idealized, in that several real effects have not been treated in this analysis. For instance, the model does not include the velocity spread in the electron beam. This velocity spread could either result from a spread in energy (i.e. spread in γ) or a spread in pitch angle (i.e. spread in α), and for most practical devices, the spread in α is expected to be more important. However in the geometry of the present model, the resonance condition is $\omega \cong n\Omega/\gamma_0$ (i.e. $k_z \cong 0$) and the relevant wavenumber $k \cong k_\perp$. Thus the velocity spread is not expected to be serious. A second limitation of this analysis is that the theory presented here is linear and although it can predict near threshold behavior well, it does not account for the non-linear saturation levels for steady-state oscillations. Finally, the present model assumes the electron beam to have sharp boundaries. A more realistic beam profile

would be one with a more gentle boundary, and this could give larger values of ε and hence lower linear efficiencies than those predicted above.

Nevertheless the present analysis has been motivated to some extent, by the need to stimulate interest in electromagnetic gain on the Bernstein modes and perhaps a formulation of a more elaborate and realistic theory. It may even stimulate experimental demonstration of some of the predictions of the present theory.

Acknowledgments
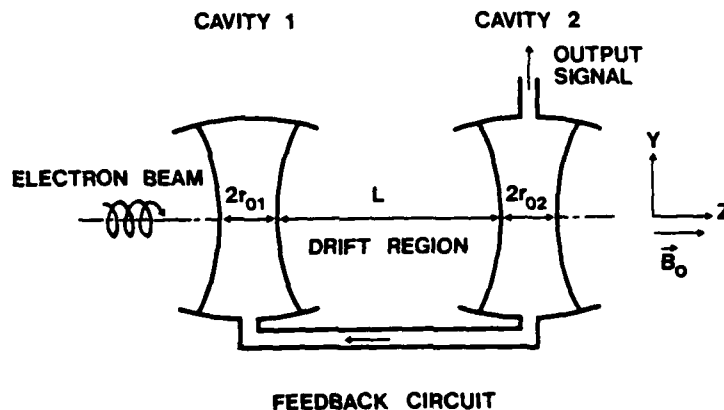
Fig. 1. Schematic diagram of quasi-optical gyroklystron.
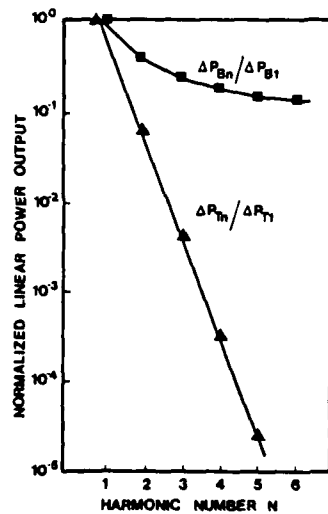
Fig. 2. Normalized linear power outputs vs cyclotron harmonic numbers for gyro-klystrons with and without coupling to Bernstein modes. Squares correspond to the values with Bernstein modes ($\Delta P_{Bn}/\Delta P_{Bn}$) triangles to those with electromagnetic interactions alone ($\Delta P_{Tn}/\Delta P_{Tl}$). Frequency $f = 65$ GHz, beam voltage $V_b = 19$ kV, beam current density $J = 5A/cm^2$, and momentum ratio $\alpha = 2$.
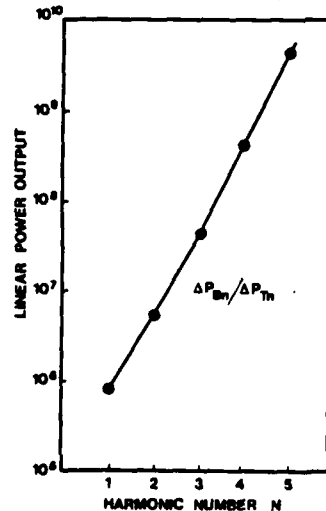
Fig. 3. Values of Bernstein modes linear power output over linear power output for electromagnetic interactions alone ($\Delta P_{Bn}/\Delta P_{Tn}$) vs cyclotron harmonic numbers. All parameters have the same values as those in Fig. 2.

References

1. G. N. Rapoport, A.K. Nemak, and V. A. Zhurakhovskiy, Radio Eng. and Electron. Phys. $\underline{12}$, 587 (1967).

2. S. V. Kolosov and A. A. Kurayev, Radio Eng. and Electron. Phys. $\underline{19}$, 65 (1974).

3. K. R. Chu, Phys. Fluids, $\underline{21}$, 2354 (1978).

4. J. L. Vomvoridis, Int. J. Infrared and Millimeter Waves $\underline{3}$ (5), in press (1982).

5. D. B. Mcdermott, N. C. Luhmann, Jr., A. Kupiszewski, and H. R. Jory, Bull. APS $\underline{27}$, 1061 (1982).

6. J. L. Hirshfield, Int. J. Infrared and Millimeter Waves $\underline{2}$, 695 (1981).

7. N. A. Ebrahim, Z. Liang, and J. L. Hirshfield, Phys. Rev. Lett. $\underline{49}$, 1556 (1982).

8. A. K. Ganguly and K. R. Chu, Int. J. Electronics $\underline{51}$, 503 (1981)

9. A. Bodeson, W. M. Manheimer, and E. Ott, "Multimode Analysis of Quasioptical Gyrotrons and Gyroklystrons" to be published in Int. J. Infrared and Millimeter Waves.

Electron Prebunching and High Harmonic Interaction in a

Bernstein Mode Quasi-Optical Gyrotron

N. A. Ebrahim, Z. Liang, and J. L. Hirshfield

Applied Physics Section, Yale University, New Haven, Conn. 06520

Abstract

Experimental evidence shows that prebunching the beam elec-
trons in a two-cavity quasi-optical gyrotron gives stronger wave-
particle interaction at high cyclotron harmonic Bernstein modes
than was observed previously without prebunching in a one-cavity
experiment. Coherent oscillations up to the ninth harmonic,
increased output power, and significant decrease in start-oscilla-
tion currents have all been observed. Output at 0.96 mm wavelength
at a magnetic field of 14.4 kG was obtained using 20 keV electrons.

Interest grows in investigations of electromagnetic gain mechanisms in the millimeter and submillimeter wave regimes, not only because of the fundamental importance of such mechanisms as new scientific phenomena, but also as a result of applications in several areas of physics. Some of these applications are in the electron-cyclotron resonance heating (ECRH) of fusion research plasmas, in high resolution imaging radars or simply as sources of rf radiation in fundamental research in astronomy and condensed matter physics. In the conventional electron cyclotron maser mechanism[1] the azimuthally phase-bunched electrons in an axial magnetic field radiate coherently at the frequency $\omega \cong N\Omega_0/\gamma$, where $\Omega_0 = |e|B_0/m_0$, $\gamma = (1 + \vec{p} \cdot \vec{p}/m_0^2 c^2)^{1/2}$, $\vec{p}$ is the electron momentum vector, B_0 is the axial magnetic field, ω is the angular frequency and N is an integer denoting the harmonic number. In order to generate submillimeter waves (f > 300 GHz) at the fundamental cyclotron frequency (N = 1) an external magnetic field in excess of 107 kG is required. Although such fields are provided by specialized superconducting coils, present practical cw uses are limited to magnetic fields less than about 60 kG. On the other hand, with pulsed systems, millimeter wave output at 0.8 mm has been reported recently using a pulsed magnetic field of 150 kG.[2] Unfortunately, certain applications such as ECRH demand long pulse or cw operation which would rule out these latter systems. Thus, if large magnetic fields are to be avoided, interaction at the high cyclotron harmonics becomes especially important.[3] However, for the electron cyclotron maser mechanism, the higher the cyclotron harmonic, the higher the threshold beam power; hence excessively large beam currents would be required. As a result, threshold conditions can become difficult to achieve for higher cyclotron harmonics.

Since the higher harmonic interaction is essentially a finite Larmor

radius effect, one solution to this problem is to employ a beam of large

orbit electrons which interact with a high order cavity resonator mode.

Although this approach lowers the value of the axial magnetic field by a

factor equal to the harmonic number, the threshold condition is highly sen-

sitive to beam transverse electron energy; high harmonic emission has been

observed based on this idea for electron energies greater than 250 keV.[4] An

alternative approach demonstrated in a recent experiment with 20 keV electrons

showed that high order harmonic interaction is possible by coupling to the

Bernstein modes on the electron beam, since these modes are unstable and

exhibit strong wave-particle interaction up to very high harmonics even for

modest beam currents.[5] The first Bernstein mode maser experiment demon-

strated harmonic interaction up to the fourth cyclotron harmonic with beam

currents less than two amperes.[5]

In this Letter, we report the first experimental observations which

show that even stronger wave-particle interaction at the higher harmonics

is possible with the electron Bernstein modes by electron prebunching in a high

quality factor quasi-optical Fabry-Perot resonator which preceeds the inter-

action and power extraction cavity. Not only do we observe interaction at

higher harmonics (up to the ninth harmonic) but we also observe a signif-

icant increase in output power and significant lowering of the threshold

condition, as compared with previous experiments without prebunching.[5]

Furthermore, submillimeter wave output at 0.96 mm has been observed with a

magnetic field of only 14.4 kG at the eighth harmonic, with beam energies

of less than 20 keV. The present experiments suggest that no feedback

circuit is necessary in order to optimize the relative phase angle between

the two cavities for efficient interaction. The second cavity automati-

cally assumes the optimum phase, such that maximum energy transfer from

the beam to the wave field occurs. To this extent, and but for the fact that the coupling in the present experiments is on the electron Bernstein modes, the present experiment may suggest a quasi-optical analogue to the complex cavity gyrotron experiment recently reported.[6]

The schematic of the experimental configuration is shown in Fig. 1; it is similar to that used in our earlier work.[5] The gyrating electrons are produced by a combination of a solid laminar-flow electron beam from a space-charge-limited Pierce gun and a spatially localized transverse magnetic field ("kicker") from a pair of Helmholtz coils. This system yields a beam of electrons gyrating in an axial magnetic field with a transverse-to-axial momentum ratio α of the order of 2.

The interaction region consists of two confocal Fabry-Perot resonators with fixed intermirror spacings L = 3.4 cm, mirror radii of curvature 11 cm and intermode frequency spacing $\Delta f = c/2L = 4.4$ GHz. In cold tests of the Fabry-Perot resonators with a sweep oscillator, a complete longitudinal mode spectrum between 60 and 72 GHz was carefully measured. The resonator spacings were then adjusted so that the mode frequency mismatch in the two cavities $\Delta\omega/\omega < 1/Q_2$, where Q_2 is the lower of the two quality factors of the cavities. The first cavity was designed to have a very high quality factor $Q_1 \sim 2 \times 10^4$. This was achieved by not having a coupling hole in this cavity, since it is the output coupling hole which determines the overall Q of this cavity. On the other hand the second cavity (cavity #2) has a low quality factor $Q_2 \sim 800$ in order to obtain high output coupling.

Table I summarizes several representative conditions under which coherent millimeter and submillimeter wave output signals were observed in the frequency range 60-320 GHz. The lower frequency limit in this experiment was set by the low-frequency cutoff of the WR-10 waveguide section used

which was about 59 GHz. The upper frequency was limited by the highest

frequency cutoff filter available to us, which was about 300 GHz. Thus

observations with axial magnetic field values above about 25 kG were

unnecessary. Observations of coherent microwave output were made by tuning

the axial magnetic field until the cyclotron harmonic frequency coincided

with a resonant mode of the Fabry-Perot, at which point oscillations

appeared in the second cavity. The output frequency was then estimated by

use of a series of waveguide cutoff filters. At 66.3 GHz, for instance,

we have observed a total of eight cyclotron harmonics at the following

magnetic fields; 24.9 kG (N = 1), 12.5 kG (N = 2), 8.3 kG (N = 3),

6.2 kG (N = 4), 5.0 kG (N = 5), 4.2 kG (N = 6), 3.6 kG (N = 7), 3.1 kG

(N = 8). The small difference between the estimated cyclotron harmonic

frequencies and the frequency of the resonant Fabry-Perot mode is probably

due to the accuracy of the axial magnetic field measurement (on the order

of 2%) and to slight pushing of the resonator frequency by the electron

beam. At 158.4 and 198.0 GHz we have observed up to the ninth harmonic,

whilst at the Fabry-Perot mode number of 71, we have observed up to the

eighth harmonic at a frequency of 312.4 GHz, in the submillimeter region.

We have also observed what appear to be the tenth and eleventh harmonics

in excess of 140 GHz, although frequency estimates show these modes to be

associated with higher order transverse modes. It is estimated that maxi-

mum microwave output power levels of approximately 30 watts in the funda-

mental have been observed at 62 GHz, an increase of nearly 15 dB from the

levels observed in the single cavity experiment. No attempt has been made

to optimize the system in terms of beam quality or magnetic field contour-

ing. Between the fourth and ninth harmonic, we did not observe a substan-

tial change in the output signal to within a factor of 2, so that the out-

put power at the higher harmonics is estimated to be in the range 0.1-1% of the power at the fundamental.

In a previous study, it was shown that the start oscillation condition for the beam current at the Nth harmonic for a single cavity could be obtained from a linear theory of the cyclotron maser instability.[5,7] Similarly, the start oscillation conditions for the unstable electron Bernstein modes could also be obtained.[8] In Fig. 2, the start oscillation conditions for the two instabilities for a single cavity ($Q \sim 800$) for the first eight harmonics at 66.3 GHz are shown for several different values of the momentum ratio α. The curves were obtained using Eqs. 1-3 of Ref. 5. The start oscillation current experimentally observed for stable oscillations are also shown for comparison. From Fig. 2, it is clear that for $\alpha = 2$, the predicted start oscillation currents from the electron cyclotron maser instability theory are orders of magnitude higher than the experimentally observed currents. Although higher α (~ 10) would tend to bring closer agreement between experiment and that theory, the near equality of measured cathode and collector currents would rule out a momentum ratio of 10 for a sizable fraction of the beam electrons. A further important observation from Fig. 2 is that experimentally observed values of the beam current are now substantially lower than those predicted for the Bernstein mode coupling in a single cavity. This is in contrast to the results of the single cavity experiment, where the operating beam currents for various harmonics, although consistent with those predicted by a Bernstein mode theory, were generally higher than the predictions.

Thus the observations of Table I and Fig. 2 strongly suggest the existence of a mechanism which substantially lowers the threshold currents, increases the output power and results in the observations of harmonic interaction up to the ninth harmonic. Theoretical analysis of quasi-optical

have been performed and the results have surpassed those of the conventional TWA devices.[13]

The gyrotron pioneers Schneider and Hirshfield used the quantum theory to predict the conditions required for stimulated emission to exceed absorption.[14,5] However, this approach is mainly of academic interest since, for the frequencies at which the cyclotron maser interaction is most interesting, one electron may fall through up to 10^8 quantum states to give up its energy to the electromagnetic field. Therefore, the classical discription is sufficient.

Hirshfield et al. first employed plasma kinetic theory to analyze the gyrotron interaction. This method treats the electron beam in the magnetic field as an electron plasma. The Maxwell-Vlasov equations form the basis for this approach. The electron distribution function (in space and momentum) has to be specified. The perturbed distribution function is found by integrating the linearized Vlasov equation along the unperturbed trajectories of the gyrating electrons. This has become a standard approach, though it is a linear theory in general. Like any other small signal theory, there are a few deficiencies in this approach. At first, nonlinear phenomena, such as saturation, can not be dealt with. As a consequence, the efficiency calculation is beyond its scope. The advantage for employing this linear theory is that it is easier to solve the problem analytically. Furthermore, it usually gives a good understanding of the basic physical effects. It seems interesting to mention that P. Sprangle et al.[15] and later K. R. Chu et al.[16] derived a formula to estimate the efficiency for TE_{nm} modes in the circular waveguide within the scope of the linear theory by deriving the relation between the wave frequency and the gyration frequency at saturation due to phase trapping, but the energy depletion mechanism is neglected in that estimate. That formula is given in the beam frame and can be easily transformed to laboratory frame by performing a Lorentzian transformation. The estimate from that formula is found to be in a good agreement with the numerical simulation results[16] except at lower beam energy, where the depletion of the electron energy is said to be the dominant saturation mechanism of the device.

the relativistic change in the electron mass plays a crucial role in the cyclotron resonance maser mechanism.

Experimentally, perhaps R. H. Pantell[3] is the first who reported an experiment involving the electron cyclotron maser mechanism in 1959. But he attributed the observed beam-wave instability to a longitudinal bunching caused by $\mathbf{v} \times \mathbf{B}$ forces. He claimed that the radiation was caused by the coupling of the TE_{11} waveguide mode with the backward traveling cyclotron wave on the magnetized electron beam. Thus some questions were still left open as to whether the cyclotron maser mechanism had in fact been observed in the experiment, since even if the axial synchronism condition had been satisfied, the results could still have been explained without involving the cyclotron maser interaction.

J. L. Hirshfield and J. M. Wachtel performed the first experiment that definitely demonstrated the existence of the electron cyclotron maser mechanism in 1964 [4,5]. They reported an experiment with 5-kV electrons traveling along an axial magnetic field. The electron beam was injected into a high Q cylindrical cavity with most of the kinetic energy transverse to the applied magnetic field.

The early experiments were with low power and low efficiency, but since 1974 the advances in gyrotron research have come at a rapid pace. The advent of the intense pulsed relativistic electron beam renewed the interest in the cyclotron maser mechanism as a source of high power microwave radiation. 800 MW at 4 cm[6], 350 MW at 2 cm[7], 8 MW at 8 mm[8] have been generated with gyrotrons. Gyrotrons built by a group of Soviet scientists at Gorkii State University have produced 1.25 MW of 45 GHz radiation with a pulse duration of 1 to 5 msec, 1.1 MW of 100 GHz radiation with pulse duration of 100 microsec. The efficiency of these gyrotron oscillators operating at the fundamental harmonic of the gyration frequency is about 34%[9]. They accomplished another impressive gyrotron experiment of 120 kW at 375 GHz with pulse duration of 0.1 msec.[10] Jory and his group did an experiment which generated 200 kW CW at 28 GHz.[11]. The experiments to heat plasmas in controlled fusion devices have been done effectively.[12] Some new configurations for gyrotrons have been examined in the experiments. The gyro-TWA experiments
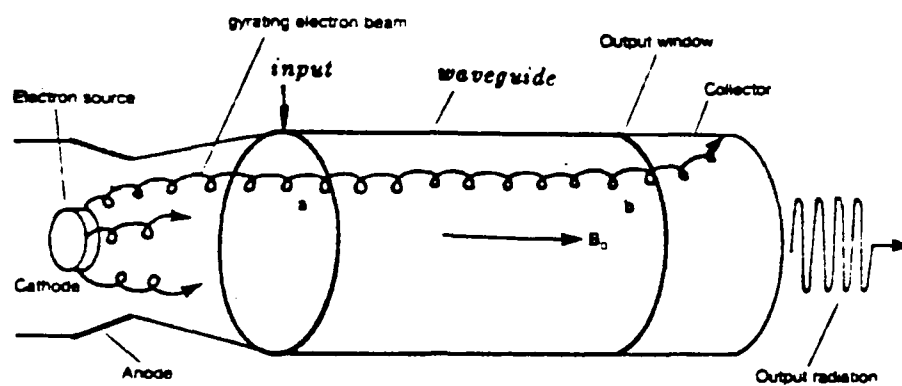
a)
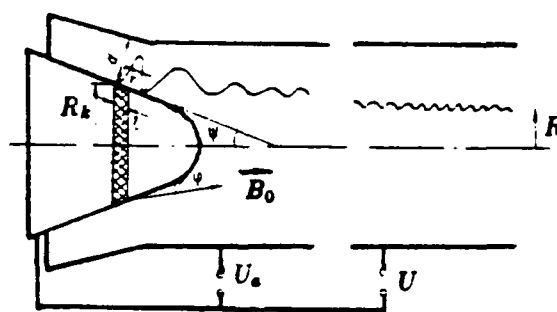
b)

Fig.1 a) The basic configuration of a gyro-TWA.
     b) A magnetron-type gun.

Chapter 1   Introduction

Because of the ability to produce or to amplify millimeter and submillimeter waves at unprecedented power level with high efficiency, gyrotron devices have been intensively investigated both theoretically and experimentally in the past two decades. Their promising applications include plasma heating, new millimeter and submillimeter wave radar systems, spectroscopy, and advanced accelerators.

This new class of microwave devices is based on the electromagnetic radiation mechanism known as the electron cyclotron maser instability, which originates from the electron azimuthal bunching due to the dependence of the electron relativistic gyration frequency on energy.

The basic configuration of a gyrotron device includes an electron beam traveling along a waveguide (or one or more cavities) which is immersed in the applied magnetic field. Since the beam-field interaction takes place in the plane transverse to the direction of wave propagation, the electrons must have a substantial part of their kinetic energy in the form of gyration motion as they move on helical orbits along magnetic field lines.

Fig.1a illustrates the basic configuration of a gyrotron traveling wave amplifier (gyro-TWA). The magnetron injection electron gun, which is commonly used in gyrotrons, is depicted in Fig.1b.

The electron cyclotron maser mechanism was recognized first by an astrophysicist R. Q. Twiss[1] in 1958. He derived the general formula for the absorption coefficient α_ω of the monochromatic radiation of angular frequency ω in an ionized medium with electrons undergoing radiative free-free transitions. Shortly after Twiss's work, A. V. Gaponov[2] published a paper to describe the classical theory of the cyclotron maser. He investigated the phase relation among those electrons gyrating in a uniform static magnetic field. It was Gaponov who realized first that

Table of Contents

ABSTRACT

THEORY OF GYROTRON TRAVELING WAVE AMPLIFIERS AT HARMONICS OF THE GYRATION FREQUENCY

Qiangfa Li

Yale University, 1984

In developing gyrotrons at millimeter and submillimeter wavelengths, a means of opera-tion at lower applied magnetic fields is desirable because of the size and weight of convetional magnets, and the expense and complexity of cryogenic magnets. This requirement can be met by operating the devices at higher harmonics of the electron gyration frequency. In the present work, a unified theory is developed for the gyrotron traveling wave amplifiers (gyro-TWA) at harmonics of the gyration frequency, both in the nonlinear regime and in the linear regime. This theory can be applied to a wide class of waveguide cross sections, arbitrary harmonic number, any waveguide mode, and generalized electron beam model. The fields in the beam-field interaction region in the waveguide are expressed in the form of an infinite series of multipoles expanded around the guiding center of the electrons. A set of equations governing the nonlinear behavior of the gyro-TWA is derived. A general dispersion equation is derived both from that set of nonlinear equations by an iteration method and from plasma kinetic theory. The latter is employed to analyze gyro-TWA devices in a systematic and generalized manner. The Laplace transformation is introduced to allow inclusion of the initial values at the input end of the waveguide. From the linear theory it is found that for a gyrotron working at s-th gyration harmonic the electrons can interact only with the $2s$-th order multipole field component. It is also found that a higher order waveguide mode is not always better than a lower order mode for the gyro-TWA working at higher harmonics. A novel out-ridged waveguide is proposed and analyzed for the use in gyrotrons. The prominent features of this new waveguide include simplicity of manufacture, freedom from local modes, good separation of lower order modes, high power handling ability, and high gain per unit length at higher gyration harmonics. A compari-sion of the gyro-TWAs with several different waveguide structures, such as the out-ridged, magnetron-type, rectangular and circular waveguides, is made through numerical examples of the gain-frequency curves computed from the linear kinetic theory.

Acknowledgement

THEORY OF
GYROTRON TRAVELING WAVE AMPLIFIERS
AT HARMONICS OF THE GYRATION FREQUENCY

A Dissertation

Presented to the Faculty of the Graduate School

of

Yale University

in Candidacy for the Degree of

Doctor of Philosophy

by

Qiangfa Li

July 1984

HARMONIC NUMBER (N)	f_{F-P}	61·7	66·3	70·9	158·4	198·0	312·4
	Mode No.m	14	15	16	36	45	71
1	B_O	23	24·9	25·9			
1	f_O	62·6	67·7	70·3			
2	B_O	11·5	12·5	13·0			
2	f_O	62·3	67·8	70·7			
3	B_O	7·7	8·3	8·6	19·5		
3	f_O	62·4	67·6	70·1	157·7		
4	B_O	5·8	6·2	6·5	14·9	18·3	
4	f_O	62·1	67·6	70·4	160·9	197·6	
5	B_O	4·6	5·0	5·3	11·6	14·7	
5	f_O	61·6	67·5	71·4	156·1	198·3	
6	B_O	3·7	4·2	4·3	9·73	12·2	
6	f_O	60·4	67·9	70·1	157·6	198·3	
7	B_O		3·6	3·7	8·3	10·5	16·5
7	f_O		68·0	70·5	157·2	198·1	311·6
8	B_O		3·1		7·4	9·1	14·4
8	f_O		67·0		159·0	196·6	311·0
9	B_O				6·5	8·1	
9	f_O				157·5	196·8	

TABLE I
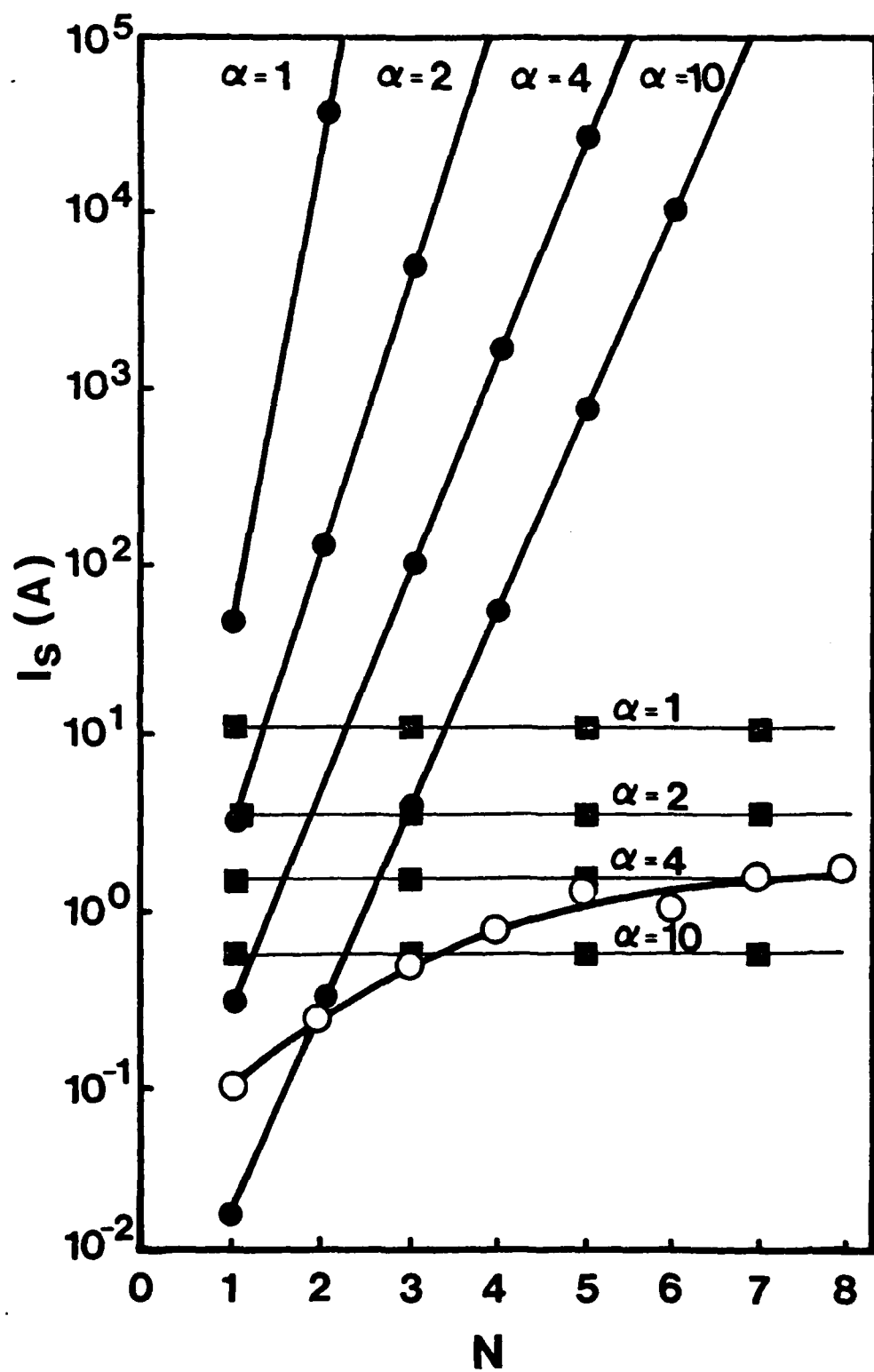
FIG. 2
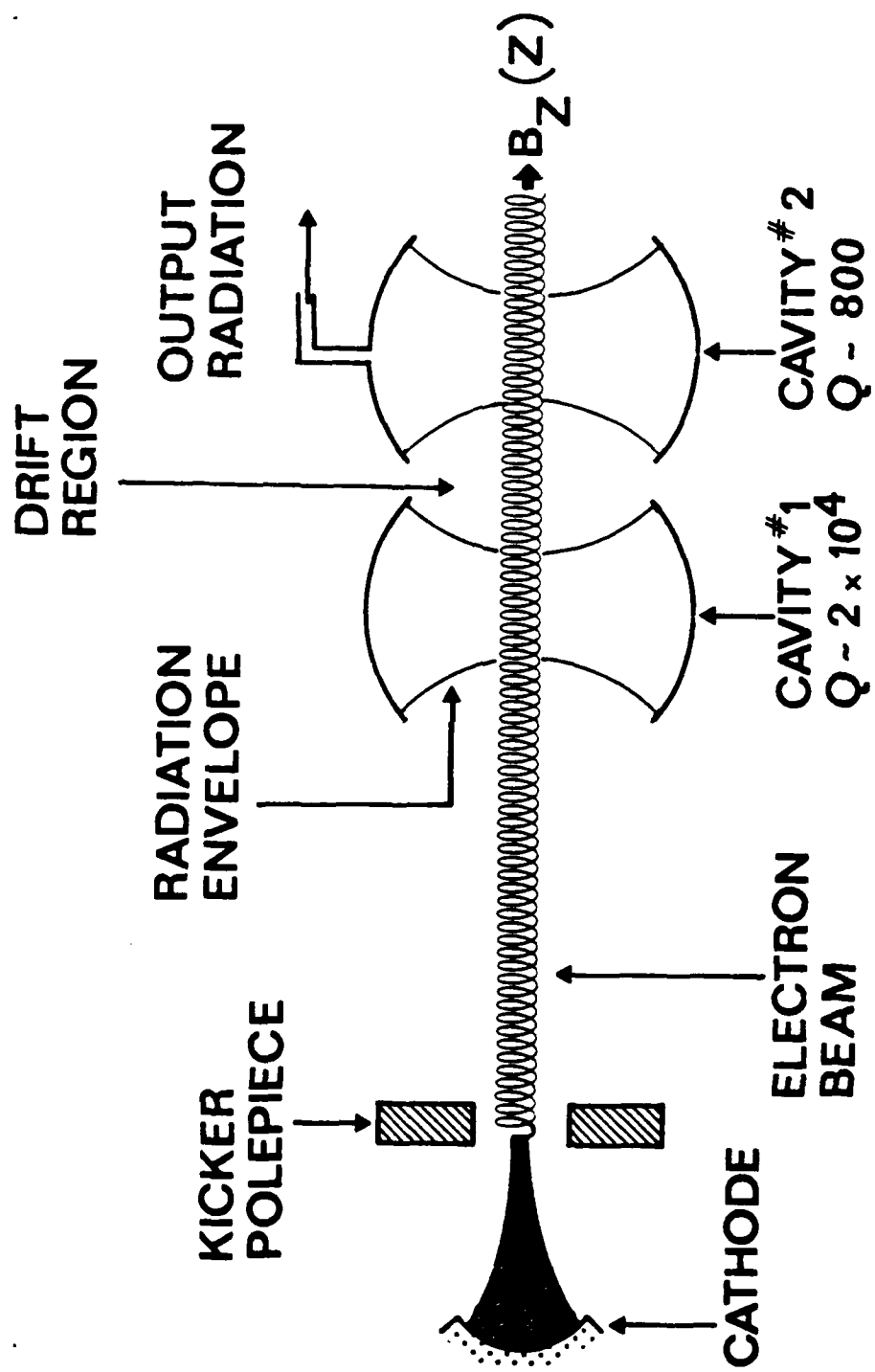
FIG. 1

CAPTIONS

FIG. 1. Schematic diagram of the experimental arrangement.

FIG. 2. Start Oscillation current versus the harmonic number.

        ● Calculated from Eq. (1), Ref. 5 (excluding Bernstein modes);

        ■ Calculated from Eq. (3), Ref. 5 (including Bernstein modes);

        ○ Experimental measurements of the start oscillation current.

TABLE I. Conditions under which coherent output signals were observed and the frequency of the observed output. Inter-mirror spacing $L = 3.4$ cm, intermode frequency $\Delta f = 4.4$ GHz. $\gamma = 1.0371$, $f_0 = N\Omega_0/2\pi\gamma$, $\Omega_0 = |e|B_0/m_0$. f_{F-P} are the resonant modes of the Fabry-Perot. B_0 is in kG and all frequencies are in GHz. N is the harmonic number. Note: although harmonics 1-2 at 158.4 GHz, 1-3 at 198.0 GHz and 1-6 at 312.4 GHz are not shown, they were clearly obtained in this experiment.

REFERENCES

1. R. Q. Twiss, Australian J. Phys. 11, 564 (1958).

2. V. A. Flyagin, A. G. Luchinin, and G. S. Nusinovich, Int. J. Infrared and Millimeter Waves 3, 765 (1982).

3. K. R. Chu, Phys. Fluids 21, 2354 (1978).

4. D. B. McDermott, N. C. Luhmann, Jr., A. Kupiszewski, and H.R. Jory, Bull. APS 27, 1061 (1982).

5. N. A. Ebrahim, Z. Liang, and J. L. Hirshfield, Phys. Rev. Lett. 49, 1556 (1982).

6. Y. Carmel, K. R. Chu, M. Read, A. K. Ganguly, D. Dialetis, R. Seeley, J. S. Levine, and V. L. Granatstein, Phys. Rev. Lett. 50, 112 (1983).

7. J. L. Vomvoridis, P. Sprangle, and W. M. Manheimer, In Infrared and Millimeter Waves Vol. 7: Coherent Sources and Applications Part II (K. J. Button, ed.), pp. 487-535 (1983) Academic Press, New York.

8. J. L. Hirshfield, Int. J. Infrared and Millimeter Waves 2, 695 (1981). The starting current formula in this reference is erroneous. The correct experssion is given in Ref. 5, Eq. (3).

9. Z. Liang, N. A. Ebrahim, and J. L. Hirshfield, Int. J. Infrared and Millimeter Waves, May (1983).

10. A. Bondeson, W. M. Manheimer, and E. Ott, Phys. Fluids, 26, 285 (1983).

gyro-klystrons based on either the electron Bernstein modes[9] or electro-magnetic interactions[10] both demonstrate that prebunching of the beam significantly enhances the interaction efficiency, but threshold currents with electromagnetic interactions alone are orders-of-magnitude higher than the values observed experimentally. The results reported in this Letter are therefore consistent with the conclusion that stronger wave-particle interaction at the higher harmonics is possible on the electron Bernstein modes by electron prebunching.

Finally, since a gyrotron based on the electron Bernstein modes is characterized by coherent output in a large number of spectral lines spanning a broad spectral range, it may have very important applications in areas where tunability is essential.

Another method in analyzing the interaction process is the Lagrangian formulation where one directly solves the equation of motion of the electrons in the applied and RF fields. For small field amplitudes, we can integrate the linearized equations for the properties of interest, then average over all the electrons is taken to obtain the properties of the electron-field interaction. This approach can be either in the linear frame or in the nonlinear frame. If rigorous relativistic kinetics is required, such as in the high power or the higher gyration harmonic gyrotron cases, the caculation has to be accomplished numerically. For the numerical solution, the computing model can include many factors and gives accurate results, but some physical insight may be lost. This approach will be dealt with in Chapter 2.

A new approach has been introduced to the Gyro-TWA nonlinear analysis. This approach is based on the concept of the soliton. The soliton is a solitary wave in a nonlinear, dispersive medium. This powerful theory can treat nonlinear, time dependent problems analytically.[17]

In developing gyrotrons at millimeter and submillimeter wavelength for plasma heating, radar system and some other purposes, there is an increasing necessity to reduce the weight and size of the devices, and consequently, to reduce the magnetic field substantially. For the amplification or generation of submillimeter waves, an impractically high applied magnetic field would be required if the device is operated at the fundamental cyclotron harmonic. For a gyrotron operating at the same frequency range but at the s-th harmonic of the gyration frequency the applied magnetic field is reduced approximately by a factor of s. This is of great importance especially for uses in compact radar systems and for some other applications, where the device size and weight are critical to the system.

However, most gyrotron oscillators and amplifers reported are at the fundamental cyclotron frequency except a few at second harmonics. Only recently, some papers theoretically investigated the properties of the magnetron-type waveguide structure to serve gyro-devices as the RF structure.[18,19] Papers on the utilization of the whispering gallery modes in the circular waveguides and some modes of the rectangular waveguides for the gyro-devices working at higher cyclotron harmonics

were also published.

Experimently, Destler et al. used a magnetron-type waveguide with 12 vanes and a 2 MV, 2 kA electron beam, and generated an output power of 250 MW most concentrated in the 12-th cyclotron harmonic.[20] The preliminary experiments on the microwave generation at higher gyration harmonics with low beam energy have been proposed and performed at Yale[21,22] and at University of Maryland[23] recently.

However, a theory on the beam-field interaction at higher harmonics is still to be developed in a generalized and systematic manner. Some basic features at the higher cyclotron harmonics still need to be explored. Since the waveguide transverse fields can be repressented by solutions of Laplace's equation, the fields in the waveguide, and consequently the forces on the electrons, can be expressed by an infinite series of multipole components expanded around the axis of the electron helical trajectories. This makes the analysis, both linear and nonlinear, capable of handling several different shapes of waveguide cross section for the *RF* structures in the gyro-TWA devices.

The waveguide structure is very important for the operation of gyrotrons at higher harmonics. A good waveguide structure may creat a suitable field pattern in the cross section of the waveguide for the beam-field interaction. Therfore, some novel waveguide structures still have to be studied.

It has been realized in general that the RF field transverse inhomogeneity in the waveguide is responsible for the interaction between the electron beam and the field in gyrotron devices at the harmonics of the electron gyration frequency.[9,24] In the present work, the analytical results both from the nonlinear theory and linear kinetic theory prove that the electron beam interaction with the field at s-th harmonics is associated only with the multipole field of order $2s$ in the waveguide, if the field is expanded around the guiding center of the electrons. In order to achieve a good coupling between the waveguide field and the beam, the operation of gyrotrons at higher gyration harmonics in general requires the waveguide to work at higher waveguide modes because the higher order multipole field components are bigger in

the higher modes. Also, a bigger beam energy is requied for gyrotrons working at the hiher harmonics. However, in this work we find that it does not always mean that a higher waveguide mode is better for a gyrotron device to work at higher harmonics than the lower waveguide mode, even though the higher waveguide mode has a higher transverse inhomogeneity in the transverse RF field. The distribution of the modes of the waveguide structure is very important for the stable and efficient operation of the devices at higher harmonics of the gyration frequency.

In this work an out-ridged waveguide structure is proposed as the new candidate for gyro-TWA (and gyrotron oscillator as well) working at higher cyclotron harmonics. This novel waveguide structure and the gyro-TWA with it are analyzed in Chapter 4. One of the features of this out-ridged waveguide is its bigger power handling ability compared to the waveguide used in the 'peniotron', since the introduction of two paires of the intruding ridges for the latter reduces the power handeling ability of the waveguide. Furthermore, these two paires of the ridges bring about locally trapped modes. The other prominent features of the out-ridged waveguide include the simplicity in manufacture, the free of the local modes, the good separation of the lower modes, and high gain per unit length at higher gyration harmonics.

In Chapter 2, by imploying the weakly irregular waveguide theory and expanding the waveguide field into an infinite series of the multipoles around the gyration centers of the electrons, a set of the equations to describe the nonlinear evolution of the electron motion in a self-consistent manner is derived. A dispersion equation is derived by iterating the solution of that set of equations. Chapter 3 is devoted to kinetic theory. The introduction of the Laplace transformation alllows one to treat the initial value problem. The small signal gain-frequency relation is obtained through the inverse Laplace transformation. The eigenvalues and the associated eigenfunctions of the proposed out-ridged waveguide and the beam-field analysis of the gyro-TWA with the out-ridged waveguide are found in Chapter 4 by applying the analytical results from Chapter 3. In Chapter 5, the small signal gain-frequency curves for gyro-TWAs with several other waveguide structrures, such as rectangu-

lar, magnetron-type and circular waveguides are computed. The advantages of the out-ridged waveguide over other waveguide structures in gyro-TWAs are demonstrated in the computed examples. Chapter 6 is devoted to a comparision of the gyro-TWAs with different waveguide structures through some examples computed from the small signal theory and some conclusions are made from the present work for the gyro-TWAs at higher harmonics of the gyration frequency.

Chapter 2   Local Field Expansion
and Nonlinear Theory

This chapter is devoted to the formulation of the basic equations for the gyrotron analysis and to the gyrotron nonlinear theory. With the equations of motion of an electron in the electromagnetic field and the local field expansion technique, the gyrotron equations are rederived in section 2.2. In section 2.3, also starting from the equations of motion of an electron in the electromagnetic field, a set of nonlinear equations, which can be applied to the gyrotrons with different waveguides, is derived in a self-consistent manner. The general gyrotron dispersion equation is derived from that set of nonlinear equations with iteration method.

2.1   Basic Equations

Maxwell's equations with sources are the basis of all the approaches of gyrotron analysis. In Gaussian units these equations are written as

$$\nabla \cdot \mathbf{B} = 0 \tag{2.1}$$

$$\nabla \times \mathbf{B} = \frac{1}{c}\frac{\partial \mathbf{E}}{\partial t} + \frac{4\pi}{c}\mathbf{J} \tag{2.2}$$

$$\nabla \cdot \mathbf{E} = 4\pi\rho \tag{2.3}$$

$$\nabla \times \mathbf{E} = -\frac{1}{c}\frac{\partial \mathbf{B}}{\partial t} \tag{2.4}$$

In this analysis, all the RF fields are assumed to be time harmonic. From Eqs.(2.1), (2.2) and (2.4), an inhomogeneous Helmholtz equation for the magnetic field can be derived as

$$\nabla^2 \mathbf{B} + \frac{\omega^2}{c^2}\mathbf{B} = -\frac{4\pi}{c}\nabla \times \mathbf{J} \tag{2.5}$$

For TE waveguide modes, i. e. , for $E_z = 0$, where z is along the axial direction of the waveguide, with the assumption $|\frac{d}{dz}\ln B_z| \ll 1$, we may write the axial component

of the magnetic field in the following form:

$$B_z = F(z)B_z^0(r_t)e^{j\omega t} \tag{2.6}$$

where r_t is the transverse coordinates, and $F(z)$ is in general a complex function of z. In the gyrotron analysis, $| \frac{d}{dz}\ln B_z | \ll 1$ is a good approximation since the beam-wave interaction is strong only in a frequency range that is close to the cutoff frequency of the interacting wave mode, where the waveguide wavelength is long compared to the scale length of the beam-wave interaction.

If the operator ∇ is written in the form $\nabla = \nabla_t + e_z\frac{\partial}{\partial z}$, then $\nabla^2 = \nabla_t^2 + \frac{\partial^2}{\partial z^2}$, and from Eq.(2.5), an equation for B_z may be written into the form

$$(\nabla_t^2 + k_c^2)F(z)B_z^0 + (\frac{\partial^2}{\partial z^2} + \frac{\omega^2}{c^2} - k_c^2)F(z)B_z^0 = -\frac{4\pi}{c}(\nabla \times \mathbf{J})\cdot e_z \tag{2.7}$$

A parameter k_c has been introduced in the above and it will be determined later. Since B_z is written in the form of Eq.(2.6) and with the assumption of the neglect of space charge effects, for TE modes, the eigenvalues and the associated eigenfunctions of the waveguide can be obtained by solving the equation

$$(\nabla_t^2 + k_c^2)B_z^0 = 0 \tag{2.8}$$

subject to the perfect conducting boundary condition on the wall of the waveguide

$$\mathbf{n}\cdot\nabla_t B_z^0 = 0 \tag{2.9}$$

where $\mathbf{n}$ is a unit vector normal to the waveguide wall surface.

Thus, for the function $F(z)$ we have the following equation

$$(\frac{d^2}{dz^2} + \frac{\omega^2}{c^2} - k_c^2)F(z) = -\frac{4\pi}{cN}\int_A (\nabla \times \mathbf{J})\cdot e_z(B_z^0)^* dA \tag{2.10}$$

where

$$N = \int_A B_z^0(B_z^0)^* dA \tag{2.11}$$

$(B_z^0)^*$ is the complex conjugate of B_z^0, and the integration is over the cross section of the waveguide.

The transverse field components for *TE* waveguide modes can be derived from the Maxwell equations in the form

$$\mathbf{B}_t = \frac{1}{k_c^2}\frac{\partial F(z)}{\partial z}\nabla_t B_z^0 e^{j\omega t} \tag{2.12}$$

$$\mathbf{E}_t = \frac{j\omega}{ck_c^2}F(z)\mathbf{e}_z \times \nabla_t B_z^0 e^{j\omega t} \tag{2.13}$$

Thus, we can write the components of the field in Cartesian coordinates from Eqs.(2.12) and (2.13) as the following

$$E_x = -j\frac{\omega}{ck_c^2}F(z)\frac{\partial}{\partial y}B_z^0 e^{j\omega t} \tag{2.14}$$

$$E_y = j\frac{\omega}{ck_c^2}F(z)\frac{\partial}{\partial x}B_z^0 e^{j\omega t} \tag{2.15}$$

$$B_x = \frac{1}{k_c^2}\frac{\partial F(z)}{\partial z}\frac{\partial}{\partial x}B_z^0 e^{j\omega t} \tag{2.16}$$

$$B_y = \frac{1}{k_c^2}\frac{\partial F(z)}{\partial z}\frac{\partial}{\partial y}B_z^0 e^{j\omega t} \tag{2.17}$$

In this way, the problem for determining the fields in the waveguide with moving electrons reduces to Eq.(2.8) which is the same equation as that for the empty waveguide; and to Eq.(2.10) which involves the electron beam and the fields in the waveguide.

For Eq.(2.10), we can have several different ways to obtain its right hand side. In this chapter and Chapter 3, three different approaches to obtain the right hand side of Eq.(2.10) will be analyzed.

It should be pointed out that if the right hand side of Eq.(2.10) is set to zero but k_c is assumed a function of z, then under the single mode assumption, Eq.(2.10) can be the basic equation for slow-varying waveguides used in gyrotrons[26-31].

2.2   Local Field Expansion

For *TE* waveguide modes, in the cross section of the waveguide, in a region small compared to the wavelength in the waveguide, we can expand the axial component of the magnetic field in the polar coordinates

$$B_z^0 = \sum_n A_n r^n e^{-jn\theta}$$

$$= \sum_n A_n (R^*)^n \tag{2.18}$$

where $R = x + jy = re^{j\theta}$. Then Eq.(2.10) can be written as

$$\left(\frac{d^2}{dz^2} + \frac{\omega^2}{c^2} - k_c^2\right)F(z) = \frac{1}{N}\int_A dA\mathbf{J}\cdot(\mathbf{E}_t)^* \tag{2.19}$$

In the polar coordinate system, in the transverse cross section of the waveguide, the synchronous field has a quasi-static structure

$$\mathbf{E}_t = -jA_n\nabla(R^*)^n \tag{2.20}$$

The equation of motion of an electron in the electromagnetic field is

$$\frac{d}{dt}\mathbf{P} + \Omega_c\mathbf{P}\times\mathbf{e}_z = -e\mathbf{E}_t \tag{2.21}$$

where $\Omega_c = \frac{eB}{mc\gamma}$, B is the total magnetic field and $\mathbf{P}$ is the momentum of the electron.

In Cartisian coodinates, the three components of this equation are

$$\frac{d}{dt}P_x + \Omega_c P_y = -eE_x \tag{2.22}$$

$$\frac{d}{dt}P_y - \Omega_c P_x = -eE_y \tag{2.23}$$

$$\frac{d}{dt}P_z = 0 \tag{2.24}$$

And the electron energy variation in time is governed by

$$mc^2\frac{d}{dt}\gamma = -e\mathbf{E}_t\cdot\mathbf{v} \tag{2.25}$$

$Eq.(2.22) + jEq.(2.23)$ gives

$$\frac{d}{dt}P - j\Omega_c P = -e(E_x + jE_y)$$
$$= \frac{je\omega}{ck_c^2}F(z)\left(\frac{\partial}{\partial x} + j\frac{\partial}{\partial y}\right)B_z(x,y) \tag{2.26}$$

where $P = P_x + jP_y$. Let the electron beam have infinitesimal cross-section, then the wave excitation in the right hand side of Eq.(2.19) becomes

$$\int_A dA\mathbf{J}\cdot\mathbf{E}_t = \langle\lambda\mathbf{v}\cdot\mathbf{E}_t e^{-j\omega t}\rangle_{\omega t}$$
$$= jA_n\lambda\frac{\mathbf{P}_t}{m}\cdot\nabla(R^*)^n$$
$$= -j\lambda\Omega_c nA_n\left(-j\frac{P}{m\Omega_c}\right)^{n-1} \tag{2.27}$$

where λ is the charge density per unit length, $\mathbf{P}_t = P_x \mathbf{e}_x + P_y \mathbf{e}_y$, and $\langle p^n \rangle_{\omega t} = \langle p^n \rangle_{\omega t_0}$ means taking the average of p^n over one period, and t_0 is the time when the electron enters the interaction region.

Setting $P = p e^{\frac{-j\omega t}{n}}$, $E_t = E_x + jE_y$, then Eq.(2.10) may be written as

$$\left(\frac{d^2}{dz^2} + \frac{\omega^2}{c^2} - k_c^2\right)F(z) = \chi \langle p^n e^{-j\omega t} \rangle_{\omega t} \tag{2.28}$$

where

$$\chi = -j\frac{n\lambda\Omega_c A_n^*}{N(jm\Omega)^n} \tag{2.29}$$

while

$$eE_t = eF(z)E_t^0 e^{j\omega t}$$

$$= \xi F(z)(p^*)^{n-1} \tag{2.30}$$

and

$$\xi = j^n \frac{enA_n}{(m\Omega_c)^{n-1}} \tag{2.31}$$

If the electron gyration frequency is approximated as

$$\Omega_c = \frac{eB}{\gamma_0 mc}\frac{\gamma_0}{\gamma}$$

$$= \Omega_{c0}\frac{(1 + \frac{p_0^2}{m^2 c^2})^{\frac{1}{2}}}{(1 + \frac{p^2}{m^2 c^2})^{\frac{1}{2}}}$$

$$\simeq \Omega_{c0}\left[1 + \frac{(P_0^2 - P^2)}{2m^2 c^2}\right] \tag{2.32}$$

then the left hand side of Eq.(2.26) becomes

$$\frac{dP}{dt} - j\Omega_c P = \frac{dp}{dt} + j\left(\frac{\omega}{n} - \Omega_c\right)p$$

$$\simeq \frac{dp}{dt} + j\left\{\frac{\omega}{n} - \Omega_{c0}\left[1 + \frac{(p_0^2 - p^2)}{2m^2 c^2}\right]\right\}p \tag{2.33}$$

Furthermore, we introduce four dimensionless quantities

$$q = \frac{p}{|p_0|} \tag{2.34}$$

$$\Delta = \frac{2}{\beta_{t0}^2}\frac{\omega - n\Omega_{c0}}{\omega}$$

$$\simeq \frac{2}{\beta_{t0}^2}\frac{\omega - n\Omega_{c0}}{n\Omega_{c0}} \tag{2.35}$$

$$\tau = \frac{2}{\beta_{t0}^2}\frac{k_z v_z}{\Omega_{c0}} \tag{2.36}$$

$$\varsigma = \frac{\beta_{t0}^2}{2}\frac{\Omega_{c0} z}{v_z} \tag{2.37}$$

Where $\beta_0 = \frac{v_0}{c}, \beta_{t0} = \frac{v_{t0}}{c}$, and Δ is the initial cyclotron resonance mismatch.

Setting

$$f_s = -j\xi 2m^2 c^2 p_0^{n-4} F(z) \tag{2.38}$$

then we may manipulate Eq.(2.26) into the form

$$\frac{dq}{d\varsigma} + jq(\Delta + |q|^2 - 1) = jf_s(q^*)^{n-1} \tag{2.39}$$

In the same way, Eq.(2.19) can be rewritten in the following form:

$$\frac{df_s^2}{d\varsigma^2} + \tau^2 f_s = I\langle q^n \rangle_{\omega t_0} \tag{2.40}$$

where

$$I = \frac{4eI_0 v_z}{N\beta_{t0}^4 \Omega_{co}^2} n^2 A_*^2 \gamma_0^{2(n-1)}$$

and f_s describes the longitudinal variation of the field in the waveguide. Eq.(2.39) and (2.40) form a set of gyrotron equations widely used in the Soviet literature, i. e., the Yulpatov gyrotron equations.[32,33] From the approximations made in the derivation of the equations, it is easy to see that the famous Yulpatov gyrotron equations are the first order approximation in the electron gyration frequency and in the field expansion and are good only for weak relativistic electron beam cases. We will require some more exact formalism to analyze the gyrotron interaction at harmonics of the gyration frequency.

2.3 Nonlinear Theory

Starting from the relativistic equation of motion of electrons in the electromagnetic field, in this section we derive a set of equations governing the nonlinear behavior of the gyro-TWA devices. Essentially, this set of equations is a set of the particle orbit equations coupled, via the source term, to the inhomogeneous wave equation in a self-consistent manner.

With the two-plate transmission line and sheet beam model, Zhurakhovskiy and Rapoport,[34,35] later Sprangle[15] derived a set of the equations to analyze the nonlinear evolution in the gyrotron devices. Flifiit et al.[36] used the method in [34, 35] to carry out the formulation of the numerical nonlinear analysis with a more realistic

circular waveguide and annular beam model. The approaches used by Destler et al.[37], Grewal et al.[38], Lindsay[39] and Lau[40] with their own special and simplified waveguide-beam models can also be classified into this ballistic method commonly used in the analysis of the conventional microwave devices. Actually, not only can the equations derived with this approach describe the nonlinear behavior, such as the saturation mechanism and the efficiency of the device, but it can also be used to get some linearized results. For the nonlinear analysis, usually we integrate that set of the derived equations numerically. Even though the nonlinear theory can offer more information on the beam-field interaction behavior, which is especially necessary for the high power gyrotron devices, the linear theory offers the basic understanding of the physics.

The assumptions made in this nonlinear analysis include the single wave model, the neglect of the space charge effect, and the initially monoenergetic electron beam. In the tenuous beam case, the single vacuum waveguide mode is a very good description which has been confirmed by the experiments[9,11]

The velocity spread of the electron beam can also be included in the nonlinear analysis, as in [15, 34].

For this nonlinear analysis, the beam and waveguide model is still that depicted in Fig.2. In this model, the beam can be either annular or concentric. Moreover, the shape of the waveguide cross-section is restricted neither to circular nor to rectangular, it can be applicable to several different shapes. In this analysis, no assumption about beam energy is made, therefore, this analysis is valid even for the fully relativistic electron beam. Of course, it can be simplified to treat field-beam interaction in the weak relativistic cases. In the following analysis, the field components in the waveguide are expanded into a series of Bessel function. The form of the coefficient in the expansion is given by the proposed out-ridged waveguide in general (see Chapter 4). When the analytical results are applied to some other waveguides, the only change that needs to make is the expansion coefficients of the fields.

Since the momentum $\mathbf{P} = \gamma m \mathbf{v}$, for the electrons in the electromagnetic field, the
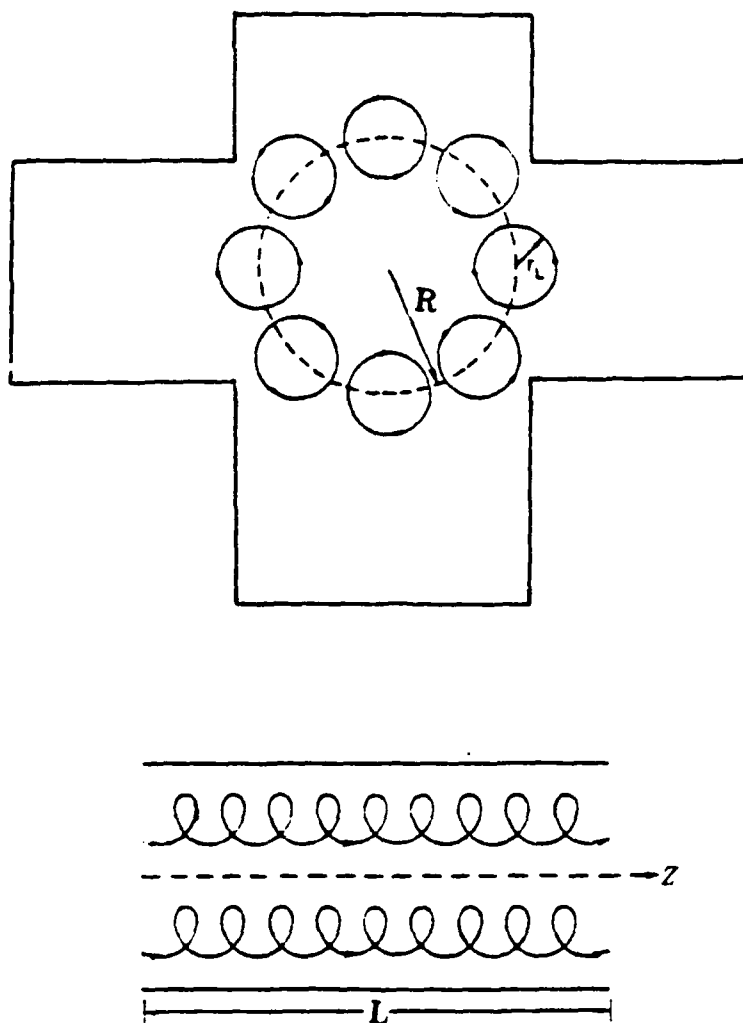
Fig.2 The beam-waveguide model.

relativistic equations of motion

$$\frac{d\mathbf{P}}{dt} = -e(\mathbf{E} + \frac{1}{c}\mathbf{v} \times \mathbf{B}) \tag{2.41}$$

$$mc^2\frac{d\gamma}{dt} = -e\mathbf{v}\cdot\mathbf{E} \tag{2.42}$$

can be written into the following equations for three components of the electron velocity in Cartesian coordinate system

$$\frac{dv_z}{dt} = -v_z\frac{d}{dt}\ln\gamma - \frac{e}{m\gamma}\left[E_z + \frac{1}{c}(v_z B_y - v_y B_z)\right] \tag{2.43}$$

$$\frac{dv_z}{dt} = -v_z\frac{d}{dt}\ln\gamma - \frac{e}{m\gamma}\left[E_z + \frac{1}{c}(v_y B_z - v_z B_y)\right] - v_y\Omega_c \tag{2.44}$$

$$\frac{dv_y}{dt} = -v_y\frac{d}{dt}\ln\gamma - \frac{e}{m\gamma}\left[E_y + \frac{1}{c}(v_z B_z - v_z B_z)\right] - v_z\Omega_c \tag{2.45}$$

In the above, $\gamma = [1 - \frac{1}{c^2}(v_z^2 + v_y^2 + v_z^2)]^{-\frac{1}{2}}$ and $\Omega_c = \frac{eB_0}{mc\gamma}$ is the electron relativistic gyration frequency.

For TE modes, the fields in the waveguide can be expressed as

$$\mathbf{B} = (B_0 + B_z)\mathbf{e}_z + B_z\mathbf{e}_z + B_y\mathbf{e}_y \tag{2.46}$$

$$\mathbf{E} = E_z\mathbf{e}_z + E_y\mathbf{e}_y \tag{2.47}$$

where $B_0\mathbf{e}_z$ is the applied magnetic field.

From the equation for γ in Eq.(2.42), it is seen that the energy change of the electrons for the TE waveguide modes is entirely from the interaction of the transverse velocity of the electron with the waveguide transverse electric field.

In general, we can express the waveguide field into an infinite series in the following equation. The coefficints B_{zn} and A_{nm} in the series are dependent upon the shape of the waveguide cross section.

$$\begin{aligned}
B_z^0 &= \sum_{n=0}^{\infty} B_{zn} \\
&= \sum_{n=0}^{\infty} B_n \frac{\sin}{\cos}(k_{z1n}z)\cos[\frac{n\pi}{h_z}(y - h)] \\
&= \sum_{n=0}^{\infty}\sum_{m=-\infty}^{\infty} A_{nm}J_m(k_c r)e^{jm\theta}
\end{aligned} \tag{2.48}$$

where the coefficient A_{nm} for the out-ridged waveguide is given by (see Chapter 4)

$$A_{nm} = \frac{1}{2}B_{z1n}\left[e^{jk_c h\cos\lambda_n} + (-1)^m e^{-jk_c h\cos\lambda_n}\right]\cos(m\lambda_n) \tag{2.49}$$

For other waveguides, A_{nm} is given through the waveguide analysis.

Setting $v = v_x + jv_y$, then we have $v_x = \frac{1}{2}(v + v^*)$, $v_y = \frac{-j}{2}(v - v^*)$, where v^* is the complex conjugate of v. Furtheremore, if the solution of v is assumed in the form

$$v = v_t e^{j\Omega_c \tau}$$

Where $\tau = t - t_0$, t_0 is the time when the particle enters the interaction space, $v_t = (vv^*)^{\frac{1}{2}}$, and the phase angle

$$\Omega_c \tau = \tan^{-1}\left(\frac{v_y}{v_x}\right)$$
$$= -\tan^{-1}\left[\frac{j(v - v^*)}{v + v^*}\right]$$

With reference to Fig.3 and from Eqs.(2.7), (2.8), on use of Graf's Bessel function addition theorem, we have

$$\mathbf{v} \cdot \mathbf{E} = v_x E_x + v_y E_y$$
$$= \frac{\omega}{2ck_c^2} F(z)\left[v\left(\frac{\partial}{\partial x} - j\frac{\partial}{\partial y}\right) - v^*\left(\frac{\partial}{\partial x} + j\frac{\partial}{\partial y}\right)\right]B_z^0 e^{j\omega t}$$
$$= -\frac{\omega v_t}{2ck_c} F(z)\sum_{n=0}^{\infty}\sum_{m=-\infty}^{\infty}\sum_{s=-\infty}^{\infty} A_{nm} J_{m-s}(k_c R)J_s'(k_c r_l)e^{j[(\omega-s\Omega_c)\tau+\omega t_0]} \qquad (2.50)$$

$$v_x B_y - v_y B_x = \frac{1}{2}(v + v^*)B_y + \frac{j}{2}(v - v^*)B_x$$
$$= \frac{j}{2}\left[v(B_x - jB_y) - v^*(B_x + jB_y)\right]$$
$$= \frac{j}{2k_c^2}\frac{\partial F}{\partial z}\left[v\left(\frac{\partial}{\partial x} - j\frac{\partial}{\partial y}\right) - v^*\left(\frac{\partial}{\partial x} + j\frac{\partial}{\partial y}\right)\right]B_z^0 e^{j\omega t}$$
$$= j\frac{v_t}{2k_c}\frac{\partial F}{\partial z}\sum_{n=0}^{\infty}\sum_{m=-\infty}^{\infty}\sum_{s=-\infty}^{\infty} A_{nm} J_{m-s}(k_c R)J_s'(k_c r_l)e^{j[(\omega-s\Omega_c)\tau+\omega t_0]} \qquad (2.51)$$

Making use of Eqs.(2.50), (2.51), then Eqs.(2 42) and (2.43) can be written into

$$\frac{d}{dt}\gamma = \frac{e\omega v_t}{2mc^3 k_c}F(z)\sum_{n=0}^{\infty}\sum_{m=-\infty}^{\infty}\sum_{s=-\infty}^{\infty} A_{nm} J_{m-s}(k_c R)J_s'(k_c r_l)e^{j[(\omega-s\Omega_0)\tau+\omega t_0]} \qquad (2.52)$$

$$\frac{d}{dt}v_z = -\frac{ev_t}{2mc\gamma k_c}\left(\frac{\omega v_z}{c^2} + j\frac{\partial}{\partial z}\right)F(z)$$
$$\sum_{n=0}^{\infty}\sum_{m=-\infty}^{\infty}\sum_{s=-\infty}^{\infty} A_{nm} J_{m-s}(k_c R)J_s'(k_c r_l)e^{j[(\omega-s\Omega_0)\tau+\omega t_0]} \qquad (2.53)$$

And Eq.(2.44) and (2.45) can be combined into one equation as

$$\frac{dv}{dt} = -v\frac{d}{dt}\ln\gamma + \frac{e}{m\gamma}\left[(E_x + jE_y) + \frac{jv_z}{c}(B_x + jB_y)\right]$$
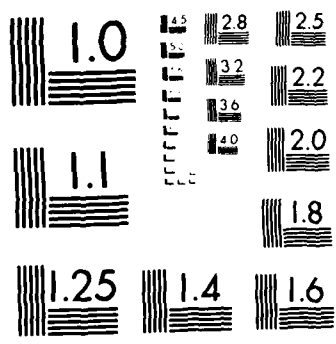$$- \frac{jeB_z^0}{mc\gamma}v - j\Omega_c v \qquad (2.54)$$

END

FILMED

DTIC

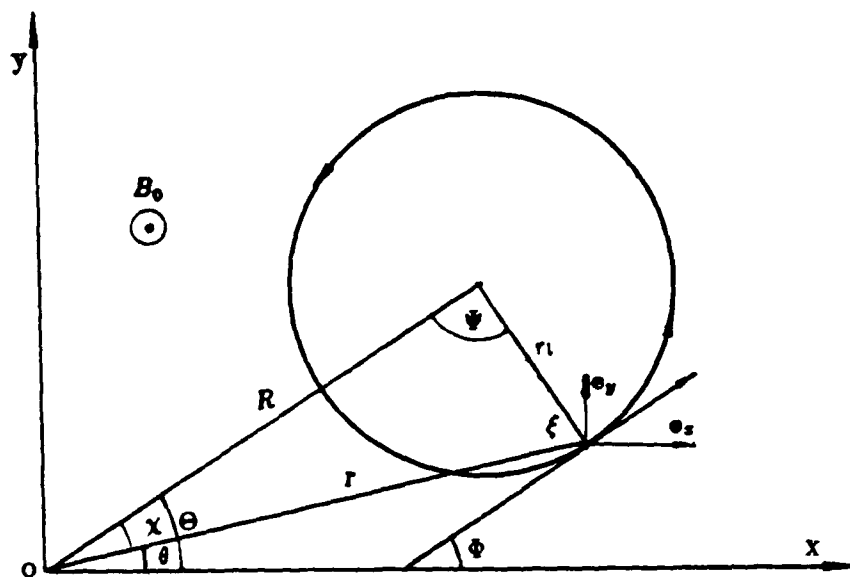MICROCOPY RESOLUTION TEST CHART

NATIONAL BUREAU OF STANDARDS 1963 A

Fig.3 The projection of an electron trajectory on the cross section of the waveguide.

In Cartisan coordinates, by equating the real and the imaginary part on both sides of Eq.(2.54) correspondingly, we obtain the following two equations:

$$
\begin{aligned}
\dot{v}_t &= -v_t \frac{d}{dt} \ln \gamma + \frac{e}{m\gamma} \left[(E_x - \frac{v_z}{c} B_y) \cos(\Omega_c \tau) + (E_y + \frac{v_z}{c} B_x) \sin(\Omega_c \tau) \right] \\
&= -v_t \frac{d}{dt} \ln \gamma - \frac{e}{mc\gamma k_c^2} \left(j\omega - v_z \frac{\partial}{\partial z} \right) F(z) \left[\cos(\Omega_c \tau) \frac{\partial}{\partial y} - \sin(\Omega \tau) \frac{\partial}{\partial x} \right] B_z^0 e^{j\omega t}
\end{aligned}
\tag{2.55}
$$

$$
\begin{aligned}
\Omega_c - \Omega_{c0} &= -\frac{e}{m\gamma v_t} \left[(E_x - \frac{v_z}{c} B_y) \sin(\Omega_c \tau) + (E_y + \frac{v_z}{c} B_x) \cos(\Omega_c \tau) \right] + \frac{eB_z}{mc\gamma} \\
&= -\frac{e}{m\gamma c k_c^2 v_t} \left(j\omega - v_z \frac{\partial}{\partial z} \right) F(z) \left[\sin(\Omega_c \tau) \frac{\partial}{\partial y} - \cos(\Omega_c \tau) \frac{\partial}{\partial x} \right] B_z^0 e^{j\omega t} \\
&\quad + \frac{eB_z^0}{mc\gamma} e^{j\omega t}
\end{aligned}
\tag{2.56}
$$

With reference to Fig.3 and on use of the Graf's addition theorem again, we have

$$
\begin{aligned}
&\left[\cos(\Omega_c \tau) \frac{\partial}{\partial y} - \sin(\Omega_c \tau) \frac{\partial}{\partial x} \right] B_z^0 e^{j\omega t} \\
&= -\frac{k_c}{2} \sum_{n=0}^{\infty} \sum_{m=-\infty}^{\infty} \sum_{s=-\infty}^{\infty} A_{nm} J_{m-s}(k_c R) J_s'(k_c r_t) e^{j[(\omega - s\Omega_c)\tau + \omega t_0]}
\end{aligned}
\tag{2.57}
$$

$$
\begin{aligned}
&\left[\sin(\Omega_c \tau) \frac{\partial}{\partial y} - \cos(\Omega_c \tau) \frac{\partial}{\partial x} \right] B_z^0 e^{j\omega t} \\
&= -\frac{k_c}{2} \sum_{n=0}^{\infty} \sum_{m=-\infty}^{\infty} \sum_{s=-\infty}^{\infty} A_{nm} J_{m-s}(k_c R) J_s(k_c r_t) e^{j[(\omega - s\Omega_c)\tau + \omega t_0]}
\end{aligned}
\tag{2.58}
$$

Then Eq.(2.56) can be written as

$$
\begin{aligned}
\dot{v}_t &= -\frac{e}{2mc\gamma k_c} \left(\frac{\omega v_t^2}{c^2} - j\omega - v_z \frac{\partial}{\partial z} \right) F(z) \\
&\quad \cdot \sum_{n=0}^{\infty} \sum_{m=-\infty}^{\infty} \sum_{s=-\infty}^{\infty} A_{nm} J_{m-s}(k_c R) J_s'(k_c r_t) e^{j[(\omega - s\Omega_c)\tau + \omega t_0]}
\end{aligned}
\tag{2.59}
$$

If a slow time scale variable is introduced as

$$
\Lambda = \frac{1}{s} [(\omega - s\Omega_c)\tau + \omega t_0],
$$

then Eq.(2.56) takes the following form:

$$
\begin{aligned}
\dot{\Lambda} &= -\frac{e}{2mc\gamma k_c^2 v_t} \left(j\omega - v_z \frac{\partial}{\partial z} \right) F(z) \left[\sin(\Omega_c \tau) \frac{\partial}{\partial y} - \cos(\Omega_c \tau) \frac{\partial}{\partial x} \right] B_z - \frac{eB_z}{mc\gamma} + \frac{\omega}{s} - \Omega_{c0} \\
&= -\frac{e}{2mc\gamma k_c^2 v_t} \left(j\omega - v_z \frac{\partial}{\partial z} - k_c v_t \right) F(z) \\
&\quad \cdot \sum_{n=0}^{\infty} \sum_{m=-\infty}^{\infty} \sum_{s=-\infty}^{\infty} A_{nm} J_{m-s}(k_c R) J_s(k_c r_t) e^{js\Lambda} + \frac{\omega}{s} - \Omega_{c0}
\end{aligned}
\tag{2.60}
$$

Where $\dot{\Lambda}$ and $\dot{v}_t$ denote the time derivatives of Λ and v_t respectively. However, there is still a problem. That is the function $F(z)$ involved in the equations obtained above. In order to get $F(z)$, we have to observe Eq.(2.10). On the right hand side of Eq.(2.10), the current density in the waveguide can be written as

$$\mathbf{J} = -\lambda \mathbf{v}$$
$$= -\lambda(v_z \mathbf{e}_z + v_y \mathbf{e}_y + v_z \mathbf{e}_z) \tag{2.61}$$

For the integral of the right hand side of Eq.(2.10), on use of Eq.(2.12) and Eq.(2.13), it can be cast as

$$\int_A dA \nabla \times \mathbf{J} \cdot \mathbf{e}_z B_z = \int_A dA [\nabla \cdot (\mathbf{J} \times B_z \mathbf{e}_z) + \nabla \times (B_z \mathbf{e}_z) \cdot \mathbf{J}]$$
$$= \frac{ck_c^2}{\omega} \int_A dA \lambda \mathbf{v} \cdot \mathbf{E} \tag{2.62}$$

It is seen from Eq.(2.62) that the axial component of the current does not contribute to the above integration and this integral is just proportional to the electron beam energy change rate averaged over the waveguide cross section. If the electron beam is idealized as having a single guiding center R, we can approximate the linear charge density as

$$\lambda = -\frac{I_0}{v_z}$$

In most cases, the beam energy is not too high, and k_z is very small, therefore, we can approximate $v_z = v_{z0}$, therefore, $\lambda = -\frac{I_0}{v_{z0}}$ is approximated as the linear charge density in the waveguide. Furtheremore, for a single gyration harmonic s,

$$\Lambda = (\frac{\omega}{s} - \Omega_c)\tau + \Lambda_0$$

where $\Lambda_0 = \frac{\omega}{s} t_0, \tau = t - t_0$. Then we may continue writing Eq.(2.62) as

$$I = \frac{ck_c^2}{\omega} \int_A dA \lambda \mathbf{v} \cdot \mathbf{E}$$
$$= -F(z)\frac{k_c}{2} \sum_{s=0}^{\infty} \sum_{m=-\infty}^{\infty} A_{sm} J_{m-s}(k_c R) \int_A dA \lambda v_t J_s'(k_c r_l) e^{js\Lambda}$$
$$= F(z)\frac{k_c I_0}{2} \sum_{s=0}^{\infty} \sum_{m=-\infty}^{\infty} A_{sm} \int_0^{2\pi} d(\omega t_0) \frac{v_t}{v_z} J_{m-s}(k_c R) J_s'(k_c r_l) e^{js\Lambda}$$
$$= F(z)\frac{sk_c I_0}{2} \sum_{s=0}^{\infty} \sum_{m=-\infty}^{\infty} A_{sm} \int_0^{2\pi} d\Lambda_0 \frac{v_t}{v_z} J_{m-s}(k_c R) J_s'(k_c r_l) e^{js\Lambda} \tag{2.63}$$

From Eq.(2.16), (2.63) we can have the following equation

$$\left(\frac{\partial^2}{\partial z^2} + \frac{\omega^2}{c^2} - k_c^2 - S\right)F(z) = 0 \qquad (2.64)$$

where

$$S = \frac{s k_c I_0}{2N} \sum_{n=0}^{\infty} \sum_{m=-\infty}^{\infty} A_{nm} \int_0^{2\pi} d\Lambda_0 \frac{v_t}{v_z} J_{m-s}(k_c R) J_s'(k_c r_l) e^{j(s\Lambda - k_s v_z \tau)} \qquad (2.65)$$

And N is the norm of the axial RF magnetic field given by Eq.(2.11).

In the above equations, the Larmor radious is $r_l = \frac{v_t}{\Omega_c}$.

Therefore, we obtained a set of the nonlinear differential equations consisting from Eqs.(2.53), (2.59), (2.60) and (2.64), that describes the nonlinear evolution of the electrons in the gyro-TWA devices. Eq.(2.64) is a secondary differential equation for one electron. If we solve this set of the differential equations numerically and consider M electrons projected on the gyration circle in a unit length of the waveguide, we have to solve a system of order $3(M + 2)$. But, if we assume there is no reflection at the output end of the waveguide, the order of this system will be reduced to $3M + 3$. For an unbunched 'cold' electron beam, the initial values are the transverse velocity, axial velocity, initial phase angle, and the initial values of $F(0)$, $F'(0)$. If the initial phases are assumed to be uniformly distributed, we can specify $\Lambda_{0i} = \frac{2i\pi}{M}$ for the i-th electron ($i = 1, 2, ..., M$). By computing the parameter γ as the function of time, therefore as a function of z, and taking the average over phases and ensemble, the energy transfer efficiency from the electrons to the waveguide fields can be obtained, and the saturation process can be determined.

Leaving this ambitious task here and what follows, we derive the linear dispersion equation for gyrotrons by iteration method.

If all the waveguide RF field components are neglected, then we obtain the lowest order solution which corresponds to the motion of the electron in a uniform static magnetic field B_0, $v_t = v_{t0}$, $v_z = v_{z0}$, $\Lambda = (\frac{\omega}{s} - \Omega_c)\tau$, $\gamma = \gamma_0$, and from Eq.(2.60) we can have

$$F(z) = e^{-j k_z z} \qquad (2.66)$$

where $\Omega_c = \frac{e B_z}{mc\gamma}$ is the electron gyration frequency. In writing Eq.(2.66), only the forward propagating wave is considered since we assume that there is no reflecting

wave at the output end of the waveguide, and $k_z = [(\frac{\omega}{c})^2 - k_c^2]^{\frac{1}{2}}$. The electron trajectory can be gotten by integrating the equation once more.

$$x = X + r_l \sin(\Omega_c \tau) \tag{2.67}$$

$$y = Y + r_l \cos(\Omega_c \tau) \tag{2.68}$$

Substituting the zero-th order solution into the nonlinear equations and integrating over t, for single harmonic number s, we obtain the solutions of the first order approximation as

$$v_t = v_{t0} - \frac{e(\omega - k_z v_{z0})}{2mc\gamma k_c \Omega_s} \sum_{n=0}^{\infty} \sum_{m=-\infty}^{\infty} A_{nm} \frac{v_{t0}}{v_{z0}} J_{m-s}(k_c R) J_s'(k_c r_l) \sin(s\Lambda - k_z z) \tag{2.69}$$

$$\gamma = \gamma_0 - \frac{e\omega v_{t0}}{2mc^3 k_c \Omega_s} \sum_{n=0}^{\infty} \sum_{m=-\infty}^{\infty} A_{nm} J_{m-s}(k_c R) J_s'(k_c r_l) \cos(s\Lambda - k_z z) \tag{2.70}$$

$$v_z = v_{z0} + \frac{e v_{t0} k_z}{2mc\gamma_0 k_c \Omega_s} \sum_{n=0}^{\infty} \sum_{m=-\infty}^{\infty} A_{nm} J_{m-s}(k_c R) J_s'(k_c r_l) \sin(s\Lambda - k_z z) \tag{2.71}$$

$$z = v_{z0}\tau - \frac{e v_{t0} k_z}{2mc\gamma_0 k_c \Omega_s^2} \sum_{n=0}^{\infty} \sum_{m=-\infty}^{\infty} A_{nm} J_{m-s}(k_c R) J_s'(k_c r_l) \cos(s\Lambda - k_z z) \tag{2.72}$$

$$\Lambda \simeq (\frac{\omega}{s} - \Omega_{c0})\tau + \Lambda_0$$
$$- \frac{e\omega\Omega_{c0} v_{t0}}{2m\gamma_0 c^3 k_c \Omega_s^2} \sum_{n=0}^{\infty} \sum_{m=-\infty}^{\infty} A_{nm} J_{m-s}(k_c R) J_s'(k_c r_l) \cos(s\Lambda - k_z z)$$
$$- \frac{e(\omega - k_z v_{z0} - k_c v_{t0})}{2mc\gamma_0 k_c^2 v_{t0} \Omega_s} \sum_{n=0}^{\infty} \sum_{m=-\infty}^{\infty} A_{nm} J_{m-s}(k_c R) J_s(k_c r_l) \cos(s\Lambda - k_z z) \tag{2.73}$$

Making use of $s\Omega_{c0} \simeq \omega$ at cyclotron resonance and the above first order approximations, considering that the second order quantities are much smaller than the first order quantities, we use the approximation $\sin \eta \simeq \eta$, $\cos \eta \simeq 1$ for small angle η, then we may write

$$\sin(s\Lambda - k_z z) \simeq \sin(\Omega_s \tau + \Lambda_0) - (\frac{\omega^2}{c^2} - k_z^2) \frac{e v_{t0}}{2mc\gamma_0 k_c \Omega_s^2}$$
$$\cdot \cos^2(\Omega_s \tau + \Lambda_0) \sum_{n=0}^{\infty} \sum_{m=-\infty}^{\infty} A_{nm} J_{m-s}(k_c R) J_s'(k_c r_l)$$
$$- \frac{e(\omega - k_z v_z - k_c v_{t0})}{2mc\gamma_0 k_c v_{t0} \Omega_s}$$
$$\cdot \cos^2(\Omega_s \tau + \Lambda_0) \sum_{n=0}^{\infty} \sum_{m=-\infty}^{\infty} A_{nm} J_{m-s}(k_c R) J_s(k_c r_l) \tag{2.74}$$

In the above equations,

$$\Omega_s = \omega - s\Omega_{c0} - k_{z0} v_{z0} \tag{2.75}$$

Substituting the above first order approximation of v_t, v_z and Eq. (2.73) into Eq.(2.52) and keeping the second order approximation terms only, we obtain

$$
\frac{1}{v_z}\frac{d\gamma}{dt} = \frac{e\omega v_{t0}}{2mc^3 v_{z0}k_c}\sum_{n=0}^{\infty}\sum_{m=-\infty}^{\infty}\sum_{s=-\infty}^{\infty} A_{nm}J_{m-s}(k_c R)J'_s(k_c r_l)sin(\Omega_s\tau + \Lambda_0)
$$

$$
-\frac{e^2\omega}{4m^2 v_{z0}c^4 k_c^2\gamma_0}\left\{\left(\frac{\omega^2}{c^2} - k_z^2\right)\frac{v_{t0}^2}{\Omega_s^2}\right.
$$

$$
\cdot\cos^2(\Omega_s\tau + \Lambda_0)\sum_{n=0}^{\infty}\sum_{m=-\infty}^{\infty}|A_{nm}|^2[J_{m-s}(k_c R)J'_s(k_c r_l)]^2
$$

$$
-\frac{(\omega - k_z v_{z0})}{\Omega_s}\sin^2(\Omega_s\tau + \Lambda_0)\sum_{n=0}^{\infty}\sum_{m=-\infty}^{\infty}|A_{nm}|^2[J_{m-s}(k_c R)J'_s(k_c r_l)]^2
$$

$$
+\frac{(\omega - k_z v_{z0} - k_c v_{t0})}{\Omega_s}\cos^2(\Omega_s\tau + \Lambda_0)
$$

$$
\left.\cdot\sum_{n=0}^{\infty}\sum_{m=-\infty}^{\infty}|A_{nm}|^2 J_{m-s}^2(k_c R)J'_s(k_c r_l)J_s(k_c r_l)\right\} \tag{2.76}
$$

The first term in the big braces in Eq.(2.76) is proportional to v_{t0}^2. There are two parts in this term. If $k_z = 0$, then this term is entirely due to the transverse force by the transverse field components, this is from the electron cyclotron maser instability; Another part which is proportional to k_z^2 is due to the force in $z-$ direction, that is, due to the Weibel instability. This Weibel part causes a change of the phase velocity of the electron motion. This can be made clear by observing Eq.(2.71). If $k_z = 0$ or $v_t = 0$, then $v_z = v_{z0}$ and Weibel instability will disappear. Thus, a conclusion we can make is that the existence of the Weibel instability is always associated with the electron transverse motion and with the propagating RF wave in the waveguide. The electron cyclotron maser part and the Weibel part always oppose each other, since their signs are different from each other. When $\omega^2 > c^2 k_z^2$, the cyclotron resonance instability dominates; otherwise, the Weibel instability dominates. When $k_z \neq 0$, there is a frequency shift due to which the amplification or oscillation frequency is shifted away from $s\Omega_{c0}$. We have seen that the energy change of the electrons is completely due to the interaction between the transverse field and velocity for TE mode interaction. The second term in the big braces is due to the change of the transverse velocity and proportional to the inverse of Ω_s; while the third term, which also inversely proportional to Ω_s, is associated with the change of the gyration phase velocity. These two terms set a threshold for the

instability. The right hand side of Eq.(2.62) may be written into the form

$$\int_A dA \nabla \times \mathbf{J} \cdot \mathbf{e}_z B_z = \int_A dA (\nabla \times \mathbf{e}_z B_z \cdot \mathbf{J})$$

$$= \frac{ck_c^2}{\omega} \int_A dA (\frac{I_0}{v_z}) \mathbf{v} \cdot \mathbf{E}$$

$$= -\frac{mc^3 k_c^2 I_0}{e\omega} \int_0^{2\pi} d\Lambda_0 \frac{1}{v_z} \frac{d\gamma}{dt} \tag{2.77}$$

Substituting Eq.(2.76) into Eq.(2.77), and taking an average over a period of the slow time scale, that is, integrating $\Omega_s \tau$ from 0 to 2π and the phase Λ_0 from 0 to 2π, from Eq.(2.65) we obtain the dispersion equation as

$$\frac{\omega^2}{c^2} - k_z^2 - k_c^2 = \frac{e\pi I_0 \omega}{4Nmc\gamma_0 v_{z0}} \left\{ \frac{\beta_t^2(\omega^2 - k_z^2 c^2)}{\Omega_s^2} \sum_{n=0}^{\infty} \sum_{m=-\infty}^{\infty} [A_{nm}]^2 [J_{m-s}(k_c R) J_s'(k_c r_l)]^2 \right.$$

$$- \frac{\omega - k_z v_{z0}}{\Omega_s} \sum_{n=0}^{\infty} \sum_{m=-\infty}^{\infty} [A_{nm}]^2 [J_{m-s}(k_c R) J_s'(k_c r_l)]^2$$

$$\left. + \frac{\omega - k_z v_z - k_c v_{t0}}{\Omega_s} \sum_{n=0}^{\infty} \sum_{m=-\infty}^{\infty} [A_{nm}]^2 J_{m-s}^2(k_c R) J_s'(k_c r_l) J_s(k_c r_l) \right\} \tag{2.78}$$

where $\beta_t = \frac{v_t}{c}$.

We can write the dispersion equation into the form

$$\frac{\omega^2}{c^2} - k_z^2 - k_c^2 = \frac{e\pi I_0}{4Nmc\gamma_0 v_{z0}} \left[\frac{\beta_t^2(\omega^2 - k_z^2 c^2)}{\Omega_s^2} H - \frac{(\omega - k_z v_{z0})}{\Omega_s} Q \right] \tag{2.79}$$

where

$$H = \sum_{n=0}^{\infty} \sum_{m=-\infty}^{\infty} [A_{nm}]^2 [J_{m-s}(k_c R) J_s'(k_c r_l)]^2 \tag{2.80}$$

$$Q = H - (1 - \frac{k_c v_{t0}}{\omega - k_z v_{z0}}) \sum_{n=0}^{\infty} \sum_{m=-\infty}^{\infty} [A_{nm}]^2 J_{m-s}^2(k_c R) J_s'(k_c r_l) J_s(k_c r_l) \tag{2.81}$$

In the circular waveguide case, for TE_{nm} mode, $k_c = \frac{p_{nm}}{a}$, where a is the radius of the waveguide and p_{nm} is the m-th root of the Bessel function $J_n(x)$; and in the above dispersion equation the coefficient A_{nm} equals unity and there is no summation involved. Comparing this dispersion equation with that derived by Chu et al.[16] For the circular waveguide TE_{nm} mode, we find that the function H is the same as H_{sm} in [16]. From Bessel equation, the first term in the function Q in Eq.(2.81) can be made the same as that in [16]. However, there is some difference in the rest of Q in Eq.(2.80) from the rest in the function Q_{sm} in [16]. The difference is due

to the different approximations made in the two different approaches to derive the dispersion equation. As pointed out in [16], in the dispersion equation the term with $Q_{,m}$ involved imposes a threshold beam energy for the instability. At higher harmonics, that term is very small compared to the term proportional to H and it can be neglected.

Chapter 3   Gyrotron Kinetic Theory

With the field components written in the forms of Eqs.(2.7) and (2.8), in Chapter 2 for nonlinear theory we derived an equation for function $F(z)$ in Eq.(2.10) which has to be solved simutaneously with other equations. In this chapter we employ plasma kinetic theory to solve this equation to get $F(z)$, furthermore, to obtain the small signal gain-frequency relation for the gyro-TWA.

Because of its relative simplicity and its easy understanding of the physical results obtained, kinetic theory has been widely used in gyrotron analysis. As a standard approach in plasma physics, the linearized Vlasov equation can be solved by the method of characteristics, and the initial value may be included by introducing a Laplace transformation. Through an inverse Laplace transformation the function $F(z)$ which describes the profile of the RF field along the waveguide with the presence of moving electrons is obtained, then the gain of the power flow of the device can be caculated. Park at al.[41] have used this approach to analyze the slow wave gyrotron amplifiers for the circular electrical waveguide modes. However, the analysis in this chapter is with a generalized waveguide-beam model shown in Fig.2 and for any TE waveguide modes.

As usual, we just find the first order perturbation of the electron distribution function. Therefore, this is a linear theory. In doing this analysis, several assumptions are made. First, it is assumed that the space charge effect can be neglected; Second, the electron beam and the RF wave in the waveguide are described by the linearized Maxwell-Vlasov equations; Third, this is a single mode analysis, the coupling with the neighboring wave modes is assumed to be negligible.

The nature of the electron helical motion in the waveguide makes the cylindrical coordinate system most suitable for this analysis. But, it is desirable that this analysis be a generalized one and can be applicable to the gyro-TWA devices with different shapes of the waveguide cross section. Therefore, this analysis is carried

out in the Cartesian coordinate system first, then a transformation to the cylindrical coordinates is made naturally by using some Bessel function identities.

Section 3.1 to 3.4 are with the derivation of the small signal gain of the device. Still in the frame of kinetic theory, the efficiency of the devices is estimated in Section 3.5. Section 3.6 is devoted to a brief discussion on the beam velocity spread problem.

3.1   Perturbed Electron Distribution Function

In addition to the Maxwell equations Eq.(2.1) to (2.4), the Vlasov equation

$$\frac{\partial f}{\partial t} + \frac{\mathbf{u}}{\gamma} \cdot \nabla f - \frac{e}{m}(\mathbf{E} + \frac{1}{c\gamma}\mathbf{u} \times \mathbf{B}) \cdot \nabla_\mathbf{u} f = 0 \tag{3.1}$$

and two coupling equations

$$\mathbf{J} = -e \int d^3 u \frac{\mathbf{u}}{\gamma} f \tag{3.2}$$

$$\rho = -e \int d^3 u f \tag{3.3}$$

together form the basic equations for plasma kinetic theory. Here $f(\mathbf{u}, \mathbf{r}, t)$ is the electron distribution function in momentum, space and time, $\mathbf{u} = \gamma\dot{\mathbf{r}}$, $\gamma = (1 + u^2)^{\frac{1}{2}}$ and $\dot{\mathbf{r}}$ stands for time derivative of $\mathbf{r}$. With the assumptions $|f_1| \ll |f_0|$, $|B_1| \ll |B_0|$, setting $f = f_0 + f_1$, $\mathbf{E} = \mathbf{E}_1$, $\mathbf{B} = \mathbf{B}_0 + \mathbf{B}_1$ and substituting these into Eq.(3.1), we have

$$\frac{\partial f_0}{\partial t} + \frac{\mathbf{u}}{\gamma} \cdot \nabla f_0 - \frac{e}{mc}(\frac{\mathbf{u}}{\gamma} \times \mathbf{B}_0) \cdot \nabla_\mathbf{u} f_0 = 0 \tag{3.4}$$

$$\frac{\partial f_1}{\partial t} + \frac{\mathbf{u}}{\gamma} \cdot \nabla f_1 - \frac{e}{mc}(\frac{\mathbf{u}}{\gamma} \times \mathbf{B}_0) \cdot \nabla_\mathbf{u} f_1 = \frac{e}{m}(\mathbf{E}_1 + \frac{\mathbf{u}}{\gamma c} \times \mathbf{B}_1) \cdot \nabla_u f_0 \tag{3.5}$$

The perturbed electron distribution function can be obtained by the method of characteristics, viz, by integrating the equation along the unperturbed electron trajectory,

$$f_1 = \frac{e}{m} \int_{t-\frac{z}{v_z}}^{t} dt' e^{-j\omega t'} (\mathbf{E}_1 + \frac{\mathbf{u}}{c\gamma} \times \mathbf{B}_1) \cdot \nabla_\mathbf{u} f_0 \tag{3.6}$$

With reference to Fig.3, we write

$$\mathbf{u} = u_t \mathbf{e}_t + u_z \mathbf{e}_z$$

$$e_t = e_x \cos \Phi + e_y \sin \Phi$$

$$u_t = (u_x^2 + u_y^2)^{\frac{1}{2}}$$

For R, the guiding center of the electrons, we have

$$\nabla_u R = -\frac{1}{\Omega_c} e_\Theta$$

$$= e_x \sin \Theta - e_y \cos \Theta \tag{3.7}$$

Furthermore, we may write

$$\nabla_u f_0 = e_z \frac{\partial f_0}{\partial u_z} + e_t \frac{\partial f_0}{\partial u_t} + \frac{\partial f_0}{\partial R} \nabla_u R$$

$$= e_z \frac{\partial f_0}{\partial u_z} + e_x \left(\cos \Phi \frac{\partial f_0}{\partial u_t} + \frac{1}{\Omega_c} \sin \Theta \frac{\partial f_0}{\partial R} \right)$$

$$+ e_y \left(\sin \Phi \frac{\partial f_0}{\partial u_t} - \frac{1}{\Omega_c} \cos \Theta \frac{\partial f_0}{\partial R} \right) \tag{3.8}$$

where $\Omega_c = \frac{eB_0}{mc\gamma}$ is the electron relativistic gyration frequency. In the Cartesian coordinate system, from Eq.(2.7), (2.8) we can write

$$\left(\mathbf{E}_1 + \frac{\mathbf{u}}{c\gamma} \times \mathbf{B}_1 \right) \cdot \nabla_u f_0 = \frac{u_t}{c\gamma} \left(B_y \cos \Phi + B_x \sin \Phi \right) \frac{\partial f_0}{\partial u_z}$$

$$+ \left[E_x + \frac{1}{c\gamma} (u_t B_z \sin \Phi - u_z B_y) \right] \left(\cos \Phi \frac{\partial f_0}{\partial u_t} + \frac{1}{\Omega_c} \sin \Theta \frac{\partial f_0}{\partial R} \right)$$

$$+ \left[E_y - \frac{1}{c\gamma} (u_t B_z \cos \Phi - u_z B_x) \right] \left(\sin \Phi \frac{\partial f_0}{\partial u_t} - \frac{1}{\Omega_c} \cos \Theta \frac{\partial f_0}{\partial R} \right) \tag{3.9}$$

The waveguide field components in the beam-field interaction region can be written in the following series form in general regardless of the shape of the waveguide cross section. However, the coefficients in the series are dependent upon the geometry of the cross section of the waveguide. Here we can use the series for the out-ridged waveguide (analyzed in Chapter 4) as the general expression. For the axial RF magnetic field in the beam field interaction region in the waveguide, we write

$$B_{1z}^0 = \sum_{n=0}^{\infty} B_{1zn}$$

$$= \sum_{n=0}^{\infty} B_{1n} \frac{\sin}{\cos} (k_{z1n} z) \cos \left[\frac{n\pi}{h_s} (y - h) \right] \tag{3.10}$$

where the notations h_s, h are in Fig.5. In the following analysis, we take the lower cosine sign in Eq.(3.10) only. For the upper sine sign, it only needs to make a simple change in the coefficient A_{nm} as we will see in Chapter 4.

From Eqs.(2.12) and (2.13) we can further write Eq.(3.9) into

$$[\mathbf{E}_1 + \frac{\mathbf{u}}{c\gamma} \times \mathbf{B}_1] \cdot \nabla_u f_0 = \frac{1}{ck_c^2}\left\{\left[\frac{1}{\gamma}\frac{\partial F(z)}{\partial z}(u_t\frac{\partial f_0}{\partial u_z} - u_z\frac{\partial f_0}{\partial u_t}) + j\omega F(z)\frac{\partial f_0}{\partial u_t}\right](\sin\Phi\frac{\partial}{\partial x} - \cos\Phi\frac{\partial}{\partial y})B_{1z}^0\right.$$

$$+ (j\omega - \frac{u_z}{\gamma}\frac{\partial}{\partial z})F(z)\frac{1}{\Omega_c}\frac{\partial f_0}{\partial R}(\cos\Theta\frac{\partial}{\partial x} + \sin\Theta\frac{\partial}{\partial y})B_{1z}^0$$

$$\left. + \frac{u_t k_c^2}{\gamma}F(z)\sin\Psi\frac{1}{\Omega_c}\frac{\partial f_0}{\partial R}B_{1z}^0\right\}. \tag{3.11}$$

Setting $k_{x1n} = k_c\sin\lambda_n$, $k_{y1n} = k_c\cos\lambda_n$ and using two Bessel identities

$$e^{jk_c r\sin(\theta+\lambda_n)} = \sum_{m=-\infty}^{\infty} J_m(k_c r)e^{jm(\theta+\lambda_n)} \tag{3.12}$$

$$e^{-jk_c r\sin(\theta+\lambda_n)} = \sum_{m=-\infty}^{\infty} (-1)^m J_m(k_c r)e^{jm(\theta+\lambda_n)} \tag{3.13}$$

then from Eq.(3.10) and with reference to Fig.3 we have

$$(\sin\Phi\frac{\partial}{\partial x} - \cos\Phi\frac{\partial}{\partial y})B_{1zn} = \frac{k_c}{2}\sum_{m=-\infty}^{\infty} A_{nm}[J_{m+1}(k_c r)e^{j\epsilon} - J_{m-1}(k_c r)e^{-j\epsilon}]e^{jm\theta} \tag{3.14}$$

$$(\cos\Theta\frac{\partial}{\partial x} + \sin\Theta\frac{\partial}{\partial y})B_{1zn} = -\frac{k_c}{2}\sum_{m=-\infty}^{\infty} A_{nm}[J_{m+1}(k_c r)e^{jx} + J_{m-1}(k_c r)e^{-jx}]e^{jm\theta} \tag{3.15}$$

$$\sin\Psi B_{1zn} = -\frac{j}{2}\sum_{m=-\infty}^{\infty} A_{nm}J_m(k_c r)(e^{j\Psi} - e^{-j\Psi})e^{jm\theta} \tag{3.16}$$

where the coefficient A_{nm} and λ_n for the out-ridged waveguide are given by (see Chapter 4)

$$A_{nm} = \frac{1}{2}B_{z1n}[e^{jk_c h\cos\lambda_n} + (-1)^m e^{-jk_c h\cos\lambda_n}]\cos(m\lambda_n) \tag{3.17}$$

$$\lambda_n = \cos^{-1}(k_{y_n}) \tag{3.18}$$

From Fig.3 and the electron orbit at equilibrium, we have a relation

$$\Psi' = \Psi - \frac{\Omega_c(z - z')}{v_z} \tag{3.19}$$

Substituting Eqs.(3.11), (3.14), (3.15), (3.16) and $t - t' = \frac{(z-z')}{v_z}$ into Eq.(3.6), we obtain the integral of the perturbed distribution function

$$f_1 = \frac{e}{m}\int_{t-\frac{z}{v_z}}^{t} dt' e^{-j\omega t'}(\mathbf{E}_1 + \frac{\mathbf{u}}{c\gamma} \times \mathbf{B}_1) \cdot \nabla_u f_0$$

$$= \frac{eN_e}{mck_c}e^{j\omega t}\sum_{n=0}^{\infty}\sum_{m=-\infty}^{\infty}\sum_{r=-\infty}^{\infty} A_{nm}e^{jm\Theta}\int_0^z dz' G(z - z')Q(z') \tag{3.20}$$

For the high power gyro-TWA devices, the efficiency is one of the most important considerations for the performances. Since the caculation of the efficiency involves saturation, which is a nonlinear process, the efficiency optimazation usually is resorted to the numerical simulation in the multiple parameter space. But, as mentioned in Introduction, an analytical efficiency scaling relation has been derived in the frame of linear theory by analyzing the phase relation at saturation.[16] Since in general the beam line

$$\omega - k_z v_z - s\Omega_c = 0$$

and the waveguide dispersion equation

$$\omega^2 - k_z^2 c^2 - k_c^2 c^2 = 0$$

intersect near at grazing angle, in the beam frame, $v_z' = 0$, this grazing condition implies that

$$\omega' \simeq s\Omega_c' \simeq ck_c \tag{3.82}$$

From the linear theory, the following condition is expected at the onset of the instability,

$$\Delta\omega' = \omega' - s\Omega_c' \tag{3.83}$$

As the saturation occurs, we expect the following relation to be held

$$\Delta\omega' = \omega' - \frac{s\Omega_c}{<\gamma_s>} \tag{3.84}$$

Where $<\gamma_s>$ means taking the average of γ over the beam ensemble at saturation. From the efficiency relation and with the assumption that $\gamma_s' \ll \gamma_0'$, we have

$$\eta' = \frac{\gamma_0' - <\gamma_s'>}{\gamma_0' - 1}$$

$$\simeq \frac{2\gamma_0'\Delta\omega_r'}{(\gamma_0' - 1)\omega_0'} \tag{3.85}$$

For fast wave devices, the second term in the right hand side of Eq.(3.79) is negligible. Setting $\omega' = \omega_0' + \Delta\omega', k_z = k_{z0}$, where ω_0' and k_{z0} are obtained from solving the beam line and the waveguide dispersion equation and substituting these into Eq.(3.78), we obtain

$$\Delta\omega_r' = \sum_{s=-\infty}^{\infty} \sum_{m=-\infty}^{\infty} A_{sm}^2 \left[\frac{\nu' k_c^2 u_i^2 c^2 J_{m-s}^2(k_c R) J_s'^2(k_c r_l)}{2\gamma N\omega_0'} \right]^{\frac{1}{3}} \tag{3.86}$$

with any shape of the cross section can be obtained. Since the solution to Eq.(2.18) may be assumed to be of the form $e^{jk_z z}$ and k_z is understood as real, we change K into k_z but the frequency ω is assumed to be complex, as a common approach in plasma physics, we obtain a general dispersion equation for the gyrotron traveling wave amplifiers as the following

$$(\frac{\omega^2}{c^2} - k_z^2 - k_c^2) = \sum_{n=0}^{\infty} \sum_{m=-\infty}^{\infty} \sum_{s=-\infty}^{\infty} \frac{\pi \nu A_{nm}^2}{\gamma N} \left\{ \frac{(\frac{\omega^2}{c^2} - k_z^2)\beta_t^2 [J_s'(k_c r_l) J_{m-s}(k_c R)]^2}{\Omega_s^2} \right. $$
$$\left. - \frac{k_c r_l \left[2\Omega_c(1 - \frac{s^2}{k_c^2 r_l^2}) J_{m-s}^2(k_c R) J_s(k_c r_l) - \frac{k_c u_z}{2}\hat{\Psi}_+ \right] J_s'(k_c r_l)}{\Omega_s} \right\} \qquad (3.77)$$

where

$$\Omega_s = \omega - \frac{k_z u_z}{\gamma} - s\Omega_c \qquad (3.78)$$

From Bessel equation we have

$$(1 - \frac{s^2}{x^2})J_s(x) = -J_s''(x) - \frac{1}{x}J_s'(x)$$

and note that $s\Omega_c \simeq \omega - \frac{k_z u_z}{\gamma}$, then the generalized dispersion equation takes the form

$$(\frac{\omega^2}{c^2} - k_z^2 - k_c^2) = \frac{\pi \nu A_{nm}^2}{\gamma N} \left[\frac{\beta_t^2 (\omega^2 - k_z^2 c^2)}{\Omega_s^2} H - \frac{(\omega - k_z v_{z0})}{\Omega_s} Q' \right] \qquad (3.79)$$

where

$$H = \sum_{n=0}^{\infty} \sum_{m=-\infty}^{\infty} [A_{nm}]^2 [J_{m-s}(k_c R) J_s'(k_r r_l)]^2 \qquad (3.80)$$

$$Q' = 2H - \sum_{n=0}^{\infty} \sum_{m=-\infty}^{\infty} [A_{nm}]^2 \left\{ 2k_c r_l J_{m-s}^2(k_c R) J_s'(k_c r_l) J_s''(k_c r_l) - \frac{k_c^2 r_l^2}{2}\Psi_+ \right\} \qquad (3.81)$$

Putting the coefficients A_{nm} to unity and removing the summations in Eq.(3.80) and (3.81), then we have a dispersion equation suitable for the TE_{nm} mode of the circular waveguide, if k_c is set to $\frac{\mu_{nm}}{a}$. Comparing to the dispersion equation derived for the TE_{nm} mode of the circular waveguide in [16], we find that H is the same as H_{sm} in [16]. As to the function Q' in Eq.(3.81) and Q_{sm} in [16], the difference is between Ψ_+ in Q' and the last two terms in Q_{sm}. In Q', the Bessel function $J_{s\pm1}(k_c r_l)$, $J_{s\pm2}(k_c r_l)$ and $J_{m-(s\pm1)}(k_c R)$, $J_{m-(s\pm2)}(k_c R)$ are also involved. In [51,52], Döhler explained that these may be important for 'peniotron' interaction. But it is still to be discussed the role of the Bessel function of order $s \pm 2$ contained in Q' in Eq.(3.81).

Where $P(L)$ is the power flow at the output end of the waveguide and $P(0)$ is the power flow at the input plane of the waveguide.

Obviously, the gain is the function of all the beam and waveguide parameters, also a function of the frequency. Thus, we can compute the gain as a function of the frequency with all the specified electron beam and waveguide parameters involved.

The commonly used $3dB$ bandwidth of the gain for an amplifier is defined as the frequency interval between the two frequencies where the gain drops down $3dB$ from the gain at the center frequency. Due to the fact that the cyclotron maser radiation is strong only when the frequency is close to the cutoff frequency of the operating waveguide mode, the gyro-TWA devices with uniform waveguide, a relatively small bandwidth is expected, usually just 1-3%. But, since this is a distributed interaction in the waveguide, some methods can be taken to alleviate this and a much bigger bandwidth can be achieved. Y.Y. Lau proposed a tapered instead of a uniform waveguide as the beam-field interaction space. Simutaneously, the applied magnetic field also is tapered to mantain the synchronization between beam and the field along the waveguide. Both from the theoretical and experimental investigations, the gyro-TWA device with tapered waveguide can achieve about 15% bandwith centered at 35 GHz frequency.[25]

Another method to increase the bandwidth is to decrease the applied magnetic field slightly below the grazing line, as many people have pointed out and confirmed in the experiments.[16,25]

Through the derivation of a dispersion equation to analyze the instability is a generally used approach in plasma physics. Here we can easily obtain a general dispersion equation from Eq.(3.50) for the gyro-TWA. The third term on the right hand side of Eq.(3.59) is proportional to the square of $\Omega_e(K)$ and is much smaller compared to the other two terms near cyclotron resonance, this makes the neglect of that term on the right hand side of Eq.(3.59) permissible. Therefore, if $D(K)$ in Eq.(3.57) is set to zero and the electron beam inhomogeneity is neglected, i. e., only the first two terms in the expression of $D_{10}(K)$ in Eq.(3.59) are taken, then for gyrotron devices a generalized dispersion equation which $\smile$ ap$_k$ cable to waveguide

Once $F(z)$ has been found, all the components of the field in any cross section in the waveguide can be obtained through $Eq.(2.7) - (2.8)$.

3.5 Gain-Frequency Relation and Efficiency

One of the most important performances for an amplifier is to achieve certain gain in a frequency interval of interest. For high power devices, the efficiency is a chief consideration. This section is used to deal with these two aspects.

Since the field components in the waveguide are assumed to be in the form in Eq.(2.7). (2.8), (2.9), and $F(z)$ is given by Eq.(3.68), so the power flow in the waveguide can be found by integrating the axial component of the Poynting vector over the cross-sectional area of the waveguide.

$$P(z) = \frac{1}{2}Re \int_A dA e_z \cdot (\mathbf{E}_t \times \mathbf{B}_t)$$
$$= \frac{1}{2}Re\left\{-jF(z)\frac{\partial F(z)}{\partial z}\left[\frac{\omega}{ck_c^4}\int_A dA\nabla_t B_z^0 \cdot (\nabla_t B_z^0)^*\right]\right\} \tag{3.72}$$

For a uniform waveguide, that part in the brackets in the above equation is independent of z. If we denote

$$D_t = -\frac{\omega}{2ck_c^4}\int_A dA\nabla B_z^0 \cdot (\nabla B_z^0)^* \tag{3.73}$$

then we can write the power flow at z and at $z = 0$,

$$P(z) = D_t Re[jF(z)\frac{dF(z)}{dz}]$$
$$= D_t\left\{\sum_{i=1}^m\left[e^{jK_iz}\frac{N(K_i)}{D'(K_i)}\right]\sum_{p=1}^m\left[K_p e^{jK_pz}\frac{N(K_p)}{D'(K_p)}\right]^*\right\} \tag{3.74}$$

$$P(0) = D_t Re[jF(0)\frac{dF(0)}{dz}]$$
$$= D_t\left[\sum_{i=1}^m\frac{N(K_i)}{D'(K_i)}\right]\left[\sum_{p=1}^m K_p\frac{N(K_p)}{D'(K_p)}\right]^* \tag{3.75}$$

If the beam-field interaction length is L, the gain in dB is defined as

$$G = 10\log\frac{P(L)}{P(0)}$$
$$= 10\log\left\{\frac{\left[\sum_{i=1}^m e^{jK_iL}\frac{N(K_i)}{D'(K_i)}\right]\left[\sum_{p=1}^m K_p e^{jK_pL}\frac{N(K_p)}{D'(K_p)}\right]^*}{\left[\sum_{i=1}^m\frac{N(K_i)}{D'(K_i)}\right]\left[\sum_{p=1}^m K_p\frac{N(K_p)}{D'(K_p)}\right]^*}\right\} \tag{3.76}$$
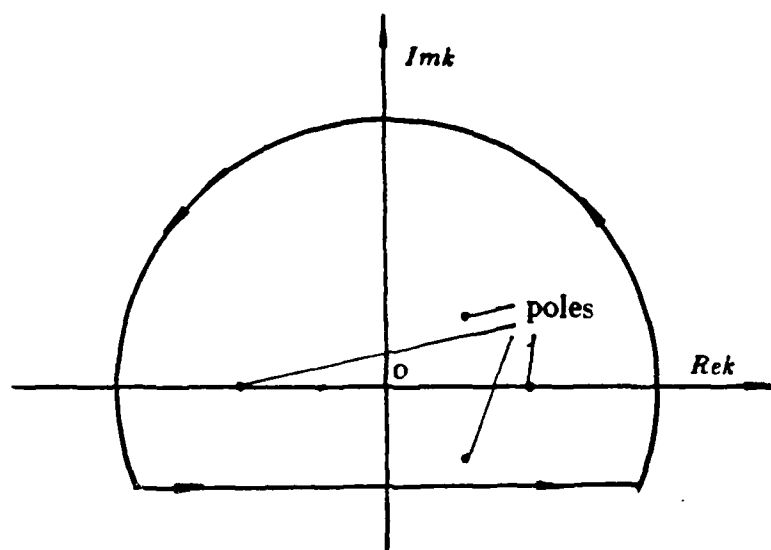
Fig.4 The contour of the integration.

$$= j \sum_{i=1}^{m} Res[e^{jK_i z} \overline{F}(K_i)] \tag{3.66}$$

where K_i is the i-th pole in the integrand. From Eq.(3.56) for $F(K)$, the poles of function $F(K)$ are the roots of its denominator $D(K)$ in Eq.(3.57).

For a generalized Lorentzian distribution in u_z

$$f_0(u_z) = D \frac{(\Delta u_z)^{2p}}{(u_z - \bar{u}_z)^{2p} + (\Delta u_z)^{2p}} \tag{3.67}$$

and a single gyration harmonic number s, there are $2 + 2p$ poles in $\overline{F}(K)$ with the Lorentzian distribution of order p in u_z. In the case $p = 1$ and also in the 'cold' electron beam case, $D(K)$ in Eq.(3.57) is a quartic function, and it is readily seen that all the singularities in $\overline{F}(K)$ are order of one. Since $\overline{F}(K)$ is in the form of Eq.(3.56), so we can write $F(z)$ in the following form by using the residue theorem.

$$F(z) = j \sum_{i=1}^{4} e^{jK_i z} \frac{N(K_i)}{D'(K_i)} \tag{3.68}$$

where $D'(K)$ is the derivative of $D(K)$ with respect to K in Eq.(3.57). At the input plane $z = 0$, if we set $F(0)$ to unity, then we have a relation

$$j \sum_{i=1}^{4} \frac{N(K_i)}{D'(K_i)} = 1 \tag{3.69}$$

Therefore, the problem of getting the function $F(z)$ is reduced to finding the poles in the function $\overline{F}(K)$, or the roots in $D(K)$. Moreover, if the output of the gyro-TWA device is well matched to the load, the wave propagating in the negative z–direction can be neglected, therefore the corresponding coefficients in Eq.(3.68) and (3.69) must be zero. $N(K)$ is given by Eq.(3.58) and $D'(K)$ can be found by taking the partial derivative of function $D(K)$ in Eq.(3.57) with respect to K.

$$D'(K) = -2[K\Omega_s^2(K) + \frac{u_z}{\gamma}\Omega_s(K)(\frac{\omega^2}{c^2} - K^2 - k_c^2)]$$
$$- \sum_{s=0}^{\infty} \sum_{m=-\infty}^{\infty} \sum_{-\infty}^{\infty} \frac{\pi \nu A_{nm}^2}{\gamma N} D_{10}'(K) \tag{3.70}$$

From Eq.(3.59) we have

$$D_{10}'(K) = \frac{2K\beta_t^2}{c^2} J_s'^2(k_c r_l) J_{m-s}^2(k_c R)$$
$$+ \frac{k_c r_l u_z}{\gamma}[2\Omega_c(1 - \frac{s^2}{k_c^2 r_l^2})J_s(k_c r_l)J_{m-s}^2(k_c R) - \frac{k_c u_t}{2}\hat{\Psi}_-]J_s'(k_c r_l)$$
$$- \frac{2u_z}{\gamma}\Omega_s(K)[2\gamma k_c r_l(1 - \frac{s^2}{k_c^2 r_l^2})J_s'(k_c r_l)J_{m-s}^2(k_c R)$$
$$- \frac{k_c u_t}{\Omega_c}\hat{\Psi}_+]J_s(k_c r_l) \tag{3.71}$$

where ϕ is the pitch angle of the electron, ψ is the Brillouin angle of the wave mode, which is defined as $tan^{-1}\psi = \frac{k_\perp}{k_z}$.

It is clear that if $v\sin\psi\sin\phi$ is very small compared to c, the speed of light in free space, i. e., if the electron beam is non-relativistic or moves with a small pitch angle or both, then the Bessel function has an argument much smaller than its order s. Since the higher the order of the Bessel function s is, the bigger the argument it needs to reach the first peak of the function value, and the peak value of the Bessel function also becomes smaller when its order increases. Therefore, when the harmonic number s increases, the coupling between the field and the electron beam becomes weaker. It is crucial to have bigger Larmor radius for higher harmonic operation. This explains why in general the gyrotrons operating at higher gyration harmonics demand high electron beam energy and big $\alpha = \frac{v_\perp}{v_z}$ to have a larger portion of the electron kinetic energy in the transverse direction.

The waveguide structure is also critical for gyrotrons working efficiently at higher gyration harmonics, since a good waveguide structure can achieve a much bigger component of the desired multipole field at the order of the harmonic number, therefore, a much bigger beam-field coupling.

3.4   Inverse Laplace Transformation, Fields

The Laplace inverse transformation of $\overline{F}(K)$ gives the function $F(z)$, with the frequency, the electron beam parameters and the waveguide parameters involved.

The Laplace inverse transformation is defined as

$$F(z) = \int_{-jC-\infty}^{-jC+\infty} dK e^{jKz}\overline{F}(K) \tag{3.65}$$

where the contour C must be large enough to include all the poles of the function $\overline{F}(K)$. The contour of the integration is depicted in Fig.4.

The inverse transformation integral may be carried out by using residue theorem in complex variable theory.

$$F(z) = \int_{-jC-\infty}^{-jC+\infty} dK e^{jKz}\overline{F}(K)$$

In the simple circular waveguide case, Eq.(3.61) reduces to the common form

$$H'_c = [J'_s(k_c r_l) J_{m-s}(k_c R)]^2 \qquad (3.62)$$

used in many papers[16,24,42].

In the expression of D_{10} in Eq.(3.59), the first term, which is proportional to H_c, is the source term; the second and the third terms impose a threshold to the instability. From this analytical result, if H_c vanishes, clearly both the cyclotron maser instability and the Weibel instability will vanish.

Since $| J_0(x) | \leq 1$, $| J_m(x) | \leq \frac{1}{\sqrt{2}}$, we conclude that for the same beam energy, the same waveguide structure, the same wave mode, and the same frequency of operation of the devices, the concentric beam has a bigger coupling with the fields than the annual beam. This offers a simple explanation for the utilization of the rotating electron layers instead of the annular beams in the most reported microwave generation experiments at higher harmonics of the gyration frequency. In the case of concentric electron beam, $R = 0$, $H_c \neq 0$ only if $m = s$. Therefore, for a single harmonic number s, the beam-field coupling coefficient becomes

$$H_c = \sum_{n=-\infty}^{\infty} (A_{nm})^2 [J'_s(k_c r_l)]^2 \qquad (3.63)$$

For the concentric beam, this means that if a gyrotron device operates at s-th gyration harmonic, the electron beam can have efficient interaction only with that order of the field multipoles which equals the harmonic number. For the other beam model, this statement is also valid if the field is expanded into multipoles around the guiding centers of the gyrating electrons.

Since near the cyclotron resonance $\Omega_c \simeq \frac{\omega - k_z v_z}{s}$, $k_c = \frac{\omega}{c} \sin \psi$, $r_l = \frac{v \sin \phi}{\Omega_c}$, and $v_z = v \sin \phi$, we can write the argument of the Bessel function as[24]

$$k_c r_l \simeq \frac{s v \sin \phi \sin \psi}{c - v \cos \phi \cos \psi} \qquad (3.64)$$

and the small argument approximation of the Bessel function can be used

$$J_s(x) \simeq \frac{x^s}{2^s s!}$$

$$\hat{\Psi}_- = \frac{2k_c^2}{k_c r_l} \Big\{ -J_{m-s}^2(k_cR)J_s'(k_cr_l)$$

$$+ [(m-s)J_{s+1}'(k_cr_l) + \frac{s+1}{k_cr_l}J_{s+1}(k_cr_l)]J_{m-(s+1)}(k_cR)$$

$$+ [(m-s)J_{s-1}'(k_cr_l) + \frac{s-1}{k_cr_l}J_{s-1}(k_cr_l)]J_{m-(s-1)}(k_cR)$$

$$- \frac{1}{2}k_cr_l J_{s+2}'(k_cr_l)J_{m-(s+2)}^2(k_cR)$$

$$- \frac{1}{2}k_cr_l J_{s-2}'(k_cr_l)J_{m-(s-2)}^2(k_cR) \Big\}. \tag{3.54}$$

$$\hat{\Psi}_+ = -\frac{2k_c^2}{k_c r_l} \Big\{ [(m-s)J_{s+1}'(k_cr_l) + \frac{s+1}{k_cr_l}J_{s+1}(k_cr_l)]J_{m-(s+1)}(k_cR)$$

$$- [(m-s)J_{s-1}'(k_cr_l) + \frac{(s-1)}{k_cr_l}J_{s-1}(k_cr_l)]J_{m-(s-1)}(k_cR)$$

$$- \frac{1}{2}k_cr_l J_{s+2}'(k_cr_l)J_{m-(s+2)}^2(k_cR)$$

$$+ \frac{1}{2}k_cr_l J_{s-2}'(k_cr_l)J_{m-(s-2)}^2(k_cR) \Big\}. \tag{3.55}$$

Finally we get $\overline{F}(K)$ in the quotient form

$$\overline{F}(K) = \frac{N(K)}{D(K)} \tag{3.56}$$

where

$$D(K) = (\frac{\omega^2}{c^2} - K^2 - k_c^2)\Omega_s^2(K) - \sum_{n=0}^{\infty}\sum_{m=-\infty}^{\infty}\sum_{s=-\infty}^{\infty} \frac{\pi\nu A_{nm}^2}{\gamma N c^2}D_{10}(K) \tag{3.57}$$

$$N(K) = jF(0)[K - \sum_{n=0}^{\infty}\sum_{m=-\infty}^{\infty}\sum_{s=-\infty}^{\infty} \frac{\pi\nu A_{nm}^2}{\gamma N c^2}D_{00}(K)] \tag{3.58}$$

where $\nu = \frac{N_s e^2}{m^2}$ is the Budker parameter and

$$D_{10}(K) = (K^2 - \frac{\omega^2}{c^2})\frac{u_l^2}{c^2}[J_s'(k_cr_l)J_{m-s}(k_cR)]^2$$

$$- k_cr_l\Omega_s(K)\Big[2\Omega_c(1 - \frac{s^2}{k_c^2r_l^2})J_s(k_cr_l)J_{m-s}^2(k_cR) - \frac{k_cu_l}{2}\hat{\Psi}_+\Big]J_s'(k_cr_l)$$

$$- \Omega_s^2(K)\Big[2\gamma k_cr_l(1 - \frac{s^2}{k_c^2r_l^2})J_s'(k_cr_l)J_{m-s}^2(k_cR) - \frac{k_cu_l}{2}\hat{\Psi}_-\Big]J_s(k_cr_l) \tag{3.59}$$

$$D_{00}(K) = \frac{u_l}{\gamma\Omega_s^2(K)}\Big\{ \frac{Ku_l^2}{\gamma^2}[J_s'(k_cr_l)J_{m-s}(k_cR)]^2$$

$$+ \frac{2k_cr_lu_z}{\gamma}\Omega_s(K)J_s(k_cr_l)J_s'(k_cr_l)J_{m-s}^2(k_cR)$$

$$- \frac{k_cu_l}{2\Omega_c}\Omega_s^2(K)J_s(k_cr_l)\hat{\Psi}_- \Big\} \tag{3.60}$$

Similar to the commonly used beam-field coupling coefficient, for a single gyration harmonic number s, we define a beam-field coupling coefficient

$$H_c = \sum_{n=-\infty}^{\infty}\sum_{m=-\infty}^{\infty} (A_{nm})^2[J_s'(k_cr_l)J_{m-s}(k_cR)]^2 \tag{3.61}$$

$$\Psi_{c-} = e^{-jm\Psi} \frac{1}{\pi r r_l^2 \sin \xi} \left\{ -k_c r_l J_{m-s}(k_c R) \cos[(m-s)\Psi - \xi] \right.$$

$$- \frac{1}{2} k_c r_l J_{m-s+2}(k_c R) \cos[(m-s+2)\Psi - \xi]$$

$$- \frac{1}{2} k_c r_l J_{m-s-2}(k_c R) \cos[(m-s-2)\Psi + \xi]$$

$$+ (m-s-1) J_{m-s-1}(k_c R) \cos[(m-s-1)\Psi - \xi]$$

$$\left. + (m-s-1) J_{m-s+1}(k_c R) \cos[(m-s+1)\Psi - \xi] \right\}. \tag{3.48}$$

$$\Psi_{c+} = e^{-jm\Psi} \frac{1}{\pi r r_l^2 \sin \xi} \left\{ \frac{1}{2} k_c r_l J_{m-s+2}(k_c R) \cos[(m-s+2)\Psi - \xi] \right.$$

$$- \frac{1}{2} k_c r_l J_{m-s-2}(k_c R) \cos[(m-s-2)\Psi - \xi]$$

$$+ (m-s-1) J_{m-s-1}(k_c R) \cos[(m-s-1)\Psi - \xi]$$

$$\left. - (m-s-1) J_{m-s+1}(k_c R) \cos[(m-s+1)\Psi - \xi] \right\}. \tag{3.49}$$

3.3   Derivation of $\overline{F}(K)$

With $\overline{J}_c(K)$ and $\overline{J}_c^\dagger(K)$ obtained in the previous section, in this section we work out the integral over the cross section of the waveguide on the right hand side of Eq.(3.36). In cylindrical coordinates, the integral is over r and θ. Making use of the relation $dr = r_l \sin \xi d\Psi$, we may convert the integral over r into an integral over Ψ. After evaluating the integral over Ψ and θ, we get

$$(\frac{\omega^2}{c^2} - k_c^2 - K^2)\overline{F}(K) - jKF(0) - \frac{d}{dz}F(0)$$

$$= \sum_{s=0}^{\infty} \sum_{m=-\infty}^{\infty} \sum_{s=-\infty}^{\infty} \frac{e^2 N_e}{mc^2} \frac{\pi A_{nm}^2}{N k_c u_t} \left[\overline{F}(K) T_1(K) - jF(0) T_0(K) \right] \tag{3.50}$$

where

$$T_1(K) = \left[\frac{K u_t}{\gamma} \frac{\partial}{\partial u_z} + (\omega - \frac{K u_z}{\gamma}) \frac{\partial}{\partial u_t} \right] [J_s'(k_c r_l) \frac{u_t^2}{\gamma \Omega_s(K)} \hat{\Phi}_+]$$

$$+ \frac{u_t^2}{2\gamma \Omega_c} J_s(k_c r_l) \hat{\Psi}_- + \frac{u_t^3 k_c}{2\gamma^2 \Omega_c \Omega_s(K)} J_s(k_c r_l) \hat{\Psi}_+ \tag{3.51}$$

$$T_0(K) = \left[\frac{u_t}{\gamma} \frac{\partial}{\partial u_z} - \frac{u_z}{\gamma} \frac{\partial}{\partial u_t} \right] J_s'(k_c r_l) \frac{u_t^2}{\gamma \Omega_s(K)} \hat{\Phi}_+$$

$$- \frac{u_t u_z}{2\gamma^2 \Omega_c} J_s(k_c r_l) \hat{\Psi}_- \tag{3.52}$$

and

$$\hat{\Phi}_+ = k_c J_{m-s}^2(k_c R) J_s'(k_c r_l) \tag{3.53}$$

$$r_\pm = R_0 \pm r_l$$

and $r_l = \frac{u_t}{\Omega_e}$ is the electron Larmor radius in the applied magnetic field, f_a is an arbitrary function of u_t, u_z, and R. The Dirac delta distribution function f_c represents the 'cold' beam with infinitely thin guiding center distribution and is normalized to be one electron per unit length. For 'cold' electron beam distribution function $f_0 = f_c$, after perfoming the integral, $\overline{J}_c(K)$ is obtained as

$$\overline{J}_c(K) = e^{j\omega t} \sum_{n=0}^{\infty} \sum_{m=-\infty}^{\infty} \sum_{s=-\infty}^{\infty} \frac{Ne^2 A_{nm}}{2\pi mck_c u_t} [Q_1(K) - jQ_0(K)] \tag{3.42}$$

where

$$Q_1(K) = \overline{F}(K)\Big\{ \Big[\frac{Ku_t}{\gamma}\frac{\partial f_a}{\partial u_z} + (\omega - \frac{Ku_z}{\gamma})\frac{\partial f_a}{\partial u_t}\Big](\Phi + \frac{u_t^2}{\gamma\Omega_e(K)})$$
$$+ \frac{u_t^2}{2\gamma\Omega_c}J_s(k_c r_l)\Psi_- + \frac{u_t^2 k_c r_l}{2\gamma\Omega_e(K)}J'_s(k_c r_l)\Psi_+ \Big\} \tag{3.43}$$

$$Q_0(K) = F(0)\Big[(\frac{u_t}{\gamma}\frac{\partial}{\partial u_z} - \frac{u_z}{\gamma}\frac{\partial}{\partial u_t})\frac{u_t^2}{\gamma\Omega_e(K)}J'_s(k_c r_l)\Phi_+$$
$$- \frac{u_t^2 u_z}{2\gamma\Omega_c}J_s(k_c r_l)\Psi_- \Big] \tag{3.44}$$

$\overline{J}_c^\dagger(K)$ is obtained by replacing Ψ_-, Ψ_+, Φ_+ with $\Psi_{c-}, \Psi_{c+}, \Phi_-$ in the expression of $J_c(K)$ correspondingly.

In the above, (see Appendix II)

$$\Phi_\pm = e^{-jm\Psi}\frac{1}{\pi r r_l^2 \sin\xi}J_{m-s}(k_c R)\cos[(m-s)\Psi \pm \xi] \tag{3.45}$$

$$\Psi_- = e^{-jm\Psi}\frac{1}{\pi r r_l^2 \sin\xi}\Big\{ -k_c r_l J_{m-s}(k_c R)\cos[(m-s)\Psi + \xi]$$
$$- \frac{1}{2}k_c r_l J_{m-s+2}(k_c R)\cos[(m-s+2)\Psi + \xi]$$
$$- \frac{1}{2}k_c r_l J_{m-s-2}(k_c R)\cos[(m-s-2)\Psi + \xi]$$
$$+ (m-s+1)J_{m-s+1}(k_c R)\cos[(m-s+1)\Psi + \xi]$$
$$+ (m-s+1)J_{m-s-1}(k_c R)\cos[(m-s-1)\Psi + \xi] \Big\}. \tag{3.46}$$

$$\Psi_+ = e^{-jm\Psi}\frac{1}{\pi r r_l^2 \sin\xi}\Big\{ \frac{1}{2}k_c r_l J_{m-s+2}(k_c R)\cos[(m-s+2)\Psi + \xi]$$
$$- \frac{1}{2}k_c r_l J_{m-s-2}(k_c R)\cos[(m-s-2)\Psi + \xi]$$
$$- (m-s+1)J_{m-s+1}(k_c R)\cos[(m-s+1)\Psi + \xi]$$
$$+ (m-s+1)J_{m-s-1}(k_c R)\cos[(m-s-1)\Psi + \xi] \Big\}. \tag{3.47}$$

the Laplace transformation of Eq.(2.17) may be manipulated further as

$$
(\frac{\omega^2}{c^2} - k_c^2 - K^2)\overline{F}(K) - jKF(0) - \frac{d}{dz}F(0)
$$

$$
= -\frac{4\pi}{Nc}\int_A \nabla \times \mathbf{J}(K)\cdot\mathbf{e}_z B_z^0
$$

$$
= \sum_{n=0}^{\infty}\sum_{m=-\infty}^{\infty}\frac{4\pi A_{nm}}{Nc}\int_0^{2\pi}d\theta\int_0^{R_*}rdr\Big\{\frac{\partial}{\partial r}[rJ_r(K)] - \frac{\partial}{\partial\theta}J_\theta(K)\Big\}J_m(k_c r)
$$

$$
= -\sum_{n=0}^{\infty}\sum_{m=-\infty}^{\infty}\frac{4\pi A_{nm}}{Nc}\int_0^{2\pi}d\theta\int_0^{R_*}drk_c r[\mathcal{J}_c(K)J_{m-1}(k_c r) - \mathcal{J}_c^{\dagger}(K)J_{m+1}(k_c r)] \quad (3.36)
$$

In the last step in writing Eq.(3.36), integration by parts has been used. Then from Eq.(3.34), we have

$$
\mathcal{J}_c(K) = -e\int d^3 u e^{j\xi}\frac{u_t}{\gamma}\overline{\mathcal{J}}_1(K)
$$

$$
= -e^{j\omega t}\sum_{n=0}^{\infty}\sum_{m=-\infty}^{\infty}\sum_{s=-\infty}^{\infty}\frac{Ne^2 A_{nm}}{mck_c}e^{-jn\Theta}\int du_t du_z d\xi e^{j s\Psi}e^{j\xi}\frac{u_t^2}{\gamma}\overline{G}(K)\overline{Q}(K) \quad (3.37a)
$$

$$
\mathcal{J}_c^{\dagger}(K) = -e\int d^3 u e^{-j\xi}\frac{u_t}{\gamma}\overline{\mathcal{J}}_1(K)
$$

$$
= -e^{j\omega t}\sum_{n=0}^{\infty}\sum_{m=-\infty}^{\infty}\sum_{s=-\infty}^{\infty}\frac{Ne^2 A_{nm}}{mck_c}e^{-jn\Theta}\int du_t du_z d\xi e^{j s\Psi}e^{-j\xi}\frac{u_t^2}{\gamma}\overline{G}(K)\overline{Q}(K) \quad (3.37b)
$$

where $\overline{Q}(K)$ is given by Eq.(3.27).

For evaluating $\mathcal{J}_c(K)$ and $\mathcal{J}_c^{\dagger}(K)$, the electron distribution function has to be specified. In order that the distribution function is general, we write it in the following form

$$
f_0(u_z, u_t, R) = f_c(u_z^0, u_t^0, R^0)f_s(u_z, u_t, R) \quad (3.38)
$$

$$
f_c(u_z^0, u_t^0, R^0) = f_u(u_z^0, u_t^0)f_R(R^0) \quad (3.39)
$$

Furthermore, we write

$$
f_u = \frac{1}{2\pi u_t}\delta(u_t - u_t^0)\delta(u_z - u_z^0) \quad (3.40)
$$

$$
f_R = \frac{1}{2\pi R}\delta(R - R_0)
$$

$$
= \frac{1}{2\pi r r_t \sin\xi}[\delta(\xi - \xi_0) - \delta(\xi + \xi_0)]\cdot\Delta(r) \quad (3.41)
$$

where

$$
\Delta(r) = \begin{cases} 1 & r_- \le r \le r_+ \\ 0 & \text{otherwise.} \end{cases}
$$

32

Making use of the convo! tion theorem, the Laplace transformation of the perturbed electron distribution function is obtained as

$$\overline{J}_1(K) = e^{j\omega t} \sum_{n=0}^{\infty} \sum_{m=-\infty}^{\infty} \sum_{s=-\infty}^{\infty} \frac{eN_e A_{nm}}{mck_c} e^{js\Psi} \overline{G}(K)\overline{Q}(K).$$ (3.30)

Where $\overline{G}(K)$ and $\overline{Q}(K)$ ar given by Eq.(3.26) and (3.27) respectively.

3.2 Perturbed Current Density

This section is for the derivation of the perturbed current density in the waveguide. Under this formalism of analysis, the axial component of the pertubed current does not contribute to the gyrotron interaction for TE wave modes, so it will be ignored.

The Laplace transformation of the perturbed current density is defined as

$$\overline{\mathbf{J}}(K) = \overline{J}_\theta(K)\mathbf{e}_\theta + \overline{J}_r(K)\mathbf{e}_r$$ (3.31)

From Eq.(3.2) and the notations in Fig.3, we have the two components of the perturbed current density as

$$\overline{J}_\theta(K) = -e \int d^3u \frac{u_t}{\gamma} \cos\xi \overline{J}_1(K)$$ (3.32a)

$$\overline{J}_r(K) = -e \int d^3u \frac{u_t}{\gamma} \sin\xi \overline{J}_1(K)$$ (3.32b)

If we introduce two quantities

$$\overline{J}_c(K) = \overline{J}_\theta(K) + j\overline{J}_r(K)$$ (3.33a)

$$\overline{J}_c^\dagger(K) = \overline{J}_\theta(K) - j\overline{J}_r(K)$$ (3.33b)

then we have

$$\overline{J}_c(K) = -e \int d^3u \frac{u_t}{\gamma} e^{j\xi} \overline{J}_1(K)$$ (3.34a)

$$\overline{J}_c^\dagger(K) = -e \int d^3u \frac{u_t}{\gamma} e^{-j\xi} \overline{J}_1(K)$$ (3.34b)

Since in general the axial RF magnetic field in the waveguide in the interaction region can be expressed in the form

$$B_{z1n} = \sum_{m=-\infty}^{\infty} A_{nm} J_m(k_c r) e^{jm\theta}$$ (3.35)

where N_e is the electron number per unit axial length, and

$$G(z - z') = \frac{1}{v_z} e^{j(\omega - s\Omega_c)\frac{z-z'}{v_z}} \tag{3.21}$$

$$Q(z) = \left[(j\omega F - \frac{u_z}{\gamma} \frac{\partial F}{\partial z}) \frac{\partial f_0}{\partial u_t} + \frac{u_t}{\gamma} \frac{\partial F}{\partial z} \frac{\partial f_0}{\partial u_z} \right] J_{m-s}(k_c R) J_s'(k_c r_l)$$

$$+ (j\omega F - \frac{u_z}{\gamma} \frac{\partial F}{\partial z} - js\frac{\Omega_c}{\gamma} F) J_{m-s}'(k_c R) J_s(k_c r_l) \frac{1}{\Omega_c} \frac{\partial f_0}{\partial R}$$

$$+ \frac{jk_c^2 u_t}{2\gamma} F[J_{m-s-1}(k_c R) + J_{m-s+1}(k_c R)] J_s'(k_c r_l) \frac{1}{\Omega_c} \frac{\partial f_0}{\partial R} \tag{3.22}$$

The Laplace transformation $\overline{F}(K)$ of function $F(z)$ is defined as

$$\overline{F}(K) = \int_0^\infty F(z) e^{-jKz} dz \tag{3.23}$$

where the imaginary part of K is chosen to be positive and large enough in magnitude so that the convergence of the integral be guaranteed.

The following two formulas for transformation are necessary to be used here.

$$L\frac{dF(z)}{dz} = jK\overline{F}(K) - F(0) \tag{3.24}$$

$$L\frac{d^2F(z)}{dz^2} = -K^2\overline{F}(K) - jKF(0) - \frac{dF(0)}{dz} \tag{3.25}$$

Thus we have the transformation for $G(z)$ in Eq.(3.21)

$$\overline{G}(K) = \int_0^\infty dz e^{-j(\omega - \frac{Ku_z}{\gamma} - s\Omega_c)z}$$

$$= j\frac{1}{\Omega_s(K)} \tag{3.26}$$

where

$$\Omega_s(K) = \omega - \frac{Ku_z}{\gamma} - s\Omega_c$$

The Laplace transfomation of $Q(z)$ in Eq.(3.22) is given by

$$\overline{Q}(K) = \overline{Q}_1(K) + \overline{Q}_0(K) \tag{3.27}$$

where

$$\overline{Q}_1(K) = j\overline{F}(K) \left\{ \left[(\omega - \frac{Ku_z}{\gamma}) \frac{\partial f_0}{\partial u_t} + \frac{Ku_t}{\gamma} \frac{\partial f_0}{\partial u_z} \right] J_{m-s}(k_c R) J_s'(k_c r_l) \right.$$

$$+ \Omega_s(K) J_{m-s}'(k_c R) J_s(k_c r_l) \frac{1}{\Omega_c} \frac{\partial f_0}{\partial R}$$

$$+ \frac{1}{2} \frac{k_c^2 u_t}{\gamma} [J_{m-s-1}(k_c R) + J_{m-s+1}(k_c R)] J_s'(k_c r_l) \frac{1}{\Omega_c} \frac{\partial f_0}{\partial R} \right\} \tag{3.28}$$

$$\overline{Q}_0(K) = F(0) \left\{ (\frac{u_z}{\gamma} \frac{\partial f_0}{\partial u_t} - \frac{u_t}{\gamma} \frac{\partial f_0}{\partial u_z}) J_{m-s}(k_c R) J_s'(k_c r_l) \right.$$

$$+ \frac{u_z}{\gamma} J_{m-s}'(k_c R) J_s(k_c r_l) \frac{1}{\Omega_c} \frac{\partial f_0}{\partial R} \right\} \tag{3.29}$$

Inserting $\Delta\omega'_r$ into Eq.(3.79) we get the efficiency of the gyrotron traveling amplifiers as

$$\eta' = \frac{2.5\gamma'_0 \Delta\omega'_r}{\gamma'_0 - 1} \qquad (3.87)$$

In Eq.(3.87) a correcting factor of 1.25 has been multiplied in order to get a good agreement with the numerical simulation results.[16] This scaling relation is valid only under the tenuous beam assumption and when the beam energy is much higher than the threshold condition for the instability. The efficiency in the laboratory frame can be obtained by a Lorentzian transformation. However, for lower beam energy, especially at fundamental cyclotron harmonics, due to neglecting the energy depletion mechanism in the saturation, this scaling relation has a bigger discrepancy with the result of the numerical simulation.

3.6   Electron Beam and Velocity Spread

For high power, efficient gyrotrons, the electron optical system must provide large current I, big $\alpha = \frac{v_t}{v_z}$ but small beam velocity spread. The beam velocity spread deteriorates the beam bunching, therefore decreases the possible output power and the efficiency of the device. The electron beam velocity spread in gyrotrons is characterized by the relative parallel and orbital velocity spread $\frac{\delta v_z}{\bar{v}_z}$ and $\frac{\delta v_t}{\bar{v}_t}$, where $\bar{v}_z$, $\bar{v}_t$ are the mean values of v_z, v_t respectively. Since the electrons basically excercise helical motion in passing through the waveguide in a conservative field, the only spread in the electron total energy is due to the space charge potential depression in the drift region, therefore a very small total energy spread can be expected, and the spread in v_z and in v_t are correlated. As a consequence, the spread in the gyration frequency of the electrons is very small. However, the spread in the Doppler-shifted cyclotron frequency through the spread in v_z can be significant.

The electron initial thermal velocity results in the orbital velocity spread. According to [43], the thermal velocity spread is estimated as

$$\frac{\delta v_t}{\bar{v}_t} \simeq 4\sqrt{\frac{m\overline{v^2}}{2eT_h}V_a}$$

where e is the electron charge in coulomb, T_h is the cathode temperature in K and V_a is the anode voltage in volt.

The roughness of the emitter surface also results in the velocity spread in the thermal velocity manner. Assuming the cathode surface grains have the form of a hemisphere of radius r_0 and h is the height of the first vertex of the electron trajectory above the cathode surface, according to [43,44], the orbital velocity spread is estimated as

$$\frac{\delta v_t}{\bar{v}_t} \simeq 1.5\sqrt{r_0/h}$$

It is seen that even a very small surface roughness of the cathode can cause a significant velocity spread, especially at millimeter wavelength since h is small.

A slightly departure of the axial symmetry of the electron beam also causes velocity spread. With the assumption of small azimuthal drift in the region of the gun, this effect is estimated as[43]

$$\frac{\delta v_t}{\bar{v}_t} = 2a\cos\psi/d$$

where a is the radial shift of the cathode, ψ is the angle between the cathode and z-axis and d is the anode-cathode gap (see Fig.1b). The electron beam space charge field playes an important role in the distribution of the electron beam velocity spread in the interaction space and also in the near emitter region since there either the transverse or parallel velocity of the electrons is small.

From the expression of $D(K)$ in Eq.(3.59) it is readily seen that the most sensitive effect is the spread in v_z through the Doppler shift frequency $\omega - k_z v_z$. The following brief discussion on the beam axial velocity spread is under the assumption of Lorentzian distribution of the beam axial velocity and is chiefly based on S. Y. Park's approach in [41]. If we assume the distribution of u_z in f_0 is the generalized Lorentzian distribution

$$f_0(u_z) = D\frac{(\Delta u_z)^{2p}}{(u_z - \bar{u}_z)^{2p} + (\Delta u_z)^{2p}} \tag{3.88}$$

Where $\bar{u}_z$ is the mean value of u_z. Changing the variable u_z into

$$\varsigma = \frac{u_z - \bar{u}_z}{\Delta u_z} \tag{3.89}$$

Then we can write the distribution function

$$f_0(\varsigma) = D \frac{1}{1 + \varsigma^{2p}} \tag{3.90}$$

and D is the normalization factor given by

$$
\begin{aligned}
D^{-1} &= \int_{-\infty}^{\infty} du_z f_0(u_z, \Delta u_z) \\
&= \frac{1}{\Delta u_z} \int_{-\infty}^{\infty} d\varsigma \frac{1}{\varsigma^{2p} + 1}
\end{aligned} \tag{3.91}
$$

Here D can be determined by the contour integral in the upper half of the complex ς-plane and we have

$$D = \frac{p}{j\pi \Delta u_z} \frac{1}{\sum_{i=1}^{p-1} \varsigma_i} \tag{3.92}$$

From Eq.(3.59), we obtain

$$
\begin{aligned}
\overline{D}_1(K) &= \int_{-\infty}^{\infty} du_z f_0(u_z, \Delta u_z) D_{10}(K) \\
&= \Delta u_z \int_{-\infty}^{\infty} d\varsigma \frac{D}{1 + \varsigma^{2p}} D_{10}(K, u_z + \varsigma \Delta u_z)
\end{aligned} \tag{3.93}
$$

For $Im(K) < 0$, if $\omega > s\Omega_c$, $D_{10}(K)$ has a pole in the lower half ς- plane and if $\omega < s\Omega_c$, $D_{10}(K)$ has a pole in the upper ς- plane.

Clearly, from Eq.(3.90) we can see that $f_0(\varsigma)$ has poles in the upper half ς- plane.

$$\varsigma_i = e^{\frac{j(2i-1)\pi}{p}} \qquad (i = 1, 2, \ldots, p) \tag{3.94}$$

Therefore, using the expression for D in Eq.(3.91), we can write

$$\overline{D}_1(K) = \sum_{i=1}^{p} \varsigma_i D_{10}(K, \overline{u}_z + \varsigma_i \Delta u_z) / \sum_{i=1}^{p} \varsigma_i \tag{3.95}$$

If the parallel velocity is the standard Lorentzian distribution with $p = 1$, then $\varsigma_1 = j$, thus we can obtain a very simple result as

$$
\overline{D}_1(K) = \begin{cases} D_{10}(K, \overline{u}_z - j\Delta u_z) & (\omega > s\Omega_c) \\ D_{10}(K, \overline{u}_z + j\Delta u_z) & (\omega \le s\Omega_c) \end{cases}
$$

This means that the effect of the spread in u_z is equivalent to a shift of the average real velocity to a complex velocity $\overline{u}_z \pm j\Delta u_z$. In the general case when $p > 1$, the velocity spread effect is the average of the shifts by $\varsigma_i \Delta u_z$ or $\varsigma_i^* \Delta u_z$.

Chapter 4   Gyro-TWA with Out-ridged Waveguide

This chapter is devoted to the proposed gyro-TWA with out-ridged waveguide. Section 4.1 is for the derivation of the dispersion equation and the field configuration in the out-ridged waveguide; Secton 4.2 is devoted to the numerical solution of the eigenvalue spectrum and the associated field components in the out-ridged waveguide by adopting the Ritz-Galerkin method.   With Ritz-Galerkin method, the field components in the waveguide can be obtained in the form of the series of the eigenfunctions.   Section 4.3 describes the computation of the gain-frequency curves of the amplifier by applying the analytical results of gyrotron kinetic theory obtained in Chapter 3 and the results in Sections 4.1 and 4.2.

Once the field structure of a certain mode in the waveguide has been obtained, the nonlinear analysis of this gyro-TWA with out-ridged waveguide can be done by integrating that set of the nonlinear equations derived in section 2.3, but it has to be resorted to numerical computation.

4.1   Out-ridged Waveguide Dispersion Equation

The cross section of the out-ridged waveguide is illustrated in Fig.5.   The cross section of the waveguide is assumed to be symmetrical about axis $y = 0$, but no assumption about axis x symmetry is made.   A detailed analysis will be presented here for TE modes only.   The derivation of the dispersion equation for TM modes is given in Appendix I.

For TE waveguide modes, if the solution to the axial magnetic field is asssumed in the form $B_x = B_x^0(x,y)e^{j(\omega t - k_z z)}$, where k_z is the axial wave number, then the equation that governing B_x^0 is

$$(\frac{\partial^2}{\partial x^2} + \frac{\partial^2}{\partial y^2} + k_c^2)B_x^0 = 0 \tag{4.1}$$
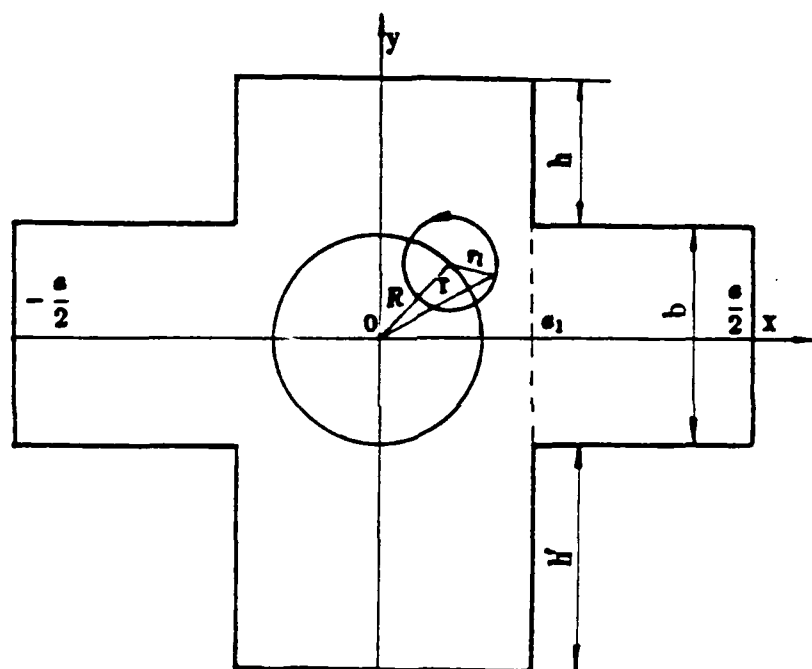
Fig.5 The cross section of the out-ridged waveguide.

subject to the boundary condition on the perfect conducting waveguide wall

$$\mathbf{n} \cdot \nabla_t B_z = 0 \tag{4.2}$$

where

$$k_c^2 = \frac{\omega^2}{c^2} - k_z^2 \tag{4.3}$$

And $\mathbf{n}$ is the unit vector normal to the waveguide wall.

For this proposed out-ridged waveguide structure, in the convenience for analyzing beam-field interaction in the generalized approach developed in Chapter 3, we adopt the standard Ritz-Galekin method to obtain the eigenvalues and the associated eigenfunctions. According to this method, the solution is expanded into the series of the eigenfunctions, each eigenfunction satisfies the boundary condition on the waveguide wall, and it is also required that the resultant expression be othogonal to each expansion function. Then the eigenvalue problem is reduced to a system of algebraic equations.

With reference to Fig.5, the solution in region I $(-a_1 \le x \le a_1)$ may be written in the form

$$B_{1z}^0(x,y) = \sum_{n=0}^{\infty} B_{1n} \frac{\sin}{\cos}(k_{x1n}x)\cos[\frac{n\pi}{h_s}(y-h)] \tag{4.4}$$

where the upper and lower functions correspond, respectively, to the magnetic and electric symmetry about y-axis and $h_s = h + h'$.

The solution written in the form in Eq.(4.4) satisfies the boundary condition Eq.(4.2). Furthermore, we define

$$k_{x1n} = \begin{cases} \sqrt{k_c^2 - (\frac{n\pi}{h_s})^2} & (k_c \ge \frac{n\pi}{h_s}) \\ -j\sqrt{(\frac{n\pi}{h_s})^2 - k_c^2} & (k_c < \frac{n\pi}{h_s}) \end{cases} \tag{4.5}$$

In region II $(\frac{-a}{2} \le x \le -a_1$ and $a_1 \ge x \le \frac{a}{2})$ the solution to Eq.(4.1) can be written as the following

$$B_{2z}^0(x,y) = \sum_{m=0}^{\infty} B_{2m} \cos[k_{x2m}(x-\frac{a}{2})]\cos[\frac{m\pi}{b}(y-\frac{b}{2})] \tag{4.6}$$

and similar to Eq.(4.5), k_{x2m} is defined as

$$k_{x2m} = \begin{cases} \sqrt{k_c^2 - (\frac{m\pi}{b})^2} & (k_c \ge \frac{m\pi}{b}) \\ -j\sqrt{(\frac{m\pi}{b})^2 - k_c^2} & (k_c < \frac{m\pi}{b}) \end{cases} \tag{4.7}$$

The other field components in region I can be derived from the Maxwell equations.

$$E_{1x} = jZ_h \frac{k_z}{k_c^2} \sum_{n=0}^{\infty} B_{1n}(\frac{n\pi}{h_e})\frac{\sin}{\cos}(k_{z1n}x)\sin[\frac{n\pi}{h_e}(y-h)] \tag{4.8}$$

$$E_{1y} = jZ_h \frac{k_z}{k_c^2} \sum_{n=0}^{\infty} B_{1n}k_{z1n}\frac{\cos}{-\sin}(k_{z1n}x)\sin[\frac{n\pi}{h_e}(y-h)] \tag{4.9}$$

$$B_{1x} = -\frac{1}{Z_h}E_{1y} \tag{4.10}$$

$$B_{1y} = \frac{1}{Z_h}E_{1x} \tag{4.11}$$

The other field components in region II are

$$E_{2x} = -jZ_h \frac{k_z}{k_c^2} \sum_{m=0}^{\infty} B_{2m}(\frac{m\pi}{b})\cos(k_{z2m}x)\sin[\frac{m\pi}{b}(y-\frac{b}{2})] \tag{4.12}$$

$$E_{2y} = jZ_h \frac{k_z}{k_c^2} \sum_{m=0}^{\infty} B_{2m}k_{z2m}\sin(k_{z2m}x)\cos[\frac{m\pi}{b}(y-\frac{b}{2})] \tag{4.13}$$

$$B_{2x} = -\frac{1}{Z_h}E_{2y} \tag{4.14}$$

$$B_{2y} = \frac{1}{Z_h}E_{2x} \tag{4.15}$$

In the above, $Z_h = \frac{\omega}{ck_z}$ is the wave impedance for TE modes. At $x = a_1$ the continuity for B_x requires

$$\sum_{n=0}^{N} B_{1n}\frac{\sin}{\cos}(k_{z1n}a_1)\cos[\frac{n\pi}{h_e}(y-h)]$$

$$= \sum_{m=0}^{M} B_{2m}\cos[k_{z2m}(a_1-\frac{a}{2})]\cos[\frac{m\pi}{b}(y-\frac{b}{2})] \tag{4.16}$$

The E_y continuity at $x = a_1$ gives

$$\sum_{n=0}^{N} B_{1n}k_{z1n}\frac{\cos}{-\sin}(k_{z1n}a_1)\cos[\frac{n\pi}{h_e}(y-h)]$$

$$= \sum_{m=0}^{M} B_{2m}k_{z2m}\sin[k_{z2m}(a_1-\frac{a}{2})]\cos[\frac{m\pi}{b}(y-\frac{b}{2})] \tag{4.17}$$

It should be noted that in Eqs.(4.16) and (4.17) the infinite series have been truncated into finite summations, and N, M are integers.

Setting

$$D_m = B_{2m}k_{z2m}\sin[k_{z2m}(a_1-\frac{a}{2})] \tag{4.18}$$

then from Eq.(4.16) we have

$$\sum_{n=0}^{N} B_{1n}k_{z1n}\frac{\cos}{-\sin}(k_{z1n}a_1)\cos[\frac{n\pi}{h_e}(y-h)] = \sum_{m=0}^{M} D_m k_{z2m}\cos[\frac{m\pi}{b}(y-\frac{b}{2})] \tag{4.19}$$

Multiplying both sides of Eq.(4.19) with $\cos[\frac{n\pi}{h_e}(y-h)]$ and integrating from $-\frac{b}{2}$ to $\frac{b}{2}$ over y, we obtain

$$B_{1n}k_{z1n}{\cos \atop -\sin}(k_{z1n}a_1)\epsilon_n h_e = \sum_{m=0}^{M} D_m E_{mn} \qquad (4.20)$$

where

$$E_{nm} = \int_{\frac{-b}{2}}^{\frac{b}{2}} dy \cos[\frac{n\pi}{h_e}(y-h)]\cos[\frac{m\pi}{b}(y-\frac{b}{2})]$$

$$= \frac{h_e b}{2\pi}\Big(\frac{1}{mb+nh_e}+\frac{1}{mb-nh_e}\Big)\Big[\sin\frac{m(b-2h)\pi}{2h_e}+(-)^n\sin\frac{m(b+2h)\pi}{2h_e}\Big] \qquad (4.21)$$

$$E_{00} = b \qquad (4.22)$$

and

$$\epsilon_n = \begin{cases} 2 & (n=0) \\ 1 & (n \neq 0) \end{cases}$$

Multiplying both sides of Eq.(4.16) with $\cos[\frac{q\pi}{b}(y-\frac{b}{2})]$ and integrating from $-\frac{b}{2}$ to $\frac{b}{2}$ over y yield

$$\sum_{n=0}^{N} B_{1n}{\sin \atop \cos}(k_{z1n}a_1)E_{qn} = B_{2q}\cos[k_{z2q}(a_1-\frac{a}{2})]\epsilon_q b \qquad (4.23)$$

Substituting Eq.(4.18) into Eq.(4.22) gives

$$\sum_{n=0}^{N} B_{1n}{\sin \atop \cos}(k_{z1n}a_1)E_{qn} = \frac{D_q\epsilon_q b}{k_{z2q}}\cos[k_{z2q}(a_1-\frac{a}{2})] \qquad (4.24)$$

From Eq.(4.20) we have

$$B_{1n} = \frac{\sum_{m=0}^{M} D_m E_{mn}}{k_{z1n}{\cos \atop -\sin}(k_{z1n}a_1)\epsilon_n h_e} \qquad (4.25)$$

Inserting Eq.(4.25) into Eq.(4.24) and moving the right hand side of Eq.(4.24) to its left hand side, we obtain a system of the equations which is the system of the dispersion equation for the out-ridged waveguide.

$$\sum_{m=0}^{M} D_m\Big\{\sum_{n=0}^{N} \frac{E_{mn}E_{qn}}{k_{z1n}\epsilon_n h_e}{\tan \atop -\cot}(k_{z1n}a_1)-\frac{\delta_{qm}\epsilon_q b}{k_{z2q}}\cot[k_{z2q}(a_1-\frac{a}{2})]\Big\} = 0 \qquad (4.26)$$

Eq.(4.26) can be written into a matrix form as the following

$$\begin{pmatrix} T_{00} & T_{01} & \ldots & T_{0n} \\ T_{10} & T_{11} & \ldots & T_{1n} \\ \ldots & \ldots & \ldots & \ldots \\ T_{n0} & T_{n1} & \ldots & T_{nn} \end{pmatrix}\begin{pmatrix} D_0 \\ D_1 \\ \vdots \\ D_n \end{pmatrix} = 0 \qquad (4.27)$$

where the element T_{mq} of matrix $[T]$ is

$$T_{mq} = \frac{E_{mn}E_{qn}}{k_{z1n}\epsilon_n h_s} \frac{\tan}{-\cot}(k_{z1n}a_1) - \frac{\delta_{qm}\epsilon_q b}{k_{z2q}} \cot[k_{z2q}(a_1 - \frac{a}{2})] \qquad (4.28)$$

and $[D]$ is a n-vector.

4.2   Waveguide Computation

The requirement that the system of equations, Eq.(4.26) has non-trivial solutions is that the determinant of matrix $T(k_c)$ be zero. If the determinant of matrix $[T(k_c)]$ is viewed as a function of k_c, then the roots of this function are the eigenvalues. This problem is then reduced to finding the roots of the function of k_c, which is denoted by $DT(k_c)$. This can be accomplished numerically. Due to the behavior of function $DT(k_c)$ which is shown in Fig.6b, and the fact that the algorithm of the most root finders converge locally, it is necesary to give a good initial quess for the root finding subroutine. Therefore, it is convenient if we scan the roots at lower order by simply computing function $DT(k_c)$ vs. k_c and take the intersections of that curve with the axis of k_c as the guesses for higher order computation of the roots. Here the Muller's method[45] is employed in making the root finding subroutine. If an eigenvalue of the waveguide has been found, the elements in the associated eigenvector may be obtained through the partitioned matrix equation.

$$[D_k] = -[T_{kk}]^{-1}[T_{k0}]D_0 \qquad (4.29)$$

D_0 can be arbitrary but subject to the subsequent normalization of the entire eigenvector $[D]$. In Eq.(4.29), the matrix $[T_{kk}]$ is the partitioned matrix of matrix $[T]$, $[D_k]$ is the vector that formed from vector $[D]$ with D_0 removed.
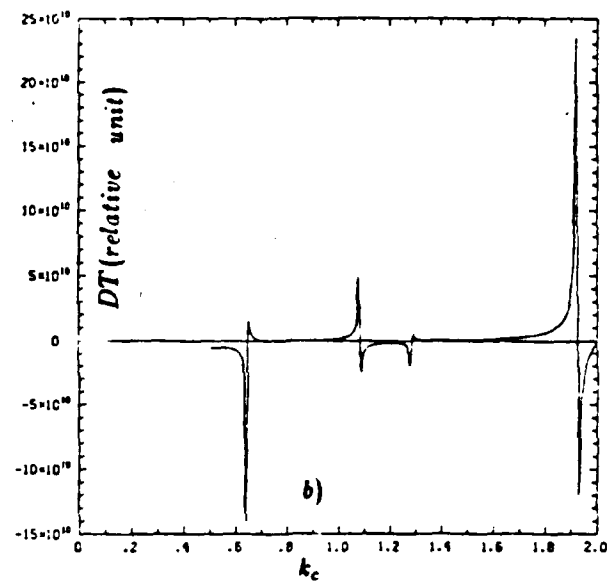
As an example of the out-ridged waveguide, the low order approximation of the determinant of matrix $[T]$, function $DT(k_c)$, is plotted in Fig.6b . The first few eigenvalues are shown in Fig.15a along with those for an rectangular example and for an magnetron type waveguide example. For one eigenvalue (TE_{11} mode), the convergence when the order gets higher is demonstrated in Table 1 by the computed results.
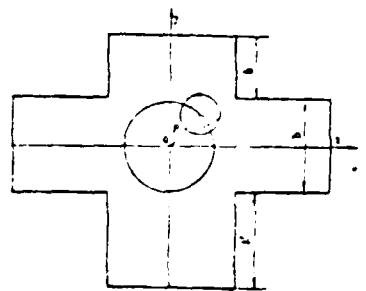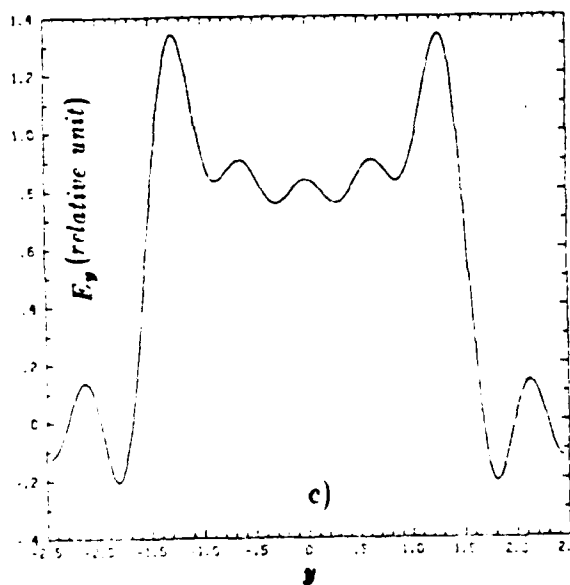
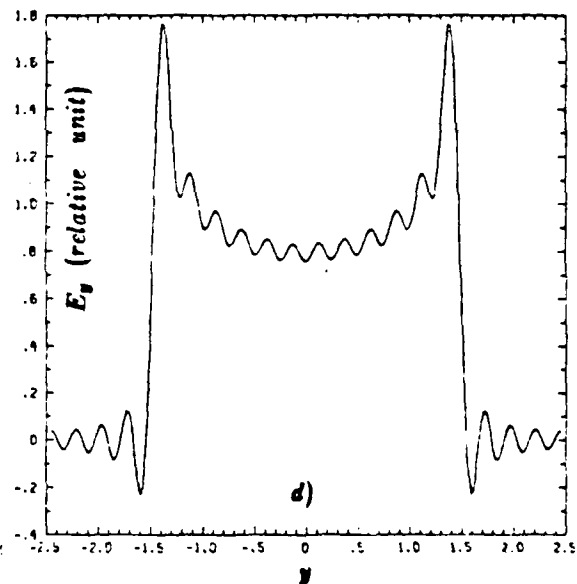$$a = .6cm \qquad b = .29cm$$
$$a_1 = .15cm \qquad h = h' = .1cm$$

a)

Fig.6 a) The dimension of the out-ridged waveguide,
b) The low order approximation of eigenvalue function,
c) For TE_{10} mode, the electric field E_y at $z = a_1$: $N = 15$, $M = 15$;
d) For TE_{10} mode, the electric field E_y at $z = a_1$: $N = 30$, $M = 30$.

Table   1

N	M	$k_c(TE_{02}\quad mode)$
10	10	.91778
15	15	.91624
20	20	.91591
25	25	.91555
30	30	.91542
35	35	.91528
40	40	.91521

The solution of Eq.(4.26) may not be acceptable in case D_0 is not the dominant component in the eigenvector. Therefore, we may have to force any component in the vector $[D(k_c)]$ to be arbitrary (for convenience we may put it to unity) in the computing program. In order to estimate the accuracy of the solution, we define an error vector $[\epsilon]$ through the following equation

$$[T(k_c)][D] = [\epsilon] \tag{4.30}$$

The maximum norm of the error vector may be roughly interpreted as the number of the significant digits in the components in $[D]$.[46] Then, the approximations to all the field components in region I and region II can be obtained by substituting the corresponding eigenvector into Eq.(4.12) to (4.20). The electrical field components for the fundamental mode TE_{01} are plotted in Fig.7a to 7d for the out-ridged waveguide with its dimensions listed in Fig.11a. The E_y field at $x = a_1$ for low order and for high order approximation are illustrated in Fig.6c and d respectively. The edge effect can be seen in the vicinity of the corners of the waveguide.

In comparision, one of the eigenvalues for this example of the out-ridged waveguide is also solved numerically by employing a PDE package PLTMG which can be used to solve boundary value problems in the form

$$\nabla(a\nabla u) + f(x, y, u, \nabla u, \lambda) = 0 \qquad in \quad \Omega$$

$$u = g_1(x, y) \qquad on \quad \Omega_1$$

$$(a\nabla u) \cdot n = g_2(x, y, u, \lambda) \qquad on \quad \Omega - \Omega_1 = \Omega_2$$

where Ω is a connected region in R^2, n is a normal unit vector on the boundary, and λ is a parameter. The coefficient functions a, f, g_i can be chosen so that the

above equation is a linear elliptic, a mildly nonlinear elliptic or a linear elliptic eigenvalue problem. Here our problem is the last case.[47] The package PLTMG uses finite element discretization based on C^0 piecewise linear triangle finite elements, adopted a procedure of a combination of inverse iteration and a multilevel iterative technique. Iterated to level 4 with the number of triangle vertices 531, the result of the eigenvalue for TE_{11} mode gives $k_c = 0.9122$. In order to check the accuracy of the result from this PDE solver at the same iteration level, the same equation on a unit circle domain subject to the same boundary condition as Eq.(4.2) is also solved using this PDE solver since this boundary value problem has an exact analytical solution $kc \simeq 3.831706$ (which is the second root of the Bessel fuction $J_0(x)$). For the unit circle domain, from this PDE solver when it is iterated to level 4 with vertices number of 542, the result is $k_c = 3.81$.

Comparing to the double ridged waveguide, which has been utilized for microwave heating, peniotron RF structure and some other purposes, this out-ridged waveguide structure is free from the trough modes. This is of big importance for gyrotrons, especially for those working at higher harmonics where the mode competetion becomes a big concern both to the stability and to the efficiency of the device. The local trough modes exist in ridged and double ridged waveguides.[16,48] It can also be seen from the eigenvalue spectrum of the out-ridged waveguide that the lower eigenvalues separated from each other very well compared to that of the magnetron-type waveguide. This lends merit to the out-ridged waveguide with a reduced mode competetion problem in gyro-TWA even when the bandwidth of the ampifier is wide.

4.3   Computation of the Gain-frequency relation

In the previous two sections the eigenvalues and the associated eigenfunctions for the out-ridged waveguide have been solved. This section deals the computation of the gain-frequency relation of the gyro-TWA with the out-ridged waveguide.
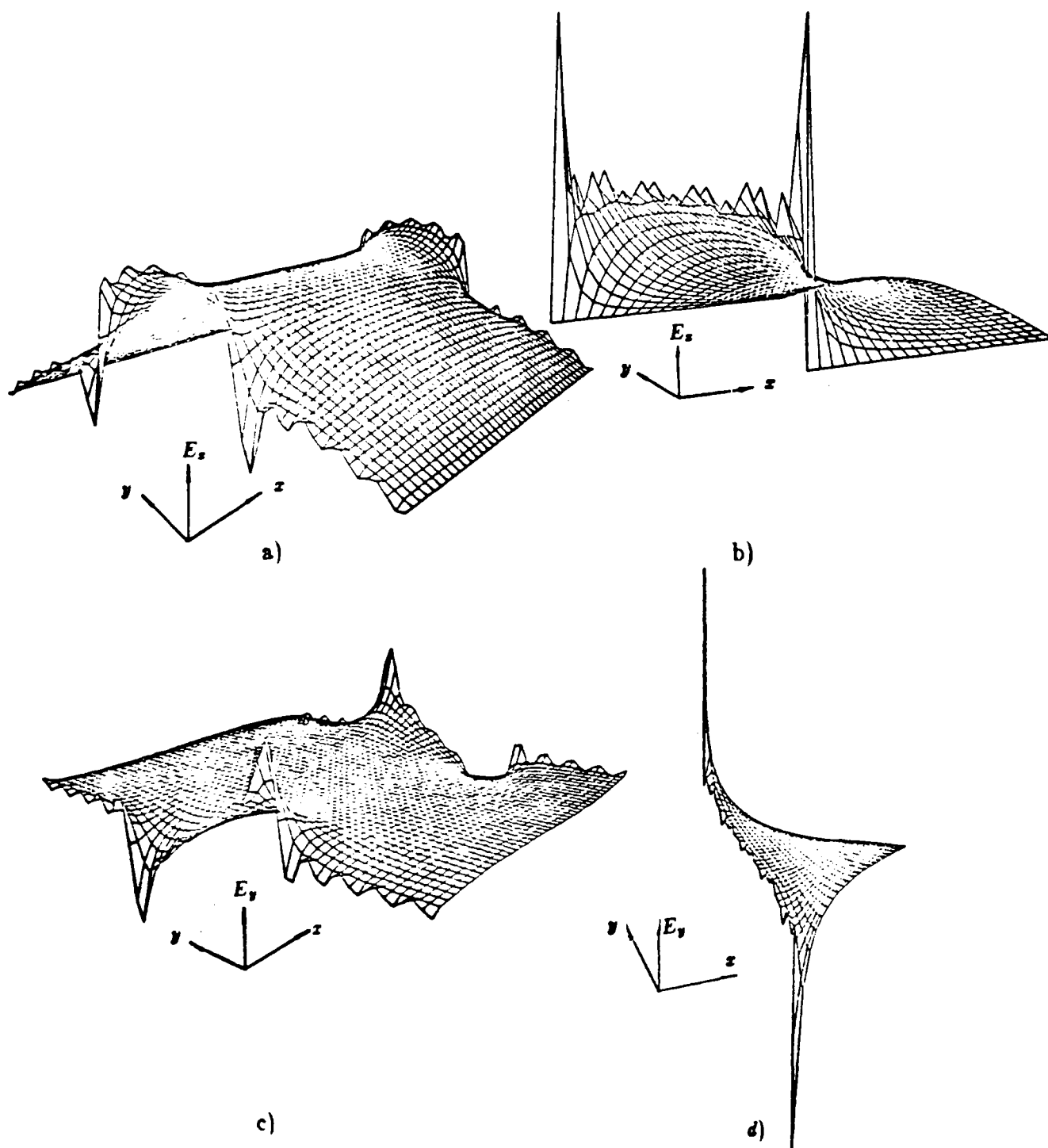
Fig.7 The electrical field transverse distribution of the TE_{01} mode.
in the outridged waveguide:
a) E_z in region I,   b) E_z in region II,
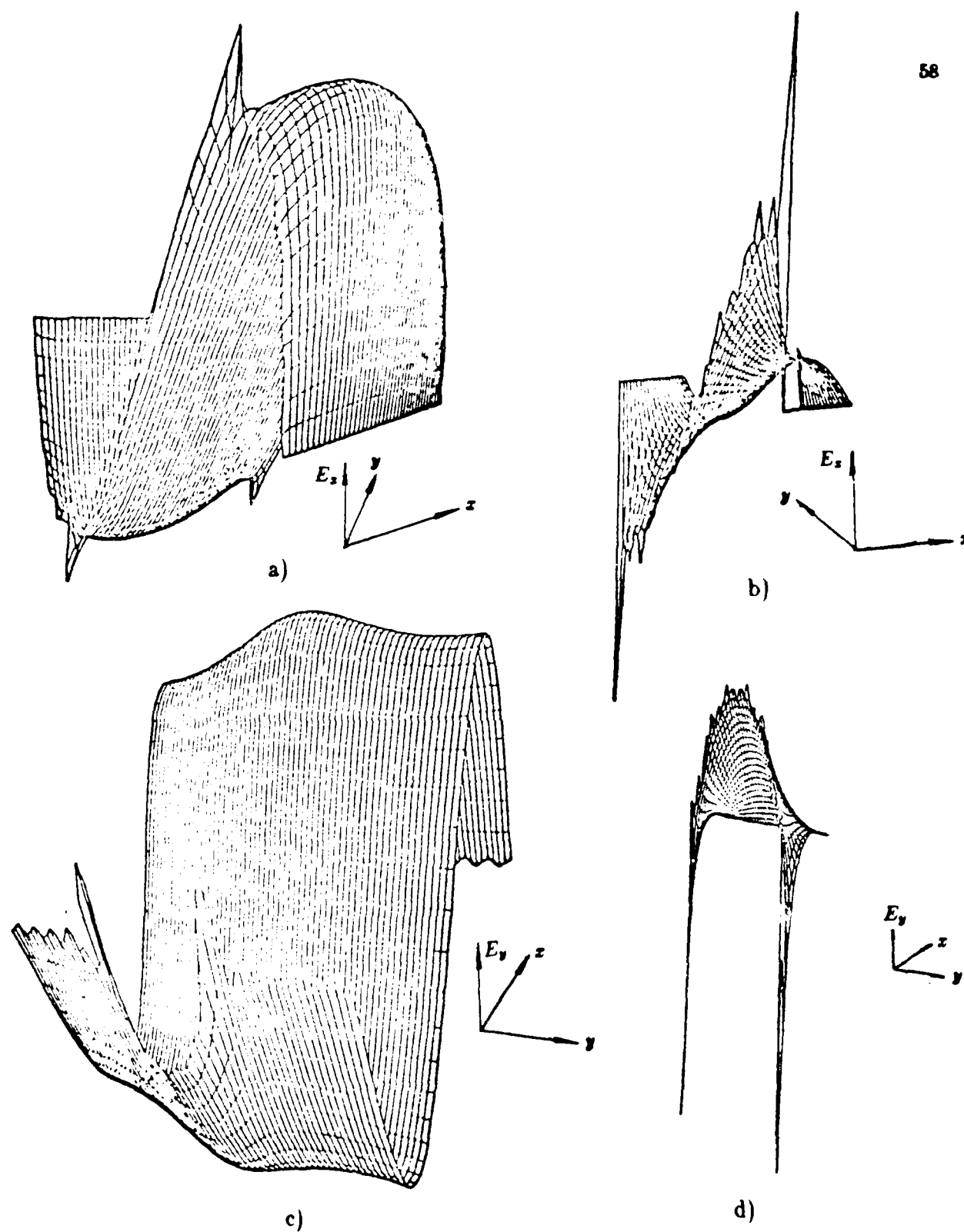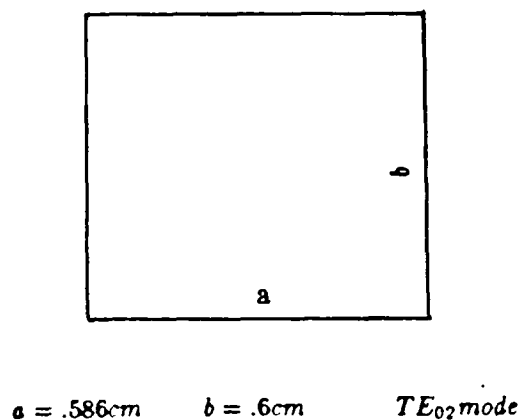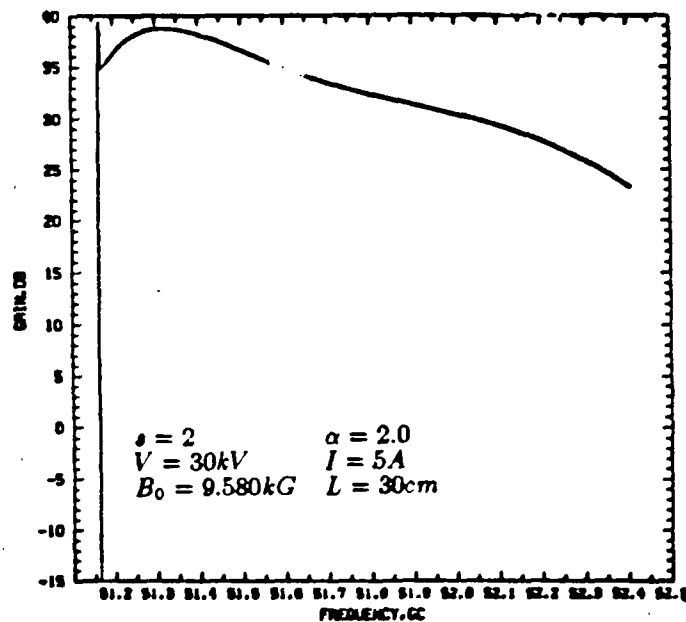c) E_r in region I,   d) E_y in region II.

Fig.8 The electrical field transverse distribution for TE_{02} mode
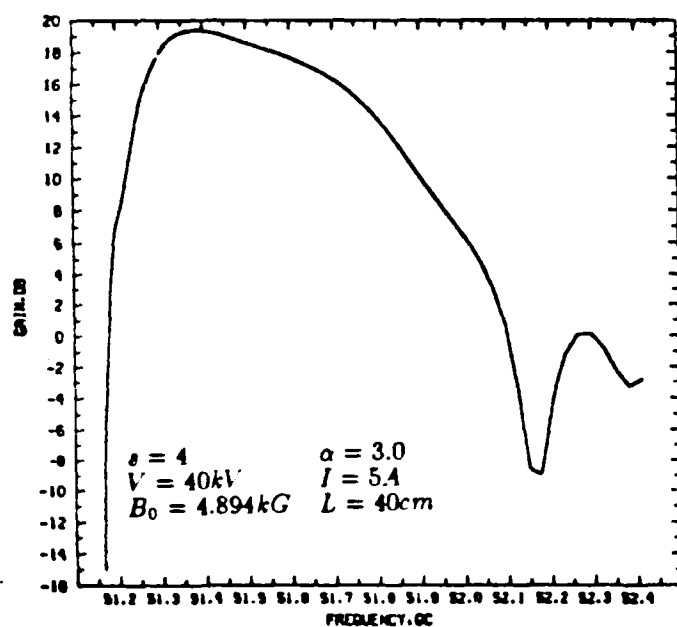in the outridged waveguide:
a) E_z in region I,   b) E_z in region II,
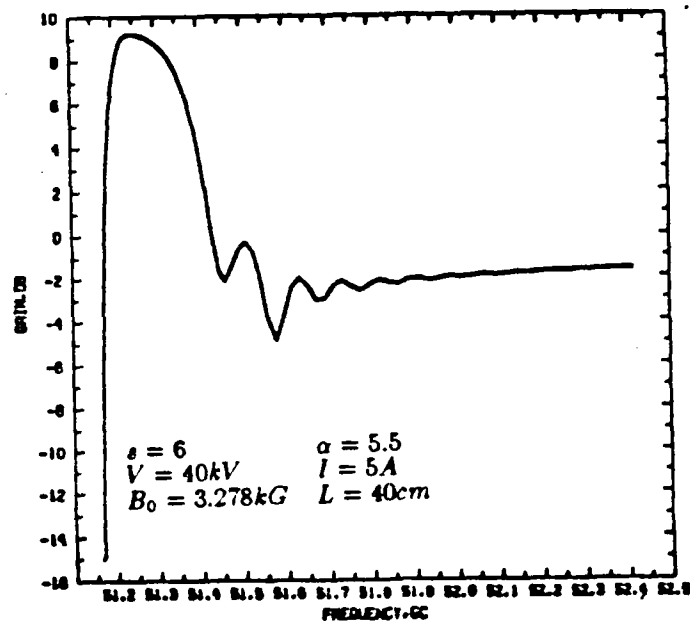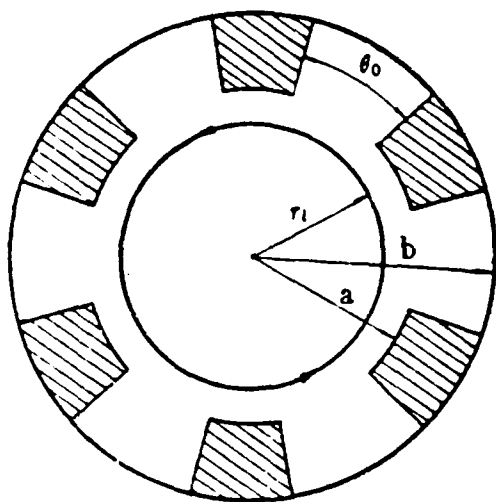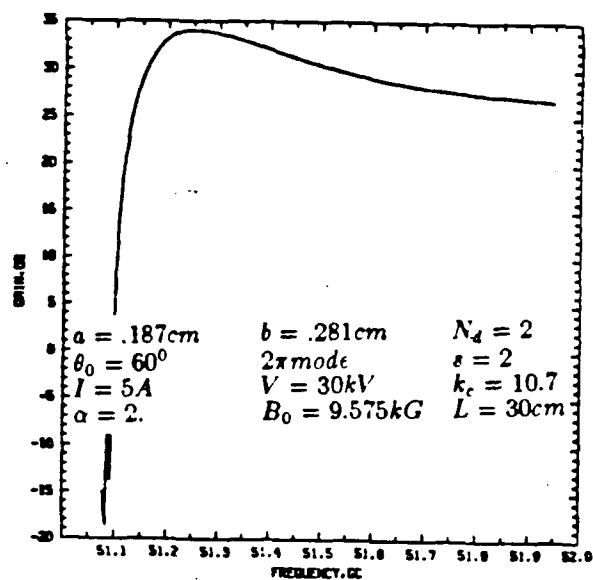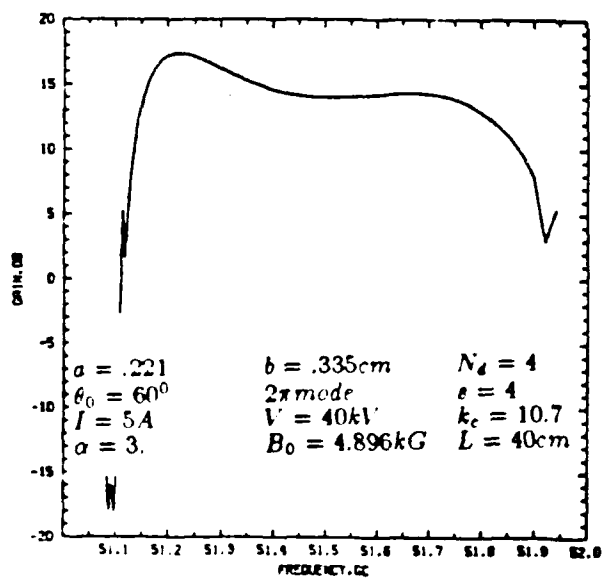c) E_y in region I,   d) E_y in region II.

a = .586cm   b = .6cm TE_{02} mode

a)

b)

$s = 2$ $\alpha = 2.0$
$V = 30kV$ $I = 5A$
$B_0 = 9.580kG$ $L = 30cm$

$s = 4$ $\alpha = 3.0$
$V = 40kV$ $I = 5A$
$B_0 = 4.894kG$ $L = 40cm$

$s = 6$ $\alpha = 5.5$
$V = 40kV$ $I = 5A$
$B_0 = 3.278kG$ $L = 40cm$

c)

d)

Fig.13a)   The cross section of the rectangular waveguide,
b) – d)With TE_{02} mode, the gain-frequency curves for $s = 2, s = 4$ and
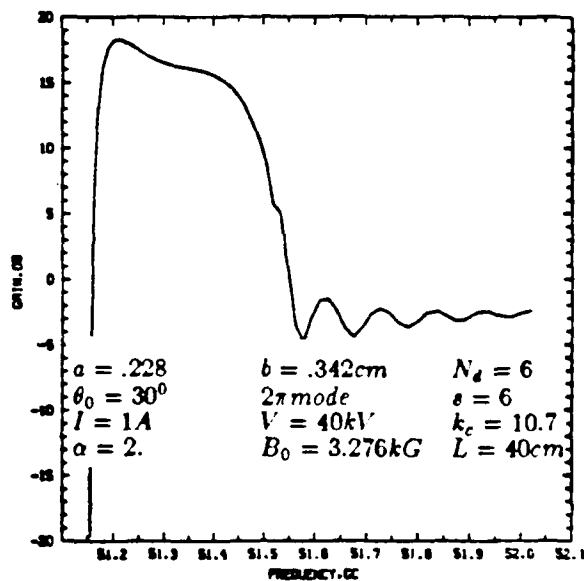$s = 6$ respectively.

a)

$a = .187cm$ $b = .281cm$ $N_d = 2$
$\theta_0 = 60^0$ $2\pi mode$ $s = 2$
$I = 5A$ $V = 30kV$ $k_c = 10.7$
$\alpha = 2.$ $B_0 = 9.575kG$ $L = 30cm$

b)

$a = .221$ $b = .335cm$ $N_d = 4$
$\theta_0 = 60^0$ $2\pi mode$ $e = 4$
$I = 5A$ $V = 40kV$ $k_c = 10.7$
$\alpha = 3.$ $B_0 = 4.896kG$ $L = 40cm$

c)

$a = .228$ $b = .342cm$ $N_d = 6$
$\theta_0 = 30^0$ $2\pi mode$ $s = 6$
$I = 1A$ $V = 40kV$ $k_c = 10.7$
$\alpha = 2.$ $B_0 = 3.276kG$ $L = 40cm$

d)

Fig.12a) The cross section of the magnetron type waveguide,
    b) – d)The gain-frequency curves for $s = 2, s = 4$ and $s = 6$ respectively.

waveguide (or combined with conical waveguide) as the RF structure. Usually, an analytical dispersion relation is derived or a partical simulation code based on directlly solving the equation of motion of electrons in the waveguide field and applied magnetic field is used to get the neccessary theoretical properties for the analysis or for the experiments in the publications.

It is well known that for TE_{mn} modes, circular waveguide has the expression for the axial magnetic field component

$$B_z = B_z^0 J_m(k_c r)e^{jm\theta} \tag{5.28}$$

Where $k_c = \frac{p_{mn}}{a}$, p_{mn} is the n-th root of the Bessel function $J'_m(x) = 0$, and a is the radious of the circular waveguide. The norm of the axial magnetic field is

$$N = \frac{a^2}{2}(1 - \frac{m^2}{p_{mn}^2})J_m^2(k_c a) \tag{5.29}$$

In applying the analytical results of gyrotron kinetic theory in Chapter 3, the gyrotron traveling wave amplifiers with circular wavegide is the simpliest case since there is no summation in the obtained equations and all the coefficients A_{mn} are just simply put to unity in the analytical results obtained in Chapter 3.

The numerical program to compute the gain-frequency functional relation with any waveguide mode and two beam models (the annular beam and the rotating electron layer beam) for circular waveguide is made available. In the example $\epsilon = 2$, the waveguide radious is chosen to have the same cutoff frequency as that of the out-ridged waveguide in $Fig.10a$ and TE_{22} the mode is chosen since for the rotating electron layer beam model the beam-field interaction can take place only when $m = \epsilon$. For $\epsilon = 4$, the operating waveguide mode is TE_{41} and the computed gain-frequency curve is in Fig.14c along with the beam parameters and the applied magnetic field value.

axis, i. e., for the rotating electron layer beam, the electron-field coupling defined in Eq.(3.61) is nonzero only for $m = s$. This means that there is actually no interaction between electron and the waveguide field for even harmonic numbers; A similar conclusion can also be made for TE wave modes with even n: there is no interaction taking place for odd number cyclotron harmonic numbers. The norm N of the axial magnetic field for rectangular waveguide is

$$N = \int_A dA B_z^0 (B_z^0)^*$$
$$= \frac{\epsilon_q}{4} ab \tag{5.26}$$

Where

$$\epsilon_q = \begin{cases} 2 & (q = 0) \\ 1 & (q \neq 0) \end{cases} \tag{5.27}$$

In the purpose to facilitate the comparison the gyro-TWA with rectangular waveguide to that with the out-ridged waveguide, in computing the gain-frequency curves of the gyro-TWA with rectangular waveguide, we choose the waveguide dimensions such that the cutoff frequency of its TE_{02} mode is the same as that of the TE_{02} mode of the out-ridged waveguide; Moreover, we choose the same beam parameters as those used for out-ridged waveguide cases. The computed gain curves are plotted in $Fig.13b$ to d with beam parameters and the applied magnetic field listed in the figures. The waveguide geometric parameters are in the below of Fig.13a.

Due to the simplicity in manufacture, the rectangular waveguide is a good choice for being utilized as the RF structure in the gyro-TWA or the gyrotron oscillators at relatively lower harmonics of the gyration frequency. Another advantage to use the rectangular waveguide in gyrotrons is that the output of the device does not have to have a mode transformer in some cases. But at higher harmonics, the gain is low, as illustrated in Fig.13.

5.3 Gyro-TWA with Circular Waveguide

Due to the relative simplicity for theoretical analysis and easiness for manufacture in the experiments, most gyrotron oscillators and amplifiers use circular

shown in Fig.12b) to d) for $s = 2$, $s = 4$ and $s = 6$ correspondinly. For $s = 2$ and $s = 4$, since the 2π mode is the best mode to choose in the magnetron-type waveguide to work as the beam-wave interaction space in the gyrotrons, we set $N_d = s$. Furthermore, we use the same beam parameters for the rotating electron layer beam as those in the computation of the gain-frequency curves for the gyro-TWAs with other waveguides for $s = 2$ and $s = 4$; For $s = 6$, the beam parameters are chosen the same as those in [18], but the waveguide dimensions have been scaled to those listed in Fig.12d from those in [18] in order to have the same frequency range of the amplifiation.

5.2   Gyro-TWA with Rectangular Waveguide

The eigenvalues and the field solution are well known for the rectangular waveguide. For TE_{qn} modes, the axial magnetic component can be expanded into a series of the Bessel function by the same approach used in Chapter 4 for the out-ridged waveguide. Since the axial magnetic field of TE_{qn} mode in the rectangular waveguide is expressed as

$$B_z = B_0 \cos[\frac{q\pi}{a}(x - \frac{a}{2})] \cos[\frac{n\pi}{b}(x - \frac{b}{2})]$$

$$= \sum_{m=-\infty}^{\infty} A_{nm} J_m(k_c r) e^{jm\theta}, \qquad (5.22)$$

we can obtain the coefficients A_{nm} in the above expansion simply by setting $h = 0$ in Eq.(3.17) in Chapter 3 and we have

$$A_{nm} = \frac{1}{2}B_0[e^{-j\frac{1}{2}k_c b \cos \lambda_n} + (-)^n e^{j\frac{1}{2}k_c b \cos \lambda_n}]\cos(m\lambda_n)$$

$$= \begin{cases} B_0 \cos(\frac{n\pi}{2})\cos(m\lambda_n) & (m - even) \\ jB_0 \sin(\frac{n\pi}{2})\cos(m\lambda_n) & (m - odd) \end{cases} \qquad (5.23)$$

where $h_s = \frac{b}{2}$ and

$$k_c = \sqrt{(\frac{q\pi}{a})^2 + (\frac{n\pi}{b})^2} \qquad (5.24)$$

$$\lambda_n = \cos^{-1}\frac{n\pi}{bk_c} \qquad (5.25)$$

It is readily seen that, for odd n and $q = 0$, $\lambda_n = \frac{\pi}{2}$. if m is even, then the coefficient $A_{nm} = 0$. For the electron beam with all the guiding centers on the waveguide

In order to be able to compute the gain-frequency curve, we have to evaluate the norm of the axial RF magnetic field for the magnetron-type waveguide over its whole cross section. The integral of the norm of the axial magnetic field can be carried out as below.

$$N = \int_A dA B_z^0 (B_z^0)^*$$
$$= \int_{A_1} dA_1 B_{z1}^0 (B_{z1}^0)^* + \int_{A_2} dA_2 B_{z2}^0 (B_z^0)^*$$
$$= I_1 + I_2 \tag{5.16}$$

where A_1, A_2 denotes the area in region I and region II respectively, and

$$I_1 = \int_{A_1} dA_1 B_{1z}^0 (B_{1z}^0)^*$$
$$= \sum_\Gamma \frac{4B_0^2 N_d^2 a^2}{\pi \Gamma^2 [Y_0'(k_c b)]^2} \sin^2(\frac{\Gamma \theta}{2})[1 + (1 - \frac{\Gamma}{k_c^2 a^2}) \frac{J_\Gamma^2(k_c a)}{[J_\Gamma'(k_c a)]^2}] \tag{5.17}$$

$$I_2 = \int_{A_2} dA_2 B_{2z}^0 (B_{2z}^0)^*$$
$$= N_d \theta_0 B_0^2 \left\{ I_{21} + [\frac{J_0'(k_c b)}{Y_0'(k_c b)}]^2 I_{22} - \frac{2J_0'(k_c b)}{Y_0'(k_c b)} I_{23} \right\} \tag{5.18}$$

$$I_{21} = \frac{a^2}{2}[J_1^2(k_c a) + J_0^2(k_c a)] - \frac{b^2}{2}[J_1^2(k_c b) + J_0^2(k_c b)] \tag{5.19}$$

$$I_{22} = \frac{a^2}{2}[Y_1^2(k_c a) + Y_0^2(k_c a)] - \frac{b^2}{2}[Y_1^2(k_c b) + Y_0^2(k_c b)] \tag{5.20}$$

$$I_{23} = \frac{a^2}{2}[J_0(k_c a)Y_0(k_c a) + J_1(k_c a)Y_1(k_c a)] - \frac{b^2}{2}[J_0(k_c b)Y_0(k_c b) + J_1(k_c b)Y_1(k_c b)] \tag{5.21}$$

From the waveguide field expansion given in Eq.(5.1) to Eq.(5.10), it is clear that in the general analytical results obtained in Chapter 3, for the gyro-TWAs with magnetron-type waveguide, $\overline{F}(K)$ is given by Eq.(3.45) with $\sum_m$ being replaced by $\sum_\Gamma$ but no summation with n, and with the coefficients A_{nm} in Eq.(3.45) being replaced by A_Γ. The programs for computing the magnetron-type waveguide eigenvalues, the coefficients in the field expansins and the gain-frequency functional relation have been accomplished. In order to facilitate the comparision to the properties of the gyro-TWAs with the other waveguides, especially those with the out-ridged waveguide, the beam parameters, applied magnetic field and the cutoff frequency of the operating waveguide mode are set the same for the gyro-TWAs working at the same harmonic of the gyration frequency. The computed gain-frequency curves are

$$B_r^{(1)} = -j\frac{k_z}{k_c}\sum_{\Gamma=-\infty}^{\infty} A_\Gamma J_\Gamma'(k_c r)e^{j\Gamma\theta} \tag{5.2}$$

$$B_\theta^{(1)} = \frac{k_z}{rk_c^2}\sum_{\Gamma=-\infty}^{\infty} A_\Gamma \Gamma J_\Gamma(k_c r)e^{j\Gamma\theta} \tag{5.3}$$

$$E_r^{(1)} = \frac{\omega}{crk_c^2}\sum_{\Gamma=-\infty}^{\infty} A_\Gamma \Gamma J_\Gamma(k_c r)e^{j\Gamma\theta} \tag{5.4}$$

$$E_\theta^{(1)} = \frac{j\omega}{ck_c}\sum_{\Gamma=-\infty}^{\infty} A_\Gamma \Gamma J_\Gamma'(k_c r)e^{j\Gamma\theta} \tag{5.5}$$

In region II ($a \leq r \leq b$), the field components can be expressed as

$$B_z^{(2)} = \sum_{\alpha=0}^{\infty} B_\alpha\left[J_\alpha(k_c r) - \frac{J_\alpha'(k_c b)}{Y_\alpha'(k_c r)}Y_\alpha(k_c r)\right]e^{j\alpha(\theta-\theta_{ol})} \tag{5.6}$$

$$B_r^{(2)} = -j\frac{k_z}{k_c}\sum_{\alpha=0}^{\infty} B_\alpha\left[J_\alpha'(k_c r) - \frac{J_\alpha'(k_c b)}{Y_\alpha'(k_c r)}Y_\alpha'(k_c r)\right]e^{j\alpha(\theta-\theta_{ol})} \tag{5.7}$$

$$B_\theta^{(2)} = \frac{k_z}{k_c^2}\sum_{\alpha=0}^{\infty} B_\alpha\frac{\alpha}{r}\left[J_\alpha'(k_c r) - \frac{J_\alpha'(k_c b)}{Y_\alpha'(k_c r)}Y_\alpha'(k_c r)\right]e^{j\alpha(\theta-\theta_{ol})} \tag{5.8}$$

$$E_r^{(2)} = \frac{\omega}{ck_c^2}\sum_{\alpha=0}^{\infty} B_\alpha\frac{\alpha}{r}\left[J_\alpha'(k_c r) - \frac{J_\alpha'(k_c b)}{Y_\alpha'(k_c r)}Y_\alpha'(k_c r)\right]e^{j\alpha(\theta-\theta_{ol})} \tag{5.9}$$

$$E_\theta^{(2)} = j\frac{\omega}{ck_c^2}\sum_{\alpha=0}^{\infty} B_\alpha\left[J_\alpha'(k_c r) - \frac{J_\alpha'(k_c b)}{Y_\alpha'(k_c r)}Y_\alpha'(k_c r)\right]e^{j\alpha(\theta-\theta_{ol})} \tag{5.10}$$

In the above,

$$\theta_{ol} = \frac{2l-1}{N_d}\pi - \frac{\theta_0}{2} \tag{5.11}$$

It is required that at $r = a$, B_z and E_θ be continuous. If in only $\alpha = 0$ term in the field expansion in region II is taken, in the same way as that in section 4.1 for the out-ridged waveguide, we obtain the approximate dispersion equation for the magnetron-type waveguide as the following:

$$\frac{J_0(k_c a)Y_0'(k_c b) - J_0'(k_c b)Y_0(k_c a)}{J_0'(k_c a)Y_0'(k_c b) - J_0'(k_c b)Y_0'(k_c a)} = \frac{N_d\theta_0}{2\pi}\sum_{\Gamma=0}^{\infty}\frac{J_\Gamma(k_c a)}{J_\Gamma'(k_c a)}\left[\frac{\sin(\frac{\Gamma\theta_0}{2})}{\frac{\Gamma\theta_0}{2}}\right]^2 \tag{5.12}$$

When $\theta' = 2n\pi + \theta$, the solution must be single valued. This demands

$$\Gamma = n + mN_d \tag{5.13}$$

where Γ and n, m, N_d all are integers. N_d is the number of the slots along the periphery of the waveguide. Then we can have

$$A_\Gamma = \frac{2N_d B_{01}}{\Gamma\pi J_\Gamma'(k_c a)Y_0'(k_c b)}\left[J_0'(k_c a)Y_0'(k_c b) - J_0'(k_c b)Y_0'(k_c a)\right]\sin\frac{\Gamma\theta_0}{2} \tag{5.14}$$

$$A_0 = \frac{2N_d B_{01}\theta}{2\pi J_0'(k_c a)Y_0'(k_c b)}\left[J_0'(k_c a)Y_0'(k_c b) - J_0'(k_c b)Y_0'(k_c a)\right] \tag{5.15}$$

Chapter 5   Gyro-TWA Devices with Other Waveguides

The gyrotron kinetic theory in Chapter 3 is a generalized one which can be applied to different waveguide structures.   In Chapter 4 the gyro-TWA with the out-ridged waveguide has been analyzed and some gain-frequency curves have been computed.   This chapter is devoted to the computation of the gain-frequency curves for gyro-TWAs with several other different shapes of the waveguides, still by applying the results obtained in Chapter 3.

5.1   Gyro-TWA with Magnetron-type Waveguide

The properties of the gyrotrons that utilize magnetron-type waveguide as the RF structure have been investigated both theoretically and experimentally.[18,19,37,43] It has been demonstrated by the experiments on microwave generation with magnetron-type waveguide open resonators that this class of the gyrotrons can achieve reasonable efficiency at higher gyration harmonics even with a modest electron beam energy.   The following simple analysis of the magnetron-type waveguide field reveals that a high beam-field coupling may be achieved if the waveguide dimensions and the waveguide mode are chosen correctly.

Fig.12a illustrates the cross section of a magnetron-type waveguide with the projection of the electron rotating layer inside the waveguide.

The Ritz-Galerkin method is employed here again to obtain the eigenvalue spectrum and the associated eigenfunctions for TE wave modes.   The axial magnetic field and other field components in region I ($r \leq a$) are expanded into the series as the following

$$B_z^I = \sum_{\Gamma=-\infty}^{\infty} A_\Gamma J_\Gamma(k_c r) e^{j\Gamma\theta} \tag{5.1}$$

in a certain frequency range and at the same harmonic number, the waveguide dimensions must be much bigger for the higher mode than the waveguide dimensions for the lower mode. But, the same beam energy gives the same Larmor radius, the beam occupies a much small portion of the waveguide cross section and has a much weaker coupling with the fields at the higher mode even though the higher mode contains more higher order multipole field. Mathematically, this can be understood by observing the behaviors of the higher order Bessel function of small argument. As a comparision with the lower mode, we take TE_{62} as an example. The electric field components of this mode in the cross section of the out-ridged waveguide are shown in Fig.9a to d . It is seen that the field is quite inhomogeneous in the waveguide. For the out-ridged waveguide having dimension as that in Fig.10a , the cutoff wavenumber of TE_{62} is 32.24; For TE_{02} mode, the cutoff wavenumber is 10.7. For a gyro-TWA designed to operate at 51.2 GHz, then the waveguide has the dimensions listed below Fig. 10a , if it operates with TE_{02} mode; the dimensions have to increase to those listed below Fig. 11a , if the gyro-TWA is still operated at 51.2 GHz but at TE_{62} mode. With all the same beam parameters as those specified for the corresponding harmonic for TE_{02} mode, the linear gain-frequency curves for gyro-TWA with out-ridged waveguide at TE_{62} mode for $s = 2$ and $s = 4$ are computed and shown in Fig. 11b and c correspondingly. It is seen clearly that the gain is lower than the corresponding one at TE_{02} mode. The first ten coefficients in the expansion of the field in the waveguide in Eq.(4.4) are listed in Table 3.

Table 3   The Coefficients B_{1n} of TE_{62} Mode

B_{10}	B_{11}	B_{12}	B_{13}	B_{14}
-0.4847	$-.5127 \times 10^{-16}$	1.090	$-.9778 \times 10^{-16}$	-3.218
B_{15}	B_{16}	B_{17}	B_{18}	B_{19}
0.1283×10^{-15}	9.623	0.1558×10^{-17}	-0.1431×10^{-2}	0.8756×10^{-20}

Eq.(4.25), the corresponding coefficient A_{nm} is equal to zero. For TE_{02} mode, the first ten coefficients in Eq.(4.4) are listed below. It can be seen that the odd n coefficients actually are equal to zero, only even n terms exist.

Table 2 The Coefficients B_{1n} of TE_{02} Mode

B_{10}	B_{11}	B_{12}	B_{13}	B_{14}
-0.7654	$-.9707 \times 10^{-17}$	1.000	$-.2937 \times 10^{-16}$	-0.8546×10^{-3}

B_{15}	B_{16}	B_{17}	B_{18}	B_{19}
-0.8612×10^{-20}	$-.1283 \times 10^{-4}$	0.4692×10^{-22}	-0.7586×10^{-4}	0.4973×10^{-23}

We may conclude that for rotating electron layer beam at this waveguide mode the beam-field interaction is practically possible only for even cyclotron harmonic number s.

However, for some other modes, for example TE_{11} mode, for even $n, B_{0n} = 0$. In this case, the cyclotron interaction can take place only for odd cyclotron harmonic numbers. This is also the consequence of the coefficients. It is worth noting that from the analysis on peniotron[49,50], they conclude that the device can only operate at even gyration harmonics in their analysis when their electrostatic field configuration approximation is used.

In order to achieve a good coupling between the waveguide field and the beam, the operation of gyrotrons at higher gyration harmonics in general requires working at higher order waveguide modes because the higher order multipole field components are bigger in higher order modes. But this does not always mean that a higher order waveguide mode is better than a lower order mode for operating a gyrotron at the higher harmonics. Since the higher order mode has a higher cutoff frequency than the lower order mode for the same waveguide geometry, if one wants to operate the device at the same harmonic with the same waveguide, one has to operate the device at higher fequency, and in consequence, apply a higher magnetic field to the device than one operates the gyrotron at a lower order waveguide mode; If the electron beam energy is kept the same, the higher magnetic field decreases the electron Larmor radius very much. As a result, the coupling between the beam and the fields becomes weaker; On another hand, if one wants to operate the device

The onset of oscillations may be troublesome in developing a high power gyrotron traveling amplifier. The reflection in the waveguide, due to the discontinuity, tapered section or some other reasons, is significant in the vicinity of the cutoff frequency of a waveguide mode[30]; And also, both from the linear theory and the nonlinear theory, the cyclotron resonant interaction is strong if the frequency is close to the cutoff frequency. Except for mode competition, these two factors perhaps are chiefly responsible for the instability of the gyrotron amplifier operation. Adopting some techniques developed for the conventional traveling amplifiers, such as the introduction of the waveguide wall loss to the amplifier, may subdue the instability of the gyro-TWA devices due to the reflections and absolute instability. If the waveguide wall has some loss due to the finite conductivity or due to the coating with lossy material on the wall, the attenuation of the waveguide in general is a function of frequency and this frequency dependence is different for different wave modes. But in general, the attenuation is most significant at the vicinity of the cutoff frequency of that mode. Therefore, it is possible to chose lossy material and to distribute it on the waveguide wall in such a way that the frequency dependence of the waveguide attenuation cancels the effect of the reflection and the over high gain near cutoff. Then we can gain the benefit in two folds: not only does it overcome the oscillation problem, but also increases the bandwidth significantly. Of course, the correct choice of the applied magnetic field and the beam parameters is also very important for the stable operation of a gyro-TWA. A comprehensive study of the stability of the gyro-TWA has to resort to the multimode analysis. In doing the numerical computation, the single mode analysis of the open resonators can offer the Q values and the reflection coefficient at the end of the tapered waveguide for all the possible oscillation modes.[27-30] However, there is no intention to study the stability of the gyro-TWAs in detail here. In the computing program, we put the waveguide attenuation into consideration by simply adopting the formula given by the perturbation method for the empty waveguide analysis.

From the numerical results of the waveguide computation, for the operating TE_{02} mode, the coefficient in the field expression, for odd n, $B_{1n} = 0$, and from
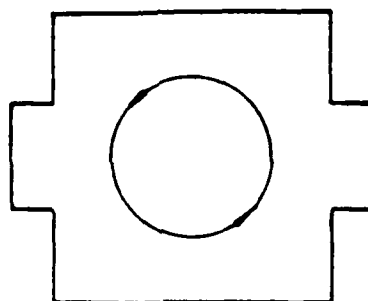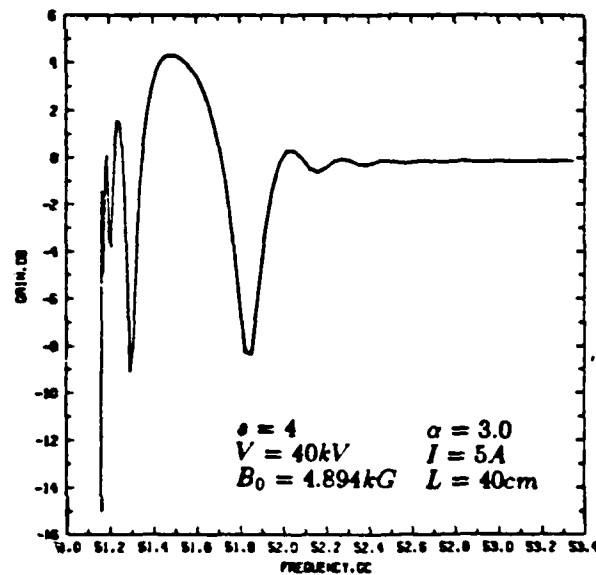
$a = 2.2cm$ $s_1 = .857cm$
$b = .662cm$ $h = h' = .57cm$

a)
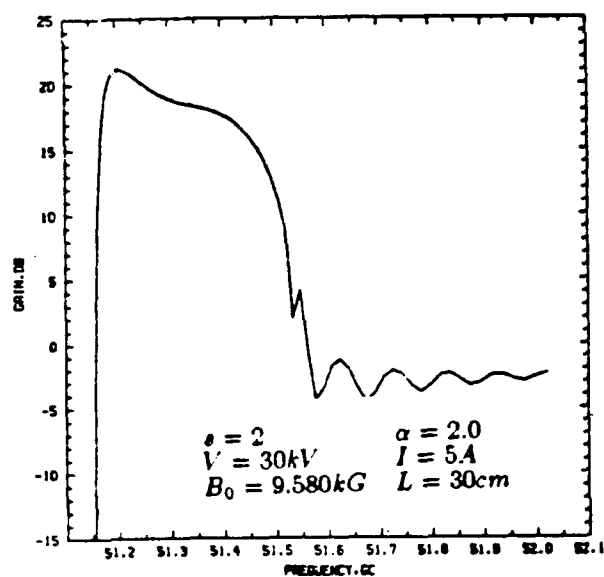
b)

c)

Fig.11a) The cross section of a gyro-TWA with the out-ridged waveguide,
    b) – c)With TE_{62} mode, the gain-frequency curves for $s = 2$ and $s = 4$
    respectively.

In computing the gain-frquency dependence by applying the analytical results developed from plasma kinetic theory in Chapter 3, in the caculation of $D(K)$ in Eq.(3.55), we need to caculate the norm N of the axial component of magnetic field of the out-ridged waveguide. This can be accomplished by evaluating the following integration of the axial magnetic field expression in section 4.1.

$$
\begin{aligned}
N &= \int_A dA B_z^0 (B_z^0)^* \\
&= \int_{A_I} dA_I B_{1z}^0 (B_{1z}^0)^* + \int_{A_{II}} dA_{II} B_{2z}^0 (B_{2z}^0)^* \\
&= \sum_{n=0}^{\infty} B_{1n}^2 \int_{x=-a_1}^{a_1} dx \int_{y=-h'}^{h} dy \cos^2(k_{x1n}x)\cos^2[\frac{n\pi}{h_s}(y-h)] \\
&\quad + 2\sum_{m=0}^{\infty} B_{2m}^2 \int_{x=-a_1}^{\frac{a}{2}} dx \int_{y=-\frac{b}{2}}^{\frac{b}{2}} dy \cos^2[k_{x2m}(x-\frac{a}{2})]\cos^2[\frac{m\pi}{b}(y-\frac{b}{2})] \\
&= \frac{h_s}{4}\sum_{n=0}^{\infty} B_{1n}^2 [2a_1 + \frac{\sin(2k_{x1n}a_1)}{k_{x1n}}] \\
&\quad + \frac{b}{2}\sum_{m=0}^{\infty} B_{2m}^2 \left\{ (\frac{a}{2}-a_1) + \frac{\sin[2k_{x2m}(\frac{a}{2}-a_1)]}{2k_{x2m}} \right\}
\end{aligned}
\tag{4.31}
$$

In the above, the coefficient A_{nm} is given by Eq.(3.21) and A_I is the area of region I, A_{II} is the area of region II.

With the formalism developed in Chapter 3, a numerical program is written and supplemented with a program solving eigenvalues and field coefficients in the series in Eq.(4.4), following the description in section 4.2. The dimensions of the example of the out-ridged waveguide are listed in the below of Fig.10a. The operating mode is chosen to be TE_{02}. The distribution of the electric field components in the cross section of the waveguide for this mode are plotted in Fig.8a to d. The reason for chosing this mode is simple. This is a relatively lower mode and it has a very good separation from the neighboring modes so the mode competition of the amplifier would not be a serious problem. The spectrum for the eigenmode is shown in Fig. 15a.

The computed gain-frequency curves are plotted in Fig.10b to d with the beam parameters for $s = 2$, $s = 4$ and $s = 6$ respectively.

For a higher mode TE_{62}, gain-frequency curves are plotted in Fig. 9b to d with the beam parameters for $s = 2$, $s = 4$ and $s = 6$ respectively.
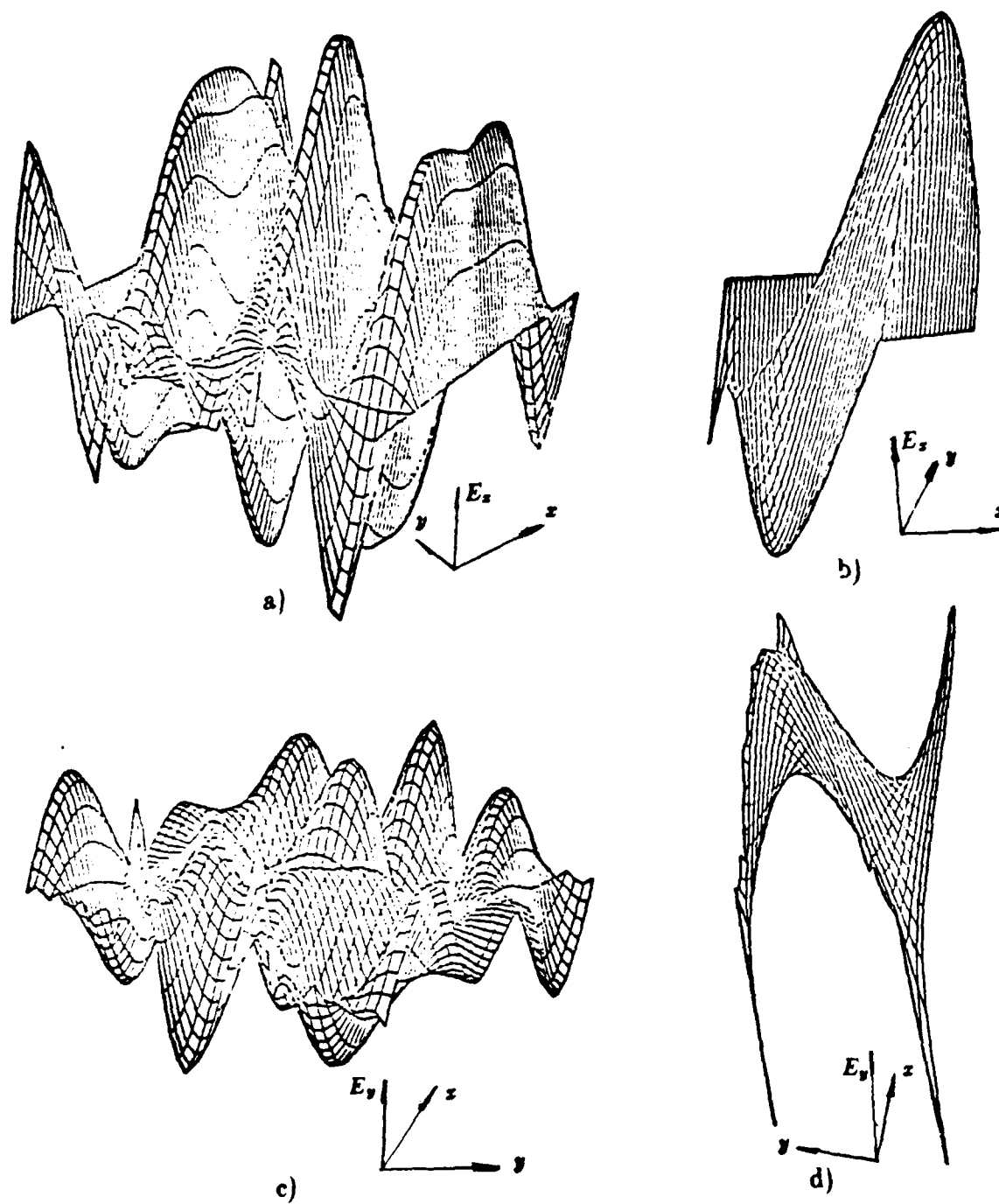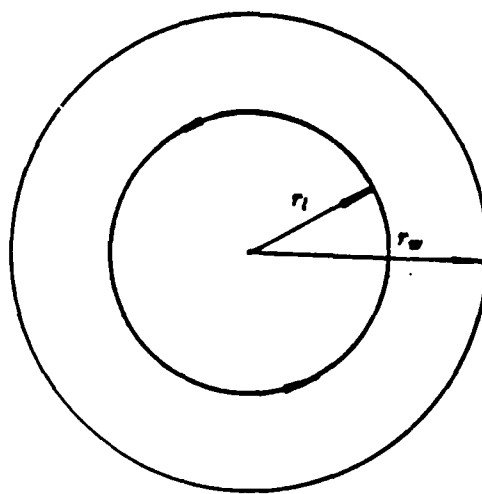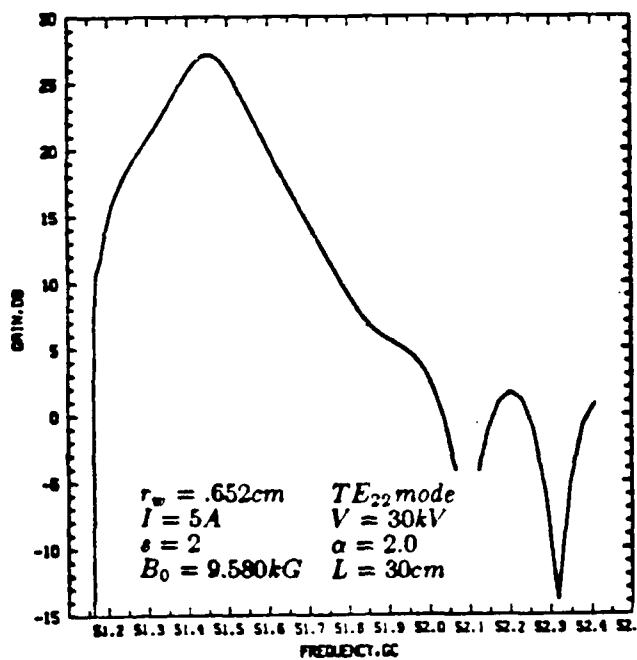
Fig.9 The electrical field transverse distribution for TE_{62} mode
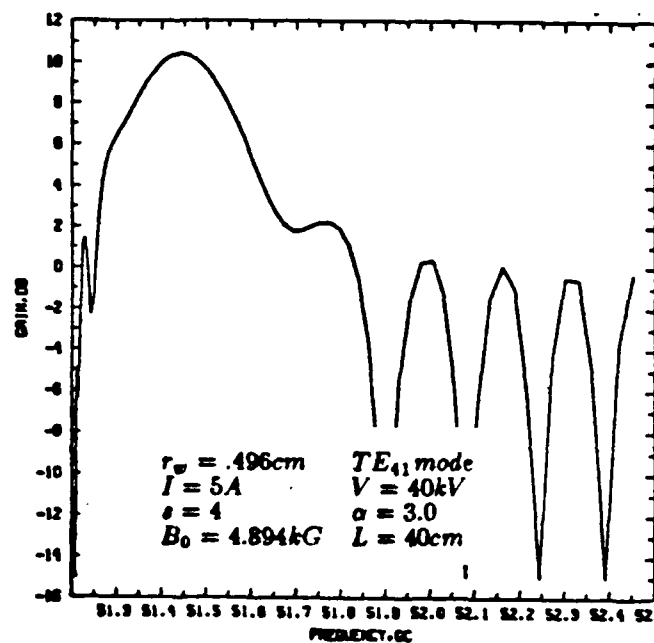in the outridged waveguide:
a) E_z in region I, b) E_z in region II,
c) E_y in region I, d) E_y in region II.

a)

$r_w = .652cm$ $TE_{22}\,mode$
$I = 5A$ $V = 30kV$
$s = 2$ $\alpha = 2.0$
$B_0 = 9.580kG$ $L = 30cm$

b)

$r_w = .496cm$ $TE_{41}\,mode$
$I = 5A$ $V = 40kV$
$s = 4$ $\alpha = 3.0$
$B_0 = 4.894kG$ $L = 40cm$

c)

Fig.14a)   The cross section of the circular waveguide,
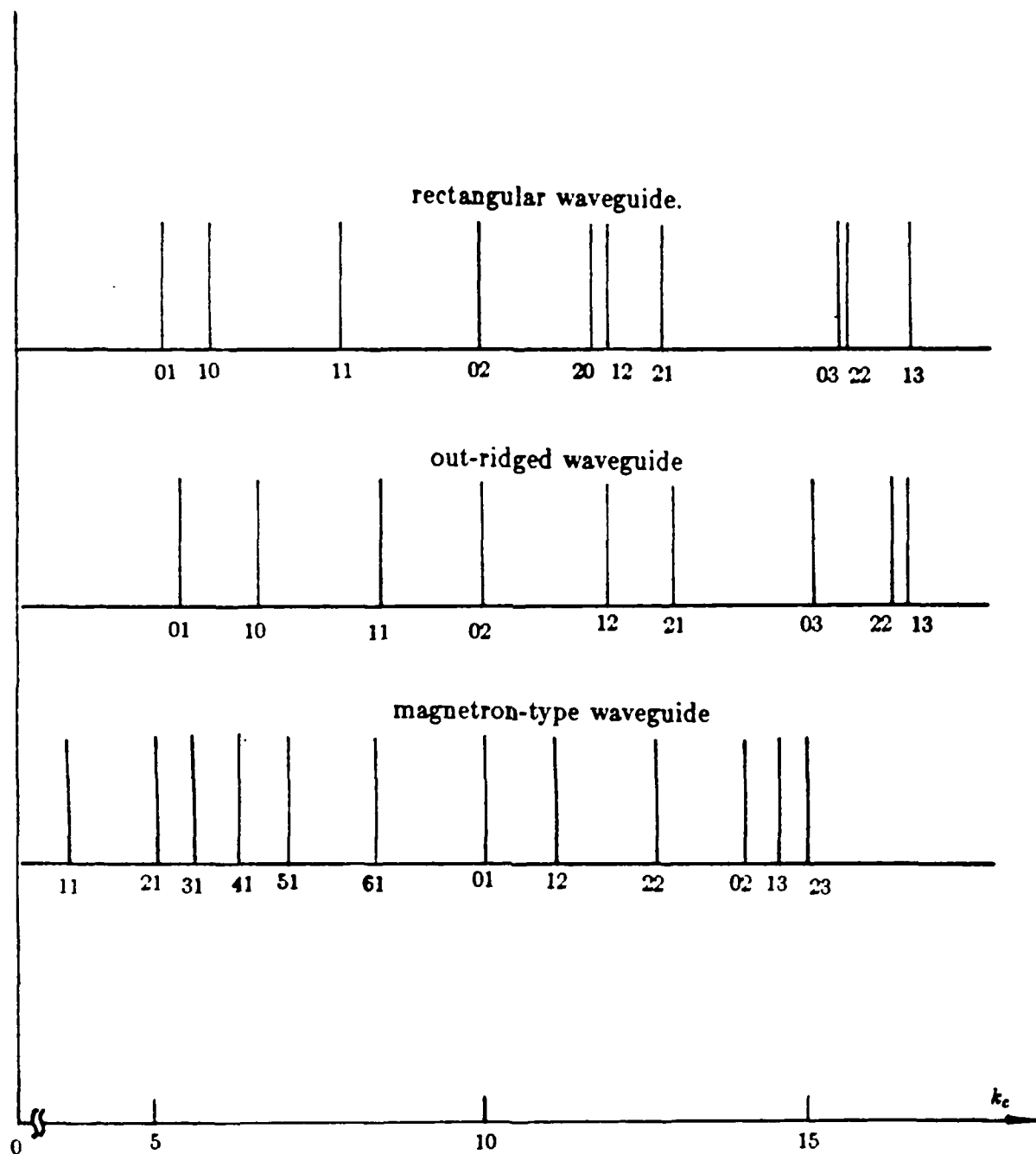   b) – c)The gain-frequency curves for $s = 2$ and $s = 4$ respectively.

Fig.15   The distribution of the first few eigenvalues.
(the numbers below the lines are the TE mode indexes).
a)   The rectangular waveguide,
b)   The out-ridged waveguide,
c)   The magnetron-type waveguide for N=6.

Chapter 6 Comparision and Conclusion

In this chapter, Section 6.1 is devoted to a comparision of the gyro-TWAs with several different waveguides analyzed in the previous chapters. In Section 6.2 some conclusions are made for the gyro-TWAs from the analysis in the present work.

6.1 Comparision

In the previous chapters, the gyro-TWAs with several different waveguide structures have been analyzed and the gain-frequency curves for some examples of the gyro-TWAs have been computed. This section is devoted to a comparision of the gyro-TWAs with different waveguides through the computed gain-frequency curves.

Even though the numerical programs are able to deal with both the annular beam and the rotating electron layer beam, all the computed examples of the gain-frequency curves are with the rotating electron layer beam only. The reason for doing this is that Eq.(3.61) indicates that the rotating electron layer beam has a bigger beam-field coupling than the annular beam; Furthermore, most of the reported experiments of microwave generation at higher harmonics of the gyration frequency utilized the rotating electron layer beam. Also, although we can treat the beam velocity spread for the Lorenzian distribution, in all the examples computed for this comparision only the 'cold' beam model are used, since the gain-frequency functional relation is not sensitive to a small velocity spread in the electron beam for fast wave devices.

For the gyrotron traveling wave amplifiers with the out-ridged waveguide and that with the rectangular waveguide, in the computation we set the same TE_{02} operating waveguide mode, the same cutoff frequency, the same beam parameters, and the same beam-field interaction length. Along with the waveguide geometric

parameters listed below Fig.10a, the gain-frequency curves are plotted in $Fig.10b$ to d for the examples of the gyro-TWAs with the out-ridged waveguide at $s = 2$, $s = 4$, and $s = 6$ respectively. The gain-frequency curves in $Fig.13b$ to d are for the examples of the gyro-TWA with rectangular waveguide at $s = 2$, $s = 4$, and $s = 6$ correspondingly, while the waveguide geometric parameters are in the below of $Fig.13a$.

It is seen from the computed results that, at $s = 2$, the gain at the center frequency of the band of the gyro-TWA with the out-ridged waveguide is 3 dB higher than that of the gyro-TWA with the rectangular waveguide at 40 dB gain level. Of cource, this is not a big difference. However, at $s = 4$, the difference of the gain at the center frequency of these two amplifiers is about 6 dB at 25 dB gain level. For $s = 6$, at 12 dB gain level, the difference in the gain is 3 dB which is a very big difference. This is to say that, as the harmonic number s goes higher, these results demonstrate that the gain of the gyro-TWA with the out-ridged wavegu le decreases much slower than the gain of the gyro-TWA with the rectangular waveguide. Therefore, the gyro-TWA with the out-ridged waveguide is much better to operate at higher harmonics than the gyro-TWA with the rectangular waveguide.

For the gyro-TWA with the magnetron-type waveguide, we always use 2π mode in the computation examples. Therefore, we set $s = N_d$ for all the examples. The gain-frequency curves are plotted in $Fig.13b$ to d.

Comparing these curves in $Fig.13b$ to d with those in $Fig.10b$ to d, we see that at $s = 2$ the gyro-TWA with the out-ridged waveguide at the center frequency has a gain 5 dB higher than that of the gyro-TWA with the magnetron-type waveguide at 40 db level. At $s = 4$, still with the same beam parameters as those for the gyro-TWA with the out-ridged waveguide at $s = 2$, the gain of the gyro-TWA with the out-ridged waveguide is 10 dB higher than that of the gyro-TWA with the magnetron-type waveguide at 20 dB level. But, comparing the gain in $Fig.10d$ with that in $Fig.13d$ at $s = 6$, it is seen that the gain of the gyro-TWA with the magnetron-type waveguide having 6 slots along the periphery of the waveguide is higher than the gain of the gyro-TWA with the out-ridged waveguide even the current in the former is smaller.

This is because that the magnetron-type waveguide structure has six slots along the periphery of the waveguide, which is a much more complicated structure than the out-ridged waveguide, therefore it is better to enhance the beam-field interaction at $s = 6$ than the later.

Comparing the gain frequency curves in Fig.10, Fig.12 and Fig.14, we see that the gyro-TWA with the out-ridged waveguide and the rectangular waveguide have a much better ability to achieve higher gain at higher harmonics than that with the circular waveguide. The gyro-TWA with the circular waveguide even for high angular number mode TE_{41}, the gain at $s = 4$ is still much lower than the gain of the gyro-TWAs with the out-ridged waveguide and with the rectangular waveguide though the latter two waveguides are working at the lower waveguide mode TE_{02}.

It is seen that the shape of the gain curves of the gyro-TWA with the circular waveguide is different from those in Fig.10 and in Fig.12. This difference is due to the different frequency dependence of the wall loss in different waveguides, which has been taken into account in the gain-frequency computation by adopting the formulas given by the pertubation method. In general, from all the computed gain-frequency curves it is seen that for any specified waveguide structure the gain of the gyro-TWA devices becomes smaller as the number of the harmonic goes higher.

In conclusion, the gyro-TWA with the out-ridged waveguide has a simple structure and up to $s = 4$, the gyro-TWA with this waveguide structure demonstrates the advantages over the gyro-TWAs with other waveguides. However, if the harmonic number is higher than 4, perhaps the magnetron-type waveguide is still a better choice than other existing waveguide structures for gyrotrons at higher harmonics.

6.2   Conclusion

In the previous chapters, the linear and the nonlinear theory of gyrotron traveling amplifier have been developed with a general beam-waveguide model. With this unified theory, if the eigenvalue and the field in the waveguide have been found, the

beam-field analysis can be accomplished either by the numerical solution to that set of the nonlinear equations or by applying the analytical results of gyrotron kinetic theory developed in Chapter 3. The general gyrotron dispersion equation is derived both from kinetic theory and from that set of the nonlinear equations which are derived from the equations of motion of the electrons in the electromagnetic field in the waveguide in the frame of the weakly irregular waveguide theory. The linear and the nonlinear theory are valid for the fully relativistic electron beam and for large orbit motion of the electrons. From the linear theory it has been proved that the gyrotron interaction at the s-th harmonic is associated with the $2s$-th order of the multipole field in the waveguide, if the field is expanded around the guiding center of the electrons.

From the computed gain-frequency curves for the specified electron beam parameters, it is seen that the gain of the gyro-TWA with any waveguide structure becomes smaller as the number of the harmonic goes higher, since the components of the higher order multipole field become smaller. This concludes that in general the gyrotrons working at higher harmonics demand higher beam energy, especially in the transverse direction. The waveguide structure in a gyro-TWA plays a very important role. This has been demonstrated by the analysis and the computed examples in the previous chapters. In this work, and also by the reported experiments of microwave generation at higher harmonics of the gyration frequency.

Through the numerical results of the examples, the advantages of the gyro-TWA with the proposed out-ridged waveguide have been demonstrated. These include the simplicity in the configuration compared to magnetron-type waveguide; the lower operating mode but still with high gain per unit length; the alleviation of the mode competition problem by the good separation of the lower modes. For a gyro-TWA with the out-ridged waveg uide, when the number of harmonic goes higher, the gain per unit length decreases much slower compared to the gyro-TWA with circular waveguide and to the gyro-TWA with the rectangular waveguide. Comparing to the waveguide utilized in 'peniotron', the out-ridged waveguide is free from the local modes or 'trough' modes. This is very important for the stability and efficiency of

the devices.

Another obvious advantage of the out-ridged waveguide is its high power handling ability compared to the magnetron-type and the 'peniotron' waveguide. Due to the two pairs of the ridges in the waveguide used in the 'peniotron', the power handling capability of the device may be reduced, so it may not be suitable for high power microwave generation or amplification.

The rectangular waveguide has a simple configuration and is also easy to manufacture, for the second harmonic operation, the coupling between the field and beam is just slightly smaller than that for the out-ridged waveguide but is poor at higher harmonics. The gyrotron traveling amplifiers with the out-ridged waveguide can achieve relatively high gain up to 4-th gyration harmonics with the moderate electron beam energy.

The configuration of the circular waveguide is simple and it has been widely utilized in gyrotron devices. From the theoretical prediction and from the experimental demonstration, the gyro-devices with the smooth circular waveguide can not go to higher gyration harmonics as beyond 3 or 4. Furthermore, the overmode operation will have a big problem of mode competition especially for wide waveband amplification.

Appendex I Derivation of the Dispersion Relation
for TM Mode of the Out-ridged Waveguide

In this derivation we still adopt the notations in Fig.5.

For TM modes, the solution of the axial electrical field in the waveguide is assumed in the form $E_z = E_z^0 e^{j(\omega t - k_z z)}$, then E_z^0 is governed by the equation

$$(\frac{\partial^2}{\partial x^2} + \frac{\partial^2}{\partial y^2} + k_c^2)E_z^0 = 0. \tag{I.1}$$

subject to the boundary condition on the perfect conducting wall

$$E_z^0 = 0 \tag{I.2}$$

where

$$k_c^2 = \frac{\omega^2}{c^2} - k_z^2 \tag{I.3}$$

The axial electric field in region I and region II can be expanded into the series of the eigenfunctions in that region.

$$E_{1z}^0(x,y) = \sum_{n=1}^{\infty} E_{1n} {\sin \atop \cos}(k_{x1n}x)\sin[\frac{n\pi}{h_s}(y-h)] \tag{I.4}$$

$$E_{2z}^0(x,y) = \sum_{m=1}^{\infty} E_{2m}\sin[k_{x2m}(x-\frac{a}{2})]\sin[\frac{m\pi}{b}(y-\frac{b}{2})] \tag{I.5}$$

The other field components in region I are derived from the Maxwell equations

$$E_{1x}^0 = j\frac{k_z}{k_c^2}\sum_{n=1}^{\infty} E_{1n}k_{x1n} {\cos \atop -\sin}(k_{x1n}x)\sin[\frac{n\pi}{h_s}(y-h)] \tag{I.6}$$

$$E_{1y}^0 = j\frac{k_z}{k_c^2}\sum_{n=1}^{\infty} E_{1n}\frac{n\pi}{h_s} {\sin \atop \cos}(k_{x1n}x)\cos[\frac{n\pi}{h_s}(y-h)] \tag{I.7}$$

$$B_{1x}^0 = -\frac{1}{Z_m}E_{1y} \tag{I.8}$$

$$B_{1y}^0 = \frac{1}{Z_m}E_{1x} \tag{I.9}$$

and in region II, the other components are

$$E_{2x}^0 = -j\frac{k_z}{k_c^2}\sum_{m=1}^{\infty} E_{2m}k_{x2m}\cos(k_{x2m}x)\sin[\frac{m\pi}{b}(y-\frac{b}{2})] \tag{I.10}$$

$$E_{2y}^0 = -j\frac{k_z}{k_c^2}\sum_{m=1}^{\infty} E_{2m}(\frac{m\pi}{b}) - \sin(k_{z2m}z)\cos[\frac{m\pi}{b}(y-\frac{b}{2})] \qquad (I.11)$$

$$B_{2z}^0 = -\frac{1}{Z_m}E_{2y} \qquad (I.12)$$

$$B_{2y}^0 = \frac{1}{Z_m}E_{2z} \qquad (I.13)$$

where $Z_m = \frac{ck_z}{\omega}$ is the TM wave impedance.

Using the continuity conditions at $z = a_1$ for E_z and B_y in the same way as that for TE modes of the out-ridged waveguide in Chapter 4, a dispersion equation can be obtained for TM modes as

$$\sum_{m=0}^{M} D_m\left\{\sum_{n=0}^{N}\frac{E_{mn}E_{qn}}{k_{z1n}\epsilon_n h_s}\frac{\tan}{\cot}(k_{z1n}a_1) - \frac{\delta_{qm}\epsilon_q b}{k_{z2q}}\cot[k_{z2q}(a_1-\frac{a}{2})]\right\} = 0. \qquad (I.14)$$

Where

$$E_{nm} = \int_{-\frac{b}{2}}^{\frac{b}{2}} dy\sin[\frac{n\pi}{h_s}(y-h)]\sin[\frac{m\pi}{b}(y-\frac{b}{2})]$$

$$= \frac{h_s b}{2\pi}(\frac{1}{mb+nh_s}-\frac{1}{mb-nh_s})\left[\sin\frac{m(b-2h)\pi}{2h_s}+(-)^n\sin\frac{m(b+2h)\pi}{2h_s}\right] \qquad (I.15)$$

$$E_{00} = 0 \qquad (I.16)$$

In matrix form, Eq. (I.14) becomes

$$[T(k_c)][D] = 0 \qquad (I.17)$$

where the element T_{mq} of the matrixis

$$T_{mq} = \frac{E_{mn}E_{qn}}{k_{z1n}\epsilon_n h_s}\frac{\tan}{-\cot}(k_{z1n}a_1) - \frac{\delta_{qm}\epsilon_q b}{k_{z2q}}\cot[k_{z2q}(a_1-\frac{a}{2})] \qquad (I.18)$$

and

$$\epsilon_q = \begin{cases} 2 & (q=0) \\ 1 & (q\neq 0) \end{cases} \qquad (I.19)$$

Then, the roots of the determinant of matrix $[T(k_c)]$ give the eigenvalues of the waveguide for TM modes.   The associated eigenfunction of a eigenvalue can be obtained by solving a system of the algebraic equations Eq.(I.14).

Appendex II   Angular Integrals

Some angular integrations in Chapter 3 are derived in the follows. For the sake of space saving, in some equations in the below the double subscripts or superscripts may occur. In those cases, the superscript or subscript on the both sides should be taken correspondingly. From Eq.(3.41),

$$f_R = \frac{1}{2\pi R}\delta(R - R_0)$$
$$= \frac{1}{2\pi r r_l \sin\xi}[\delta(\xi - \xi_0) - \delta(\xi + \xi_0)]\cdot\Delta(r) \qquad (II-1)$$

where

$$\Delta(r) = \begin{cases} 1 & r_- \le r \le r_+ \\ 0 & \text{otherwise.} \end{cases}$$
$$r_\pm = R_0 \pm r_l$$

Using Graf's addition theorem and with reference to Fig.3, we can have

$$\Phi^\pm_{m-s} = \int_{-\pi}^{\pi} d\xi\, e^{\pm j\xi} e^{-js\Psi} J_{m-s}(k_c R) f_R$$

$$= \frac{1}{2\pi r r_l \sin\xi_0} e^{-jm\Psi} \sum_{s=-\infty}^{\infty} J_{m-s-s'}(k_c r_l) J_{s'}(k_c r) \int_{-\pi}^{\pi} d\xi\, e^{j(s'\pm 1)\xi}[\delta(\xi + \xi_0) + \delta(\xi - \xi_0)]\cdot\Delta(r)$$

$$= \frac{1}{\pi r r_l \sin\xi_0} e^{-jm\Psi} J_{m-s}(k_c R)\cos[(m-s)\Psi \pm \xi_0]\cdot\Delta(r) \qquad (II-2)$$

Since

$$\cos\Psi = \frac{\partial R}{\partial r_l} = \frac{r}{R}\cos\xi$$

$$\sin\Psi = \frac{\partial R}{r\partial\xi_0} = \frac{r}{R}\sin\xi$$

we can have

$$e^{j\Psi}\frac{\partial f_R}{\partial r_l} = \frac{\partial f_R}{\partial R}\frac{\partial R}{\partial r_l} + j\frac{\partial f_R}{\partial R}\frac{r}{R}\sin\xi$$
$$= \frac{\partial f_R}{\partial r_l} + j\frac{1}{r}\frac{\partial f_R}{\partial\xi} \qquad (II-3)$$

Thus, we have

$$\int_{-\pi}^{\pi} d\xi\, e^{j(s'\pm 1)\xi} e^{j\Psi}\frac{\partial f_R}{\partial R} = \frac{\cos(s'\pm 1)\xi\cdot\Delta(r)}{\pi r r_l^2 \sin\xi_0}\frac{(s'+2)}{s'} \qquad (II-4)$$

$$\int_{-\pi}^{\pi} d\xi e^{j(s'\pm1)\xi} e^{-j\Psi} \frac{\partial f_{cR}}{\partial R} = -\frac{\cos(s'\pm1)\xi\cdot\Delta(r)}{\pi r r_i^2 \sin\xi_0} \frac{s'}{(s'-2)} \qquad (II-5)$$

$$\Psi_{m-s-1}^{\pm} = e^{-jm\Psi} \int_{-\pi}^{\pi} d\xi e^{\pm j\xi} e^{j(m-s-1)\Psi} J_{m-s-1}(k_c R) e^{j\Psi} \frac{\partial f_R}{\partial R}$$

$$= \frac{1}{\pi r r_i^2 \sin\xi_0} e^{-jm\Psi} \left\{ -\frac{1}{2} k_c r_l J_{m-s}(k_c R) \cos[(m-s)\Psi - \xi_0] \right.$$

$$- \frac{1}{2} k_c r_l J_{m-s-2}(k_c R) \cos[(m-s-2)\Psi \pm \xi_0]$$

$$\left. + (m-s\pm1) J_{m-s-1}(k_c R) \cos[(m-s-1)\Psi \pm \xi_0] \right\} \qquad (II-6)$$

$$\Psi_{m-s+1}^{\pm} = e^{-jm\Psi} \int_{-\pi}^{\pi} d\xi e^{\pm j\xi} e^{j(m-s-1)\Psi} J_{m-s+1}(k_c R) e^{j\Psi} \frac{\partial f_R}{\partial R}$$

$$= \frac{1}{\pi r r_i^2 \sin\xi_0} e^{-jm\Psi} \left\{ -\frac{1}{2} k_c r_l J_{m-s}(k_c R) \cos[(m-s)\Psi - \xi_0] \right.$$

$$+ \frac{1}{2} k_c r_l J_{m-s+2}(k_c R) \cos[(m-s+2)\Psi \pm \xi_0]$$

$$\left. - (m-s\pm1) J_{m-s+1}(k_c R) \cos[(m-s+1)\Psi \pm \xi_0] \right\} \qquad (II-7)$$

Thus, we can obtain the following several integrals:

$$\Psi_+ = \Psi_{m-s-1}^+ + \Psi_{m-s+1}^+$$

$$= e^{-jm\Psi} \frac{1}{\pi r r_i^2 \sin\xi_0}$$

$$\left\{ -\frac{1}{2} k_c r_l J_{m-s-2}(k_c R) \cos[(m-s-2)\Psi + \xi_0] \right.$$

$$+ \frac{1}{2} k_c r_l J_{m-s+2}(k_c R) \cos[(m-s+2)\Psi + \xi_0]$$

$$+ (m-s\pm1) J_{m-s-1}(k_c R) \cos[(m-s-1)\Psi + \xi_0]$$

$$\left. - (m-s\pm1) J_{m-s+1}(k_c R) \cos[(m-s+1)\Psi + \xi_0] \right\} \qquad (II-8)$$

$$\Psi_- = \Psi_{m-s-1}^+ - \Psi_{m-s+1}^+$$

$$= e^{-jm\Psi} \frac{1}{\pi r r_i^2 \sin\xi_0} \left\{ -k_c r_l J_{m-s}(k_c R) \right.$$

$$\left\{ -k_c r_l J_{m-s}(k_c R) \cos[(m-s)\Psi + \xi_0] \right.$$

$$+ (m-s\pm1) J_{m-s-1}(k_c R) \cos[(m-s-1)\Psi + \xi_0]$$

$$+ (m-s\pm1) J_{m-s+1}(k_c R) \cos[(m-s+1)\Psi + \xi_0]$$

$$- \frac{1}{2} k_c r_l J_{m-s-2}(k_c R) \cos[(m-s-2)\Psi + \xi_0]$$

$$\left. - \frac{1}{2} k_c r_l J_{m-s+2}(k_c R) \cos[(m-s+2)\Psi + \xi_0] \right\} \qquad (II-9)$$

$$\Psi_{c+} = \Psi^-_{m-s-1} + \Psi^-_{m-s+1}$$

$$= e^{-jm\Psi} \frac{1}{\pi r r_i^2 \sin \xi_0}$$

$$\left\{ -\frac{1}{2} k_c r_l J_{m-s-2}(k_c R) \cos[(m-s-2)\Psi - \xi_0] \right.$$

$$+ \frac{1}{2} k_c r_l J_{m-s+2}(k_c R) \cos[(m-s+2)\Psi - \xi_0]$$

$$+ (m-s \pm 1) J_{m-s-1}(k_c R) \cos[(m-s-1)\Psi - \xi_0]$$

$$\left. - (m-s \pm 1) J_{m-s+1}(k_c R) \cos[(m-s+1)\Psi - \xi_0] \right\} \qquad (II-10)$$

$$\Psi_{c-} = \Psi^-_{m-s-1} - \Psi^-_{m-s+1}$$

$$= e^{-jm\Psi} \frac{1}{\pi r r_i^2 \sin \xi_0} \left\{ -k_c r_l J_{m-s}(k_c R) \right.$$

$$\left\{ -k_c r_l J_{m-s}(k_c R) \cos[(m-s)\Psi - \xi_0] \right.$$

$$+ (m-s \pm 1) J_{m-s-1}(k_c R) \cos[(m-s-1)\Psi - \xi_0]$$

$$+ (m-s \pm 1) J_{m-s+1}(k_c R) \cos[(m-s+1)\Psi - \xi_0]$$

$$- \frac{1}{2} k_c r_l J_{m-s-2}(k_c R) \cos[(m-s-2)\Psi - \xi_0]$$

$$\left. - \frac{1}{2} k_c r_l J_{m-s+2}(k_c R) \cos[(m-s+2)\Psi - \xi_0] \right\} \qquad (II-9)$$

Appendex III   Radial Integrations

For the sake of saving space, some of the following derivations double subscripts are used. In any case, the sub- and supper-scripts must be be taken correspondinly. From the Graff's addtion thorem and with reference to Fig.3, we have

$$J_m(k_c r)e^{jm\xi} = \sum_{s=-\infty}^{\infty} J_{m-s}(k_c R)J_s(k_c r_l)e^{js\Psi} \qquad (III-1)$$

and since $dr = r_l \sin \xi d\Psi$, we may write

$$[\Phi^{\pm}_{m-s}]_r = \int_{r_1}^{r_2} dr k_c r e^{jm\theta} \Phi^{\pm}_{m-s} J_{m\mp 1}(k_c r)$$

$$= \frac{k_c}{2\pi} J_{m-s}(k_c R) \int_{-\pi}^{\pi} d\Psi e^{j(m\mp 1)\xi} e^{j\mp(m-s)\Psi}$$

$$= \frac{k_c}{2\pi} J_{m-s}(k_c R) \sum_{s=-\infty}^{\infty} J_{m\mp s'}(k_c r_l)J_{s'}(k_c R) \int_{-\pi}^{\pi} d\Psi e^{\mp j(m-s\pm s')\Psi}$$

$$= k_c J^2_{m-s}(k_c R)J_{s\mp 1}(k_c r_l) \qquad (III-2)$$

$$[\Psi_{s-}]_r = \int_{-\pi}^{\pi} dr k_c r e^{jm\theta} \Psi_{s-} J_{m\mp 1}(k_c r)$$

$$= \frac{k_c}{r_l}\{-k_c r_l J^2_{m-s}(k_c R)J_{s\mp 1}(k_c r_l) + (m-s\pm 1)J^2_{m-s-1}(k_c R)J_{s+2}(k_c r_l)$$

$$+ (m-s\pm 1)J^2_{m-s+1}(k_c R)J_{s-2}(k_c r_l)$$

$$- \frac{1}{2}k_c r_l J^2_{m-s-2}(k_c R)J_{s+1}(k_c r_l)$$

$$- \frac{1}{2}k_c r_l J_{m-s+2}(k_c R)\cos[(m-s+2)\Psi \pm \xi_0]\} \qquad (III-4)$$

$$[\Psi_{s+}]_r = \int_{-\pi}^{\pi} dr k_c r e^{jm\theta} \Psi_{s+} J_{m\mp 1}(k_c r)$$

$$= \frac{k_c}{r_l}\{(m-s\pm 1)J^2_{m-s-1}(k_c R)J_{s+2}(k_c r_l)$$

$$- (m-s\pm 1)J^2_{m-s+1}(k_c R)J_{s-2}(k_c r_l)$$

$$- \frac{1}{2}k_c r_l J^2_{m-s-2}(k_c R)J_{s+1}(k_c r_l)$$

$$+ \frac{1}{2}k_c r_l J_{m-s+2}(k_c R)\cos[(m-s+2)\Psi \pm \xi_0]\} \qquad (III-5)$$

Thus, we obtain the following several quantities as

$$\hat{\Phi} = [\Phi^-_{m-s}]_r - [\Phi^+_{m-s}]_r$$

$$= 2k_c J^2_{m-s}(k_c R) J'_s(k_c r_l) \qquad (III-6)$$

$$\hat{\Psi}_- = [\Psi_-]_r - [\Psi_{c-}]_r$$

$$\frac{2k_c^2}{k_c r_l} \Big\{ -k_c r_l J^2_{m-s}(k_c R) J'_s(k_c r_l)$$

$$+ [(m-s) J'_{s+1}(k_c r_l) + \frac{s+1}{k_c r_l} J_{s+1}(k_c r_l)] J^2_{m-s-1}(k_c R)$$

$$+ [(m-s) J'_{s-1}(k_c r_l) + \frac{s-1}{k_c r_l} J_{s-1}(k_c r_l)] J^2_{m-s+1}(k_c R)$$

$$- \frac{1}{2} k_c r_l J'_{s-2}(k_c r_l) J^2_{m-s+2}(k_c R)$$

$$- \frac{1}{2} k_c r_l J'_{s+2}(k_c r_l) J^2_{m-s-2}(k_c R) \Big\} \qquad (III-7)$$

$$\hat{\Psi}_+ = [\Psi_+]_r - [\Psi_{c+}]_r$$

$$\frac{2k_c^2}{k_c r_l} \Big\{ [(m-s) J'_{s+1}(k_c r_l) + \frac{s+1}{k_c r_l} J_{s+1}(k_c r_l)] J^2_{m-s-1}(k_c R)$$

$$- [(m-s) J'_{s-1}(k_c r_l) + \frac{s-1}{k_c r_l} J_{s-1}(k_c r_l)] J^2_{m-s+1}(k_c R)$$

$$+ \frac{1}{2} k_c r_l J'_{s-2}(k_c r_l) J^2_{m-s+2}(k_c R)$$

$$- \frac{1}{2} k_c r_l J'_{s+2}(k_c r_l) J^2_{m-s-2}(k_c R) \Big\} \qquad (III-8)$$

References

[1] R. Q. Twiss, "Radiation transfer and the possibility of negative absorption in radio astronomy," Aust. J. Phys., Vol. 11, pp. 564-579, Dec., 1958.

[2] A. V. Gaponov, "Addendum," Izv. VUZ. Radiofizka, Vol. 2, p. 837, 1959.

[3] R. H. Pantell, "Backward wave oscillations in an unloaded waveguide," Proc. IRE, vol. 47, p. 1146, June 1959.

[4] J. L. Hirshfield and J. M. Wachtel, "Electron cyclotron maser," Phys. Rev. Lett. 38 vol. 12, pp. 533-536, 1964.

[5] J. L. Hirshfield, I. B. Bernstein and J. M. Wachtel, "Cyclotron resonance interaction of microwaves with energetic electrons," J. Quantum Electronics, vol. QE-1, pp. 237-245, 1965

[6] V. L. Granatstein, M. H. Herdon, P. Sprangle, Y. Garmel, and J. A. Nation, "Gigawatt microwave emission from an intense relativistic electron beam," IEEE Trans. Microwave Theory Tech., vol. MTT-22, pp. 1000-1005, 1974.

[7] M. Friedman and M. Herndon, "Emission of coherent microwave radiation from a relativistic electron beam propagating in a spatially modulated field," Phys. Fluids vol. 16, pp. 1982-1995, 1973.

[8] N. I. Zaytsev, T. B. Pankratowa, M. I. Petelin, and V. A. Flyagin, "Millimeter and submillimeter waveband gyrotrons," Radio Eng. Electron Phys. vol. 19, pp. 103-107, May 1974.

[9] A. A. Andronov, V. A. Flyagin, A. V. Gaponov, A. L. Godenberg, M. I. Petelin, Infrared Physics, Vol. 18, p. 385, 1978.

[10] V. L. Granatstein, M. E. Read, I. R. Branet, Infrared and Millimeter Waves, vol. 5, K. J. Button ed., Academy, New York, 1982.

[11] H. Jory, S. Evans, J. Moran, J. Shively, D. Stone, and G. Thomas, "200 kW pulsed and CW gyrotrons at 28 GHz," 1980 IEDM Technical Digest, 12.1, pp. 304-307.

[12] V. V. Alikaev, G. A. Babrovskii, V. I. Poznyak, K. A. Razumova, V. V. Sannikov,

and A. A. Shmarin, Fiz. Plazmy 2, pp. 390-395, 1976. (Soviet J. Plasma Phys. 2, pp. 212-215 ,1976)

[13] R. S. Symons and H. R. Jory, S. Hegji and P. Ferguson, "An experimental gyro-TWT," IEEE Trans. Microwave Theory Tech., pp. 181-184, March 1981.

[14] J. Schnedier, "Stimulated emission of radiation by relativistivc electrons in a magnetic field," Phys. Rew. Lett. 2, pp. 504-505, 1959.

[15] P. Sprangle and A. T. Drobot, "The linear and self-consistent nonlinear theory of the electron cyclotron maser instability," IEEE Trans. Microwave Theory Tech. pp. 313-317, vol. MTT-25, No.6, 1977.

[16] Kwo Ray Chu, A. T. Drobot, H. H. Szu and P. Sprangle, "Theory and simulatior of the gyrotron traveling wave amplifier operating at cyclotron harmonics," IEEE Trans. Microwave Theory Tech. pp. 313-317, vol. MTT-28, No. 4, 1980.

[17] G. T. Thomas, "Solitons and nonlinear gyro-TWT Theory," Int. J. Electronics, 1981, Vol. 11, No. 4, pp. 395-413.

[18] Y. Y. Lau and L. R. Barnett, "Theory of a low magnetic field gyrotron (Gyro-magnetron) ," IJIMW 3, pp. 619-644,1982.

[19] K. R. Chu et al. , "Theory of harmonic gyrotron oscillator with sloted resonant structure," IJIMW., Jan., pp. 121, 1984.

[20] W. W. Destler, R. L. Weiler, and C.D. Striffler, "High power generation from a rotating E layer in a magnetron-type waveguide," Appl. Phys. Lett. 38(7), pp. 570-572, 1 April, 1981.

[21] J. L. Hirshfield, "Cyclotron harmonic maser," IJIMW,2, pp. 695-704,1981

[22] N. A. Ebrahim, Z. Liang, and J. L. Hirshfield, "Bernstein-mode quasioptical maser experiment," Phys. Review Lett., 49, No. 21(1556), 1982

[23] Won Namkung,"Observation of micriwave generation from a cusptron device," Phys. Fluids 27(2), pp. 329-330, Feb., 1984.

[24] V. L. Bratman, N. S. Ginzburg, G. S. Nunsinovich, M. I. Betelin, and P. S. Strelkov, "Relativistic gyrotrons and cyclotron autoresonance masers," Int. J. Electronics, 1981, Vol. 51, No. 4, pp. 541-567.

[25] Kwo Ray Chu, et al., "Theory of a wide-band distributed gyrotron traveling

ampllifier," IEEE Trans. ED, Vol. ED-28, pp. 866-871, 1981.

[26] S. N. Vlasov, G. M. Zhislin, I. M. Orlova, M.I.Petelin,and G.G. Rogaecheva, "Irregular waveguides as open resonators," Radiophysics and Quantum Electronics, vol. 121, No. 8, pp. 972-978, Aug. 1969.

[27] Li Qiangfa, "Theoretical analysis of open resonators in the form of waveguide with slow-varied cross section," Acta Physica Sinica, Vol. 29, No. 11, Nov., 1980.

[28] Li Qiangfa and Xu Cheng he, "Microwave network theory of open resonators in the form of waveguide with slowly-varying cross-section," Acta Physica Sinica, Vol. 30, No. 7, July, 1981.

[29] Zhou Lezhu, Xu Chenghe, and Gong Zhonglin, "General theory and design of microwave open resonators," IJIMW 3, 117-136, 1982.

[30] Q. F. Li and K. R. Chu, "Analysis of open resonators," IJIMW 3, pp. 705-723, 1982.

[31] I. B. Bernstein, Lale K. Divringi and Timothy M. Smith, "The theory of irregular waveguides and open resonators," IJIMW 4, pp. 57-117, 1983.

[32] V. A. Flyagin, A. V. Gaponov, M. I. Petelin and V. K. Yulpatov, "The gyrotron,"
IEEE, Trans. Microwave Theory Tech., Vol. MTT-19, pp. 547-555, 1971.

[33] A. V. Gaponov, A. I. Flyagin, A. L. Godenberg, G. S. Nusinovitch, S. E. Tsimring, V. G. Vsov, and S. N. Vlasov, "Powerful millimetre-wave gyrotrons," Int. J. Electronics, 1981, Vol. 51, No. 4, pp. 277-302.

[34] V. A. Zhurakhovskiy, "Using an average method to integrate relativistic nonlinear equations for phase synchronous instruments," Radiotech. Electron. 9, No. 8, pp. 1527-, 1964.

[35] G. N. Rapport, A. K. Nemak and V. A. Zhurakhovskiy, "Interaction between helical electron beams and strong electromagnetic fields at cyclotron- frequency Harmonics," Radiotech. Electron. 12, No. 4, pp. 633-641, 1967.

[36] A. W. Fliflit, M. E. Read, K. R. Chu, and R. Steeley, "A self-consistent field theory for gyrotron oscillators: application to a low Q gyromonotron," Int. J. Electronics, 1982, Vol. 53, No. 6, pp. 501-521.

[37] W. W. Destler, R. E. Weiler, and C. D. Striffler, "High power generation from a rotating E layer in magnetron-type waveguide," Appl. Phys. Lett. 38(7), pp. 570-572, 1 April, 1981.

[38] M. S. Grewal and J. A. Byers, "A computational study of the negaive mass instability in the nonlinear regime," Plasma Physics, Vol. 11, pp. 727-738, 1969.

[39] P. A. Lindasay, "Self-consistent large-signal interaction in a TWT gyrotron," Int. J. Electronics, 1981, Vol. 51, No. 4, 379-393.

[40] Y. Y. Lau, M. J. Baird, L. R. Barnett, K. R. Chu, and V. L. Granastein, "Cyclotron maser instability as a resonant limit with space charge wave," Int. J. Electronics, 1981, Vol. 51, No. 4, pp. 331-340.

[41] S. Y. Park, J. M. Baird, and J. L. Hirshfield, "Linear theory of gyro-slow-wave amplifier for TE_{0n}-modes in a dielectric-loaded cylindrical waveguide," Report for NRL, 20 Nov., 1981.

[42] K. R. Chu, "Theory of electron cyclotron maser interaction in a cavity at the harmonic frequencies," Phys. Fluids, 21(12), Dec. 1978.

[43] S. E. Tsrimring, Izv. VUZ. Radiofiz., vol. 15, No. 8, 1247, 1972.

[44] V. K. Lygin and S. E. Tsimring, Isv. VUZ, Radiofizika, 21, 1363, 1978.

[45] S. D. Conte and Carl de Boor, Elementary numerical analysis, Third Edition, McGraw-Hill Book Company, 1980.

[46] J. P. Montgomery, "On the complete eigenvalue solution of ridged Waveguide," IEEE, Trans. Microwave Theory Tech., Vol. MTT-19, pp. 547-555, 1971.

[47] R. E. Bank, PLTMG User's Guide (at Yale), 1982.

[48] D. Dasgupta et al., "Eigenvalue spectrum of rectangular waveguide with two symmetrically placed double ridges," IEEE Trans. Microwave Theory Tech., Vol MTT-29, pp. 47-51, 1981.

[49] G. Döhler, D. Gallagher, and R. Moats, "The Peniotron: A fast wave device for efficient High power MM wave generation," Int. Electron Meeting, Dec. 4-6, 400, 1978.

[50] S. P. Kuznetrov, D. I. Trubetskov, and A. P. chetverikov, "Nonlinear theory of

the peniotron," STPL, 6(10), 495, Oct., 1980. ~~495, Oct., 1980,~~

[51] G. Döhler, "Peniotron interaction in gyrotrons: I. Qualitative analysis," Int. J. Electronics, Vol. 56, No. 5, pp. 617-627, 1984.

[52] G. Döhler, "Peniotron interaction in gyrotrons: II. Quantitative analysis," Int. J. Electronics, Vol. 56, No. 5, pp. 629-640, 1984.

END

FILMED

6-85

DTIC